Heterotypic cell-cell interactions between Kras^{G12D} cells and normal neighbours in early pancreatic cancer

William Hill

PhD Thesis
2018

Acknowledgements

First I would like to thank my supervisor Dr. Catherine Hogan for all the guidance and support you've provided every step of my PhD and for being a great inspiration.

I would also like to thank Derek Scarborough and Mark Isaac from the histology services and the team from the barrier unit including Elaine Taylor, Michael Quirk, Asif Jeelani and Paul Chapman for all their assistance and help.

I am also grateful to everyone who I have worked with at ECSCRI who have made it such a great environment to do my PhD in. In particular, I would like to thank current and past members of Hogan lab including: Sean Porazinski for patiently teaching me so much and Andreas Zaragkoulias for all his help on the pancreas project. The fellows Joaquin de Navascues, Florian Siebzehnrubl and Lee Parry have also been a great help through my project. I have been fortunate to supervise several great undergraduate students including Rebecca Bennion, Matt Jones and Clare Moscrop.

On a more a personal note I would like to thank my parents and family for the constant support and eoncouragement. I would like to thank all my friends who have always been there for me since undergrad: Abby, Alice, Laura, Cat, Mia, Rosh, Huw, Swg, Lew, Danny, Jake, and Charlie. Last but by no means least, thank you to Imogen for everything.

Table of Contents

List of Figures

List of Tables

Abbreviations

2D - Two-dimension

3D - Three-dimension

ADM - Acinar-ductal metaplasia

APC - Adenomatous polyposis coli

BMMA - Butyl methyl methacrylate

BMP - Bone morphogenetic protein

BSA - Bovine Serum Albumin

CA-19 - Carbohydrate 19

CC3 - Cleaved caspase 3

cdc42 - Cell division control protein 42

CIL - Contact inhibition of locomotion

CK-19 - Cytokeratin 19

CreERT = Cre recombinase-Estrogen receptor fusion transgene

ctDNA - Circulating tumour DNA

dEph - *Drosophila* Eph

dH2O - Distilled H20

Dlg - Disc large-1

DMEM - Dulbecco's Modified Eagle Medium

DNA - Deoxyribonucleic acid

dpi - Days post injection

E-cadherin - Epithelial cadherin

ECM - Extracellular matrix

EGF - Epidermal growth factor

EGFR - Epidermal growth factor receptor

EMT - Epithelial-mesenchymal transition

F-actin - Filamentous actin

FBS - Foetal bovine serum

GAP - GTPase activating protein

gDNA - Genomic deoxyribonucleic acid

GDP - Guanine diphosphate

GEF - Guanine nucleotide exchange factor

GTP - Guanosine triphosphate

HEPES - 4-2-hydroxyethyl)-1-piperazineethanesulfonic acid

hESC - Human embryonic stem cell

IP - Intraperitoneal

IPMN - Intraductal papillary mucinous neoplasm

JNK - c-Jun N-terminal Kinase

Lgl - Lethal (2) giant larvae

MCN - Mucinous cystic neoplasm

MDCK - Madin-Darby canine kidney cells

mRNA - Messenger ribonucleic acid

NCC - Neural crest cell

NGS - Normal Goat Serum

OCT - Optimal cutting temperature

P/S - penicillin/streptomycin

PanIN - Pancreatic intraepithelial neoplasia

PBS - Phosphate buffered saline

PCR - Polymerase chain reaction

PDAC - Pancreatic ductal adenocarcinoma

PDE – Pancreatic ductal epithelial

PDK4 - Pyruvate dehydrogenase 4

Pdx1 - Pancreatic and duodenal homeobox 1

PFA - Paraformaldehyde

PI3K - Phosphatidylinositide 3-kinase

PKA - Protein kinase A

RFP - red fluorescent protein

ROCK - Rho associated protein kinase

RT - Room temperature

RTK - Receptor tyrosine kinase

S.D - Standard deviation

S1P - Sphingosine 1-phosphate

S1P2 - Sphingosine 1-phosphate receptor 2

Ser - Serine

SFK - Src family kinase

TAE - Tris-acetate-EDTA

TBS - Tris buffered saline

tdRFP - Tandem dimer red fluorescent protein

TGF-α - Transforming growth factor alpha

Thr - Threonine

UV - Ultraviolet

WASP - Wiskott-Aldrich syndrome protein

Wg - wingless

WT - wild type

YAP - yes associated protein

Abstract

At the initial stages of tumourigenesis, transformation occurs in a single cell within a healthy epithelial sheet. Competitive interactions between normal and Ras-transformed cells can drive the elimination of mutant cells from tissues to protect from carcinogenesis. Moreover, we have previously demonstrated that normal cells detect and eliminate Ras-transformed cells via differential EphA2 signalling. $Kras^{G12D}$ expressing cells (Kras^{G12D} cells) initiate and drive the earliest stages of pancreatic cancer yet it is unclear if normal pancreatic cells can eliminate oncogenic cells. Here we use low level, stochastic induction of $Kras^{G12D}$ mutations in the pancreas to model the interaction of normal and transformed epithelial cells. We show that Ras-transformed cells adopt a contractile morphology and are eliminated from healthy tissue when present at low numbers. When surrounded by normal cells, Kras^{G12D} cells become segregated, increase in compactness and are often extruded. We find that E-cadherin-based cell-cell contacts are downregulated and internalised in mutant cells when surrounded by normal neighbours in an EphA2-dependent manner. Our evidence also suggests that normal cells suppress progression of Ras-transformed cells to an early disease state. Together, this study suggests that non-transformed pancreatic epithelial cells can eliminate Kras^{G12D} cells from the tissue via EphA2 signalling. These data identify a novel putative tumour-suppressive mechanism in the adult pancreas that mutant cells must first overcome to drive tumourigenesis. Understanding the earliest stages of pancreatic carcinogenesis will provide insight into how risk factors promote disease and may elucidate how pancreatic cancer spreads around the body.

Chapter 1: Introduction

1.1   The Mammalian Pancreas

The pancreas is a glandular organ that forms part of both the digestive and endocrine system (Jain and Lammert, 2009). It is located in the upper left part of the abdomen behind the stomach and is divided into four regions: head, neck, body and tail. The exocrine pancreas consists of acinar and ductal cells (Figure 1.1A). The acinar cells form the bulk of the pancreas and generate digestive enzymes that are stored in zymogen granules. They are organised into grape-like clusters at the termini of a branching ductal system (Bardeesy and DePinho, 2002). The ducts form a network of tubes of increasing size that add mucous and bicarbonate to the acinar-secreted enzyme mix and empty into the duodenum (Grapin-Botton, 2005). The endocrine pancreas is made up of four cell types that are organised into Islet of Langerhans and secrete hormones into the bloodstream (Figure 1.1B). The α- and β- cells regulate the usage of glucose by producing glucagon and insulin, respectively. Pancreatic polypeptide and δ-cells produce pancreatic polypeptide and somatostatin to modulate the secretory properties of other pancreatic cell types (Jain and Lammert, 2009). To control and carry out these functions the pancreas is highly innervated and contains a network of blood vessels (Brunicardi et al., 1995).

1.2 Epithelial Biology

The pancreas, as with most organs, consists of layers of cells termed epithelia and have several functions such as: form a physical barrier to protect tissues, regulate the exchange of chemicals between the underlying tissue and lumen, secretion of hormones into the circulatory, enzymes and other products into ducts and also provide sensation (Alberts, 2013). The role of epithelial tissues is closely associated with the junctional complexes formed between cells and the polarity of epithelial tissues (Figure 1.2).

Epithelial cell polarity is established by complex but coordinated events involving the multiprotein complexes: Par, Crumbs and Scribble (Rodriguez-

Boulan and Macara, 2014). This generates spatially distinct domains at the apical surface, the tight junction, and the lateral and basal surfaces (St Johnston and Ahringer, 2010). Stable cell polarity also relies on the asymmetric delivery of apical and basolateral proteins to the correct surface (Apodaca et al., 2012).

The orientation of epithelial polarity requires extrinsic signals that arises from the extracellular matrix (ECM) (Gumbiner, 1996). Most cells also contact a supporting matrix with a large variety of cell surface proteins interacting with the underlying extracellular matrix (ECM) for structure and cell migration (Bonnans et al., 2014). The integrin family is central to these cell-matrix interactions. Between cells, tight junctions link epithelial cells closely together to form a barrier and enable regulation of ion transport across epithelial layers. The mechanical attachment between adjacent cells is carried out by adherens junctions that consist of cadherins, such as E-cadherin, and catenins such as p120-, α- and β-catenin and are linked to the actin cytoskeleton (Alberts, 2013). This linkage to the actin cytoskeleton can generate force and the linkage of cadherins to the actin network is finely regulated. Desmosomes are another class of cell-cell junction that confers mechanical resilience on cell layers. Together these junctions mediate cell-cell and cell-ECM adhesion and allow epithelial layers to act as a coherent dynamic sheet (Trepat and Sahai, 2018). Epithelial integrity and homeostasis are central to survival with alterations to these systems resulting in cancer.
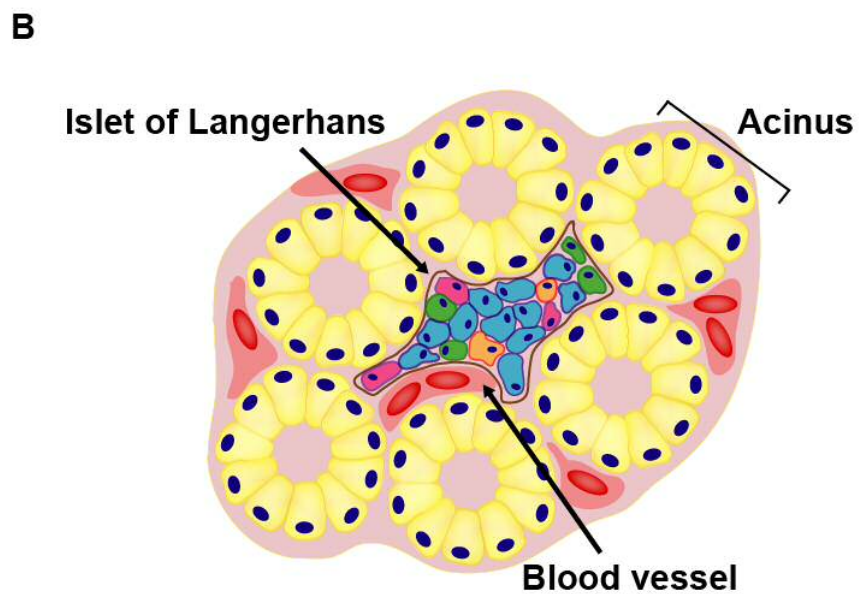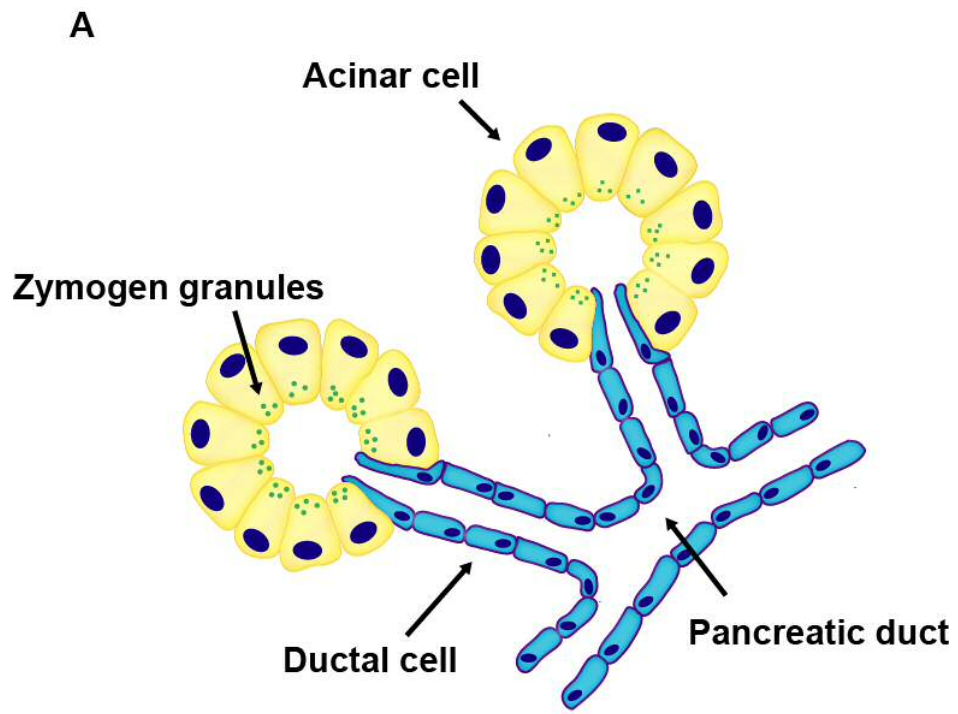
Figure 1.1: Exocrine and endocrine compartments of the pancreas.
Grape-shaped acinar cells produce enzymes stored in zymogen granules
that travel down ducts to the intestine. The hormone-secreting islets are
found scattered throughout the tissue. Figure based on Bardeesy &
DePinho, 2002.
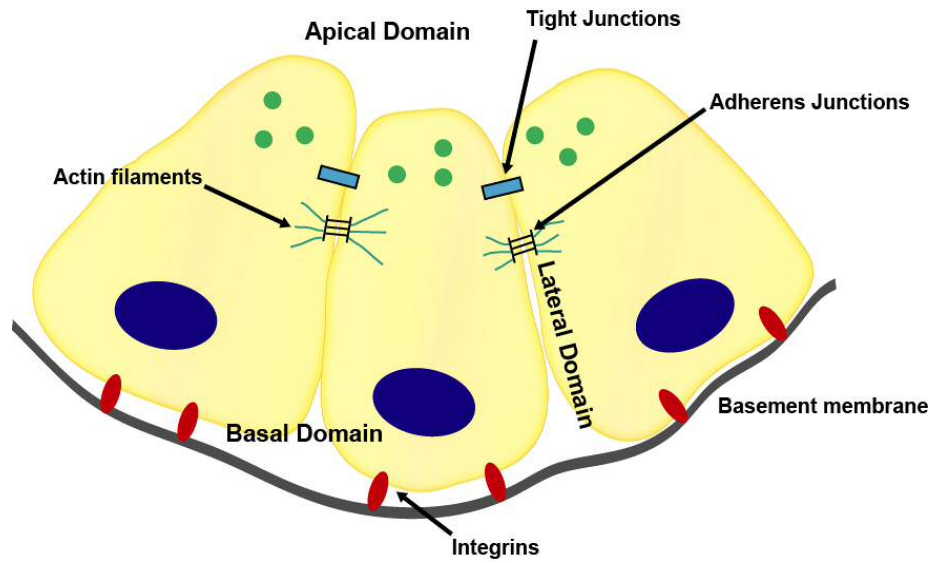
Figure 1.2 Epithelial Polarity and Junctional complexes. Several junctional complexes perform different functions within epithelial tissues. Tight junctions perform a barrier function and enable active regulation of ions. Adherens junctions generate cell-cell adhesion and can transmit force through the linkage with the actin cytoskeleton. Cell-matrix interactions are facilitated through integrins. The basement membrane provides directional cues that allows the establishment of polarity.

Pancreatic Cancer

1.2.1 Incidence

Pancreatic cancer is one of the most deadly forms of the disease. An estimated 9,921 new cases were diagnosed in the UK in 2015 and associated with 9,263 deaths in 2016 (Cancer Research UK, 2017). It is currently the fourth highest cause of cancer death in developed countries and is predicted to become the second leading cause of cancer-related mortality by 2030 (Rahib et al., 2014). Less than 5% of patients survive for at least five-years after diagnosis in the UK and this survival rate has remained unchanged for the last 40 years (Cancer Research UK, 2017).

1.2.2 Risk factors

One of the major determinants of pancreatic cancer risk is age with over 90% of patients diagnosed >50 years old (Deutsch et al., 1999). With regards to preventable risk factors, tobacco smoking is the most characterised. It has been estimated that smoking is attributable to 15-30% of cases. Smoking tobacco can increase the risk of pancreatic cancer by up to threefold and a dose-risk relationship has been identified (Bosetti et al., 2012). Other factors such as obesity and low physical activity have also been linked to development of this disease (Behrens et al., 2015).Obesity is thought to promote a chronic pro-inflammatory state and hyperinsulinaemia that may increase risk (Raimondi et al., 2009; Xu et al., 2018). Chronic pancreatitis, an inflammatory disease of the pancreas, is believed to increase risk of pancreatic cancer by more than tenfold. Diabetes can be both a consequence of early-stage pancreatic cancer and a risk factor for the disease with long-term diabetes approximately doubling the risk of pancreatic cancer (Bosetti et al., 2014). However, the precise mechanism for increased likelihood of developing the disease cause by different risk factors is not well understood.

1.2.5 Diagnosis of Pancreatic cancer

One of the major contributors to the dismal prognosis of pancreatic cancer is due to late diagnosis. Pancreatic cancer is difficult to diagnose in part because the clinical manifestations are non-specific and occur late in disease progression. Symptoms include unexplained weight loss, nausea, new-onset diabetes and jaundice (Freelove and Walling, 2006).Diagnosis typically requires expensive and invasive techniques such as contrast-enhanced computed tomography and endoscopic ultrasound with needle biopsy. At the time of diagnosis around 80% of patients have advanced, metastatic disease that is not suitable for surgical intervention (Siegel et al., 2016). However, patients diagnosed with localised disease are eligible for surgery which increases the 5-year survival by >5-fold to 25%.

Being able to diagnose the disease earlier would markedly improve patient survival but faces a number of challenges. Although the lifetime risk for developing PDAC is 1.5%, and only 1 in 8000 individuals will be diagnosed each year (Siegel et al., 2016). This low incidence in the general population in combination with expensive and invasive tests demands that any screening technology is highly sensitive with a low false positive rate. Use of biomarkers is a promising area of research for diagnosis and disease monitoring of pancreatic cancer. Currently, in individuals known to have a high risk for developing PDAC, the blood biomarker cancer antigen 19-9 (CA-19) can be used to aid diagnosis and monitor disease. However, it has a number of limitations with low sensitivity (78.2%), specificity (70%) and false positive (5-10%) limiting its use (Becker et al., 2014; Poruk et al., 2013). Furthermore, it is difficult to differentiate between pancreatic cancer and other non-malignant diseases such as liver cirrhosis (Duffy et al., 2010) and CA-19 is not expressed in all patients (Poruk et al., 2013). Circulating tumour DNA (ctDNA) encoding mutant KRAS have shown encouraging results with detection in 43% of patients before metastasis. Efforts to use mutant KRAS has also been hampered by the finding that Kras-mutations are common in an age-dependent manner even in people devoid of pancreatic malignancy (Lu et al., 2002; Parsons and Meng, 2009; Yakubovskaya et al., 1995; Yan et al., 2005). Similarly, the presence of circulating tumour cells from may also provide a fruitful diagnostic but both ctDNA and circulating cells are

only detected in a subset of pancreatic cancer patients (Sausen et al., 2015). More recently, the EphA2 receptor has been identified as a potential extracellular vesicle biomarker for pancreatic cancer (Liang et al., 2017). Although promising, it is imperative to understand how biology impacts biomarkers in disease initiation and progression.

1.3   Biology of Pancreatic Cancer

Pancreatic ductal adenocarcinoma (PDAC); the most common form of pancreatic cancer accounts for 95% of cases and arises from the exocrine compartment of the pancreas.

Multiple studies have identified Kirsten rat sarcoma viral oncogene homolog (KRAS) mutations as the initial event in the development of human PDAC (Almoguera et al., 1988; Habbe et al., 2008; Hingorani et al., 2003). Outside of *KRAS* mutations the genetic landscape of pancreatic cancer primarily consists of only a handful of other mutations: CDKN2A, TP53, and SMAD4. Activating mutations in *KRAS* are found in up to 95% of patients with inactivating mutations in *TP53*, *CDKN2A* and *SMAD4* occurring in 50-80% of cancers (Biankin et al., 2012; Jones et al., 2008; Waddell et al., 2015; Witkiewicz et al., 2015). PDAC is associated with several distinct precursor lesions including pancreatic intraepithelial neoplasia (PanIN), intraductal papillary mucinous neoplasm (IPMN) and mucinous cystic neoplasm (MCN) (Morris et al., 2010a). The stepwise progression of PanIN lesions to invasive PDAC has been most well characterised, summarised in Figure 1.3. They are classified based on histology into three stages of increasing cellular and nuclear atypia (Bardeesy and DePinho, 2002; Hruban et al., 2004; Morris et al., 2010a) (Figure 1.2): PanIN 1A (flat duct lesions), PanIN 1B (papillary duct lesions), PanIN 2 (papillary duct lesions with dysplasia) and PanIN3 (also known as carcinoma-*in-situ*). Support for the stepwise model comes from increasing PanIN stage associated with increasing mutational burden. For example, loss of p16^{INK4A} protein is associated with PanIN 2 and PanIN 3, with a higher frequency in PanIN 3 (Wilentz et al., 1998). Nuclear accumulation of TP53 or SMAD4 loss is also most commonly observed in PanIN-3, with higher frequency of somatic mutation of both genes in invasive cancer (DiGiuseppe et al., 1994; Wilentz et al., 1998, 2000). Moreover,

although *KRAS* mutations are present in all PanIN stages and PDAC, the proportion of cells containing *KRAS* mutations increase with PanIN grade (Kanda et al., 2012). This suggests that in humans early PanIN lesions expand clonally and contain *KRAS* wild-type cells that are lost as disease advances. The mutational burden of Kras-transformed cells in PanIN lesions then increases, lesions become higher grade and eventually develop into PDAC. Recently, a revised 2-tier classification system has recommended for patients which describes current PanIN-2 and neoplasms with intermediate grade dysplasia as low grade (Basturk et al., 2015). With the term 'high grade' lesion reserved for the uppermost end of the spectrum including carcinoma in situ.

Another key feature of pancreatic cancer is an abundant and dense collagenous stroma and accounts for up to 90% of the tumour volume (Neesse et al., 2015). The stroma consists of both cellular elements: pancreatic stellate cells, infiltrating immune cells, endothelial cells and neuronal cells and extracellular matrix (ECM) proteins: collagens, fibronectin and laminin as well as non-collagenous proteins like glycoproteins and glycosaminoglycans (Von Ahrens et al., 2017; Neesse et al., 2015; Sousa and Kimmelman, 2014; Stromnes et al., 2014). This results in restricted nutrients and oxygen gradients with complex cross-talk between the stroma and cancer (Tape et al., 2016).

Pancreatic cancer is an extremely deadly disease and one reason for this is the highly invasive and metastatic capabilities of PDAC. It has been demonstrated in murine models that cells can disseminate from the earliest stages of pancreatic carcinogenesis (Hendley et al., 2016; Rhim et al., 2012, 2014). Before frank metastasis could be detected, mutant cells were able to seed the liver with circulating tumour cells widely associated with epithelial-to-mesenchymal (EMT) characteristics (Rhim et al., 2012)(Figure 1.2). Furthermore, genetic analysis has indicated that precancerous neoplastic cells migrate through the ductal system and seed precursor lesions in the pancreas (Makohon-Moore et al., 2018), suggesting cells can spread early in disease progression but not necessarily to seed other organs. Recently, livers from PDAC patients were found to harbour single disseminated cancer cells that can grow following resection of the primary tumour (Pommier et al., 2018). Strikingly, these cells were found to be cytokeratin-19 (CK19) negative. Expression of CK19 in acinar cells is thought to follow *Kras^{G12D}* mutations as the initial event in

pancreatic cancer. In acinar cells, expression of oncogenic *Kras^{G12D}* results in a CK19, duct-like progenitor via a process known as acinar-ductal metaplasia (ADM), that gives rise to precursor lesions (Houbracken et al., 2011).
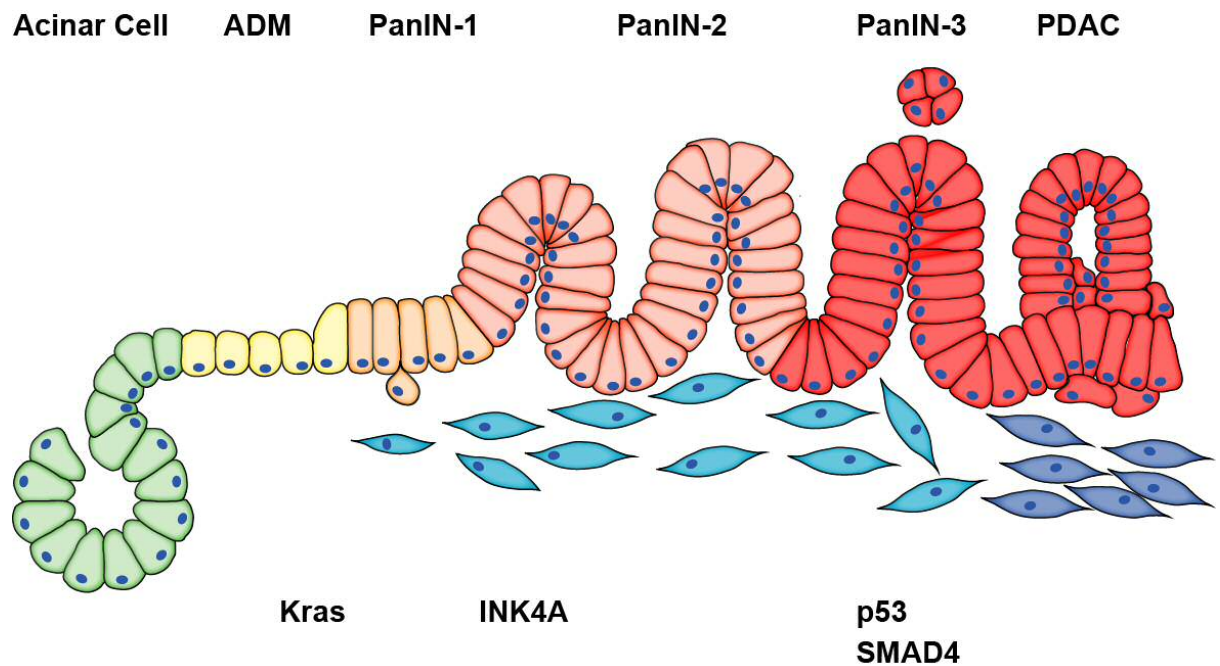
Figure 1.3: Progression of PDAC. Activating mutations to *Kras* in acinar cells are sufficient to initiate pancreatic intraepithelial neoplasia (PanIN) and pancreatic ductal adenocarcinoma (PDAC). PanINs are classified on morphology with increasing cellular atypia and mutations burden as disease progresses. Oncogenic cells can escape basally from PanIN-1 lesions to metastasise to the liver. In addition to epithelial changes desmoplastic changes occur in the stroma. Figure is based on Morris et al., 2010.

1.3.1 Acinar-Ductal Metaplasia

Histologically, PDAC resembles the exocrine ductal compartment of the pancreas, however, mouse models using lineage-specific oncogene activation suggested that the ductal compartment is refractory to Kras mutations (Brembeck et al., 2003; Guerra et al., 2007). It was later observed that oncogenic Kras^{G12D} can convert acinar cells into duct-like cells and PanINs and this leads to PDAC (Carriere et al., 2007; Guerra et al., 2007; Habbe et al., 2008; Morris et al., 2010a; Shi et al., 2013). This acinar-ductal-metaplasia (ADM) process has been an intense area of study in recent years. In the absence of activating *Kras* mutations ADM is a common and reversible process to protect the pancreas and help regenerate the organ following inflammation (e.g. pancreatitis) or damage (Houbracken et al., 2011; Liou et al., 2013). ADM can also result from loss of cell-cell contact signalling; with several studies demonstrating that loss of cell-cell junctions and E-cadherin based cell-cell adhesions capable of driving ADM (Hall and Lemoine, 1992; Hendley et al., 2016; Hezel et al., 2008; Shi et al., 2013). Oncogenic Kras^{G12D} expression also facilitates ADM, but in contrast to the damage response, this is irreversible and can lead to PanIN lesion formation (Baer et al., 2014; Collins et al., 2014; Kopp et al., 2012; Storz, 2017). A summary of ADM can be found in Figure 1.4.

During the process of ADM, a number of transcription factors associated with mature acinar fate are turned off, with increased expression of factors typically found in both mature ductal cells and embryonic pancreatic progenitors (Kopp et al., 2012; Krah et al., 2015; Prévot et al., 2012; Zhu et al., 2007). Specifically, acinar genes such as *Mist1*, *Cpa1* or those encoding elastase and amylase are silenced (Shi et al., 2013). With induction of genes such as *CK19* and *Sry*-related high-mobility group box 9 (Sox9) (Liou et al., 2013). ADM can then lead to the formation of early PanIN lesions but to progress to more invasive carcinoma, it is thought another insult in the form of a secondary mutation (Bardeesy and DePinho, 2002; Hingorani et al., 2005), or inflammation (Guerra et al., 2011) is required to progress to PDAC.

Although the use of acinar-specific Cre promoters has demonstrated that mutant acinar cells can give rise to PDAC in animal models (Habbe et al., 2008), the progression of pancreatic cancer in humans is less well understood.

Human acinar cells can undergo ADM (Liu et al., 2016) but a variety of pancreatic lesions have been identified in humans and whether PDAC occurs via a stepwise process is not clear. Indeed, PanIN-like lesions can be induced by PDAC in normal, adjacent tissue (Ferreira et al., 2017). This suggests that lesions could arise from a variety of cellular origins. It is also conceivable that PanIN lesions are a protection mechanism from the progression of tumourigenesis by confining aberrant cells into proliferative-restricting cysts similar to the intestine (Cortina et al., 2007).
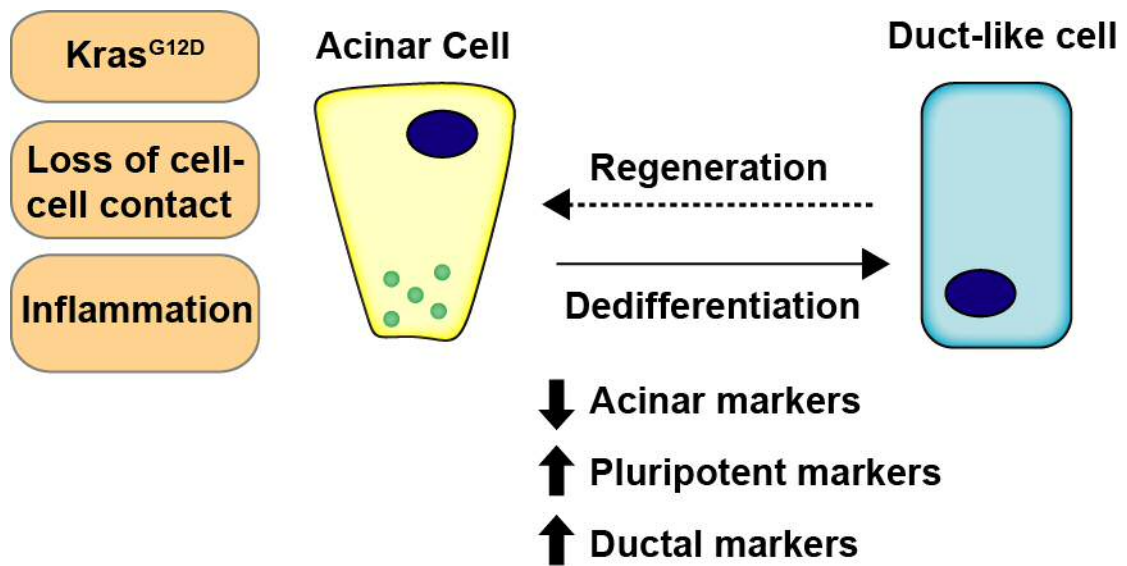
Figure 1.4: Acinar-ductal metaplasia (ADM) in the pancreas. A number of insults to pancreatic cells such as *Kras^G12D* expression, loss of cell-cell contacts or inflammation can induce dedifferentiation to a more duct-like cell. In response to inflammation this process is reversible but in the presence of Kras^G12D it is irreversible and can initiate pancreatic cancer precursor lesion formation. Figure is based on Storz, 2017.

1.3.2 RAS/MAPK Signalling in Pancreatic Cancer

RAS/MAPK signalling is integral to all parts of PDAC development. Mutational activation of KRAS is found in around 95% of PDAC tumours (Biankin et al., 2012), can drive disease in mouse models (Hingorani et al., 2003) and $Kras^{G12D}$ expression is required for the maintenance of precancerous lesions (Collins et al., 2014). This demonstrates that oncogenic *Kras* expression is critical for the initiation, growth and maintenance of PDAC.

KRAS is a member of the Ras family of small GTPases which includes: HRAS, NRAS and KRAS and together constitute the most frequently mutated oncogene family in human cancer (Prior et al., 2012). However, the mutation of family members is associated with different cancers; for example, *HRAS* is frequently mutated in melanoma and bladder whereas *KRAS* mutations are found in ovary, lung, colon and pancreas. Furthermore, the mutation frequency of *KRAS* can vary between cancer types. In PDAC, $KRAS^{G12D}$ mutations are dominant whereas a relatively high frequency of G13 mutations are found in colorectal cancer (Hobbs et al., 2016). This suggests different Ras isoforms and mutations are important for different forms of cancer.

The RAS family of proteins have been involved in cell differentiation, proliferation, migration and apoptosis (Cox and Der, 2010). RAS proteins become active when bound to guanine triphosphate (GTP) and inactive when bound to guanine diphosphate (GDP). RAS proteins have an intrinsic GTP-GDP cycling ability which is regulated by guanine nucleotide exchange factors (GEFs) and GTPase activating proteins (GAPs), that stimulate nucleotide exchange and the intrinsic GTP hydrolysis activity of RAS respectively. In the active, RAS-GTP bound form it interacts with a spectrum of downstream effectors to regulate a wide range of signalling networks. Mutations to residues G12 and G13 lead to constitutive activation of KRAS, holding it in the KRAS-GTP form promoting persistent signalling to downstream effectors. Downstream of KRAS are a diverse range of signalling pathways. In PDAC, the KRAS signalling pathways activated in PDAC are: Raf/Mek/Erk, PI3K/Pdk1/Akt and Ral GEF pathway (Collisson et al., 2012; Eser et al., 2013; Feldmann et al., 2010; Lim et al., 2005).

In summary, *Kras^{G12D}* mutations lock KRAS in the active GTP-bound form which is required for the initiation and development of PDAC. Other RAS isoforms can be mutated but are not as important in PDAC.

1.3.4 Models of Pancreatic Ductal Adenocarcinoma

Our understanding of how KRAS signalling contributes to the progression and development of PDAC has largely come from mouse models. However, initial studies of *Kras* mutational activation in murine models were unsuccessful. Expression of mutant *Kras* under acinar and ductal promoters resulted in ductal lesions and mixed acinar and ductal carcinomas (Grippo et al., 2003) or periductal inflammation (Brembeck et al., 2003), but not PDAC. This could have been a result of differences in *Kras* output between the endogenous and lineage specific promoters. The development of the Cre-inducible conditional allele targeted to the endogenous *Kras* locus allowed temporal and spatial control using the endogenous promoter (Hingorani et al., 2003; Tuveson et al., 2004).

Cre recombinase is an enzyme that recognises *loxP* sites on DNA and can excise the segment between them (Hoess et al., 1984). Artificial integration into the genome allows targeting of specific DNA sequences to inactivate and activate genes of interest. Activation is typically achieved with a *loxP-STOP-loxP* cassette at the start of a gene; Cre activation then removes a stop codon and permits gene expression. Control of Cre activation can be provided by using different cell type specific promoters to drive *Cre* expression. The first models to accurately recapitulate PDAC used Cre-recombinase under the control of promoters of pancreatic progenitor genes such as pancreatic duodenal homeobox 1 (*Pdx1*) and *Ptf1a* (also known as *p48*) which target Kras^{G12D} to almost all cells in the developing pancreas (Hingorani et al., 2003). These early studies using Cre-LoxP system demonstrated that physiological levels of KRAS^{G12D} induced lesions that recapitulate the full spectrum of human PanINs. Moreover, animals developed invasive and metastatic PDAC at a low frequency over 1 year (Hingorani et al., 2003). However, even in these models whereby *Kras^{G12D}* is expressed in almost every cell in the pancreas during development, only a small number of lesions formed with most of the tissue histologically normal. This suggests other factors are involved in lesion formation.

These models were then expanded to investigate the contribution of different cell types in PDAC. It has been demonstrated that expression of $Kras^{G12D}$ in adult mature acinar cells results in spontaneous PanIN lesion formation (Habbe et al., 2008). However, the ductal exocrine compartment appears more refractory to tumourigenesis with expression of $Kras^{G12D}$ alone insufficient to drive tumourigeneis. Recent work has demonstrated that two mutant $p53^{R172H}$ alleles in addition to oncogenic Kras is required to initiate PDAC from the ductal compartment in adult mice (Bailey et al., 2016). Moreover, it appears that PDAC originating from ductal cells progresses to PDAC via tubular lesions distinct from PanIN lesions (Ferreira et al., 2017). Therefore, both ductal and acinar cells can be a cell of origin for PDAC although duct-derived PDAC requires additional mutations and displays distinct pathophysiology.

The original $Kras^{G12D}$-driven models have also been combined with mutations and loss-of-function alleles for tumour suppressors commonly mutated in PDAC. It is important to note that in these current models, simultaneous activation of $Kras^{G12D}$ and loss of tumour suppressor occurs, in contrast to human tumour progression where aberrations accumulate over time. Loss of tumour suppressors in combination with oncogenic *Kras* expression accelerates disease and can alter the type of precursor lesion that develops, metastatic behaviour and the differentiation state of the malignant disease (Morris et al., 2010a). This illustrates the plasticity of the pancreas, with the same pancreatic cells developing a range of distinct phenotypes based on a few mutations. Studies of murine models has also indicated that mutational 'inactivation' and complete loss of protein can have different functions. Mice expressing mutant $p53^{R127H}$ can promote the metastasis of PDAC, in contrast to genetic loss of p53 which does not (Morton et al., 2010). This model, *Pdx1-Cre; Kras$^{LSLG12D/+}$;p53^{R172H}* (KPC) has become one of the most widely used models of PDAC for several reasons. They develop a spectrum of premalignant lesions that progress to PDAC with 100% penetrance. Tumours accurately recapitulate the extensive stroma and moderately differentiated ductal morphology observed in human patients. The KPC model also develop co-morbidities such as cachexia and jaundice and develop lung and liver metastases, the most commonly observed sites in humans (Gopinathan et al., 2015).

Other murine models have used the tamoxifen inducible Cre (Cre^ERT). In this model, the Cre enzyme is fused with a modified oestrogen receptor (ERT) that prevents translocation of the Cre protein into the nucleus (Feil et al., 1996). This results in the Cre^ERT construct only translocating to the nucleus upon binding of tamoxifen which provides temporal control of recombination. This also provides spatial control as tamoxifen dose can be titrated to lower the number of cells in which recombination takes place. Recently, this model has been used to study early pancreatic cancer in the adult and shows differential changes based on whether recombination occurs on a global or much lower level (Krah et al., 2015). Loss of the acinar determinant *Ptf1a* in around a quarter of acinar cells resulted in no histological change after 6 weeks, but deletion in >65% of cells drove rapid dedifferentiation (Krah et al., 2015). This suggests the interaction of normal and transformed cells impacts disease initiation and proposes that heterotypic interactions may be important in the initiation of PDAC.

1.4 Cell Competition

The heterotypic interaction of two different cell populations can have a major impact on the fate of aberrant cells and tumourigenesis. It has been demonstrated that normal cells can remove aberrant or defective cells through a process known as cell competition. Cell competition is a cell fitness-sensing mechanism that compares the relative fitness of a cell with its neighbour and is essential for proper development of embryos and tissue homeostasis in adults (Bowling et al., 2018; Morata and Ripoll, 1975; Moreno et al., 2002). Through competition and the sensing of relative fitness, those cells deemed less fit than their neighbours are eliminated (i.e., become "losers"), with the fitter population ("winners") undergoing compensatory proliferation (Figure 1.4). Importantly, loser cells lost through this mechanism are viable in different contexts. Cell competition was first described in *Drosophila melanogaster* imaginal wing discs by Morata and Ripoll (1975). Analysis of cells carry a heterozygous mutation in *Minute* (a ribosomal protein) found that heterozygous animals are viable and display a developmental delay due to slower proliferation. However, analysis of mosaic flies found that in heterozygous animals, *Minute*^+/- cells undergo apoptosis when

surrounded by normal, wild-type cells (Figure 1.4). This first demonstrated that tissues sense differential growth rates within a tissue and eliminate the slower-growing population. This early work also established a number of rules governing cell competition. Cell competition was found to be regionally modulated and sensitive to tissue type. For example, *Minute* hemizygous clones are more strongly outcompeted in the centre of the wing disc compartment, than at the periphery (Simpson, 1979). The proximity of winners and loser cells is important for cell competition but are not transmitted across compartment boundaries, indicating not only local but lineage specific cell interactions are essential (Simpson and Morata, 1981). Furthermore, cell competition can have a number of different effects on the loser cell population. Although classically associated with inducing apoptosis in loser cell populations (Moreno et al., 2002) loser cells can also be induced to undergo senescence (Bondar & Medzhitov, 2010), differentiation (Shiozawa et al., 2011) or extrusion (Hogan et al., 2009).

Evidence that cell competition is conserved in mammals was demonstrated using mouse cells carrying a heterozygous mutation in ribosomal protein L24 (Oliver et al., 2004). In chimera animals, mutant cells are eliminated by wild-type neighbours whereas they survive in a heterozygous mutant animal. The mutant cells displayed a growth disadvantage, but could generate viable mice in isolation. Evidence for cell competition in mammals also arises from a rat liver regeneration model (Oertel et al., 2006). Adult hepatocytes were found to be replaced by transplanted foetal hepatocytes over time, with apoptosis of adult hepatocytes at the border with foetal repopulating hepatocytes. Recently, the importance of cell competition in murine embryo has been highlighted with around 35% of cells eliminated via p53 mediated competition in normal development (Bowling et al., 2018). Mosaic activation of Myc *in vivo* has also been shown to induce apoptosis-dependent cell competition in several tissues and organs in developing mice (Clavería et al., 2013; Villa del Campo et al., 2014). The investigation of Myc in cell competition has identified a number of concepts of cell competition, for example, that relative-fitness levels are important rather than absolute fitness values. This was first demonstrated in *Drosophila* where cells overexpressing *dMyc*, the homolog of the mammalian proto-oncogene *c-Myc* induce the death of surrounding, normal growing, wild-type cells (De La Cova et al., 2004; Moreno and Basler, 2004). Wild-type cells

confronted with fitness-enhanced cell overexpressing non-tumourigeneic levels of Myc become losers and are eliminated (Figure 1.4) from the wing disc epithelium, a phenomenon known as supercompetition.

So far, cell competition appears to be a general feature of metazoan tissues that is important for expanding or eliminating cell lineage variants. Although cell competition drives changes in cellular properties, total tissue size does not alter suggesting homeostasis is preserved. With mutations predicted to occur in every cell division and the exposure to environmental factors also inducing DNA damage, adult tissues can be considered a patchwork of mutant clones. Indeed, sun-exposed skin is a patchwork of mutated cells with 18-32% of normal skin cells containing a carcinoma driver mutation (Martincorena et al., 2015). Therefore, cell-competitive interactions could play a lifelong role in homeostasis of tissues.
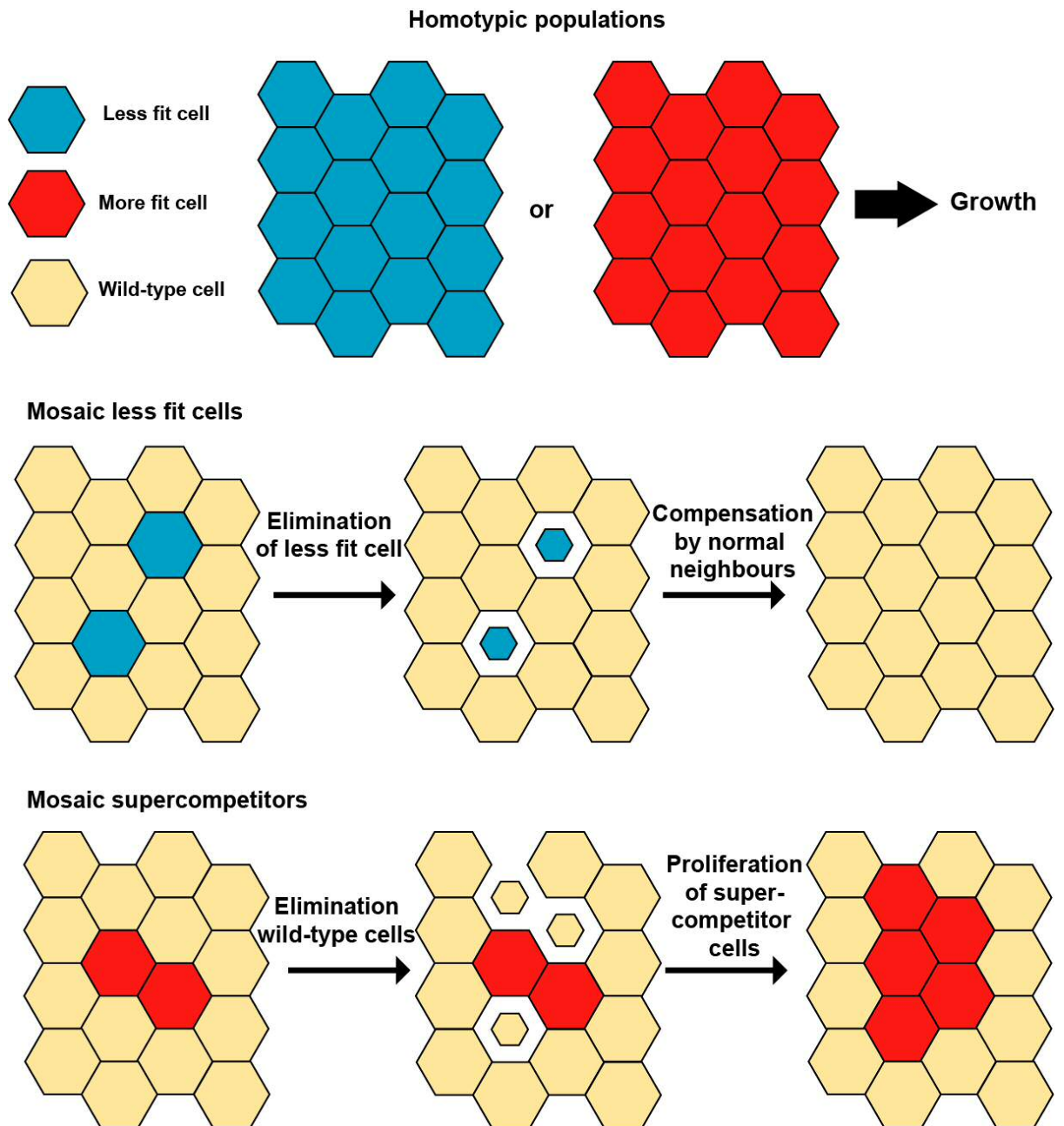
Figure 1.5: Types of cell competition. Cells that are viable in homotypic environments but are less fit (e.g. *Minute$^{+/-}$*) are eliminated via apoptosis when surrounded by fitter neighbours. In supercompetition, more fit cells (e.g. cMyc overexpressing cells) induce apoptosis in the surrounding less fit, wild-type neighbours.

1.4.1 Triggers of Cell competition.

A defining feature of cell competition is the elimination of aberrant cells only when confronted with more-fit cells. Three broad categories of changes to cells are known to trigger cell competition: those leading to metabolic changes, those causing sharp signalling differences and those disrupting apical-basal polarity (summarised in Table 1.1)

In many studies of cell competition, the two competing populations display different growth rates, for example, *Minute* lose clones grow slower than wild-type counterparts (Morata and Ripoll, 1975). However, it is now clear that differences in growth rate alone are not sufficient to induce loser cell elimination by cell competition. Overexpression of cell-cycle regulators such as *cyclin-D* and *cyclin-dependent kinase 4 (Cdk4),* are not sufficient for cells to acquire a winner status and eliminate slower-growing wild-type cells (De La Cova et al., 2004). Conversely, decreasing proliferation of cells in a mosaic fashion via insulin signalling also does not induce cell competition in the slower growing cells (Böhni et al., 1999; Verdu et al., 1999). Furthermore, cell competition can be induced in post-mitotic cells in *Drosophila* follicular epithelium leading to apoptosis of losers and hypertrophy of winners (Tamori and Deng, 2013).

A number of mutations that alter proliferation and cause cell competition alter protein synthesis. The *Minute* and *Bst* mutations disrupt ribosomal proteins and MYC is known to regulate protein synthesis so alterations to this process may be the underlying trigger (Dang, 2012; Eilers and Eisenman, 2008; Meyer and Penn, 2008). In addition to this, metabolic pathways that impact cell proliferation may trigger cell competition. For example, MYC can activate glycolysis and regulate metabolism during cell competition (De La Cova et al., 2014). Difference in energy metabolism have also been shown to be required for elimination of slow-growing cells in immortalised cell models (Penzo-Méndez et al., 2015). Therefore, proliferation may only be a readout of the different properties of winner and loser cells.

1.4.1.1 Signalling Pathways that trigger Cell Competition

The second set of mutations that induce cell competition affect signalling pathways. Sharp differences in bone morphogenetic protein (BMP)/Dpp (Moreno et al., 2002; Sancho et al., 2013), Wnt/Wg (Vincent et al., 2011), JAK-STAT (Rodrigues et al., 2012), Hippo signalling (Mamada et al., 2015; Tyler et al., 2007), Notch signalling (Alcolea and Jones, 2015) and p53 mutations (Watanabe et al., 2018) have all been shown to induce cell competition and are summarised in Table 1.1.

The first signalling pathway found to regulate cell competition was the BMP/Dpp pathway. *Minute*$^{+/-}$ mutant clones in *Drosophila* have lower levels of Dpp signalling which causes apoptosis (Moreno et al., 2002). In mammals, pluripotent cells with decreased BMP signalling are also eliminated via an apoptosis-dependent mechanism (Sancho et al., 2013).

Differences in both WNT/Wg and JAK-STAT signalling between cells can also induce cell competition. Work in *Drosophila* models has demonstrated that cells with low WNT/Wg signalling levels are eliminated when surrounded by normal neighbours. Conversely, cells with higher levels of Wnt/Wg signalling via *Axin* or *APC* mutations, behave as supercompetitors and eliminate surrounding wild-type cells (Suijkerbuijk et al., 2016; Vincent et al., 2011). Similarly, in JAK-STAT signalling, wild-type cells eliminate JAK-STAT signalling deficient cells with sustained activation of this pathway producing supercompetitors (Rodrigues et al., 2012).

Another pathway that can induce cell competition is the Salvador-Warts-Hippo signalling pathway. In mouse cell cultures, activation of the Hippo signalling pathway in fibroblasts leads to elimination by normal neighbours (Mamada et al., 2015). Furthermore, inhibition of the Hippo pathway by *Yorkie* or *Tead4* overexpression leads to cells becoming supercompetitors and elimination of wild-type cells (Mamada et al., 2015; Neto-Silva et al., 2010; Tyler et al., 2007; Ziosi et al., 2010).

Sharp signalling differences can also alter differentiation balance within an epithelium (Alcolea and Jones, 2015). Inactivation of Notch in single murine oesophageal epithelial progenitor cells results in these cells producing more progenitor daughters (Alcolea et al., 2014). Moreover, mutant cells promote the

differentiation of neighbouring wild type cells and hence the elimination of normal cells from the tissue.

Finally, it has recently been demonstrated that in MDCK cells and intestinal organoids expressing mosaic expression of mutant p53 results in elimination of transformed cells (Watanabe et al., 2018). Although p53 is generally considered a sensing mechanism for cell competition, with this role discussed later, cells expressing mutant $p53^{R273H}$ undergo necroptosis when surrounded by normal epithelial cells.

1.4.1.2 Polarity genes and Disruption of Epithelial Integrity in Cell Competition

Mutation of several different proteins involved in maintenance of apical-basal polarity are also known to induce cell competition. In *Drosophila*, mutation to *Scribble, Lethal giant larvae (Lgl),* or *Discs Large (Dlg)* in all cells leads to neoplastic overgrowth and tumours. However, mutation of these genes in a mosaic fashion in *Drosophila* or MDCK cells *in vitro* leads to apoptosis of mutant cells by normal neighbours (Agrawal et al., 1995; Brumby and Richardson, 2003; Chen et al., 2012; Igaki et al., 2006; Norman et al., 2012; Tamori et al., 2010; Woods and Bryant, 1991). This suggests that cell competition does not just function to remove aberrant cells but also removes oncogenic cells. Indeed, overexpression of *dMyc* in *Lgl* mutant clones promotes retention of transformed cells and promotes neoplastic outgrowth (Froldi et al., 2010; Menendez et al., 2010). Further indication that cell competition measures relative fitness, not absolute fitness levels, is that polarity deficient cells are not eliminated when surrounded by *Minute*$^{+/-}$ mutant cells (Froldi et al., 2010)

Factor/Pathway	Role in Cell Competition	Difference	Reference
Minute	Heterozygous mutants are eliminated	Growth	(Morata and Ripoli, 1975)
Myc	High expressing cells are supercompetitors	Growth	(Claveria et al., 2013; de la Cova et al., 2004)
BMPs	Low levels associated with loser status	Signalling	(Moreno et al., 2002; Sancho et al., 2013,)
Hippo	Activation associated with loser cells whilst nuclear YAP associated with supercompetitor status	Signalling	(Neto-Silva et al., 2010; Ziosi et al., 2010)
JAK/STAT	Low levels associated with loser status and high levels with supercompetitors	Signalling	(Rodrigues et al., 2012)
Notch	Notch mutant cells promote differentiation and loss of wild type neighbours	Signalling	(Watanabe et al., 2018)
p53	p53 mutant cells undergo necroptosis and are basally extruded	Signalling	(Alcolea et al., 2014)
Wingleess (Wg)	Low levels associated with loser status and high levels with supercompetitors	Signalling	(Vincent et al., 2011)
Scribble	Scribble mutant cells are eliminated by normal neighbours	Polarity	(Brumby and Richardson, 2003; Igaki et al., 2006; Norman et al., 2012)
Discs large (Dlg)	Dlg mutant cells are eliminated by normal neighbours	Polarity	(Igaki et al., 2006)
Lethal giant larvae (Lgl)	Lgl mutant cells are eliminated by normal neighbours	Polarity	(Agrawal et al., 1995; Tamori et al., 2010)

Table 1.1: Summary of cell competition triggering signals

1.4.2 Mechanisms of Sensing Cell Competition.

A core concept of cell competition is how cells sense the relative fitness levels of surrounding neighbours. Three main theories have been put forward to explain the context-dependent elimination of less-fit cells: 1) competition for growth factors/ nutrients, 2) direct cell fitness comparison and 3) mechanical sensing.

1.4.2.1 Competition for ligands

An initial model to describe cell competition is that cells compete for a limiting factor necessary for survival. For example, neurons competing for a

limited pool of extracellular nutrients or growth factors required for viability (Raff, 1992). This is supported by the fact that damage to growth or survival factor pathways leads to cell competition (Moreno et al., 2002; Senoo-Matsuda and Johnston, 2007). However, more recent studies suggest this model is too simplistic and does not occur in most competitive situations. Mouse pluripotent cells with defective BMP signalling are removed when surrounded by normal neighbours, however excess of BMP ligands cannot prevent this process (Sancho et al., 2013). If BMP were a limiting factor then the level of competition could be modulated by BMP levels, however, varying BMPs in co-culture systems does not alter cell competition intensity (Sancho et al., 2013). Furthermore, different types of cell competition take place in mammalian culture conditions in which growth factors are provided in excess (Hogan et al., 2009; Mamada et al., 2015; Norman et al., 2012; Tamori et al., 2010). Therefore, it is likely other pathways are more relevant in competitive interactions.

1.4.2.2 Direct-Sensing of Fitness

Another proposed model of cell competition is that fitness levels are communicated directly between cells. In this mechanism, the molecules exposed on the surface of cells reports the fitness status of a cell. Evidence for this mechanism arose with the discovery of *Flower* genes which encode a transmembrane calcium channel ubiquitously expressed in *Drosophila* (Rhiner et al., 2010)*.* It has been demonstrated that less fit cells upregulate specific Flower isoforms that promote apoptosis, only when surrounded by cells expressing the ubiquitous Flower isoform. The isoforms associated with decreased fitness, termed Flower-lose isoforms, have been detected in *Drosophila* cell competition models induced by *Minute*, *Myc* and *Scribble* (Rhiner et al., 2010). Moreover, the expression of Flower-lose isoforms is sufficient to induce cell competition when surrounded by cells expressing the ubiquitous isoform (Levayer et al., 2015; Rhiner et al., 2010). Although it is not yet clear how differences in *Flower* isoform expression are established and the relevance to mammals.

A mechanism for the recognition of less-fit cells has recently been proposed that is similar to the detection of pathogens. The innate immune system can recognise both non-self, such as microbial infection, and altered-self, such

as cancer cells. Therefore, this could provide a potential mechanism to distinguish fitness levels between cells. In support of this, during cell competition the Toll and Immune Deficiency signalling pathways are rewired to drive loser cell elimination. For example, in *dMyc* overexpressing or *Minute*^{+/-} mutant cells, the elimination of loser cells requires Toll-related receptors (TRRs)(Meyer et al., 2014). However, it is not precisely understood how different fitness levels in cells results in TRR activation. Therefore, although differences in signalling proteins presented by less-fit loser cells appear to be important for establishing winners and losers, how decreased fitness leads to alterations in these surface markers is unclear.

1.4.2.3 Mechanical Cell Competition

A final model of sensing fitness has been proposed based on mechanical stress. This was first proposed based on mathematical modelling of populations of cells with non-uniform proliferation rates (Shraiman, 2005). Faster-growing cells will compress the slower-growing surrounding cells and once the level of mechanical stress is sufficient it will drive apoptosis, relieving the overall tissue pressure. Evidence for this model comes from developing *Drosophila* tissue where cell crowding leads to delamination or forcing out of cells (Marinari et al., 2012).

More recently, p53 levels have been identified as important in mechanical cell competition. It was found that *Scribble* knockdown Madin-Darby Canine Kidney (MDCK) cells *in vitro* have a basal level of p53 activation which makes them hypersensitive to mechanical stress (Wagstaff et al., 2016). When these mutant cells were surrounded by normal neighbours they become compacted and eliminated. Upon compression by normal neighbours, *Scribble* knockdown cells activate ROCK and p38 which further increased p53 and led to apoptosis. Indeed, p53 appears to be a general mechanism for fitness sensing, separate to it's classical DNA-damage response. Cells with stress-induced p53 activity are outcompeted by fitter cells in the mouse haematopoeitc system (Bondar and Medzhitov, 2010). Moreover, elevated p53 expression labels defective cells for competitive elimination in murine development (Bowling et al., 2018).

Tension generated at the interface between winner and loser cells can also control mechanical competition. Interface contractility is generated between wild-type cells and cells expressing transcription factors for different fates (Bielmeier et al., 2016). Actomyosin accumulates at the boundary between normal and aberrantly-specific cells with contractility in single aberrant cells causing apoptosis. However, in larger clusters of mis-specified cells the contractile forces induced cyst formation.

Furthermore, in *dMyc*-induced cell competition in *Drosophila* the probability of elimination of wild-type cells correlates with surface area in contact with mutant cells (Levayer et al., 2015). With tension differences between mutant and normal cells promoting intercalation, normal cell elimination and the subsequent invasion of tissue by oncogenic cells.

1.4.3 Cell competition in Cancer

Newly arisen, pre-cancerous cells are produced in normal epithelial sheets and must overcome the barriers that act to maintain homeostasis in order to form a tumour. It therefore follows that the interaction of normal and mutant cells can lead to cell competition.

A number of observations support a tumour-suppressive role for cell competition. For example, polarity or *Rab5* knockdown cells produce neoplastic lesions in mutant animals but are eliminated by surrounding wild-type cells via cell competition (Agrawal et al., 1995; Ballesteros-Arias et al., 2014; Brumby and Richardson, 2003; Chen et al., 2012; Gateff, 1978; Igaki et al., 2006; Norman et al., 2012; Tamori et al., 2010). Furthermore, in the mouse thymus, bone-marrow-derived progenitors consistently replace T-lymphocyte precursors. A cell-competition-type mechanism is thought to drive the elimination of older bone marrow progenitors by younger cells due to a decreasing responsiveness to interleukin-7 over time (Martins et al., 2014). If this cell competition is inhibited and older cells are no longer replaced then T cell acute lymphoblastic leukaemia arises.

In addition to the tumour-suppressive role of cell competition, a number of studies have also demonstrated a tumour-promoting role at multiple stages of

tumourigenesis. The overexpression of *dMyc* provided the first evidence of cell competition promoting tumourigenesis. With *dMyc* overexpression sufficient to transform mutant cells into supercompetitors and eliminate surrounding wild-type cells (De la Cova et al., 2004). The oncogenic role of MYC is well characterised and this supercompetitor role led to the suggestion that elimination of neighbours allows expansion of early-stage tumours (Moreno, 2008). However, the elimination of wild-type cells by *dMyc* overexpressing winner cells does not give rise to tumours and is phenotypically silent in both mice and *Drosophila* (Clavería et al., 2013; De La Cova et al., 2004; Moreno and Basler, 2004). This led to the suggestion that cell competition is limited to aiding the expansion of pre-cancerous lesions that require a second oncogenic hit for tumour formation. The replacement of normal cells by a cancer-primed cell population that is morphologically normal is termed field cancerisation (Braakhuis et al., 2003; Slaghter et al., 1953). It has been demonstrated that competitive interactions can drive clonal expansion of a mutant cell population (Alcolea et al., 2014). Inactivation of Notch in single oesophageal epithelial progenitor cells promotes the differentiation and hence loss from the tissue of neighbouring wild type cells. Moreover, mutant cell division produces more progenitor cells and less differentiating cells leading to clonal expansion and a field change (Alcolea et al., 2014).

However, several studies in *Drosophila* have demonstrated that elimination of wild-type cells by mutant cells can also promote tumour progression. In the *Drosophila* intestine *APC* $^{-/-}$ mutant cells kill surrounding normal cells and form adenomas (Suijkerbuijk et al., 2016). Importantly, preventing cell competition, by inhibition of apoptosis, restores tissue homeostasis and contains adenoma expansion. This demonstrates a requirement for cell competition to drive expansion of mutant cells. Furthermore, in the *Drosophila* wing disc, once clusters of less-fit cells reach a certain size cell competition also promotes tumourigenesis. Wild-type cells eliminate *Rab5* knockdown cells, however, once clusters reach about 400 cells in size the apoptosis in mutant cells at the boundary of normal:mutant cells is not sufficient to remove the cluster. The mutant cells further away from wild-type cells survive and proliferate. Moreover, the apoptosis of mutant cells at the boundary promotes tumour growth of cells further from the border (Ballesteros-Arias et al., 2014).

Together, this suggests cell competition can act as both a tumour-suppressive and tumour-promoting mechanism depending on context and stage of tumour formation.

1.4.4 Ras and Cell Competition

The three *Ras* genes are the most commonly mutated oncogenes in cancer with mutations found in around 16% of all human tumours (Prior et al., 2012). It has also been found to be involved in cell competition. Cells deficient in Ras/Raf/MAPK signalling can be outcompeted by wild-type neighbours (Prober and Edgar, 2000). However, expression of constitutively active Ras turns cells into supercompetitors with apoptosis in surrounding wild-type cells (Karim and Rubin, 1998).

Use of mammalian MDCK cells has demonstrated a role for cell competition between mammalian cells expressing *Ras^{V12}*, referred to as Ras^{V12} cells, and normal neighbours *in vitro*. When Ras^{V12} cells are surrounded by normal neighbours, the transformed cells undergo two independent phenomenon in a non-cell autonomous manner. Mutant cells are either apically extruded from the monolayer, or form dynamic basal protrusions and invade the basal matrix (Hogan et al., 2009). When Ras^{V12} cells are plated alone no cell extrusion or basal invasion occurs. Basal invasion occurs in mutant cells that avoid extrusion at protracted time points. Cdc42 and ROCK activity are required in Ras^{V12} cells and E-cadherin-based cell-cell adhesions in normal cells were required for efficient extrusion. It was also found that extrusion is independent of apoptosis suggesting a different mechanism to the homeostatic elimination of apoptotic cells that occurs via sphingosine-1-phsophate (S1P) (Gu et al., 2011). It has since been demonstrated that Src-transformed, ErbB2-transformed cells, and cells expressing constitutively active YAP are also apically extruded *in vitro* (Chiba et al., 2016; Kajita et al., 2010; Leung and Brugge, 2012; Wu et al., 2015).

Recent work has begun understanding the molecular mechanisms of how normal and Ras^{V12}-transformed cells interact and changes that occur at the interface (Figure 1.6). In normal cells neighbouring Ras-transformed cells, the cytoskeletal protein filamin accumulates (Kajita et al., 2014). Filamin recruits vimentin at the basal side of cell-cell contact sites to generate contractile force

thought to squeeze transformed cells out apically. This suggests normal epithelial cells sense that neighbouring cells are aberrant and actively eliminate them from the epithelium.

In the Ras^{V12}-transformed cells surrounded by normal cells a variety of molecular changes have also been characterised. When Ras-transformed cells surrounded by normal neighbours, the actin-binding protein Epithelial Protein Lost In Neoplasm (EPLIN) is accumulated (Ohoka et al., 2015). EPLIN does not accumulate in Ras^{V12} cells cultured alone. In co-cultures, EPLIN activates protein kinase A (PKA), myosin-II and induces enrichment of caveolae-containing microdomains. This facilitates apical extrusion of mutant cells surrounded by normal neighbours. In Ras^{V12} cells surrounded by normal neighbours, Rab5 also accumulates and endocytosis is enhanced (Saitoh et al., 2017). This disrupts E-cadherin-based cell-cell adhesions and promotes mutant cell extrusion.

Physical forces are also important for the extrusion of Ras^{V12}-cells surrounded by normal cells and therefore this could be considered a form of mechanical cell competition. The activity of myosin-II is increased in Ras^{V12} cells and transformed cells become round and tall with the enhanced tensile force (Hogan et al., 2009; Kajita et al., 2014). Filamin in the normal cells can crosslink actin and act as a mechanotransducer/sensor (Ehrlicher et al., 2011). Redistribution of N-WASP is also observed during apical extrusion of Ras-transformed cells (Wu et al., 2014). At the interface between normal and Ras^{V12} cells N-WASP is reduced at the apical junctions and increased at the lateral membrane; increasing lateral tension and promoting extrusion.

More recently, apical cell extrusion has been investigated *in vivo* using murine models. Expression of Ras^{V12} in a mosaic fashion in the crypt epithelia in combination with *in vivo* time lapse imaging observed dynamic apical extrusion of mutant cells (Kon et al., 2017). In this study, organoid models of the intestinal epithelium were also generated and recapitulated apical extrusion. In organoids EPLIN accumulates in Ras^{V12} cells surrounded by normal neighbours with pyruvate dehydrogenase kinase 4 (PDK4) – mediated metabolic changes in mutant cells also promoting the extrusion of Ras^{V12} cells (Kon et al., 2017). Evidence for the extrusion of Ras^{V12}-transformed cells has also been observed from the pancreatic ductal and lung epithelium using CK19-driven Cre recombinase (Sasaki et al., 2018). However, <1% of pancreatic cancer patients

have Hras mutations (Hobbs et al., 2016; Prior et al., 2012) and the cell of origin in pancreatic cancer is still unclear (Yamaguchi et al., 2017), so further work is required to establish the role of cell competition in pancreatic cancer.

It is also unclear as to whether extrusion of Ras^{V12} mutant cells is tumour-suppressive or tumour-promoting. Apical extrusion of epithelial cells in the body will typically result in mutant cells in a lumen, for example the intestinal lumen. This will not only remove the cells from the supporting extracellular matrix, promoting programmed cell death via anoikis (Frisch and Francis, 1994), but will also subject the extruded cell to harsh physical conditions (e.g., stool, urine, digestive fluids). Thus, apical extrusion may be considered as cancer-preventative. However, extrusion can also allow sporadic mutant cells to escape the suppressive epithelium and proliferate (Leung and Brugge, 2012), or colonise other sites within the pancreas (Makohon-Moore et al., 2018). With *Kras^{V12}* associated with anoikis resistance (Zhang et al., 2017), it is conceivable that extrusion allows Ras-transformed cells to evade the suppressive microenvironment and proliferate outside the native niche. The interaction of Ras-transformed and Ras-wild type cells may also be maintained at later stages of tumourigenesis. As spatial analysis of *Kras^{G12D}* mutant cells using RNA in situ hybridisation has demonstrated that mutant cells intimately mix with *Kras* wild-type cells even within tumours (Baker et al., 2017), these interactions may be relevant to multiple stages of tumourigenesis.

1.4.4.1 Extrusion in homeostasis

Although extrusion of oncogenic cells can occur from epithelial sheets extrusion is also cellular process that occurs within non-transformed epithelial to maintain homeostasis. To maintain homeostasis as a tight barrier an epithelium requires a fine balance of growth and apoptosis which occurs via several mechanisms. One classical mechanism for this is contact inhibition; with high cell density inhibiting cell proliferation (Eagle and Levine, 1967; Stoker and Rubin, 1967). Another homeostatic mechanism is the elimination of apoptotic cells. In this process, apoptotic cells are identified by neighbouring cells and pushed out of the epithelium by actomyosin-mediated contractile forces (Gu et al., 2011;

Rosenblatt et al., 2001). It has also been demonstrated that overcrowding induces extrusion of live cells (Eisenhoffer et al., 2012; Marinari et al., 2012).

To remove dying cells from an epithelium extrusion occurs via a distinct extrusion mechanism. Sphingosine 1 phosphate (S1P) from apoptotic MDCK cells interacts with the G-protein-coupled receptor Sphingosine 1 Phosphate receptor 2 (S1P$_2$) which activates Rho mediated contraction (Gu et al., 2011). This leads to the formation of a basal actomyosin ring at the base of surrounding cells to squeeze the cell out and draw together neighbouring cells to prevent gaps in the epithelial barrier. Overcrowding has also been shown to lead to extrusion via S1P and myosin contraction, however extrusion from overcrowding also requires the stretch-activated channel Piezo1 (Eisenhoffer et al., 2012). Other work investigating crowding-induced extrusion of live cells in *Drosophila* found that cells progressively lose junctions with the surrounding cells (Marinari et al., 2012). This is followed by loss of apical area, recruitment of a contractile myosin II ring in neighbouring cells and extrusion. Modulating cell growth and density altered extrusion, suggesting overcrowding induced mechanical forces triggers extrusion in crowded regions.

Recently, computer simulations of the epithelium have found similarities between molecules in liquid crystals, with cells forming a dense and polarised monolayer (Kawaguchi et al., 2017; Saw et al., 2017). Epithelia cells can spontaneously orientate and align towards singular points, known as topological defects. The head of these coordinated flow of cells generates compressive stress that promotes extrusion. Although blocking crowding induced extrusion can cause atypical cellular accumulation in zebrafish (Gu et al., 2015), the organism-wide consequences of inhibiting this extrusion appear relatively mild.

Cell extrusion can also determine the fate of a cell in development. For example, in lung development random cell subpopulations of bronchial epithelia are extruded and undergo epithelial-to-mesenchymal transition (EMT)-like migration before colonising lung branch points as committed neuroendocrine progenitors (Kuo and Krasnow, 2015). Furthermore, extrusion of embryonic neural crest cells (NCCs) from the dorsal neural epithelia is key in development of craniofacial structures (Le Douarin and Kalcheim, 1999). Extruded cells undergo EMT and migrate to multiple destinations to differentiate into neurons and glia of the peripheral nervous system (Berndt et al., 2008; Thiery et al., 2009).

Thus, cell extrusion also allows the initiation of migration and subsequent differentiation during development. In addition to the active elimination of aberrant cells extrusion occurs in epithelial tissues to control tissue dynamics and aid the movement of cells in development.

Ras-transformed cell extrusion
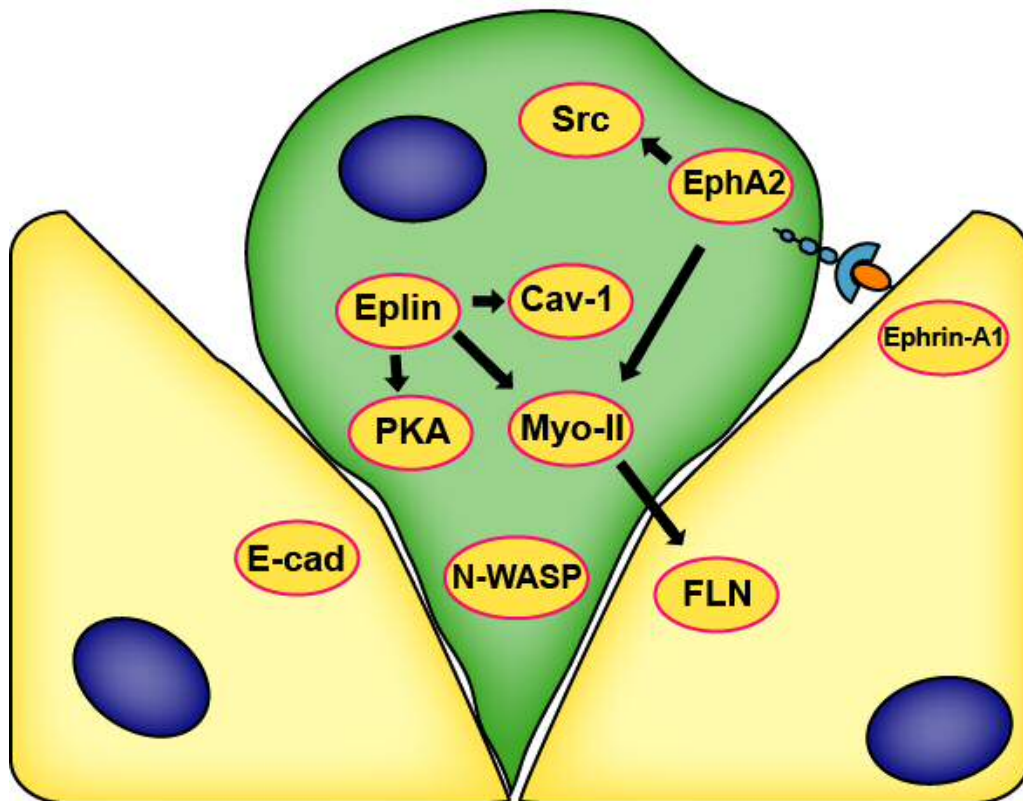
Figure 1.6: Mechanism of extrusion of Ras^{V12} cells. In Ras-transformed cells (green) and the surrounding normal neighbours (yellow) various signalling pathways are modulated leading to extrusion of mutant cells.

1.4.7 EphA2-dependent elimination of Ras^{V12} cells.

Although the trigger for extrusion of non-transformed cells in apoptosis and overcrowding has been elucidated, how oncogene-transformed cells are detected and eliminated is less clear. To investigate the signals underlying detection of Ras^{V12} cell extrusion we have previously used a cell confrontation assay to amplify the boundary between Ras-transformed and normal MDCK epithelial cells *in vitro* (Porazinski et al., 2016). EphA2 is elevated in Ras^{V12} cells at the mRNA and protein level (Macrae et al., 2005) and allows detection of mutant cells by the surrounding normal epithelia. The interaction of normal and Ras^{V12} cells then induces ephrin-A-EphA2 signals which drives repulsion and is accompanied by EphA2 dependent increased contractility of mutant cells. *Drosophila* Eph receptor (dEph) was also detected in segregating clones of Ras^{V12} cells and is functionally required for segregation of Ras^{V12} cells from wild-type cells in *Drosophila* wing imaginal discs. Therefore, Ras-transformed cells arising in normal epithelial sheets generates ectopic EphA2 boundaries causing segregation and extrusion of mutant cells. Furthermore, we have demonstrated that normal epithelial cells can trigger EphA2-dependent Ras^{V12} repulsion at the level of the single cell (Hill and Hogan, 2017). Dropping low numbers of normal cells onto confluent monolayers of Ras^{V12}-transformed cells demonstrated that even small clusters of normal cells can drive repulsion and enhanced contractility of Ras-transformed cells. Expression of a dominant-negative EphA2, which lacks a functional intracellular domain, was also sufficient to inhibit Src-transformed cell extrusion (Porazinski et al., 2016).

1.7 Eph-Ephrin Signalling

EphA2 is a member of the Eph receptor tyrosine kinase (RTK) family. Eph (from 'erythropoietin-producing hepatocellular carcinoma cell line') receptors were first identified in 1987 and are divided into two subfamilies (Hirai et al., 1987). The type A Eph receptors (EphA1-EphA2 and EphA10) bind and activate five type A ephrins (ephrin-A1-ephrinA5) and the type B Eph receptors (EphB1-EphB4 and EphB6), bind and activate three type B ephrins (ephrin-B1-B3). A

degree of promiscuity exists between and within subfamilies, for example, EphB2 can bind ephrin-A5 and EphA3 binds ephrin-A3, -A4 and –A5 (Noberini et al., 2012).

Both Eph receptors and ephrin ligands are membrane tethered, thus signalling occurs from direct cell-cell contact (Davis et al., 1994). Forward Eph-ephrin signalling in the receptor expressing cell consists of Eph-receptor interaction with ephrin ligand on a neighbouring cell and leads to activation of the Eph receptor kinase domain and often leads to cell repulsion (Figure 1.7). Following ligand interaction, Eph receptors cluster together and become phosphorylated at key tyrosine residues (Kania and Klein, 2016). However, it has also been established that reverse signalling can occur through ephrin ligands and this can elicit either cell repulsion or adhesion (Cowan and Henkemeyer, 2001; Jørgensen et al., 2009; Palmer et al., 2002; Xu and Henkemeyer, 2009). This generates a large amount of signalling complexity which is further complicated by how both Eph receptors and ephrins cluster, impacting signalling. Both Ephs and ephrins need to be clustered to trigger efficient activation (Davis et al., 1994), with activation driving receptor and ligand tetramers to form, producing large signalling arrays. The size of an array correlates with the degree of cellular response (Smith et al., 2004). Another layer of complexity in signalling is generated by the finding that Eph receptors can interact *in cis* with ephrins on the same cell membrane (Hornberger et al., 1999; Yin et al., 2004). This has been demonstrated to inhibit forward signalling through the Eph receptor (Yin et al., 2004). Also, Eph receptors can signal in a ligand-independent manner when overexpressed, such as in tumourigenic cells. For example, EphA2 can be activated by growth factors in serum via AKT phosphorylation of EphA2 serine 897, leading to increased cell migration and invasion (Miao et al., 2009). Recently, it has also been identified that extracellular vesicles (exosomes) can contain Eph receptors and can lead to Eph-ephrin signalling without direct cell contact (Gong et al., 2016).
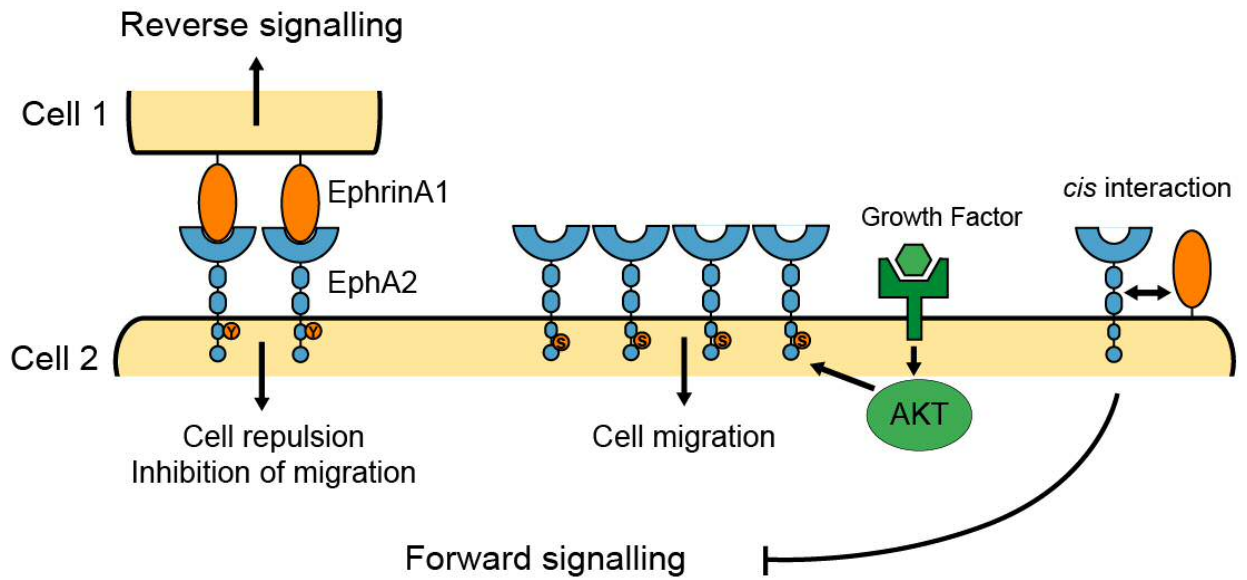
Figure 1.7: Principles of Eph signalling. Interaction of membrane bound Eph receptor and ligand can lead to signalling in both cells. Eph receptors can also be activated independently of ligand. The interaction of receptor and ligand, *in cis,* on the same membrane can inhibit classical downstream signalling.

1.7.2 Functions of Eph-Ephrin Signalling

Due to the complexity of Eph-ephrin signalling, the intracellular signalling pathways downstream of individual Ephs are yet to be fully elucidated. What is known is that Eph-ephrin signalling plays a key role in tissue organisation both in development and adult homeostasis and can regulate adhesion, repulsion and influence cell migration.

In the developing embryo, Eph-ephrin interactions ensure correct migration and cellular positioning. The combination of repulsion and attraction generated by Eph-ephrin signalling allows delicate balance to control neuronal growth cone migration (Wang and Anderson, 1997). The formation of different compartments with sharp borders is essential for development in vertebrates (Bronner-Fraser, 1999; Langenberg and Brand, 2005) with Eph-ephrin signalling critical to this process (Cayuso et al., 2015). For example, in the brain Eph receptors and ephrin ligands are expressed in complementary patterns. Signalling leads to cellular repulsion to inhibit cell intermingling which is vital for correct brain development (Twigg et al., 2004). During early development, segregation from a homologous population of cells into distinct cell types is the basis for different tissue and organ formation. Somatogenesis has been used to model segregation and boundary formation and how this is associated with dynamic morphological changes such as mesenchymal-to-epithelial transitions. Eph-ephrin signalling has been found to underly the formation of this morphological boundary and cell epithelialisation in early development (Barrios et al., 2003; Watanabe et al., 2009). In the developing pancreas, defective Eph signalling causes disorganised epithelia with a loss of cell-cell contacts leading to branching defects (Villasenor et al., 2010).

Eph receptors also play key roles in tissue maintenance and cell sorting in adult tissues. In the small intestine Eph-ephrin signalling regulates correct cell compartmentalisation (Batlle et al., 2002). At the base of each crypt stem cells proliferate and differentiate to produce the distinct cell lineages required, with progenitors migrating up the villus passively. EphB receptors are Wnt signalling target genes and highly expressed at the base of the crypt whereas ephrin-B ligands are found in differentiated cells further up the villus. The repulsive force generated by EphB-ephrinB interactions restricts the mixing of differentiated and

proliferating cells. Another intestinal cell lineage, Paneth cells, retain elevated EphB levels after differentiation which inhibits travelling up the villus, with these cells held at the base of the crypt.

Eph-ephrin signalling can control sorting at both the level of cells and tissues due to the variety of effects they can have on cell adhesion, repulsion and migration. For example, forward signalling through EphA2 can lower integrin function to reduce cell migration and integrin-mediated adhesion (Miao et al., 2000). Conversely, EphB1-ephrinB1 signalling can increase adhesion via $\alpha 1\beta 5$ integrin activation (Huynh-Do et al., 1999). Indication that adhesion is dictated by the combination of Eph and ephrins expressed and present at the surface.

At the molecular level, to regulate repulsive and attractive forces upon cell-cell contact, Eph-ephrin signalling can modulate Rho family GTPases (Noren and Pasquale, 2004). The Rho GTPase family controls cell movement by regulating the formation of actin structures required for cell migration. With Eph-ephrin signalling known to both promote and inhibit the activation of three key members of this family: Rac1, Cdc42 and RhoA (Pasquale, 2010; Pasquale et al., 2008). To alter these small GTPases, Eph receptors and ephrins act via GTPase-activating proteins (GAPs) and guanine nucleotide exchange factors (GEFs). With regulation of GAPs and GEFs allowing both activation and inhibition of Rho GTPases by Eph receptors to control repulsion. For example, stimulation of neural cells with ephrinA5 leads to growth cone collapse via activation of Rho causing cell retraction (Wahl et al., 2000). Cell repulsion also requires the adhesive properties of Eph-ephrin binding are overcome, either by cleavage of ligand from the membrane (Hattori et al., 2000) or endocytosis (Marston et al., 2003; Zimmer et al., 2003). Although it is worth noting that control of Rho GTPases can regulate other functions. For example, EphA2 forward signalling can promote epithelial characteristics by inhibiting RhoA (Wakayama et al., 2011), and enhance endothelial angiogenic responses via Rac1 (Hunter et al., 2006). It has also been reported that upon Eph-ephrin interaction, cleavage and shedding of E-cadherin at the interface occurs establishing differential adhesion that contributes to cell segregation (Solanas et al., 2011).

In contrast to the function of other RTKs, Eph receptors do not generally regulate cell growth through the Ras pathway and frequently inhibit Ras

signalling. Stimulation of EphA receptors with ephrin-A1 has been demonstrated to inhibit the Ras/MAPK pathway and inhibit cell proliferation in prostatic epithelial cells and endothelial cells (Miao et al., 2001). Furthermore, EphA2 is a direct transcriptional target of the Ras/MAPK pathway with EphA2-ephrin-A1 forward signalling negatively regulating activation of Ras (Macrae et al., 2005). Therefore, EphA2 can be considered to act in a negative feedback loop with Ras/MAPK signalling in some contexts.

Eph-ephrin signalling has also been implicated in contact inhibition of locomotion (CIL). This is the process by which cells collide and stop migrating before repolarising and migrating in a different direction (Abercrombie and Heaysman, 1954). In prostate cancer cells, the balance between repulsive EphA and attractive EphB signalling was found to alter CIL (Astin et al., 2010). EphA2 and EphA4 act together to coordinate CIL, whereas EphB3 and EphB4 upregulation leads to inhibition of CIL and increased invasion.

1.7.3 EphA2 in cancer

With the variety of effects Eph-ephrin signalling can have on a cell, it is not surprising that changes to Eph receptors are implicated in tumourigenesis. EphA2 receptor is important for detection and extrusion of Ras-transformed cells and so will be primarily discussed. EphA2 is upregulated in an array of different cancers including: breast, glioblastoma, prostate, melanoma and ovarian with elevated levels associated with advanced disease and poor prognosis (Andres et al., 1994; D'Amico et al., 2001; Duxbury et al., 2004; Kataoka et al., 2004; Landen et al., 2006; Walker-Daniels et al., 1999; Zelinski et al., 2001). However, the mechanisms by which EphA2 signalling promotes tumourigenesis are complex and are not well characterised with evidence for both a tumour suppressive and tumour promoting role, suggesting context-dependent functions. When stimulated by ephrin ligands EphA2 appears to have a tumour suppressive function. Upon ligand binding, EphA2 becomes autophosphorylated at cytoplasmic tyrosine residues, and recruits p120Ras-GAP to downregulated Ras-GTP (Dail et al., 2006; Miao et al., 2001). Autophosphorylation of EphA2 also supressing activated Akt (Miao et al., 2009). Using a shRNA screen for tumour suppresses *in vivo* in a Kras^{G12D}-drive murine lung adenocarcinoma

model identified EphA2 as a key tumour suppressor (Yeddula et al., 2015). Loss of EphA2 was found to promote cell proliferation via activation of the Ras/MAPK and hedgehog pathway and drive tumourigenesis. But when overexpressed EphA2 can become activated in a ligand-independent manner and promoter tumourigenesis. For example, in the absence of ligand, tyrosine residues on the receptor are not phosphorylated allowing Akt signalling. Activated Akt can then phosphorylate EphA2 at cytoplasmic serine residues which promotes a migratory phenotype in part via Rho GTPases (Hiramoto-Yamaki et al., 2010; Miao et al., 2009). Moreover, expression of EphA2 alone in mammary MCF10A cells is sufficient to confer tumourigenicity in mice (Zelinski et al., 2001).

In addition to a role in tumour growth EphA2 has also been implicated in tumour metastasis. Overexpression of EphA2 is strongly associated with increased metastatic burden in colorectal cancer (Saito et al., 2004). However, in pancreatic ductal adenocarcinoma (PDAC) EphA2 levels is decreased in metastatic tumours compared to non-metastatic tumours (Mudali et al., 2006). This suggests EphA2 could promote a mesenchymal phenotype and so must be downregulated during mesenchymal-epithelial transition (MET). In PDAC, genetic disruption of EphA2 has also been shown to reduce invasion and metastasis *in vivo* (Gundry et al., 2017). We have also previously identified that EphA2 drives the extrusion of Ras-transformed cells using *in vitro* models of early disease (Porazinski et al., 2016). What effect this may have on tumour growth or spread is unclear and requires further investigation. Thus, Eph-ephrin signalling is a cell-cell contact dependent, multi-layered and complex signalling pathway that precisely controls organisation at both the cell and tissue level. It allows cells to sense their immediate surroundings and react appropriately, for example by repulsion of a neighbouring cell. Aberrant expression of EphA2 is implicated in cancer, particularly Ras-drive carcinomas, and can both promote and suppress tumourigenesis.

In summary, epithelial tissues have several mechanisms to maintain homeostasis with competitive interactions between normal and aberrant cells driving the elimination of single less fit cells surrounded by normal neighbours. These competitive interactions can also drive the extrusion of mutant cells with Ras-transformed cells eliminated via a process that requires EphA2. *Kras^{G12D}*

mutations drive the initiation of PDAC yet is unclear how pancreatic tissues homeostasis is restored following the emergence of mutant cells.

1.8 Aims and Objectives

Kras^{G12D} transformed cells initiate pancreatic cancer and these transformed cells emerge within normal epithelial sheets. We know from cell competition studies that the interaction of mutant cells with normal neighbours can have both negative and positive effects on the transformed cell. Furthermore, it has been demonstrated that EphA2 signalling drives the segregation and elimination of Ras-mutant cells. The principal aim of this study was to investigate whether these interactions occur at the earliest stages of pancreatic cancer; when Kras^{G12D} cells arise within a normal pancreatic epithelium and what effect this may have on the fate of transformed cells. Specifically, the objectives were:

Establish *in vivo* mouse models to investigate the fate of Kras^{G12D} cells surrounded by normal neighbours over time within the context of a tissue. The requirement of EphA2 for these interactions will also be assessed.

Second, an *in vitro* model of primary pancreatic cell culture will be developed to investigate heterotypic interactions between normal and transformed cells. This will allow further elucidation of Kras^{G12D} and normal cell interactions at the level of the single cell over time to decipher the underlying mechanism. Furthermore, the downstream signalling mechanisms underlying normal:mutant cell interactions and fate of transformed cells will be examined.

Chapter 2: Materials and Methods

2.1   Experimental Animals

2.1.1 Animal Husbandry

All experiments in this thesis were performed in murine models (*mus musculus*) or with tissues and cell cultures derived from mouse tissue. All animals were maintained on an outbred background and housed in a specified pathogen-free (SPF) facility in accordance with institutional animal care guidelines and UK Home Office regulations, under valid personal and project licenses. Animals were given access to Standard diet (Special Diet Service UK, expanded diet) and fresh water *ad libitum* and maintained on a 12:12 hour light-dark schedule.

Once mice had reached 6 weeks of age or older they were bred in trios of one male and two females or duos of one male and one female as required. At approximately 4 weeks of age, pups were weaned and separated based on sex. At point of weaning ear biopsies were also taken for identification and genotyping.

2.2 Genetic Mouse Models

To investigate mosaic Kras^{G12D} induction in the pancreas requires both temporal and spatial control of recombination (Figure 2.1). To this end a *Pdx1-CreERT* transgene was utilised to drive expression of a tamoxifen inducible form of Cre recombinase/oestrogen receptor fusion protein in the endocrine, exocrine and duct tissue of the pancreas. The expression of a mutant KRAS protein was achieved by employing a model whereby the *Kras2* locus was targeted with a cassette containing the oncogenic form of the KRAS2 protein with the glycine at position 12 substituted with an aspartic acid. A loxP flanked stop codon was included upstream of the sequence so mutant transcript was only expressed after Cre-mediated recombination. To mark cells where recombination had occurred an inverted sequence coding for tandem-dimer red fluorescent protein (tdRFP) was inserted in intron 1 of the Rosa26 locus (Luche et al., 2007). Inverted loxP sites are arranged around these sequences so that two cre-mediated events

were required for expression; both excision of the stop codon and inversion of the *tdRFP* sequence. To investigate the role of EphA2 a transgenic model was also used whereby EphA2 was disrupted. A vector was used to disrupt the EphA2 gene within the extracellular domain resulting in the gene to encode an expected non-function truncated protein (Brantley-Sieders, 2004). Previously, characterisation of N-terminal and C-terminal EphA2 expression demonstrated that neither the full length nor a truncated form of EphA2 is present in these mice and thus can be considered a EphA2 null mouse (Amato et al., 2016). A summary of the animal models and abbreviations used in this thesis is presented in Table 2.1.

Abbreviation	Genotype
KC	*Pdx1-Cre^{ERT}; Rosa26^{tdRFP}; LSL-Kras^{G12D}*
Control	*Pdx1-Cre^{ERT}; Rosa26^{tdRFP}*
KC-Eph	*Pdx1-Cre^{ERT}; Rosa26^{tdRFP}; LSL-Kras^{G12D}; EphA2*
RFP-Eph	*Pdx1-Cre^{ERT}; Rosa26^{tdRFP}; EphA2*

Table 2.1 Glossary of Animal models
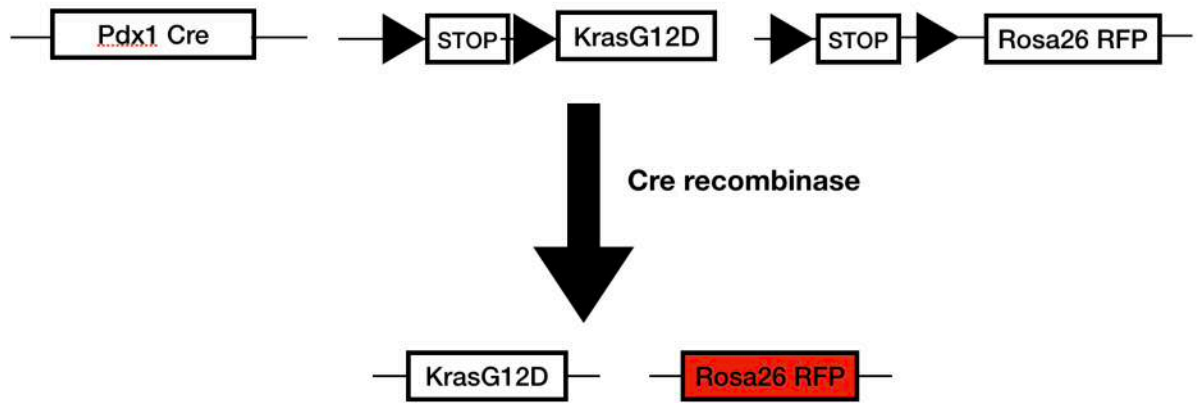
Figure 2.1: Genetic model of Kras^{G12D} expression in the pancreas. Cre recombinase activity in pancreatic cells results in excision of a stop codon and expression of *Kras^{G12D}* from the endogenous locus and RFP from the Rosa26 promoter.

2.3 Experimental Procedures

All experiments involving animals were conducted according to the UK Home Office regulations under valid personal and project licenses and in accordance with the Animal [Scientific Procedures] Act 1986. Experimental procedures were carried out in designated procedure rooms.

2.3.1 Identification of Experimental Cohorts

2.3.1.1 Ear Biopsy for identification and genotyping

For identification purposes ear biopsies were taken at weaning using a 2 mm ear punch (Harvard apparatus). DNA extraction from these biopsies was then used for genotyping. Biopsies were also taken from experimental cohorts at time of death to confirm genotype.

2.3.1.3   DNA extraction

Ear biopsies were collected and stored at -20°C until processing. Samples were then digested in 250 μL cell lysis buffer (VWR) containing 0.4 mg/mL proteinase K (Sigma) overnight at 42°C with agitation. The following day, samples were cooled to room temperature and 100 μL of protein precipitation solution (VWR) was added. The samples were then briefly mixed by inversion and insoluble debris and protein were pelleted by centrifugation at 16,000 G for 10 minutes at room temperature. The DNA was precipitated by adding the supernatant to 250 μL of isopropanol (ThermoFisher Scientific) in a DNase free eppendorf. The solution was mixed by inversion and DNA was pelleted by centrifugation at 16,000 G for 15 minutes. The supernatant was discarded and the pellet was washed with 70% ethanol. The DNA was pelleted by centrifugation at 16,000 G for 10 minutes and supernatant discarded. The pellet was air dried for 30 minutes at room temperature and resuspended in 250 μL of DNase/Rnase free water (Ambion). DNA was then stored at 4°C or at -20°C for long-term storage.

2.3.1.4 PCR Protocol

PCR was carried out in tube strips (0.2 mL thin walled, Alpha Laboratories). To each tube 3 µL of gDNA extracted from ear biopsies 47 µL of PCR mix (Table 2.2) was added. Primer sequences can be found in Table 2.3. The reaction was then run in a GS4 thermocycler (G storm) with the cycling times found in Table 2.2.

2.3.1.5 Gel electrophoresis of PCR products

Agarose gels were made by dissolving agarose (Bioline) 2% (w/v) in Tris-acetate-EDTA (TAE) buffer (National Diagnostic) and heating in a microwave at full power for 3 minutes and 10 seconds with agitation at regular intervals. After cooling slightly, 5 µL Safeview (NBS biologicals) was added per 100 mL. This was mixed gently to avoid bubbles and the gel was then cast into moulds with combs. Once set, the combs were removed and the gel placed into an electrophoresis tank and covered with 1x TAE. Following this 10 µL of each PCR sample was added to individual wells and run alongside a 100 bp ladder (PCR Biosystems). The samples were run at 120 V for approximately 30 minutes and then visualised using a GelDoc UV Transilluminator (Bio-Rad) and images taken with the GelDoc software (Bio-Rad). Genotypes were then established based on PCR product sizes in Table 2.3.

PCR Mix	*Pdx1-Cre*	*Kras*^{G12D}	*EphA2*^{tm1Jrui}	*Rosa26*^{tdRFP}
Template DNA	3 µL	3 µL	3 µL	3 µL
Distilled Water	21.8 µL	21.7 µL	21.7 µL	21.7 µL
2x Hot Start Taq Mix Red (PCR Biosystems)	25 µL	25 µL	25 µL	25 µL
Primer 1 (100 mM)	0.1 µL	0.1 µL	0.1 µL	0.1 µL
Primer 2 (100 mM)	0.1 µL	0.1 µL	0.1 µL	0.1 µL
Primer 3 (100 mM)	N/A	0.1 µL	0.1 µL	0.1 µL
PCR Cycling conditions				
Initial Denaturation	3 min; 94°C	3 min; 94°C	3 min; 94°C	3 min; 94°C
Cycle number	35	35	35	35
Step 1: Denaturation (Time; Temp)	30 sec;94 °C	30 sec;94 °C	30 sec;94 °C	30 sec;94 °C
Step 2: Annealing (Time; Temp)	30 sec; 55°C	30 sec;68 °C	30 sec; 60°C	30 sec; 56°C
Step 3: Extension (Time; Temp)	1min; 72°C	1min; 72°C	1min; 72°C	1min; 72°C
Final	5min; 72°C	5min; 72°C	5min; 72°C	5min; 72°C
	Hold at 4°C	Hold at 4°C	Hold at 4°C	Hold at 4°C

Table 2.2 Genotyping PCR reaction conditions

Gene	Forward primer (5' - 3')	Reverse primer (5' - 3')	Product Size
Pdx1-Cre	CTG GAC TAC ATC TTG AGT TGC	GGT GTA CGG TCA GTA AAT TTG	650 bp
Kras^{G12D}	WT Forward: TGT CTT TCC CCA GCA CAG T	CTG CAT AGT ACG CTA TAC CCT GT	WT = 250bp
	Mut Forward: GCA GGT CGA GGG ACC TAA TA		Mutant=100bp
EphA2^{tm1Jrui}	TGT CAC TTG CGA ACA GTG CT	WT: CGC TAT CAC ACT CAG CAG GA	WT=414 bp
		Mutant: GTG GAG AGG CTT TTT GCT TC	Mutant=280bp
Rosa26^{tdRFP}	AAG ACC GCG AAG AGT TTG TCC	Mutant: GTG GAG AGG CTT TTT GCT TC	WT = 209 bp
		WT: TAA GCC TGC CCA GAA GAC TCC	Mutant = 310 bp

Table 2.3 Primer sequences used for genotyping and product sizes. Kras^{G12D}, EphA2 and RFP genotyping also includes primer for wild-type (WT) and mutant alleles.

2.4   Experimental Cohorts induction

After PCR was used to identify the genotype of mice they were randomly placed into control and experimental cohorts at 42 – 56 days of age. Cre-recombinase translocation to the nucleus and hence recombination was induced by intraperitoneal injection (IP) of tamoxifen. Stocks of 10 mg/mL tamoxifen (Sigma) were generated by dissolving tamoxifen in corn oil (Sigma) overnight at 37°C with agitation. This was then diluted 1:1000 to produce 10 µg/mL of tamoxifen. Animals were then administered 100 µL of 10 µg/mL in a single injection to produce a 1 µg dose respectively. For high dose tamoxifen was dissolved in corn oil at 20 mg/mL and dissolved in the same manner as before. Mice were then injected with 9 mg/40 g of body weight every other day for 3 injections over 5 days.

2.5 Tissue sample preparation

To avoid degradation of RNA and protein, all tissues were dissected immediately after animal sacrifice.

2.5.1 Dissection of mice

Mice were culled following a schedule 1 approved method of culling (e.g. cervical dislocation) and dissected upon confirmation of death by permanent cessation of circulation. The abdomen was sprayed with 70% ethanol and a V-shaped incision from the genital area up to the diaphragm. The gut and colon can then be pulled outside the abdominal cavity, revealing the pancreas next to the spleen and stomach, allowing excision of the pancreas.

2.5.2 Fixation of tissue

Once removed the pancreas was cut transversely into 3 segments. The segment corresponding to the tail was placed in optimal cutting temperature (OCT) compound (Agar Scientific) and orientation recorded before being rapidly frozen in dry ice. Samples were stored at -80°C until processing for cryosectioning and RFP analysis. The middle section was fixed in ice cold 2% paraformaldehyde (ThermoFisher scientific) and then stored at 4°C for 24 hours before embedding for 3D immunofluorescence tomography. The final segment was fixed in ice cold 10% neutral buffered formalin (Sigma) for 24 hours at 4°C. Samples were then stored in 70% ethanol in distilled H_2O for 4°C until processing for immunohistochemistry.

2.6 Tissue Analysis

2.6.1 Sectioning of frozen tissue

Following tissue sample preparation pancreas frozen in OCT was cut on a Leica CM1860 UV cryostat. Each block of OCT was brought up to $-20^{\circ}C$ and then 10 μm sections were cut from the tail and placed on glass slides. Slides were then placed in 50 mL falcon (Sigma) and stored at -80°C until imaging. For RFP area and cluster analysis 5 sections were collected with each slice separated by at least 50 μm.

2.6.2 Tile-scan frozen tissue

After sections were generated they were imaged on a LSM 710 confocal microscope (Zeiss). Each slide was rapidly thawed before the whole tissue area was imaged using tile-scans for RFP and brightfield.

2.6.3 Laser Capture Microdissection (LCM)

Frozen tissue sections were also used for laser capture microdissection of RFP positive and RFP negative tissue. Each slide was rapidly thawed and regions of interest (ROI) were marked manually on a PALM Microbeam Laser Micro-dissector (Zeiss). ROI were then catapulted into the cap of a 0.2 mL Eppendorf containing 15 μL Buffer ATL (Qiagen) and stored at -80°C.

2.6.3.1 Genomic DNA isolation from Laser Capture Micro-dissected Tissue

Once all microdissected tissue samples had been collected gDNA was then extracted using a MinElute DNA purification kit (Qiagen) which provided all reagents unless stated. Firstly, 10 μL of proteinase K was added to the sample before pulse-vortexing for 15 seconds. Samples were then incubated at 56°C for 1 hour before adding 25 μL of Buffer ATL. To this 50 μl of Buffer AL and 50 μL of ethanol were added before thoroughly mixing and incubating at room temperature for 5 minutes. This was then passed through a QIAmp MinElute column by centrifuging at 6000 g for 1 minute. The column was then washed with 500 μL Buffer AW1 and then 500 μL of Buffer AW2 by centrifuging as before. The column was then dried by centrifuging at 20,000 g for 3 minutes before elution of the DNA using DNase/Rnase free water.

2.6.3.2 PCR for recombined Kras^{G12D} allele

To test for recombination at the Kras^{G12D} locus a PCR reaction was carried out that would differentiate between: the wild-type *Kras* allele, the *LSL-Kras^{G12D}* allele and the *Kras^{G12D}* allele where Cre recombinase has excised the stop codon. To 3 μL of DNA was added 47 μL of PCR as described in Table 2.1 with the following

3 primers: 5'GTC TTT CCC CAG CAC AGT GC 3', 5'CTC TTG CCT ACG CCA CCA GCT 3', 5' AGC TAG CCA CCA TGG CTT GAG TAA GTC TGC 3'. Cycling conditions were the same as EphA2 genotyping from Table 2.1 with a product size of 500 bp for the non-recombined Kras^{G12D} allele, 622 bp for the wild-type allele and 650 bp for the recombined Kras^{G12D} allele where Cre has excised the LoxP-Stop-LoxP cassette.

2.6.4 Immunohistochemistry (IHC)

5 μm formalin-fixed paraffin-embedded (FFPE) sections were produced by Derek Scarborough in the Histology Core Service, School of Biosciences, Cardiff University, before staining was carried out. IHC and quantification of staining was carried out by Dr Andreas Zaragkoulias, a Postdoctoral research associate within the lab. Sections were deparaffinised and rehydrated by passage through Xylene down a decreasing gradient of ethanol washes: 100%, 95% and 75% each for 5 minutes. Antigen retrieval was then carried out using citrate buffer (2.94 g Sodium citrate tribasic dehydrate (Sigma) in 1 L dH$_2$O, pH 6). Citrate buffer was heated in a pressure cooker for 5 minutes at 1000W before immersing slides and heating for a further 10 minutes before leaving the slides to cool at room temperature. Endogenous peroxidase was blocked by incubation in 3% hydrogen peroxide (Sigma) in distilled H$_2$O (dH$_2$O). Sections were then blocked in 5% normal goat serum (NGS) in tris-buffered saline (TBS) for 30 minutes at room temperature before incubation in primary antibody (anti-Ki67 1:100 (Abcam), anti-Cleaved Caspase 3 1:100 (Cell signalling)) overnight at 4°C in a humidity chamber. Slides were then washed for 3 x 5 minutes in TBS before incubation in secondary antibody. A biotinylated goat anti-rabbit (DAKO) secondary was used at 1:200 for 30 minutes at room temperature before washing in 3 x TBS for 5 minutes each again. A Vectastain ABC kit (Vector labs) was used for binding of HRP to the antibody complex and carried out according to manufacterer's protocol. Staining was visualised using 3,3'-diaminobenzidine tetrehydrochloride (DAB) (DAKO) before dehydration and mounting of slides. Whole tissue sections were imaged using a Zeiss Axioscan Z1 before counting of positive nuclei and measurement of tissue area was carried out in Zeiss blue software.

2.7 Primary cell isolation – Acinar epithelia

2.7.1 3D Acinar Culture

Mice were culled and pancreas removed as previously described (Section 2.5.1) and then rinsed in 1 x Hank's Balanced Salt Solution (HBSS, ThermoFisher scientific). The pancreas was then sliced into small 1 to 3 mm^3 pieces by mechanical dissociation using Noyes scissors and centrifuged at 450 g for 2 minutes at 4°C. The supernatant was aspirated and discarded to remove cell fragments and blood cells. Then 10 mL of collagenase IA solution (HBSS 1x containing 10 mM HEPES (ThermoFisher), 200 U/mL of collagenase IA (Sigma), and 0.25 mg/mL trypsin inhibitor (Sigma)) was added. This was incubated for 20-30 minutes at 37°C. During this time (every 5 minutes) mechanical dissociation by pipetting back-and-forth in pipettes of decreasing size (25, 10, and 5 mL serological pipettes). To stop the enzymatic reaction 10 mL of cold buffered washing solution (HBSS 1x containing 5% Foetal Bovine Serum (FBS) and 10 mM HEPES (ThermoFisher scientific)). This was then spun at 450 g for 2 minutes at 4°C and the supernatant removed and discarded. The pellet was then washed a further 3 times in 10 mL of buffered wash solution each time and centrifuged at 450 g for 3 minutes and 4°C to allow aspiration of the wash.

The cellular pellet was then resuspended in 7 mL of acinar culture media (Table 2.4). This mixture was then allowed to pass through a 100 μm filter to remove non-digested fragments but allow pancreatic acinar structures (10-15 cells) to pass through. This solution was then added dropwise to HBSS containing 30% FBS and acinar cells were pelleted (450 g, 2 minutes at 4°C). Acinar cells were then resuspended in 12 mL of acinar culture media. The acini were then left overnight to eliminate contaminant cells and cellular remnants that have adhered overnight.

After leaving in suspension overnight the acini were transferred and seeded on collagen matrix scaffolds. For this, 300 μL of type I Rat tail collagen solution (Corning, 2.31 mg/mL in 17mM NaOH) was used to coat the glass of 35 mm glass bottom well plates (MatTek). To each well, 300 μL of collagen was

added to cover the glass insert and then 200 μL removed to produce a thin coat. This was dried for around 1 hour at 37°C. The acini suspension was mixed at 1:1 ratio with 2.7 mg/mL type I Rat tail collagen with 17 mM NaOH and plated on top of collagen coating.

Reagent	Concentration	Supplier
Waymouth's media with 2.5% FBS		ThermoFisher scientific
Penicillin/Streptomycin	1x	ThermoFisher scientific
Serum Trypsin Inhibitor	250 ng/mL	Sigma
recombinant epidermal growth factor	25 ng/mL	ThermoFisher scientific
Dexamethasone	1 μg/mL	Sigma

Table 2.4 Acinar epithelial media composition

2.8 Primary cell isolation – Ductal epithelia

2.8.1 2D Ductal culture

Collagen plates were first prepared to culture primary pancreatic epithelia. The collagen mix was generated consisting of PBS (1x) with phenol red and NaOH (17 mM). Collagen was used at 2.31 mg/mL and diluted in filter sterilised water. Following this, 2 mL of collagen was plated in each well of a 6-well plate (Greiner) and incubated for at least one hour at 37°C.

Next, the cells were harvested and isolated. Mice were culled and the pancreas was then carefully removed as previously described (Section 2.5.1) and rinsed in G solution (HBSS (ThermoFisher scientific), 1x penicillin/streptomycin (P/S, ThermoFisher scientific), 1x Fungizone (ThermoFisher scientific) and 5 mM D-glucose (Sigma)). Mechanical cutting of the tissue was then carried out to produce fragments around 1 mm^2 and this was digested using 25 mL of 1 mg/mL collagenase at 37°C with stirring for 15 – 20 minutes. Once digested, 20 mL of G solution was used to transfer the digested

tissue through a 40 μm nylon strainer. Flow through was discarded and the strainer was washed to collect the remaining tissue. This tissue was then washed with G solution and spun down at 200 g for 3 minutes using half deceleration. The supernatant was discarded and the pellet was washed twice more using G solution. The cells were then digested using trypsin at room temperature for 5 minutes and this reaction was then stopped by adding soybean trypsin inhibitor (Sigma) to a final concentration of 0.6 mg/mL. Following this the cells were washed with DMEM six times to completely remove any trace of collagenase, spinning down at 200 g for 3 minutes with half deceleration after each wash to pellet cells. Finally, the pellet was resuspended in 12 mL PDEC media (Table 2.5) and plated onto 6-well plates. Cells were cultured at 37°C and 5 % CO_2 and passaged once they have reached high confluency.

Reagent	Concentration	Supplier
DMEM/F12 + 15 mM HEPES, 3.2 mg/mL glucose		ThermoFisher scientific
Nu-Serum IV culture supplement	5%	Collaborative biomedical products
Penicillin/Streptomyocin	1x	ThermoFisher scientific
D-Glucose	5 mg/mL	Sigma
Nicotinamide	1.22mg/mL	Sigma
Soybean Trypsin Inhibitor type I	0.1 mg/mL	Sigma
ITS+ Cell culture supplement	5 mL/L	BD Biosciences
Bovine pituitary extract	25 µg/mL	BD Biosciences
EGF	20 ng/mL	BD Biosciences
Dexamethasone	1 uM	Sigma
Cholera toxin	100 ng/mL	Sigma
3,3,5-tri-iodo-L-thyronine	5 nM	Sigma

Table 2.5: Ductal epithelia media composition

2.8.2 Passaging Pancreatic Ductal Epithelial Cells

Upon reaching or nearing confluency, cells were passaged by splitting at no more than 1:4 ratios. Firstly, new collagen coated plates were generated as previously described (Section 2.8.1). Following this the cell-collagen mix was removed from the well plates and incubated in 5 mg/mL collagenase V (Sigma) for 20 minutes at 37°C. The mix was then spun at 200 g for 3 minutes with half deceleration and supernatant discarded. The pellet was then digested in trypsin for 5 minutes at 37°C and digestion stopped by adding soybean trypsin inhibitor to a final concentration of 0.6 mg/mL. Next the suspension was washed using DMEM (Gibco) and pelleted by centrifugation at 200 g for 5 minutes with half deceleration. The pellet was washed a further 6 times washing in the same manner before resuspension in PDEC media and plating onto collagen coated plates. Pancreatic ductal epithelial cells were used after the first or second passage to ensure reproducible results

2.9 Tumour Derived Cell lines

2.9.1 Cell culture

Primary murine pancreatic tumour-derived epithelial cells lines KR, KP and KRE were a gift from Dr Jennifer P. Morton (Beatson Institute, Glasgow). All cells were maintained in DMEM including GlutaMAX and D-Glucose supplemented with 10% FBS (ThermoFisher). Cells were incubated at 37°C and 5% CO_2 in 10 cm cell culture plates (Greiner) with media changed every 2-3 days and passaged when confluent.

When cells became 80-90% confluent they were split at a ratio between 1:6-1:10. To remove cells, media was aspirated and cells washed with warm PBS (ThermoFisher) and then 1 mL of 0.25% trypsin/EDTA (Invitrogen) was added and incubated at 37°C for 5 minutes. Once cells had detached 5 mL of normal growth media was added to inactivate trypsin activity before splitting at appropriate ratios (KR 1:6, KP 1:10, KRE 1:10).

2.9.2 Long term Storage of cell lines

Low passage cell lines were frozen and cryo-stored in liquid nitrogen. Cells were detached from culture as described previously before resuspending in growth media containing 10% dimethyl sulfoxide (DMSO; Sigma) and aliquoted at >$1x10^6$ cells/mL in cryotubes (Nunc). Cells were then frozen at -80°C in a cryo-freezing vessel containing isopropanol (ThermoFisher) for 24 hours before transferring to liquid nitrogen.

To raise cells from long term storage, cells were rapidly defrosted in a water bath at 37°C for 2 minutes. Cells were then plated in complete growth media and once attached to the surface (~1 hour) media was changed to remove any trace of DMSO.

2.9 Cell Interaction experiments

2.9.1 Cell-cell mixing

To investigate direct cell-cell interactions cells were pre-mixed before plating to generate heterotypic cell-cell interactions. To distinguish between cell populations, it was necessary to use a cell tracker dye to label one population. This was achieved using CellTracker Orange CMRA Dye (ThermoFisher scientific) which is soluble; once taken up by cells it becomes cell-impermeable. Cells were washed twice with PBS and then incubated in serum-free DMEM with 4 μM CellTracker for one hour at 37°C and 5% CO_2. Once labelled, cells were washed twice more with PBS and split as described previously. Cells were then mixed with $2.5x10^6$ primary ductal cells mixed with $5x10^4$ labelled tumour-derived cells. This mixture was then plated in 4 well plates (Nunclon Delta Surface, ThermoFisher scientific) coated with 300 μl of rat tail type I collagen (Corning). Cells were grown for 48 hours until confluent and fixed with 4% PFA.

2.9.2 Ligand-Cell collision assay

To investigate the interaction of ephrin ligands with Eph receptors on pancreatic cells a stripe assay was carried out whereby cells are seeded into one well of a cell culture insert (Ibidi) with clustered ligand in the other (Porazinski et al., 2016). Once the insert is removed cells migrate and proliferate towards and then interact with the ligand stripe. This work was carried out by Rebecca Bennion, a Cardiff University undergraduate student under my supervision.

To begin, Fc- proteins are preclustered with goat anti-human IgG antibody (Jackson Immunoresearch) at 1:2 molar ratio. To precluster Fc-proteins and for each well to be coated, 10 μg of Fc-ephrin A ligand and 10 μg of Fc control (R&D Systems) were incubated for 30 minutes at room temperature with 2.4 μl of IgG antibody, with PBS added to make a final volume of 100 μL. One well of a cell culture insert (Ibidi) was then coated with 100 μL of this suspension for 30 minutes at 37°C, followed by washing with PBS and standard ductal epithelial growth media (Table 2.3) once for 1 minute each. To visualise the stripe, a secondary anti-goat antibody (ThermoFisher scientific) was incubated with the stripe in the cell culture insert for 1 hour before washing with PBS and standard ductal epithelial growth media as before. Cells were then seeded into the neighbouring well of the insert and allowed to adhere for 3 hours before the cell insert was carefully removed. Samples were then fixed after approximately 96 hours once cells had migrated and interacted with the stripe. Immunofluorescence was then carried out for F-actin and nuclei stained with Hoescht 33342 as described in Section 2.10.3.

2.10 Immunofluorescence

2.10.1 Preparation of Mowial

Coverslips were mounted using Mowiol solution. To prepare Mowiol solution 12 g glycerol (Sigma) and 4.8 g Mowiol 4-88 (Calbiochem) were added to 12 mL of H_2O and mixed overnight at room temperature. The following day 24

mL of 0.2 M Tris (pH 8.5) was added and the solution mixed at 50°C for at least 45 minutes until dissolved. Aliquots were then stored at -20°C until required.

2.10.2 Staining of Acinar cells

Staining of 3D acinar clusters was optimised for clusters of primary cells within collagen gel and was carried out in the glass-bottomed culture dishes. Cells were initially fixed in 4% PFA for 30 minutes at RT before permeablisiation in 0.5% TritonX100 in PBS for 30 minutes. Samples were then washed in PBS once and Glycine Wash buffer (0.1 M glycine in H_2O) three times for 10 minutes each. Blocking was then carried out in cyst block buffer (Table 2.5) for 1 hour before overnight incubation with primary antibody at specific concentrations (Table 2.6) at 4°C. This was followed by 3 x 20 minute washes of cyst block buffer were used. Following this, incubation with a suitable fluorescent secondary antibodies (Alex Fluor^{TM} 488 or 647 conjugate, Life technologies) at 1:200 dilution in cyst block buffer for 3 hours at RT in the dark. Secondary antibodies with emission spectra in green (488) and far red (647) were chosen to permit visualisation of cell tracker. Following this, three more washes in cyst block buffer were carried out, each for 20 minutes. Nuclei were then stained for by incubation in Hoescht 33342 (Life technologies) for 15 minutes at room temperature in the dark before mounting of samples in Mowial. Imaging was carried out on a Zeiss LSM 710 confocal microscope.

Reagent	Concentration	Supplier
NaCl	130 mM	Sigma
Bovine Serum Albumin (BSA)	1%	Sigma
Tritonx100	0.20%	Sigma
Tween20	0.05%	Sigma
FBS	10%	ThermoFisher scientific

Table 2.6 Cyst block buffer components. Added to distilled H_2O

2.10.3 Staining of Ductal cells

Immunofluorescence staining of 2D pancreatic ductal epithelial monolayers was carried out following established protocols. Throughout this protocol phosphatase inhibitors; sodium orthovanadate and sodium fluoride were both added to all solutions at 1 mM when staining for phosphorylated proteins to inhibit any residual phosphatase activity. All steps were carried out at RT unless otherwise stated. To begin staining, cells were fixed for 10 minutes in 4% PFA followed by 3 x 5 minute washes in TBS. Cells were then permeabilised in 0.25% TritonX-TBS for 10 minutes before blocking in 3% BSA-TBS for 1-2 hours. Cell were then incubated in primary antibody (Table 2.7) in 3%-TBS overnight at 4°C. Following this samples were washed in TBS for 3x 5 minutes before incubating in secondary antibody (1:200, Life technologies) and phalloidin (1:200, Invitrogen) for 1 hours at room temperature. Samples were washed thrice more for 5 minutes each in TBS before incubation with Hoescht 33342 (Life technologies) for 2 minutes. Following this a final H$_2$O wash was carried out for 5 minutes before mounting in Mowiol. Imaging was carried out on a Zeiss LSM 710 confocal microscope.

Antibody	Supplier	Concentration	Source
anti-EphA2 D7	Millipore 05-480	1:200	Mouse
anti-EphA2 8B6	CST-129275	1:200	Mouse
anti-E-cadherin	BD Transduction 610182	1:500	Mouse
anti-Sox9	Millipore AB5535	1:1000	Rabbit
anti-Amylase	Sigma A8273	1:200	Rabbit
anti-phosphorylated Src (Y416)	CST-21015	1:50	Rabbit
anti-phosphorylated Myosin II (Thr18/Ser19)	CST-36745	1:50	Rabbit
anti-RFP	Creative Diagnostics H83194	1:500	Rabbit

Table 2.7 Antibodies for Immunofluorescence

2.11 3D Immunofluorescence Tomography

To visualise interactions of normal and Kras[G12D] pancreatic cells *in vivo* in 3D a recently developed technique known as 3D immunofluorescence tomography was utilised (Parfitt et al., 2012). This involves embedding of tissue in butyl-methyl methacrylate (BMMA) plastic and cutting serial sections of 2 μm. Slides can be filled with up to 3 ribbons of serial section with each ribbon up to 20 slices or 40 μm. Immunofluorescence of serial sections on slides and subsequent imaging of each section was carried out. Each image can then be aligned to generate a 3D reconstruction of the tissue.

2.11.1 Butyl-methyl Methacrylate (BMMA) formulation

To formulate BMMA, butyl methacrylate and methyl methacrylate monomer solutions (Polysciences) were mixed 1:4 and the reducing agent dithiothreitol was added to a concentration of 5 mM. The photo-initiator, benzoin ethyl ether (Sigma) was also added (0.3% of total volume). Finally, BMMA solution was degassed with N_2 for 30 minutes to remove oxygen which inhibits polymerisation. BMMA solution was stored at -20°C to prevent heat and ambient light inducing polymerisation.

2.11.2 Sample processing

Following fixation of tissue in 2% PFA in PBS for at least 24 hours, samples were embedded in low melting point 3% agarose (Bioline) to orient tissue appropriately. Tissues were then dehydrated in 50%, 70% then 95% ethanol for 30 minutes each at room temperature before a final incubation in 100% ethanol for a further 30 minutes. Following dehydration, samples were infiltrated with BMMA. Samples were incubated with 25%, 50% and 75% BMMA in ethanol for at least 12 hours each at room temperature. Then tissues were submerged and rotated in 100% BMMA for 24 hours at 4°C. For polymerisation of BMMA each sample was placed in a BEEM gelatin capsule and sealed before being placed under UV light for 20 hours at 4°C.

2.11.3 Serial Sectioning

Serial sections 2 μm thick were cut using a diamond knife (DiATOME) on a Leica EM UC7 Ultramicrotome. Cutting was carried out by Dr Geraint Parfitt, a research fellow at Cardiff University. By addition of an adhesive (Pattex) to the top and bottom of the block to bind each section together forming a ribbon. Ribbons of 12-20 sections were then floated onto a Poly-L-Lysine coated slide (ThermoFisher scientific). Chloroform vapour was used when required to expand the sections ensuring sections lay flat before mounting onto slides.

2.11.4 Immunostaining of Serial Sections

Ribbons of serial sections were incubated in acetone for 10 minutes to remove BMMA before rehydration in 95%, 75%, 50% ethanol and PBS each for 10 minutes. Antigens were unmasked by heating sections in 1X citrate buffer (2.94 g Sodium citrate tribasic dehydrate (Sigma) in 1 L H_2O, pH 6) in a pressure cooker. Citrate buffer was heated in a microwave at 1000 W for 10 minutes before submersing slides in the buffer. The pressure cooker was then heated in a microwave for a further 10 minutes. Slides were then cooled in PBS before blocking of non-specific antibody binding. This was carried out by incubating in 5% normal goat serum in PBS for 30 minutes. Tissues were then incubated in primary antibody at the appropriate concentration (Table 2.5) overnight at 4°C. Slides were then washed in PBS for 3 x 5 minutes before incubation in secondary antibody (Life technologies) for 2 hours at room temperature. Sections were then incubated in Hoescht 33342 (1:5000 in PBS) for 5 minutes before mounting in 50:50 Glycerol:PBS.

2.11.5 Three-Dimensional Reconstruction

Individual sections were imaged on a Zeiss LSM 710 confocal microscope. The same position in each section was manually selected, checked for focus and then imaged in each channel. The individual montage images were

then merged in Fiji (Version 2.0) to form a single stack maintaining the sequence of sections. For every image acquisition, at least two channels of information were collected with one representing nuclei. Data sets could then be interleaved and co-aligned using the common nuclei channel. Image alignment and three-dimensional reconstruction was performed with the AlignSlices module in the Amira 5.4 Software package (Visage Imaging) with semi-automated alignment. Reconstructions were then exported as TIFF files for analysis in Fiji and Imaris software packages.

2.12 Imaging

Fluorescent imaging was carried out on a Zeiss LSM 710 confocal microscope. Samples were stored at 4°C and brought up to room temperature before imaging. Imaging settings were kept the same for each individual protein in each system. All image files were saved and analysed as .CZI files. Samples from IHC were imaged using a Zeiss Axioscan Z1 slide scanner to image the whole tissue section.

2.13 Image Analysis

2.13.1 Calculating RFP percentage area

The percentage area of RFP in a whole tissue section was calculated as the area of RFP as a proportion of the total tissue area and quantified in Fiji software (Version 2.0). RFP and brightfield image channels captured from cryosections were split and then a ROI was drawn around intact tissue and area measured. The RFP channel was then cropped using the tissue ROI to remove any fluorescence outside the tissue. The maximum was then increased to the same level for all images to improve quality of thresholding. Fluorescence was then defined using Auto Threshold by the Default method. The area of RFP was then calculated by Analyse Particles using a size threshold of 100 μm to remove background and count masks generated. The total area of RFP was then

calculated in excel and normalised to tissue area to produce a percentage area of RFP for each slice. For each biological replicate 5 whole tissue slices were analysed.

2.13.2 In Vivo Cluster Analysis

To calculate the density of clusters of RFP *in vivo* individual clusters were quantified using Fiji software and total area of tissue quantified as before. Clusters were then binned on size using GraphPad Prism6 and normalised to the area of each tissue slice. This generated the density of different sized clusters per tissue and was repeated for each biological replicate. This was then plotted in GraphPad.

2.13.3 In Vitro Quantification

To quantify contractility and segregation of transformed cells from 2D ductal epithelial cultures cell area and Index of Sphericity were calculated. Cell area was calculated by manual segmentation of cells based on membrane fluorescence using Fiji. Area was then measured for each cell. Index of Sphericity is a recently described mathematical model that quantifies how much an object shape deviates from the ideal shape of a circle (Ionescu-Tirgoviste et al., 2015). As the Index of Sphericity tends more towards 1, the object is more spherical. It considers two parameters: i) the shape perimeter measured on a 2D surface and ii) a relative parameter, namely the mean shape diameter. The mean shape diameter is determined from the perimeter and area of an irregular shape. The ratio between the perimeter and mean diameter of a perfect circle is π and thus the deviation from this can be quantified to measure the divergence from a perfect circle. The area and perimeter of a CMRA labelled cluster was measured manually in Fiji before calculation of the Index of Sphericity.

2.13.4 3D In Vivo Quantification of Volume

To calculate the volume of RFP positive cells *in vivo,* tissue stained for E-cadherin and RFP and nuclei was imaged and 3D reconstructions generated using immunofluorescence tomography. Three-dimensional reconstructions were then imported into Imaris (Version 9.2, Bitplane). Segmentation was then carried out using the ImarisCell module using Cell Membrane Region Detection based on E-cadherin immunofluorescence. Cell membrane detection algorithms are a collection of automatic tools and were adjusted and optimised for a small ROI before expanding to the whole 3D image. RFP positive cells were then selected and volume recorded.

2.14 Statistical Analysis

Statistical analysis was carried in GraphPad Prism6. Error bars on graphs represent standard deviation. Data was tested for normal distribution using a Shapiro-Wilk normality test. For comparison of normally distributed data an unpaired Welch's *t*-test was carried out with a p value of <0.05 taken as a significant difference. Data that were found to be not normally distributed were compared using a Mann Whitney U two-tailed test with significant difference accepted with $p < 0.05$.

Chapter 3: Characterising Kras^{G12D} normal heterotypic cell-cell interactions *in vivo*

3.1 Introduction

At the initial stage of carcinogenesis transformation occurs in a single cell within a normal epithelium. However, what happens at the interface between the mutant cells and the surrounding normal neighbours is not clearly understood. Recent studies have demonstrated that mutant cells can be eliminated from epithelial tissues *in vitro* via cell competition with normal neighbours. For example, it has been shown that Ras^{V12}-, Src- or ErbB2- transformed cells are apically extruded when surrounded by normal epithelial cells (Hogan et al., 2009; Kajita et al., 2010; Leung and Brugge, 2012). Extrusion *in vitro* is dependent on E-cadherin-based cell-cell adhesions and signalling to the actin-myosin cytoskeleton. Importantly, when transformed cells are cultured alone apical extrusion does not occur suggesting that extrusion is cell-context dependent. Recently, differential EphA2 has been demonstrated to be the underlying signalling causing repulsion and extrusion of Ras mutant cells *in vitro* and was found to be evolutionary conserved in *Drosophila* (Porazinski et al., 2016). Cell-cell interactions between normal and Ras^{V12} cells triggers ephrin-A-EphA2 signalling which induces repulsion of mutant cells. In the absence of EphA2 signals, Ras^{V12} cells integrate with normal cells and adopt a pro-invasive morphology.

EphA2 is a member of the Eph family of receptor tyrosine kinases, which are involved in cell segregation and tissue boundary formation required through development and to maintain organised tissues in complex organisms (Kania and Klein, 2016). Alterations to EphA2 has been linked with breast, prostate, lung, ovarian, cervical, oesophageal and colorectal cancer (Andres et al., 1994; D'Amico et al., 2001; Duxbury et al., 2004; Kataoka et al., 2004; Landen et al., 2006; Walker-Daniels et al., 1999; Zelinski et al., 2001). Moreover, increased EPHA2 expression in tumour cells correlates with poor prognosis in breast and oesophageal cancer with EphA2 knockout reducing tumour growth and metastasis in ErbB2-driven breast cancer in mice (Brantley-Sieders et al., 2008).EphA2 has also been studied in pancreatic cancer patient samples; with EphA2 is elevated in primary tumour and the loss of EphA2 was associated with

metastasis (Mudali et al., 2006). Although abnormal expression of EphA2 has been reported during tumourigenesis the precise role is unclear, with a role in cell competition not explored.

Recently, a number of studies have begun elucidating a role for cell competition at the earliest stages of Ras-driven carcinoma. Using mouse-derived organoid and *in vivo* imaging has demonstrated that single Ras[V12] cells are apically extruded from the intestinal epithelium (Kon et al., 2017) and cleared in adult murine skin models (Brown et al., 2017). In the developing pancreas, there is some evidence that selective loss of Kras[G12D] mutant cells occurs (Morton et al., 2010). Moreover, cellular extrusion has been identified from precursor lesions in the pancreas (Hendley et al., 2016; Rhim et al., 2012). Recently, one study found evidence of extrusion of single Ras[V12] cells from the pancreatic ductal epithelium *in vivo* (Sasaki et al., 2018). This work also investigated the process by which extrusion is overcome and found a high-fat diet and chronic inflammation could inhibit extrusion. The number of mutant cells has also been demonstrated to determine if cell competition promotes or prevents tumourigenesis. Small clusters of oncogenic Ras expressing cells can be eliminated from *Drosophila* epithelia by contractile forces between aberrant and normal cells however these forces drive cyst formation in larger mutant clusters (Bielmeier et al., 2016). In very large clusters of Rab5 mutant cells (around 400 cells) cell competition-dependent apoptosis at the boundary of normal:mutant cells can drive proliferation and tumour formation (Ballesteros-Arias et al., 2014). These studies suggest that cell context-dependent changes occur to extrude cells with oncogenic Ras. However, whether this impedes tumourigenesis or can promote tumour formation and invasion and precisely how it occurs *in vivo* is still unclear.

Mutations to Ras are integral to many forms of cancer with *Kras* mutations known to have a causal role in human pancreatic ductal adenocarcinoma (PDAC). Mutational activation of KRAS is present in >90% of PDAC and represents the most frequent and earliest genetic alteration, being found in >95% of low-grade human pancreatic intraepithelial neoplasia (PanIN) 1A lesions (Habbe et al., 2008; Kanda et al., 2012; Morris et al., 2010a). Moreover, *Kras[G12D]* expression in the murine pancreas is sufficient to initiate pancreatic intraepithelial neoplasias (PanINs) which can progress with long latency to PDAC, fully

recapitulating the human disease in mouse models (Hingorani et al., 2003). Furthermore, using an inducible and reversible expression of Kras^{G12D} mouse model has demonstrated that continuous Kras^{G12D} is required; with rapid regression of primary and metastatic lesions and tumours following inactivation of Kras^{G12D} (Collins et al., 2014). Kras^{G12D} mutations are predicted to occur decades before tumour formation (Yachida et al., 2010), indicating a large window for diagnosis and disease monitoring. Therefore, Kras^{G12D} mutations can be considered the initial and driver mutation of the early disease states in PDAC and may occur long before tumour formation.

Pancreatic cancer is the fifth leading cause of cancer deaths in the UK. It has a median survival measured in months and a 5-year survival of <5 % (Cancer Research UK, 2017). The poor prognosis is due to the aggressive nature of the disease and a lack of symptoms resulting in only 10-20 % of patients diagnosed with surgically resectable cancer, the only cure (Mayo et al., 2012). Better understanding of the initial stages of pancreatic cancer is imperative to improving patient prognosis.

The aims of this chapter were to investigate the role of cell-cell interactions on the fate of newly emerged mutant cells in the murine pancreas *in vivo*. It aims to answer: i) whether *Kras^{G12D}* expressing mutant cells are eliminated by normal neighbours, ii) is EphA2 required for the loss of transformed cells and iii) if cluster size dependent changes are occurring *in vivo*.

3.2 Results

3.2.1 *Pdx1-Cre^{ERT}* drives recombination in the pancreas with high efficiency

In order to study the interaction of *Kras^{G12D}* expressing mutant cells (Kras^{G12D} cells) and normal neighbours it was first necessary to generate an *in vivo* model of mosaic Kras^{G12D} cells. To this end animals bearing the *Pdx1-Cre^{ERT}* transgene (Gu et al., 2002) were crossed with (*Lox-STOP-Lox) LSL-Kras$^{G12D/+}$* mice (Jackson et al., 2001). To label recombined cells, animals were crossed with the *ROSA26$^{LSL-RFP}$* reporter transgene (Luche et al., 2007). This resulted in *Pdx1-Cre; Rosa26^{tdRFP}; Kras^{G12D}* mice which will be referred to as KC from now on. In these animals, tamoxifen drives Cre-mediated excision of the *LSL* cassette and expression of *Kras^{G12D}* and *RFP*. Control mice for RFP studies were *Pdx1-Cre^{ERT}; ROSA26$^{LSL-RFP}$* with tamoxifen leading to RFP labelling of Kras wild-type pancreatic cells. Breeding pairs were kindly provided by Jen Morton and Owen Sansom at the Beatson Institute, Glasgow and re-derived into a SPF unit.

To investigate the interaction of normal and mutant cells it was necessary to generate tissue with mosaic expression of *Kras^{G12D}*. To achieve this a low level of tamoxifen was administered to induce low levels of recombination within the tissue. Control animals at 6-8 weeks of age were injected with 1 µg and 1mg of tamoxifen by IP injection. At 7 days post-induction (dpi) the pancreas was harvested, frozen in optimal cutting temperature (OCT) compound and sectioned on a cryostat. Five sections of 10 µm each and at least 50 µm apart were cut and imaged using the tile-scan function on a Zeiss LSM710 confocal microscope to capture the whole section (Figure 3.1A). The area of RFP was then quantified using ImageJ and calculated as a percentage of the total tissue area (Figure 3.1B). Induction using 1 µg "low dose" of tamoxifen resulted in 20.8% ± 3.7 (± standard deviation, n=5) of the tissue positive for RFP. As animals were all of a similar weight and due to the precision of induction it was not necessary to control dose based on animal weight to generate a reproducible percentage area with low inter-variation. Induction with 1mg of tamoxifen led to 24% ± 17 (n=2) and as this was similar to 1 µg but with higher variation the 1 µg dose was used in future experiments. The pancreata from animals not bearing the RFP transgene

were found to be negative for RFP fluorescence. Age-matched animals that had not been induced with tamoxifen had a percentage area of RFP of 1.3% ± 0.4 (n=2) (Figure 3.1B). This indicates low level induction with tamoxifen results in around 20% recombination within the tissue with minimal background induction.

As a control for studying heterotypic cell-cell interactions it was also necessary to generate tissue with widespread $Kras^{G12D}$ expression. To induce widespread recombination, and hence most cells expressing $Kras^{G12D}$ and RFP, previous work has used a dosage system consisting of one intraperitoneal (IP) injection of 9 mg /40 g of bodyweight every other day for a total of 3 injections (Gidekel Friedlander et al., 2009). Control mice ($Pdx-1-Cre^{ERT}$; $ROSA26^{LSL-RFP}$) at 6 – 8 weeks of age were injected following this regime and the pancreas was harvested and RFP area quantified as before (Figure 3.1A, B). Using this "high" tamoxifen dosage resulted in a percentage area of RFP positive tissue (± standard deviation) of 80.5 % (Figure 3.1B). This indicates that at this dose using a $Pdx1$-driven Cre, most cells in the pancreas have undergone recombination as the vast majority of the tissue is RFP positive. This demonstrates the capability of the system to generate a model of cell-cell interactions whereby most recombined cells are surrounded by recombined neighbours.

Together, this shows that the levels of recombination within the murine pancreas can be controlled by dosage of tamoxifen and the system can generate two scenarios; one with a large number of normal-mutant cell interaction (low dose) and a second with a predominance of mutant-mutant cell interactions (high dose). This allows characterisation of the fate of Ras-transformed cells over time in the murine pancreas *in vivo* and recapitulates the initial genetic event occurring in a single cell within a healthy epithelium.

The RFP transgene consists of a "tandem-dimer2" RFP (tdRFP) variant which consists of two genetically modified DsRed subunits covalently fused resulting in a very bright variant. Due to this brightness even spurious read-through across the transcript could result in background fluorescence (Luche et al., 2007). To overcome this the tdRFP was inserted in reverse orientation relative to ROSA26 transcription. This in combination with two unique pairs of loxP sites, one pair in parallel and the other in opposite orientation, means that two Cre-mediated recombination events are required for activation (Luche et al., 2007). As Cre-mediated recombination can vary between loci (Liu et al., 2013),

and two recombination events are required for *RFP* but only one for *Kras*[G12D] expression it was necessary to confirm that RFP faithfully labelled cells expressing *Kras*[G12D]. To this end laser capture microscopy was used to excise RFP positive and RFP negative tissue from induced KC animals 7 dpi. Genomic DNA was then extracted from these samples and a PCR was carried out for the recombined, non-recombined and wild-type allele (Figure 3.1C). It was observed that RFP positive tissue produced two bands corresponding to the 622bp product from the WT allele and the 650bp product from the recombined *Kras* allele with no band identified at 500bp from the unrecombined *Kras* allele (Figure 3.1D). This suggests a similar level of recombination efficiency at the two loci and that RFP accurately labels cells with mutant *Kras*[G12D]. Laser capture microdissection was also carried out for RFP negative tissue. This produced two bands at 500bp and 622bp corresponding to the non-recombined *LSL-Kras*[G12D] locus and the WT allele respectively. However, a faint band was also observed at 650bp suggesting that a low level of RFP negative cells have undergone Cre-mediated recombination at the *Kras*[G12D] locus. This suggests that some cells have recombined at the mutant *Kras*[G12D] allele but are not expressing RFP. Although it could not be ruled out that some Kras[G12D] cells are not RFP positive this demonstrates that the system is robust and RFP accurately marks mutant cells.

The pancreas consists of both exocrine and endocrine compartments with *Pdx1* reported to be expressed in both compartments in the adult (Jonsson et al., 1994; Offield et al., 1996). During development *Pdx1* is expressed in all pancreatic lineages, however in the adult the expression pattern is less clear. To investigate which cell type was undergoing recombination, fixed tissue was stained with anti-RFP and anti-E-cadherin to examine recombined cells and allow identification of cell type by morphology (Figure 3.1E). It was observed that of the exocrine compartment both acinar and ductal cells were positive for RFP (Figure 3.1E, white arrows and white arrowheads, respectively). RFP positive cells were also identified within islets (Figure 3.1E, dashed line). This suggests that *Pdx1* is expressed within both the exocrine and endocrine compartment in the adult. Furthermore, acinar cells were observed to make up the largest contribution to the RFP positive area.

Expression of *Kras*[G12D] leads to constitutive activation of KRAS and the MAPK signalling pathway (Macrae et al., 2005). To investigate markers KRAS

activation immunohistochemistry for phosphorylated ERK (pERK) was carried out however no positive signal was observed at 7 or 35 dpi. in KC mice (data not shown) and it has previously been reported that pERK is not a robust read-out of KRAS activation in the pancreas (Ji et al., 2009). However, expression of $Kras^{G12D}$ is sufficient to induce PanIN lesions and increase the amount of KRAS-GTP present, demonstrating activation of oncogenic KRAS (Bailey et al., 2016; Collins et al., 2012; Ferreira et al., 2017; Guerra, 2013; Habbe et al., 2008; Hingorani et al., 2003, 2005). Moreover, we have previously found pERK levels to be cyclical upon Ras activation in MDCK cells. Therefore, pERK is not appropriate to use as a readout of $Kras^{G12D}$.

Together, this describes the development of an *in vivo* model of normal:mutant cell interactions in the adult murine pancreas *in vivo* with RFP providing a surrogate for $Kras^{G12D}$ expression.

A Cryosections

Low dose   High dose

endogenous RFP

B

RFP % area vs Dose (High, Medium, Low, Uninduced)

C

LSL-KrasG12D   A→ C→ →B [STOP] Exon 1   C + B = 500bp

WT   A→ B→ Exon 1   A + B = 622bp

Recombined KrasG12D   A→ B→ Exon 1   A + B = 650bp

D

RFP-   RFP+

650 bp
622 bp
500 bp

E

RFP E-cadherin Nuclei
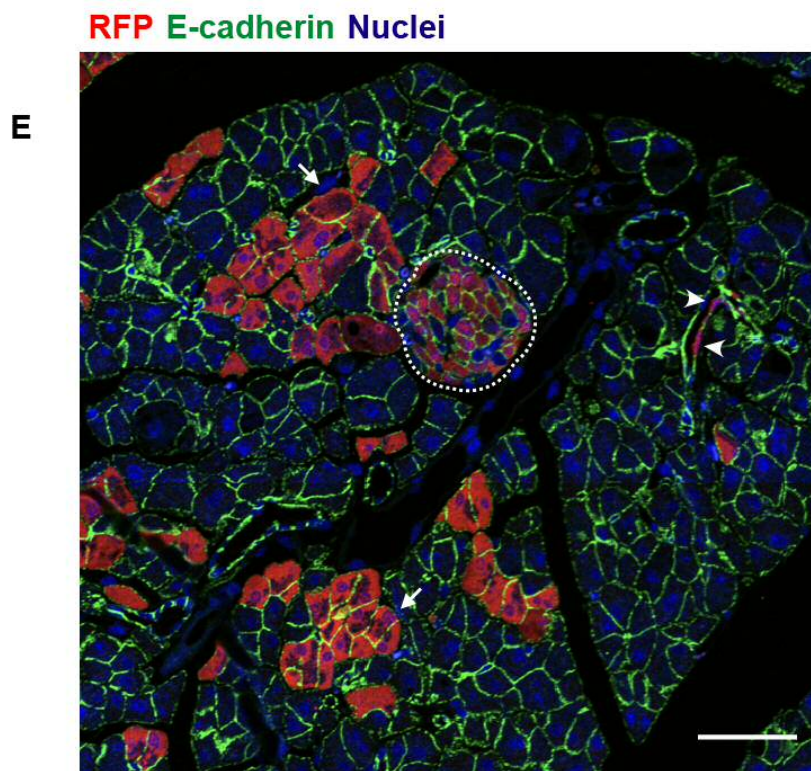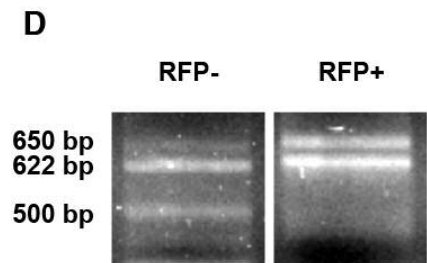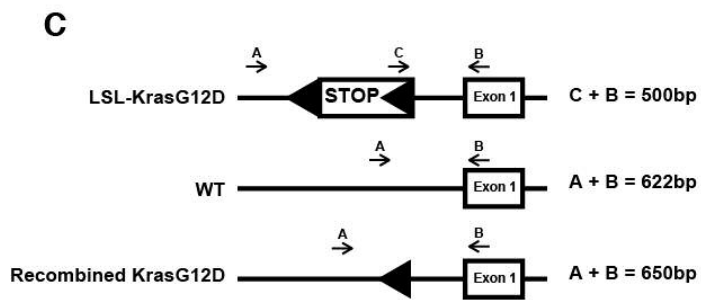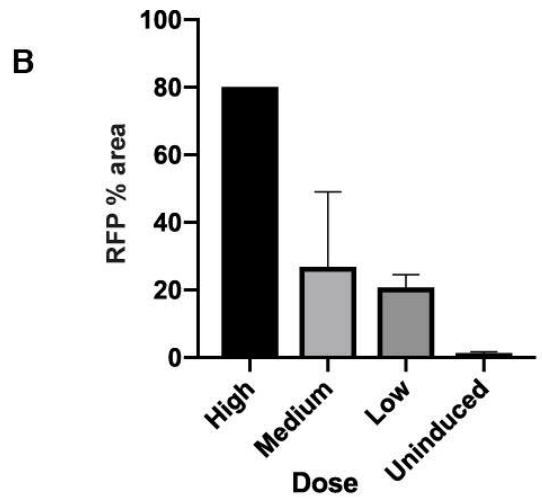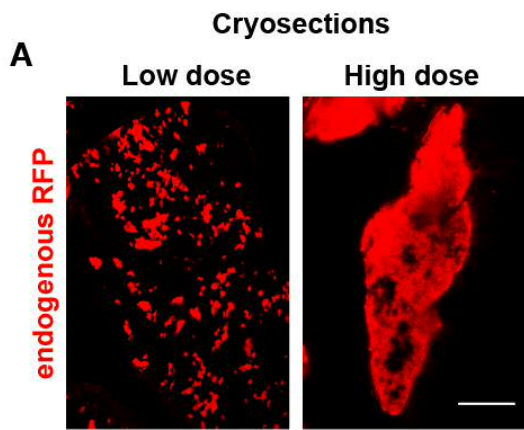
Figure 3.1: Developing a model of Kras^{G12D}:normal cell interaction with an RFP reporter. By regulating the dose of tamoxifen the level of recombination as measured by RFP % area can be controlled (A). High dose (3x9mg/40g) achieves 80.5% (n=1) area of recombination in the tissue, medium dose (1x 1mg) resulted in 24%±20 (n=2) and low dose (1x 1ug) induced 20.8%±3.7 (n=5). Background induction in uninduced mice is low at 1.3%±0.4 (n=2) (B). A diagram of primer binding sites (C) shows the method of detection of Kras locus recombination by PCR. Using laser capture microscopy to extract RFP positive cells followed by PCR using the primers from (C) indicates RFP positive cells have also recombined at the *Kras^{G12D}* locus. In RFP negative tissue wild-type (WT) and unrecombined Kras$^{LSL-G12D}$ alleles were detected. However, a weaker band correspondingly to recombined Kras$^{1LOX-G12D}$ was detected in RFP negative tissue indicating in a small proportion of non-RFP labelled cells express oncogenic *Kras^{G12D}*. (E) Confocal image of fixed murine pancreas tissue harvested 7 dpi. with low dose tamoxifen. Fixed tissue is stained with anti-RFP antibody (red), anti-E-cadherin (green) and Hoescht (blue). RFP is detected in exocrine acinar cells (white arrows), ductal epithelial cells (white arrowheads) and endocrine islets (dashed white line), indicating Pdx-1-driven Cre expression. Scale bars, 500 μm (A), 100 μm (E).

3.2.2 Developing a sample representative of intravariation through the pancreas

Once the method of induction had been established it was investigated whether an RFP sample from the tail was representative of the whole pancreas. As the pancreas is the second largest gland in the body and is reported to have differences in cell composition, blood supply and innervation through the tissue (Dolenšek et al., 2015) the RFP levels through the pancreas were quantified. A whole KC pancreas was harvested 14 days after induction with 1 μg of tamoxifen, embedded in OCT for sectioning on a cryostat. Initially, a 10 μm slice was collected every 50 μm for the first 300 μm from the tail as the tail sample. Then a slice was collected every 250 μm throughout the rest of the pancreas with representative tile scans from the beginning, middle and end depicted in Figure 3.2A. The RFP percentage area of each slice was then calculated by quantitative analysis of both the total tissue and RFP area using ImageJ (Figure 3.2B). It was observed that the average percentage area of RFP in the tail sample (first 300 μm) was 4.1 % ± 0.7. Through the rest of the pancreas the percentage area of RFP appears to have only low variation with all values except one within 2% of the average tail sample. Moreover, no general trend of RFP change was observed through the pancreas. This quantifies the variation of recombination within the pancreas and suggests that values attained from a tail sample provide an approximate representation of the whole pancreas.

A

B
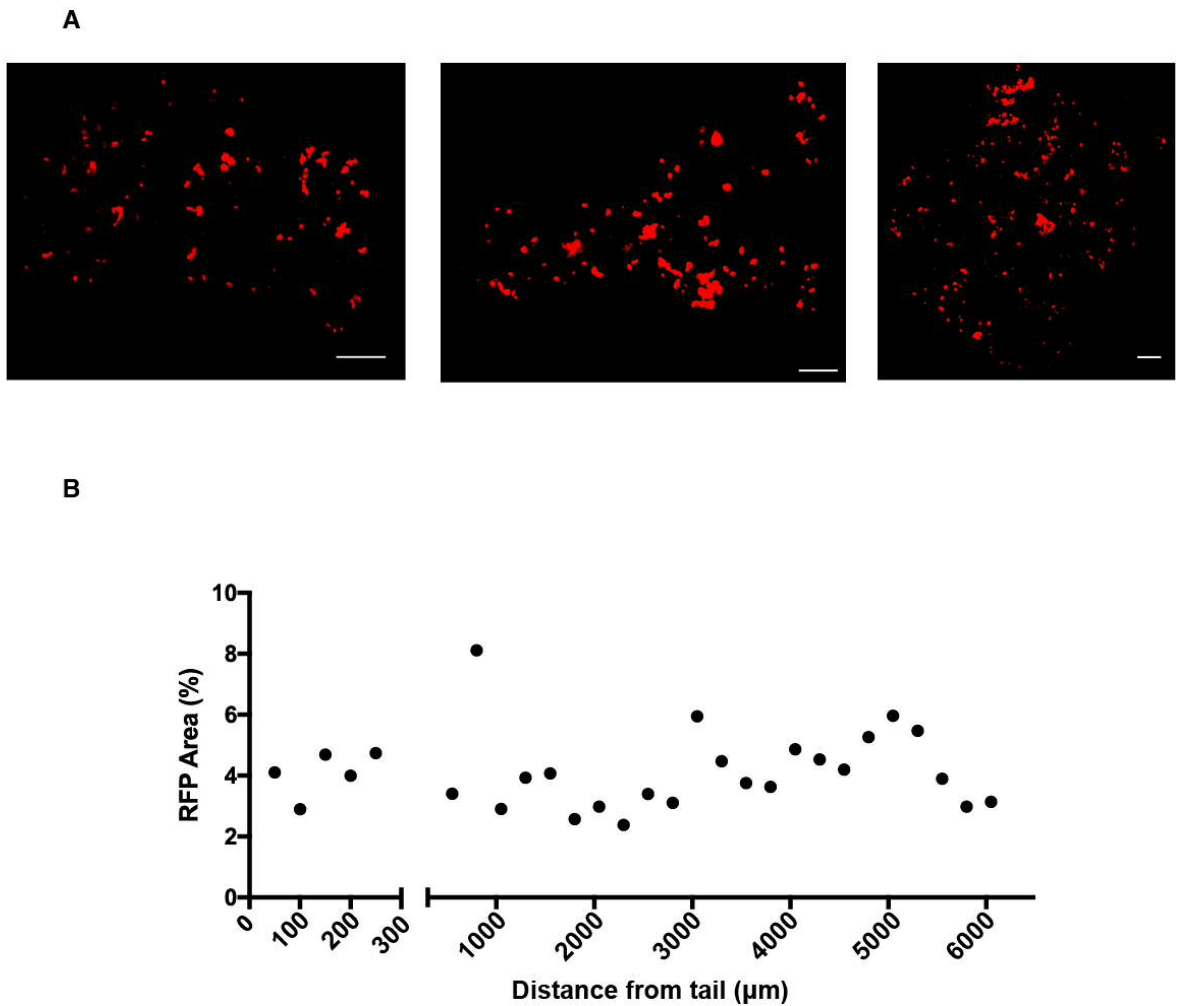
Figure 3.2: Levels of recombination are similar through the murine pancreas. (A) At 14 dpi the whole pancreas was sectioned from the tail, imaged with tile scans and are stitched to show entire tissue sections representative images of RFP (red) from tissue sections from the start, middle and end (left to right). (B) Quantification of RFP percentage area identified the variation through the pancreas and suggests 5 slices from 300 μm in the tail is representative of the whole organ. Scale bar, 500 μm.

3.2.3 The percentage area of cells expressing oncogenic *Kras* decreases over time

Having validated the low dose model of *Kras*^{G12D} recombination in the pancreas to establish mosaic expression in the pancreas, the fate of mutant cells was investigated over time.

Cohorts of KC and control animals (Kras wild-type) were injected with 1 μg of tamoxifen at 6-8 weeks of age and tissue harvested at 7 and 35 days post induction. These time points were chosen as loss of Kras^{G12D} cells from the pancreas was previously suggested to take place over a period of 28 days using constitutive Cre activation *in utero* (Morton et al., 2010). A section of 10 μm was cut every 50 μm in the tail of the pancreas until 5 sections were collected. Tile-scans of the tissue were then captured and stitched before quantification of the total tissue area and RFP area using ImageJ (Figure 3.3A). All images were captured using the same settings and analysed using the same parameters and thresholding method. Quantification of RFP percentage levels (± standard deviation) at 7 dpi revealed similar levels of recombination in control and KC pancreata (Control = 20.8 % ± 3.7 Vs. KC = 27.6 % ± 5.0) (Figure 3.3B). This suggests that the initial levels of recombination within control and KC animals are similar. No difference was observed between male and female animals so both sexes were pooled in all experiments. To understand tissue dynamics over time in the pancreas, *Pdx1-Cre; Rosa26*^{tdRFP} control cohorts were also generated for later time points (Figure 3.3B). It was found that the percentage area of RFP positive tissue in controls did not significantly change between 7 and 35 dpi (7 days = 20.8 % ±3.7 Vs. 35 days = 24.6 % ±1.8, Welch's t-test, p= 0.09). This suggests that RFP is stable and provides a robust model to track cellular changes over time.

Next, the percentage area of RFP in KC animals was analysed over time. Interestingly, at 35 dpi the percentage area of RFP was significantly decreased compared to 7 dpi (7 days = 27.6% ± 5.0 Vs. 35 days = 8.5% ± 3.0, Welch's unpaired *t*-test, p= 0.0036) (Figure 3.3B). This indicates that over 28 days approximately 69% of *Kras*^{G12D} expressing cells are lost from the tissue. As separate cohorts of induced animals were generated for each time point, rather than lineage tracing in single animals, Kras wild-type controls were compared to

KC animals at each time point. Quantification of RFP demonstrated that a significantly decrease between control and KC mice had occurred by 35 dpi (Control = 24.6% ± 1.83 Vs. KC = 8.5% ±3.03, Welch's unpaired t-test, p= <0.0001). This suggests that stochastic induction of mutant $Kras^{G12D}$ expression in a low number of cells drives drastic changes to the tissue resulting in a large decrease in RFP area, implying a loss of mutant cells.

Together, this data indicates that labelled, Kras wild-type cells are relatively unchanged over 28 days but when $Kras^{G12D}$ cells are present at low numbers, they are eliminated.
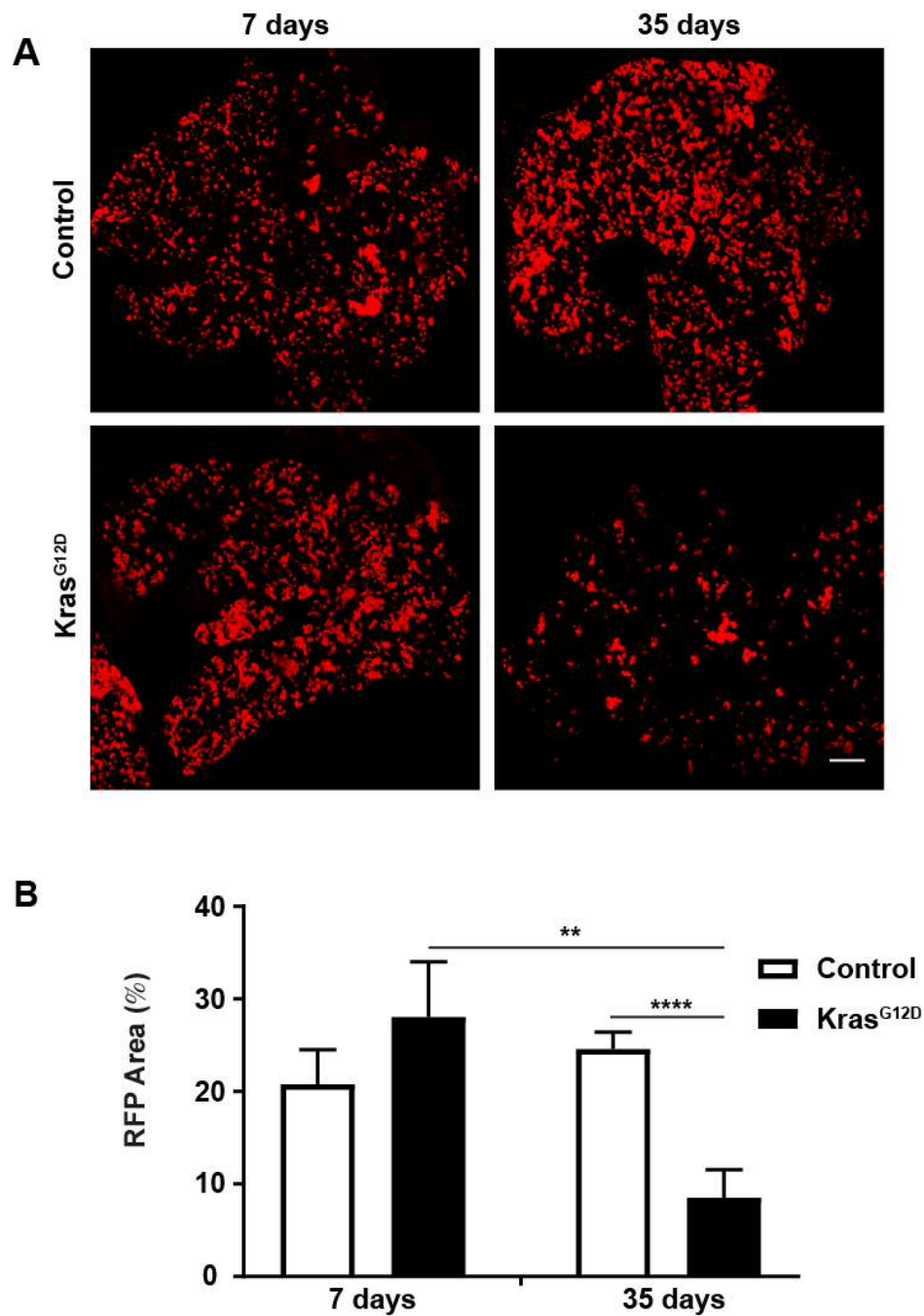
Figure 3.3: Loss of Kras^{G12D} mutant cell area over time. KC (*Pdx1-Cre; Rosa26^{tdRFP}; Kras^{G12D}*) animals and controls (*Pdx1-Cre; Rosa26^{tdRFP}*) were induced using a low dose of tamoxifen via IP injection and tracked over time. Representative images of sectioned pancreata harvested at 7 and 35 dpi. with RFP imaged using tile-scans (A). The percentage area of RFP was then quantified as a readout of Kras^{G12D} cell area (black bars) and Kras wild type cell area (Control, white bars) (B). A significant decrease in area of *Kras^{G12D}* expressing cells was observed at 35 dpi. compared to 7 days. Moreover, at 35 dpi. the area of mutant Kras cells was significantly lower than Kras WT controls. Data represents mean ± s.d. n = 4-6 biological replicates. Statistical analysis was carried using Welch's two-tailed *t*-test with *P<0.05 and ****P<0.0001. Error bars are standard deviation. Scale bar, 500 μm

3.2.4 The loss of RFP is not a cell-autonomous process and requires normal neighbours

After observing that the presence of Kras^{G12D} cells at low numbers in the pancreas resulted in a decrease in RFP area, it was necessary to test whether this is a result of a cell intrinsic mechanism or requires normal neighbours. We have previously identified the autonomous upregulation of EphA2 as the process by which Ras mutant cells are triggered to be eliminated from epithelial monolayers (Porazinski et al., 2016). Ras mutant cells were not eliminated when surrounded by other Ras mutant cells suggesting a requirement of non-transformed epithelial cells. To test the requirement of non-transformed neighbours the dose was increased to generate widespread recombination within the pancreas and the RFP area over time was tracked.

Cohorts of KC animals, at 6-8 weeks of age, were injected with the high dose and the pancreas was harvested at 7 and 35 dpi. Sections of frozen tissue were then imaged using tile-scans to image RFP in the whole section as before and quantified using ImageJ (Figure 3.4A). By increasing the amount of tamoxifen administered the percentage area of RFP increased to 70.7 % ± 8.7 in KC animals 7 dpi (Figure 3.4B). In this setting, the interaction of normal and mutant cells decreases whilst homotypic Kras^{G12D}:Kras^{G12D} cell interactions increase. Control mice (Kras wild-type) were also induced in the same manner and resulted in a RFP area of 80.5 % at 7 dpi. This suggests that the levels of recombination induced in KC and controls is similar at 7 dpi and allows direct comparison at later time points.

The RFP distribution was then imaged at 35 dpi to investigate how mutant cell area changes over time in this scenario. It was found that no significant change in RFP percentage area was observed between 7 and 35 days in the KC model (35 days = 75.3 % ± 7.1 Vs. 7 days = 70.7 % ± 8.7, Welch's t-test p = 0.5012) (Figure 3.4B). This indicates that over the same time period that led to loss of RFP when mutant cells are present at low numbers, RFP area is stable when mutant cells are present at high numbers. Furthermore, no significant difference in RFP percentage area was observed between Kras WT and Kras^{G12D} tissues at 35 dpi following high dose induction (Control = 66.3 % ± 10.0 Vs. KC = 75.3 % ± 7.1, Welch's t-test p = 0.2636). The area of RFP was also compared

at high dose for Kras wild-type, RFP labelled cells over time. Between 7 and 35 dpi levels of RFP in control mice were observed to undergo a small decrease (7 days = 80.5 % Vs. 35 days = 66.3 % ± 10.0). However, further investigation is required to increase the number of biological replicates to understand if the loss of RFP area in controls over time is a consistent and significant trend.

Together these data demonstrate that when *Kras*^{*G12D*} expressing cells are present at a high number within the pancreas the overall percentage area of mutant cells does not decrease over time. This suggests that mutant cells are not lost when present in tissues at high numbers and indicates a requirement for normal neighbours in the elimination of Kras^{G12D} cells.

A

B
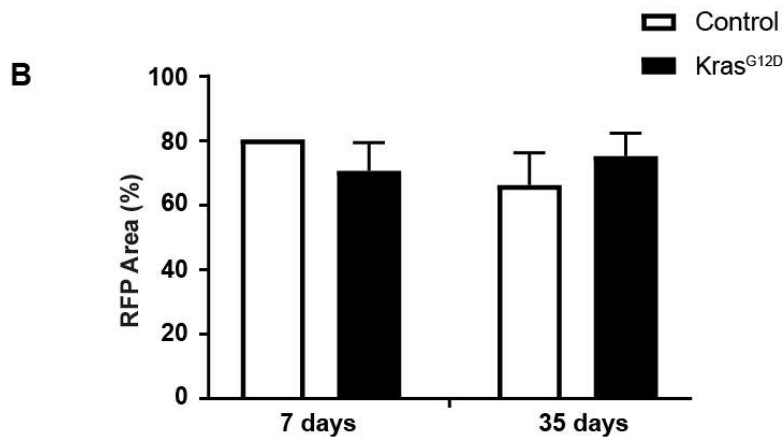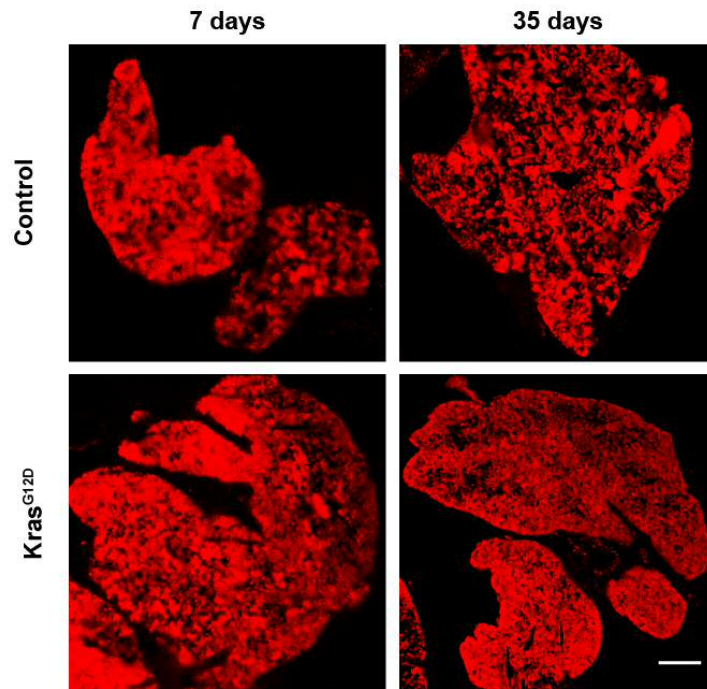
Figure 3.4: Area of RFP is unchanged over time in high dose. To examine the requirement of heterotypic interactions between normal and mutant cells for the decrease in RFP area widespread recombination was induced using a high dose of tamoxifen. KC (*Pdx1-Cre; Rosa26^tdRFP; Kras^G12D*) and control mice (*Pdx1-Cre; Rosa26^tdRFP*) were injected with 1 injection of 9 mg/40 g every other day for a total of 3 injections and tissue harvested at 7 and 35 days post-induction. (A) Representative images of cryosections of whole tissue slices imaged as a tile-scan. (B) Quantification of RFP area demonstrates no significant change in control (hite bars) or KC mice (black bars) between 7 and 35 dpi. At 35 dpi the area of Kras mutant cells is similar to RFP labelled Kras WT cells suggesting that mutant cell area does not decrease when Kras cells at present at high numbers. Statistical analysis was carried using Welch's two-tailed *t*-test. Data represents mean ± s.d. n = 3 biological replicates except for control 7 days where n = 1. Scale bar, 500 μm

3.2.5 Elimination of sporadic Kras^{G12D} cells from normal tissues requires EphA2

Previously, we have demonstrated that cells expressing oncogenic Ras are detected by normal neighbours by elevated EphA2 in mutant cells (Porazinski et al., 2016). Cell-cell interactions between normal and Ras-transformed cells triggers EphA2 signalling in mutant cells. This leads to repulsion and extrusion of Ras-transformed cells from non-transformed monolayers. It follows that the EphA2 signalling could be driving the decrease in RFP area of Kras^{G12D} cells in the pancreas by elimination.

To investigate if EphA2 signalling is required for the loss of Kras^{G12D} cells, the KC model was crossed onto animals expressing an inactive form of EphA2 (Brantley-Sieders, 2004), generating *Pdx1-Cre^{ERT}; LSL-Kras$^{G12D/+}$; Rosa26$^{LSL-RFP}$; EphA2^{tm1Jrui}*, referred to from now on as KC-Eph. This model uses an in-frame translation stop-codon inserted into exon 5 (Shi et al., 2012), that renders the absence of a full length or truncated protein (Amato et al., 2016), similar to a null. Controls for this cohort included *Pdx1-Cre^{ERT}; Rosa26$^{LSL-RFP}$; EphA2^{tm1Jrui}* and will be referred to as RFP-Eph. To explore whether functional EphA2 is required for the decrease in RFP area, animals were induced at 6-8 weeks of age and harvested 7 and 35 days later.

First it was necessary to investigate whether EphA2 deficiency altered the induction level by tamoxifen injection, by analysing RFP area at 7 dpi in RFP-Eph controls. Quantification of RFP percentage area at 7 dpi in RFP-Eph controls showed a similar level of recombination to KC and control mice (Figure 3.5B). There was no significant difference in RFP area at 7 days post-induction between control and RFP-Eph (Control = 20.8 % ± 1.8 Vs. RFP-Eph = 29.1 % ± 11.6 Welch's unpaired *t*-test, p = 0.1928). This suggests that EphA2-deficiency does not alter initial levels of induction and demonstrates that at 7 dpi this EphA2-deficient mouse model is comparable with the KC model allowing direct comparison at later time points.

Next, RFP-Eph mice were used to investigate the effect of loss of functional EphA2 on RFP over time. At 35 dpi it was found that the area of RFP was 24.0 % ± 3.2 (Figure 3.5A, C). There was no significant difference between

control and RFP-Eph in this model at 35 days post-induction (Control = 24.6 % ± 1.8 Vs. RFP-Eph = 24.0 ± 3.2, Welch's unpaired t-test, p =0.71). Furthermore, there is no significant change in RFP area over time in RFP-Eph mice (7 days = 29.1 % ± 11.6 Vs. 35 days = 23.98 % ± 3.2, Welch's unpaired t-test, p = 0.3910). Together, these data show that EphA2-deficiency alone does not alter RFP area over time following induction with low dose tamoxifen.

Having established that EphA2-deficiency had no effect on RFP area in controls, the functional requirement of EphA2 in elimination of $Kras^{G12D}$ cells in KC mice could be studied. Analysis of RFP area at 7 dpi showed that the percentage area of RFP was not significantly different to controls at the same time point (Control = 20.8 % ± 3.7 $Pdx1$-Cre^{ERT}; KC-Eph= 32.9 % ± 15.5, Welch's unpaired t-test, p = 0.216). This indicates that induction levels are similar at early time-points. The loss of mutant cells over time was then investigated in the KC-Eph model. At 35 dpi it was observed that there was significantly more RFP in KC-Eph then KC mice (KC-Eph = 23.12 % ± 1.34 Vs. KC = 8.5 % ± 3, Welch's unpaired t-test, p = <0.0001). Moreover, the area of $Kras^{G12D}$ cells returned to similar levels as controls suggesting that EphA2-deficiency is sufficient to completely rescue loss of RFP within the context of normal neighbours.

In conclusion, these data indicate that functional EphA2 is required for the loss of RFP when labelling $Kras^{G12D}$ cells surrounded by normal neighbours *in vivo* which could infer that EphA2-deficiency leads to retention of mutant cells.
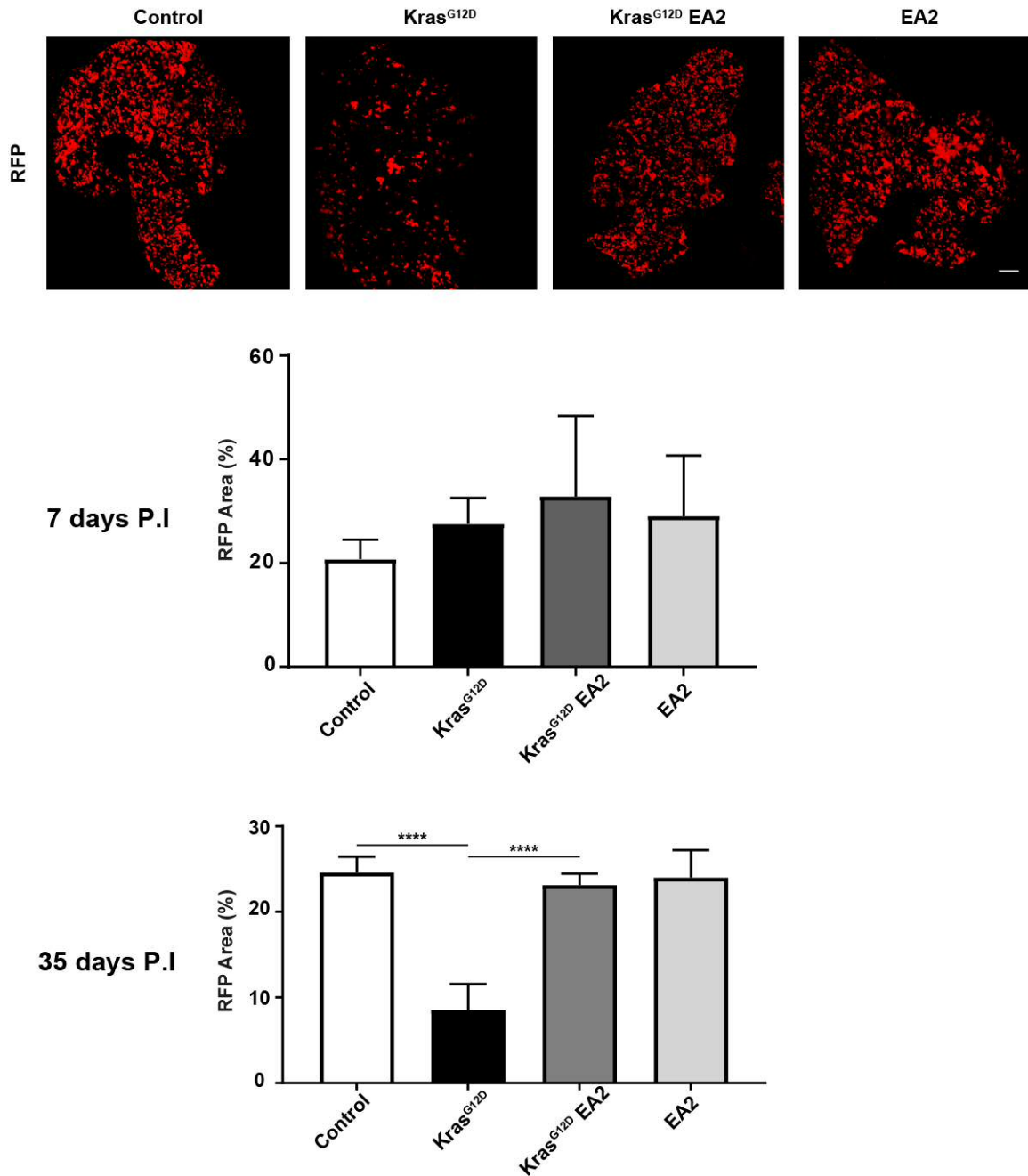
Figure 3.5: Loss of RFP area at low dose requires functional EphA2 *in vivo*.
(A) Representative images of RFP from tile scans of whole tissue sections at 35
dpi. of control (*Pdx1-Cre^{ERT}; Rosa26^{LSL-RFP}*), Kras^{G12D} (*Pdx1-Cre^{ERT}; LSL-
KrasG12D; Rosa26^{LSL-RFP}*), Kras^{G12D} EA2 (*Pdx1-Cre^{ERT}; LSL-KrasG12D;
Rosa26^{LSL-RFP}; EphA2^{tm1Jrui}*) and EA2 (*Pdx1-Cre^{ERT}; Rosa26^{LSL-RFP}; EphA2^{tm1Jrui}*)
mice. (B) Quantification of RFP percentage area at 7 days post induction shows
similar levels of recombination between Kras EA2 and controls. Loss of functional
EphA2 also had no effect on RFP area over time with EA2 (*Pdx1-Cre^{ERT};
Rosa26^{LSL-RFP}; EphA2^{tm1Jrui}*) comparable to controls. (C) At 35 days post-induction
there is no significant difference between Kras EA2 and controls. However, EphA2-
deficiency leads to a significant increase in RFP area compared to Kras^{G12D} cells
and a return to levels similar to controls. Statistical comparison was carried out
using Welch's unpaired *t*-test. Data represent mean ± s.d. with n = 4-6 biological
replicates. P < 0.0001 = ****. Scale bar, 500 μm.

3.2.6 Clusters of *Kras^{G12D}* expressing cells are eliminated from normal pancreatic tissue

Characterising RFP levels in the tissue provides a global view of changes to labelled cells however it does not provide information on RFP cluster dynamics. Clusters can undergo dynamic changes such as merging, splitting and/or elimination. Moreover, RFP percentage area considers both number and size of individual cells and so to gain insight into these dynamic changes individual clusters were defined and treated discretely (Figure 3.6A). As the loss of RFP was only observed in the low dose this was the focus of this analysis.

Using the same tile-scans used for RFP area analysis, segmentation and quantification of clusters was carried out for KC and control animals. The data were then visualised using a boxplot to observe the distribution of $Kras^{G12D}$ cluster sizes over time and compared to control (Figure 3.6B). In control mice at 7 dpi the median was 1263 μm^2 with 25% percentile and 75% percentile 466 μm^2 and 3487 μm^2 respectively, with an interquartile range (IQR) of 3021 μm^2. There is no significant change in the distribution of cluster sizes in control mice between 7 and 35 dpi (p = 0.11, Mann-Whitney *t*-test). This suggests that over time the distribution of Kras wild type clusters is similar. Next, the clusters from KC animals were analysed (Figure 3.6B). Direct comparison between control and KC mice at 35 days could not be carried out as cluster distributions are significantly different at 7 dpi (p = <0.0001, Mann Whitney *t*-test). This could be a result of difference in the induction profile between animal models or indicate dynamic changes to Kras^{G12D} clusters have occurred by 7 days. At 35 dpi a significant increase in the distribution of Kras^{G12D} cluster sizes was observed (p = <0.0001, Mann Whitney *t*-test). This has resulted in a 39% increase in the median mutant cluster size in KC mice between 7 days (1051 μm^2) and 35 dpi (1710 μm^2). When compared to the stable cluster distribution over time observed in control mice this suggests a dynamic shift towards an increase in the size distribution of Kras^{G12D} clusters.

To characterise further the changes to *Kras^{G12D}* clusters over time, the total number of clusters was calculated for each biological replicate and normalised to area (Figure 3.6C). This provided an overview of how the number of clusters was changing over time. At 7 dpi it was found that the density of

clusters induced was similar in KC and control animals (Control = 37.5 mm^{-2} ± 5.6 Vs. KC = 31.3 mm^{-2} ± 5.4). Over time in controls, no significant change in the number of Kras wild-type clusters was observed (7 days = 37.5 mm^{-2} ± 5.6 Vs. 35 days = 44.3 mm^{-2} ± 10.0, Welch's unpaired t-test, p =0.2314). A significant decrease in clusters was observed between KC and control animals at 35 dpi (Control = 44.4 mm^{-2} ± 10.0 Vs. KC = 18.1 mm^{-2} ± 5.7, Welch's unpaired t-test, p = 0.0072). In addition, there was a significant decrease in the number of *Kras^{G12D}* clusters over time (7 days = 31.3 mm^{-2} ± 5.4 Vs. 35 days = 18.1 mm^{-2} ± 5.8, Welch's unpaired t-test, p = 0.0252). This suggests approximately 43% of mutant clusters are lost within this time frame.

Together, these results demonstrate that clusters of Kras^{G12D} cells are eliminated from normal pancreatic tissue over time. Moreover, dynamic changes appear to be occurring to clusters leading to an increase in the size distribution of Kras^{G12D} clusters over time. These data provide insight into changes to Kras^{G12D} clusters at the level of the tissue over time.
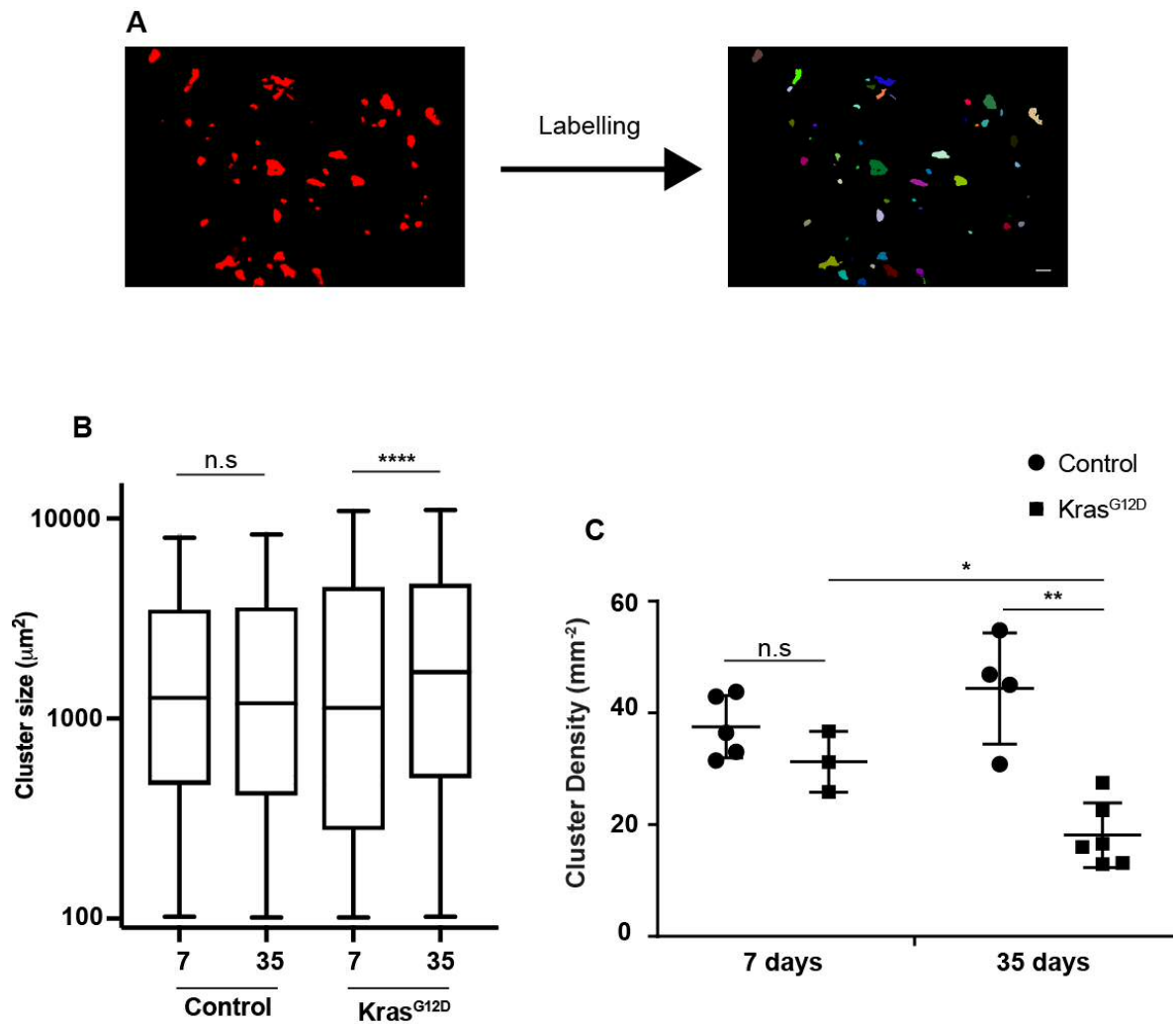
Figure 3.6: Cluster analysis indicates that clusters of *Kras^{G12D}* cells are lost *in vivo*.
(A) Method of segmentation of RFP clusters resulting in labelling and quantification of individual cluster. (B) Tukey-style boxplot showing distribution of clusters in control (*Pdx1-Cre^{ERT}; Rosa26^{LSL-RFP}*) at 7 dpi (n= 17892 clusters) and 35 dpi (n = 12967 clusters) and Kras^{G12D} (*Pdx1-Cre^{ERT}; LSL-Kras^{G12D}; Rosa26^{LSL-RFP}*) at 7 dpi (n = 15263 clusters) and 35 dpi. (n = 6089 clusters). There is no significant difference between control cluster distributions over time (p = 0.11, Mann-Whitney test). There is a significant increase in the size of Kras^{G12D} clusters (p=<0.0001, Mann-Whitney test). ≥4 mice for each time point and genotype were analysed in B. Line across box is median. Box boundaries indicate 25th and 75th percentile. Whiskers indicate 1st and 99th percentiles. (C) There is no significant difference in density of clusters at 7 dpi between control (circles) and Kras^{G12D} clusters (squares). There is a significant decrease in the density of Kras^{G12D} clusters at 35 days compared to 7 days. There is also significantly less clusters at 35 days in KC compared to control mice. Cluster density was compared using Welch's unpaired *t*-test. Each point represents a biological replicate with horizontal line depicting mean ± s.d. P <0.05 = *, P<0.01 = **. Scale bar, 500 μm.

3.2.7 Cluster size dependent changes to *Kras*^{G12D} mutant clusters *in vivo*

Previously, within this chapter I have demonstrated that the area of Kras^{G12D} cells decreases over time, and this is accompanied by a decrease in the number of mutant clusters indicating that changes to the size of mutant clusters may be occurring. Understanding changes to clusters of specific sizes could help elucidate the mechanism by which transformed cells are being lost in the pancreas. Furthermore, previous work using *Drosophila* and *in silico* models of extrusion has demonstrated that the size of an aberrant cluster impacts its fate (Bielmeier et al., 2016), with the mechanical force generated from heterotypic interactions sufficient to extrude small mutant clusters but not larger clusters. In larger clusters of mutant cells competition-dependent apoptosis can even promote tumourigenesis (Ballesteros-Arias et al., 2014).

To investigate how the distribution of Kras^{G12D} clusters was changing over time the density of clusters was broken down by cluster size. Previous studies have used this to understand changes to specific cluster sizes over time and a loss of small clusters (Bielmeier et al., 2016). Attempts at identifying nuclei whilst retaining endogenous RFP signal proved technically challenging and so individual cells were not able to be counted in clusters. Thus, size of cluster was used as a readout. This was done for each biological replicate with cluster sizes binned every 200 μm^2 as this is the approximate size of a normal acinar cell (Houbracken and Bouwens, 2017); with the mean and standard deviation plotted at the centre of each bin. The x-axis was cropped at a point where all samples had reached a plateau to improve clarity of visualisation.

First, it was necessary to examine labelled Kras wild-type clusters to observe how these change over time *in vivo*. As expected with stochastic labelling of cells, as the cluster size increases the frequency of that cluster decreases; smaller clusters are more frequent than larger clusters (Figure 3.7A). In control animals, the density of clusters of different sizes was observed to be similar between 7 and 35 days post-induction. This supports the distribution of cluster sizes observed in Figure 3.6. However, a slight increase in the number of small clusters (<1000 μm^2) was observed in control mice over time. Overall, this suggests that labelled Kras wild-type clusters are relatively unchanged during this timeframe.

Next, the distribution of RFP labelled *Kras*^{G12D} clusters of different sizes was examined over time. The number of small clusters decreased between 7 and 35 dpi in KC mice (Figure 3.7B). A significant decrease was observed for the cluster bin 200 μm^2 (Welch's *t*-test, p = 0.0051), with a trend to decreasing density of clusters <600 μm^2. Whereas the density of larger clusters (>600 μm^2) at the later time point is comparable to 7 dpi. This suggests that small Kras^{G12D} clusters are lost *in vivo* over time. This could explain the increased size of Kras^{G12D} clusters, when comparing distributions, observed in Figure 3.6. This suggests that small clusters of Kras^{G12D} cells are being eliminated from normal pancreatic tissue *in vivo*.

As individual clusters were not traced over time it is also necessary to compare control (*Pdx1-Cre*^{ERT}; *Rosa26*$^{LSL-RFP}$) with KC animals at 35 days post-induction. The distribution of KC and controls at 35 dpi can be directly compared because the distribution of clusters is similar at 7 dpi (Figure 3.7C), although KC animals appeared to have slightly more clusters <500 μm^2 at this time point. Examining KC and control at 35 dpi it appears that the number of *Kras*^{G12D} clusters of all comparable sizes is decreased. A significant decrease in the density of most cluster sizes up to and including 4400 μm^2 was observed between control and KC mice (Table 3.1). This is in contrast to comparing KC animals over time which suggested that only small clusters are decreased. Together, these data provide evidence that cluster size may have an impact on the fate of a cluster with small clusters of Kras^{G12D} cells preferentially lost from tissues. Although dynamic changes to larger cluster cannot be ruled out, this work provides further insight into size-dependent changes to Kras^{G12D} clusters over time and identifies a possible threshold size below which mutant cluster are eliminated by normal tissue.
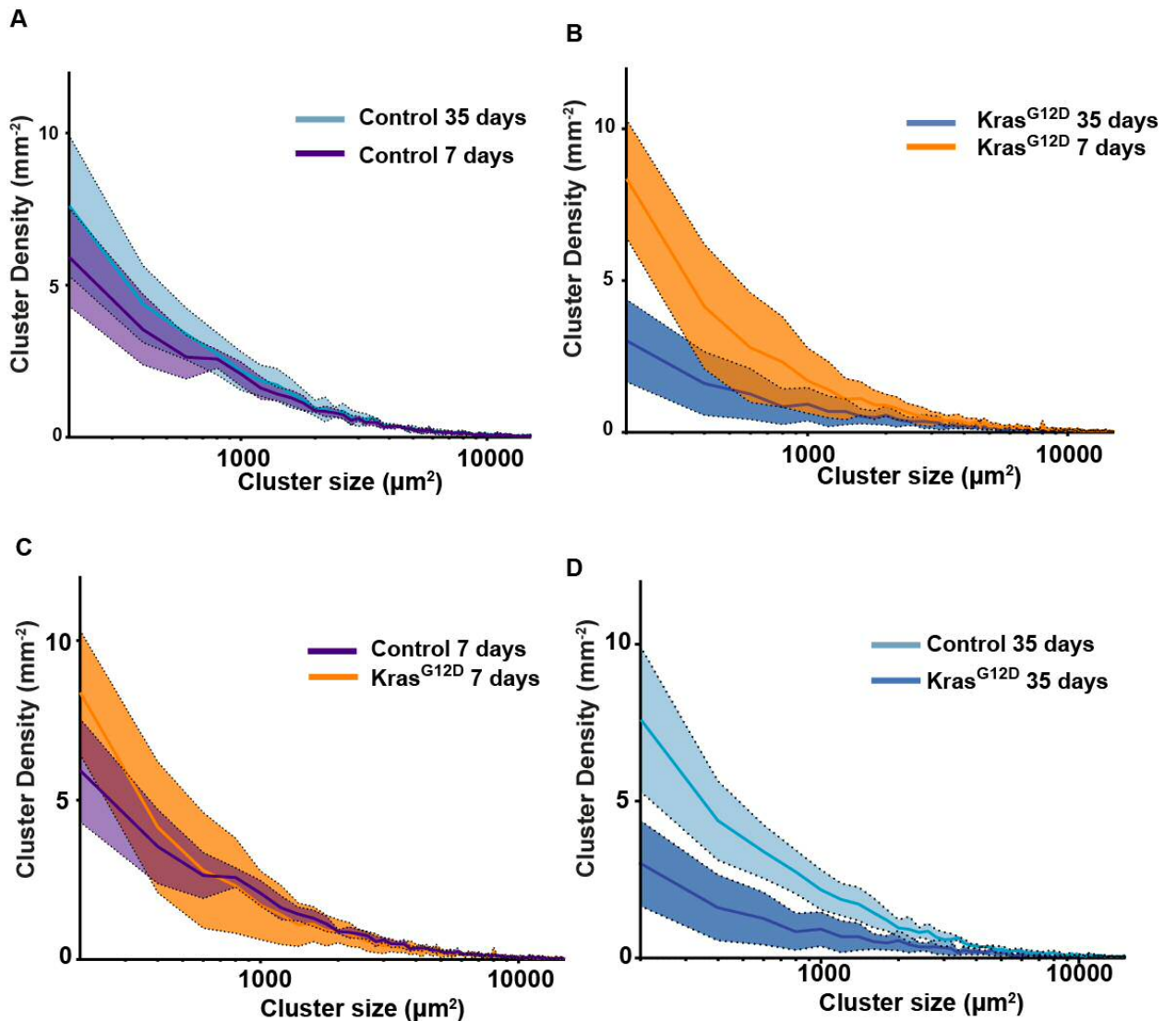
Figure 3.7: Small clusters of *Kras^{G12D}* cells are preferentially eliminated *in vivo* when surrounded by normal neighbours. Frequency distribution graphs of different cluster sizes. (A) The distribution of *Kras* WT control (*Pdx1-Cre^{ERT}; Rosa26^{LSL-RFP}*) clusters is similar at 7 and 35 days post induction. (B) The density of small *Kras^{G12D}* clusters (<600 μm^2) decreased between 7 and 35 dpi in Kras^{G12D} (*Pdx1-Cre^{ERT}; LSL-KrasG12D; Rosa26^{LSL-RFP}*) with a similar number of larger clusters present at these two time points. (C) The frequency of clusters of different sizes is similar between control and Kras at 7 days post induction. Shown for clarity (D) The density of *Kras^{G12D}* clusters of all sizes is lower at 35 dpi when compared to control at the same time point. Data represents mean ± s.d. (shaded area) from 4-6 biological replicates.

Cluster size (μm2)	p-value Control 35 days Vs. Kras^{G12D} 35 days	Fold change	Control clusters analysed (n=4)	Kras^{G12D} clusters analysed (n=4)
200	0.0095	2.5	2190	1035
400	0.0121	2.7	1303	478
600	0.0067	2.7	991	378
800	0.0044	3.3	805	269
1000	0.0381	2.4	637	278
1200	0.01	2.7	554	202
1400	0.0194	2.5	516	214
1600	0.019	2.7	435	183
1800	0.0144	2.5	357	164
2000	0.0357	1.7	284	170
2200	0.0907	2.1	286	135
2400	0.0095	2.3	228	120
2600	0.0217	2.4	257	122
2800	0.0317	1.9	200	106
3000	0.1251	1.8	178	103
3200	0.0628	1.9	168	93
3400	0.0095	3.8	176	79
3600	0.0337	1.9	140	79
3800	0.0011	2.1	116	68
4000	0.0272	1.8	109	79
4200	0.0003	2.0	99	63
4400	0.0008	2.2	98	62
4600	0.4276	1.2	90	77
4800	0.2399	1.6	80	67
5000	0.0879	1.8	85	61
5200	0.2974	1.4	77	60

Table 3.1: Table of p-values for comparing control and KC at 35 days. Table listing p-values calculated to test for statistical difference in relative loss RFP clusters per cluster size bin utilising either a Welch's unpaired *t*-test or a Mann-Whitney *t*-test. Red = p-value <0.05. The analysis suggests *Kras^{G12D}* expressing clusters of less than 4600 μm^2 are significantly under-represented in the data set.

3.2.8 Characterising the effects of EphA2-deficiency on mutant and normal clusters over time

As clusters of *Kras*^{G12D} cells are eliminated and as EphA2 is required for the decrease in RFP area *in vivo* the requirement of EphA2 for the elimination of mutant clusters was investigated.

First it was necessary to establish whether loss of functional EphA2 affects RFP cluster density over time (Figure 3.8A). As expected, in the RFP-Eph model RFP clusters occur at a similar density to controls at 7 dpi (RFP-Eph = 38.3 mm^{-2} ± 12.76 Vs. Control = 37.5 mm^{-2} ± 5.6). The loss of functional EphA2 also did not result in changes to the number of clusters over time in RFP-Eph mice (7 days = 38.3 mm^{-2} Vs. 35 days = 36.2 mm^{-2} ± 11.0). Furthermore, the distribution of clusters of different sizes in RFP-Eph mice is similar at 7 and 35 dpi (Figure 3.9A). In summary, this suggests that loss of EphA2 alone does not lead to changes to total number of clusters or clusters of a specific size.

Next the effect of EphA2-deficiency on Kras^{G12D} clusters was investigated. At 7 dpi, the density of Kras^{G12D} clusters in KC-Eph mice was similar to controls and KC (Figure 3.8A). However, at 35 dpi significantly more RFP clusters were observed in KC-Eph mice compared to KC (KC = 18.1 mm^{-2} ± 5.8 Vs. KC-Eph = 44.3 mm^{-2} ± 11.8, Welch's unpaired *t*-test, p = 0.0048). This suggests that loss of functional EphA2 is required for the observed decrease in clusters. As the density of clusters in KC-Eph animals not only increased but returned to similar levels as controls this suggests that EphA2-deficiency inhibits Kras^{G12D} cell loss and is sufficient to completely abrogate the loss of Kras^{G12D} clusters.

Following this the density of clusters was broken down by cluster size to further elucidate the effect of EphA2-deficiency on Kras^{G12D} clusters. This demonstrated that in EphA2-deficient animals the density of Kras^{G12D} clusters of all sizes was similar over time (Figure 3.9B). Analysis of individual cluster sizes up to 5000 μm^2 showed no significant change in density between 7 and 35 dpi (Welch's *t*-test and Mann-Whitney test, all p >0.05). Moreover, a significant increase in Kras^{G12D} clusters up to 4200 μm^2 in size was observed KC-Eph mice when compared with KC mice (Table 3.2). This supports the hypothesis that EphA2-deficiency leads to the retention of clusters of Kras^{G12D} cells up to 4200 μm^2. Not only was a significant increase in the density of clusters <4200 μm^2

observed but the density in an EphA2-deficient model returned to a similar level as controls (Figure 3.9C), with no significant difference between the density of clusters up to 5000 μm^2 in KC-Eph mice compared with Kras wild-type control.

In summary, EphA2-deficiency alone does not alter the distribution of clusters of different sizes over time. However, EphA2-deficiency leads to a significant increase in the number of Kras^{G12D} clusters present at 35 dpi up to 4200 μm^2 in size. Furthermore, the number of clusters in KC-Eph mice at 35 dpi is similarto *Kras* wild-type controls. This suggests a size threshold of around 4400 μm^2 below which Kras^{G12D} clusters surrounded by normal neighbours are preferentially lost in an EphA2-dependent manner.
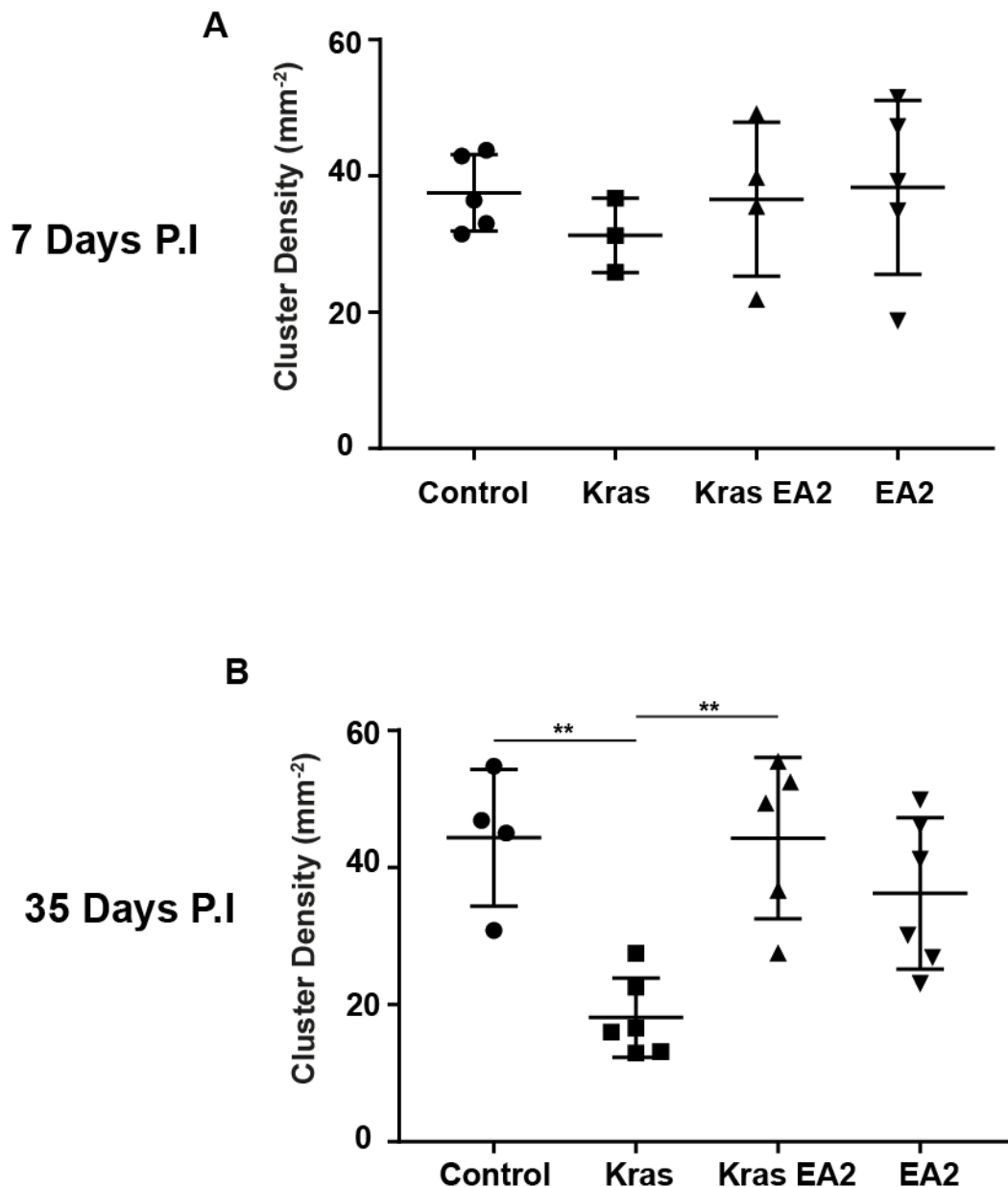
Figure 3.8: EphA2 is required for the elimination of mutant clusters within the context of a normal epithelium. (A) At 7 dpi there is no significant difference in cluster density between control (*Pdx1-Cre^ERT^; Rosa26^LSL-RFP^*, n = 17892 clusters), Kras^G12D^ (*Pdx1-Cre^ERT^; LSL-KrasG12D; Rosa26^LSL-RFP^*, n = 15263 clusters) Kras^G12D^;EA2 (*Pdx1-Cre^ERT^; LSL-KrasG12D; Rosa26^LSL-RFP^; EphA2^tm1Jrui^*,n = 13422 clusters) and EA2 (*Pdx1-Cre^ERT^; Rosa26^LSL-RFP^; EphA2^tm1Jrui^*,n = 16942 clusters). This allows direct comparison of later time points between genotypes. (B) After 35 dpi the number of Kras WT clusters on a background of EphA2-defiency (EA2) is not significantly different to control or Kras^G12D^; EA2. There are significantly more Kras^G12D^ clusters in EphA2-deficient mice at 35 dpi. than KC mice. With the number of clusters in Kras EA2 similar to control this suggests loss of EphA2 completely inhibits normal neighbour driven elimination. Data represents mean ± s.d. with each point representing a biological replicate. Cluster density was compared using Welch's unpaired *t*-test. P<0.001 = **
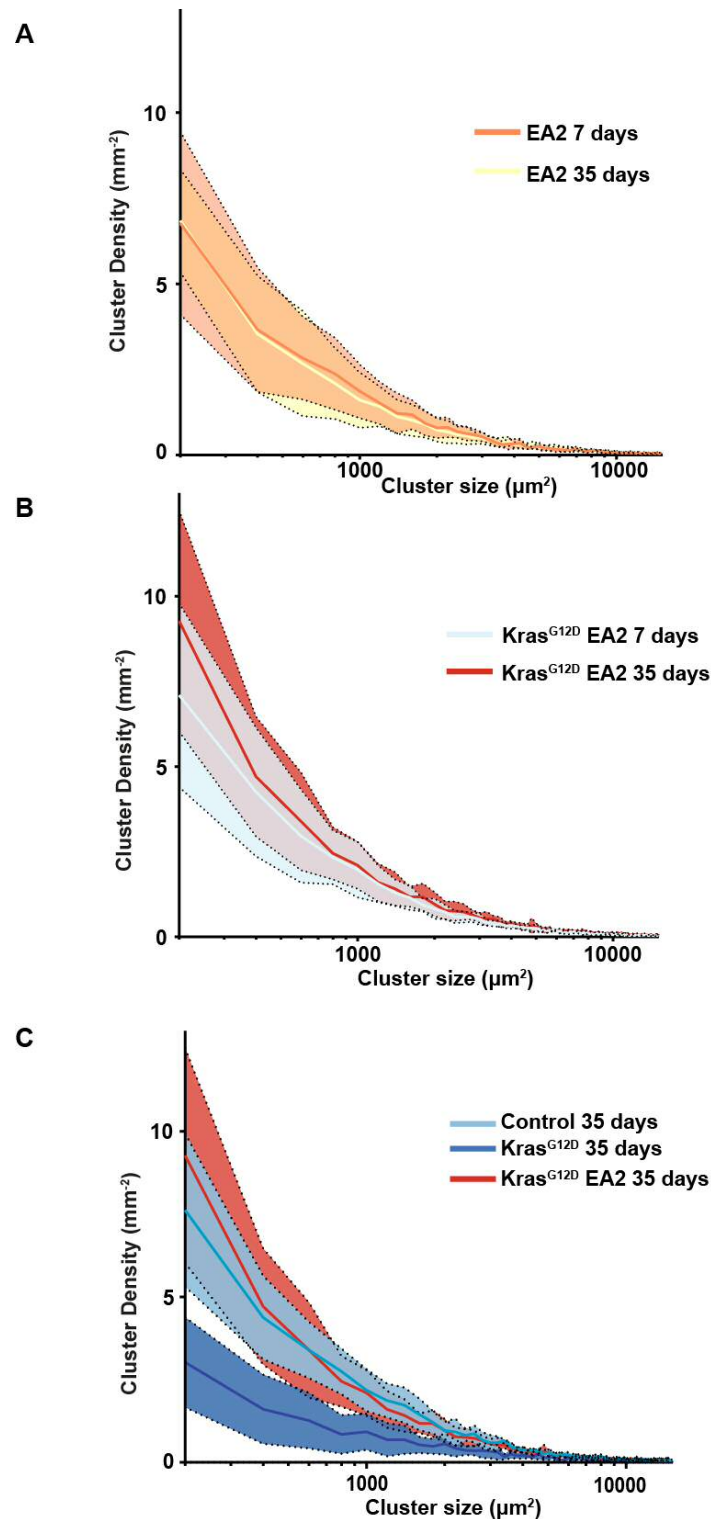
Figure 3.9: Elimination of small clusters of *Kras^G12D* cells requires EphA2 *in vivo*.
(A) The distribution of Kras WT clusters in a model of EphA2 loss of function, EphA2 (*Pdx1-Cre^ERT; Rosa26^LSL-RFP; EphA2^tm1Jrui*), remains relatively changed between 7 (n=16942 clusters) and 35 dpi (n=23305). (B) The density of *Kras^G12D* clusters on a EphA2 LOF background, Kras^G12D EphA2 (*Pdx1-Cre^ERT; LSL-KrasG12D; Rosa26^LSL-RFP; EphA2^tm1Jrui*) was also similar at 7 (n=13422 clusters) and 35 dpi. (n=18402 clusters). (C) Kras^G12D clusters in EphA2-deficient mice appear at similar levels to Kras WT controls (n=12967 clusters) at the same time point, suggesting EphA2 is required for the elimination of small clusters from the pancreas. Data represents mean ± s.d. (shaded area) from 4-6 biological replicates.

Cluster size (mm2)	p-value Kras EA2 35 days Vs. KrasG12D 35 days	Fold change	KrasG12D clusters analysed (n=4)	KrasG12D EA2 clusters analysed (n=5)
200	0.0094	3.1	1035	3686
400	0.0125	2.9	478	1951
600	0.0254	2.7	378	1462
800	0.0057	2.9	269	1053
1000	0.016	2.3	278	897
1200	0.0211	2.3	202	687
1400	0.0313	2.1	214	604
1600	0.0047	2.2	183	503
1800	0.0133	2.4	164	494
2000	0.0823	1.7	170	408
2200	0.0603	1.8	135	334
2400	0.0303	2.1	120	331
2600	0.0168	2.1	122	317
2800	0.0318	1.8	106	274
3000	0.069	1.7	103	226
3200	0.139	1.7	93	227
3400	0.0043	3.1	79	218
3600	0.0766	1.7	79	183
3800	0.0041	1.9	68	157
4000	0.0138	1.8	79	161
4200	0.0091	1.8	63	143
4400	0.0584	1.8	62	134
4600	0.7836	1.1	77	121
4800	0.2017	2.0	67	123
5000	0.0643	1.9	61	131
5200	0.2931	1.3	60	105

Table 3.2: Table of p-values for EphA2-deficient and KC mice at 35 dpi. Table listing p-values calculated to test for statistical difference in relative loss RFP clusters per cluster size bin utilising either a Welch's unpaired *t*-test or a Mann-Whitney *t*-test. Red = p-value <0.05. The analysis suggests *Kras*[G12D] expressing clusters of less than 4600 μm^2 are significantly increased in an EphA2-deficient model in the data set.

3.2.9 Tissue-wide homeostasis is unaltered by mosaic $Kras^{G12D}$ expression

Homeostasis of a tissue can lead to several population changes which would alter the dynamics of RFP area and cluster distribution. For example, proliferation and apoptosis of RFP positive tissue can lead to increased or decreased cluster size respectively. Moreover, labelling of a stem cell pool can lead to neutral drift and clone expansion or loss (Lopez-Garcia et al., 2010; Snippert et al., 2010).

To elucidate tissue homeostasis of the pancreas, tissue-wide changes in proliferation and apoptosis were examined using the cell specific markers Ki67 (Scholzen and Gerdes, 2000) and cleaved caspase 3 (CC3)(Kujoth et al., 2005) respectively. Staining and counting was carried out by Dr. Andreas Zaragkoulias, a Postdoctoral research associate in the lab after I had generated the tissue. Cohorts of mice at 6 - 8 weeks of age were injected with 1 ug of tamoxifen and pancreas harvested at 7 and 35 days post-induction and analysed by immunohistochemistry (Figure 3.10). The limitation of the assay was the technical inability to co-localise RFP with homeostasis specific markers, therefore whole tissue sections were quantified. At 7 dpi there was no significant difference between the number of Ki67 positive cells in KC and controls (Control = 71.1 mm^{-2} ±11.8 Vs. KC = 79.0 mm^{-2} ± 16.8, Welch's unpaired t-test, p= 0.84). This suggests at 7 dpi proliferation is similar in Kras^{G12D} expressing mosaic tissues and Kras wild-type controls. Moreover, at 35 dpi the density of Ki67 positive nuclei is no significantly different (Control = 26.7 mm^{-2} ± 3.7 Vs. KC = 25.5 mm^{-2} ± 12.8, Welch's unpaired t-test, p= 0.87). However, a significant decrease occurs between 7 and 35 dpi in both Kras wild-type control (7 days = 71.1 mm^{-2} ± 11.8 Vs 35 days = 26.7 mm^{-2} ± 3.7, Welch's unpaired t-test, p= 0.0032) and KC mice (7 days = 79.0 mm^{-2} ± 16.8 Vs 35 days = 25.5 mm^{-2} ± 12.8, Welch's unpaired t-test p=0.0018). Although this suggests that proliferation decreases between 7 and 35 dpi in both experimental and control; the level of proliferation is similar between control and KC mice at both time points. This suggests that proliferation of tissue is unchanged by expression of $Kras^{G12D}$.

In cell competition, a number of studies have demonstrated that loser cells undergo apoptosis and are eliminated from epithelial tissues (Amoyel et al., 2014;

Clavería et al., 2013; Moreno et al., 2002; Norman et al., 2012; Wagstaff et al., 2016). Moreover, the dynamics of RFP clusters can be altered by differential apoptosis between tissues. However, analysis of the apoptotic marker CC3 demonstrated a similar number of apoptotic cells in KC mice and controls at both time points. No significant change to the number of CC3 positive nuclei was found between control and KC mice at 7 (Control = 1.46 mm^{-2} ±0.19 Vs. KC = 1.24 mm^{-2} ±0.54, Mann Whitney test p = 0.1667) or 35 dpi (Control = 1.07 mm^{-2} ± 0.44 Vs. 1.08 mm^{-2} ± 0.23, Welch's unpaired *t*-test p = 0.9679). This suggests that the rate of apoptosis is unchanged in tissues by expression of *Kras^{G12D}* in tissues. Furthermore, the density of apoptotic cells is unaltered over time. Although it can not be ruled out that Ras-transformed cells undergo apoptosis and are eliminated before 35 dpi, by which point levels of apoptosis returns to normal. These data suggest that apoptosis is not driving the loss RFP and hence Kras^{G12D} mutant cells from the pancreas over time. This suggests cell competition is not inducing apoptosis of loser cell and compensatory proliferation of winner cells is not occurring.
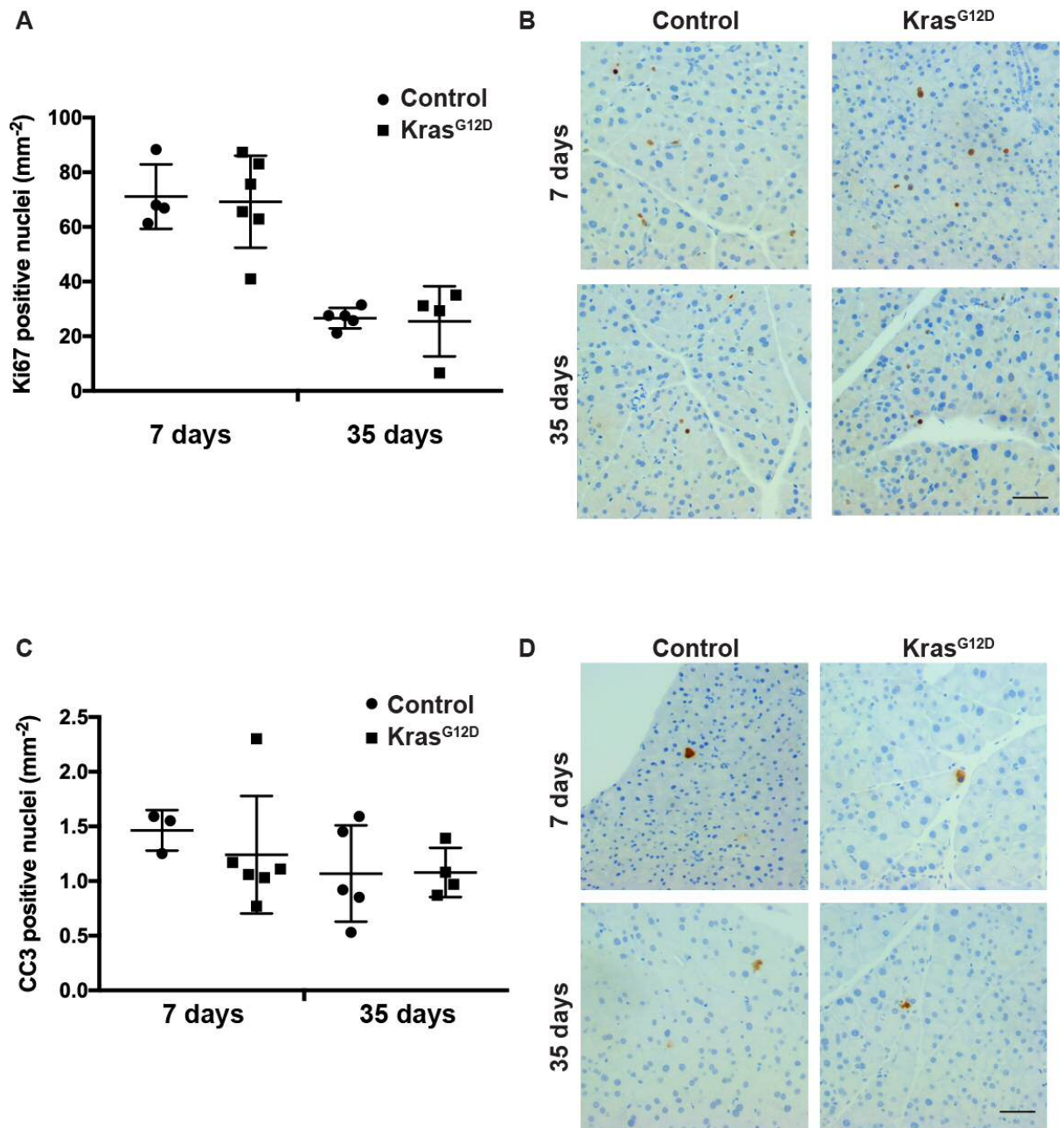
Figure 3.10: Homeostasis is unperturbed during Kras^G12D cell elimination. Immunohistochemistry for proliferation (Ki67) and apoptosis by Cleaved Caspase 3 (CC3) in control (*Pdx1-Cre;Rosa26^LSL-RFP*) and Kras^G12D (*Pdx1-Cre;Rosa26^LSL-RFP*; *Kras^G12D*). Levels of Ki67 were not significantly different between control and Kras^G12D mice at 7 and 35 dpi although a decrease was observed over time in both conditions (A, B). Levels of CC3 were not significantly different between control and Kras^G12D mice at either time point (C, D). Moreover, CC3 did not significantly change over time in control or Kras^G12D mice. Data represents mean ± s.d. with each point a biological replicate. Scale bar, 50 μm.

3.3 Discussion

A number of studies have investigated the interaction of normal and Ras mutant cells *in vitro*. In MDCK cell lines, Hogan *et al.* (2009) demonstrated that Ras^{V12}-transformed cells surrounded by normal epithelia cells are apically extruded from a monolayer. When Ras^{V12} cells are cultured alone apical extrusion does not occur suggesting that normal neighbours are required. More recently, we have demonstrated that differential EphA2 signalling between normal and mutant cells promotes the detection and elimination of Ras^{V12} cells (Porazinski et al., 2016). Differential EphA2 expression between normal and mutant cells triggers repulsion between normal:mutant cells and increased contractility of Ras^{V12} cells. Mutations to *Kras* are sufficient to drive the earliest stages and are considered the initial mutation in pancreatic cancer (Collisson et al., 2012; Hingorani et al., 2003; Kopp et al., 2012) Recent studies have suggested that Ras mutant cells can be extruded *in vivo* (Kon et al., 2017; Sasaki et al., 2018). Moreover, cell competition is typically studied in developing or rapid turnover tissues (Amoyel et al., 2014; Bowling et al., 2018; Moreno et al., 2002) using constitutive activation of oncogenic *Hras* (Ras^{V12}) (Hogan et al., 2009; Kajita et al., 2014).. However, whether cell competition is occurring between normal and Ras-transformed pancreatic cells is unclear. Therefore, this study aimed to characterise the effect of mosaic *Kras*^{G12D} expression in the adult pancreas, which is a slow turnover tissue (Magami et al., 2002).

3.3.1 Modelling heterotypic cell-cell interactions in the murine pancreas *in vivo*

Animal models of pancreatic cancer have provided new insight into disease initiation and progression. In this study, the *Pdx1-Cre*^{ERT}; *Rosa26*^{tdRFP}; *Kras*$^{G12D/+}$ (KC) mouse model was used to provide temporal and spatial control over expression of oncogenic Kras in the adult pancreas and trace transformed cells using an RFP reporter. By titrating the level of tamoxifen, single or small clusters of cells could be induced to express *Kras*^{G12D} and investigate the requirement of heterotypic interactions with non-transformed neighbours in fate of mutant cells. Using genetic mouse models requires careful consideration of a number of factors.

One important consideration for murine models is the timing of *Cre* expression. A previous study has investigated the fate of *Kras^{G12D}* transformed cells from the pancreas using the same promoter (*Pdx1*) without the tamoxifen-sensitive human oestrogen ERT domain (Morton et al., 2010). This results in recombination in every cell of the pancreas from E8.5 and it was observed that GFP positive *Kras^{G12D}* mutant cells were lost 2-6 weeks after birth from the developing pancreas. From this the authors suggested that *Kras^{G12D}* expressing cells are outcompeted by wild-type pancreatic cells via differential cell fitness between the two populations of cells. This suggests that interactions between normal and *Kras^{G12D}* mutant cells could lead to the selective loss of mutant cells but use of an embryonic activation model of PDAC has several limitations. Firstly, the developing pancreas has proliferation rates and a dynamic cellular composition markedly different to the adult pancreas (Grapin-Botton, 2005; Magami et al., 2002). The turnover in the adult pancreas is relatively slow with the half-life of an acinar cell around 132 days (Nakayama et al., 2003). Moreover, expression of *Kras^{G12D}* during the development of the epithelium of other tissues has been reported to cause defects in the adult (Fan et al., 2008). Expression of *Kras^{G12D}* in ovary development was found to block differentiation causing abnormal ovary follicle development and impaired response to hormone in the adult. Finally, human PDAC is an adult-onset malignancy (Gidekel Friedlander et al., 2009) with almost half (47%) of new cases in people aged 75 and over in the UK (Cancer Research UK, 2017). Thus, to better understand the relevance to adult disease, *Kras^{G12D}* expression was induced and studied in adult mice.

Generating tissues mosaic for *Kras^{G12D}* expression is required to understand normal-mutant cell-cell interactions. This can be achieved by controlling the number of pancreatic cells in which Cre recombinase drives recombination at the *LSL-Kras^{G12D}* locus. This level of control can be achieved by fusion of Cre-recombinase with an altered ligand-binding domain for the human oestrogen receptor (Hoess et al., 1984). This results in a Cre^{ERT} construct and a protein that will only enter the nucleus and drive recombination at LoxP sites in the presence of tamoxifen. Therefore, by titrating the amount of tamoxifen delivered to animals the number of cells undergoing recombination can be altered. However, use of the Cre-LoxP system requires careful interpretation and experimental approach. For example, it is not always possible to extrapolate from

one recombination event to another as alleles can have different susceptibilities to Cre-mediated recombination (Liu et al., 2013; Vooijs et al., 2001). To investigate whether RFP recombination was associated with recombination of $Kras^{G12D}$ we used laser capture microdissection to verify that RFP positive tissue only contained cells which had also recombined at the $LSL\text{-}Kras^{G12D}$ allele. This suggests that RFP accurately marks mutant cells in this system.

Another consideration of the Cre-LoxP system is the promoter which drives Cre expression. The use of pancreas-specific Cre driver lines has allowed targeting of the specific compartments and lineages within the pancreas (Magnuson and Osipovich, 2013). In this study, the pancreatic progenitor *Pdx1* gene was used to drive expression of Cre. The *Pdx1* gene is expressed in pre-pancreatic endoderm starting at E8.5 and as development progresses it becomes more abundant in Beta-cells with lower levels in the exocrine compartment (Jonsson et al., 1994; Offield et al., 1996). Thus, during development Pdx1-Cre driver lines can drive recombination in all pancreatic cell types, however, the expression pattern of *Pdx1* in the adult is less clear. Although *Pdx1* is typically associated with the endocrine lineage in adults; in this study recombination also occurred in the acinar compartment and ductal compartment. This suggests that in this mouse model *Pdx1* expression is sufficient in these cell types to produce Cre-recombinase. It is also possible that *Pdx1* marks a subpopulation of adult pancreatic cells. Several studies have indicated that the acinar cell population is heterogeneous (Wollny et al., 2016) and *Pdx1* has been proposed to mark adult stem/progenitor cells (Gidekel Friedlander et al., 2009). However, the high dose in this system was sufficient for recombination in the vast majority of cells. This suggests that *Pdx1* expression is not the limiting factor in selecting which cells recombine and indicates that a subpopulation of *Pdx1* positive cells are not being selected to recombine. In the analysis used within this study it was difficult to distinguish specific cell types within and therefore make conclusions on the different compartments. However, although different cell types were found to be labelled using this promoter acinar cells were mainly considered in RFP analysis as acinar cells make up over 80% of the pancreas and made up the vast majority of labelled cells. Therefore, it was assumed that changes in RFP was a result of changes predominantly from the exocrine acinar compartment, although changes to other cells types cannot be ruled out.

In summary, this study has generated a model to study heterotypic interactions of normal and Kras[G12D] mutant cells in the adult murine pancreas. This model provides both temporal control and control over the amount of tissue-wide recombination within the pancreas.

3.3.2 Kras[G12D] mutant cells are lost in vivo when surrounded by normal neighbours

Once a system of mosaic *Kras[G12D]* expression in the murine pancreas had been established the fate of Kras[G12D] transformed cells could be investigated over time. No significant change to RFP area in low dose Kras wild type controls was observed overtime. However, when RFP-labelled Kras[G12D] cells were present in the pancreas at low numbers a significant decrease in RFP was observed. The human body has evolved a number of defence mechanisms for the removal of aberrant cells (Fuchs and Steller, 2015). In the initiation of pancreatic cancer, a single normal cell acquires an initiating driver gene mutation, however, it is thought that in most cases this initiating mutation causes the cell to undergo apoptosis or senescence, or to be lost owing to immune surveillance or during a bottleneck event of tissue turnover (genetic drift) (Makohon-Moore and Iacobuzio-Donahue, 2016). To investigate if autonomous changes to mutant cells is inducing a decrease in RFP area widespread recombination was induced resulting in around 75% of the pancreas expressing *Kras[G12D]*. With this high level of Ras-transformed cells present in the tissue, between 7 and 35 days post induction, no significant decrease in RFP level was observed. Previous work has also demonstrated that in zebrafish immune cells are recruited to single Ras-transformed cells and can engulf and eliminate the mutant cell (Feng et al., 2010). Ras-transformed cells can also be cleared in murine models by natural killer cells (Johnson et al., 1990). However, as no change in RFP was observed when mutant cells were present at high numbers this suggests the immune system is not the primary method of clearance for Kras[G12D] cells in the pancreas. Indeed, although immune infiltrate is considered to occur early within tumourigenesis they are typically associated with ADM events and PanIN lesions (Liou et al., 2015, 2017). Therefore, this work suggests that Kras[G12D] cells in the pancreas are eliminated by non-transformed epithelial neighbours.

Normal epithelial cells can eliminate mutant neighbours by cell competition (Morata and Ripoll, 1975). The loss of mutant cells from the pancreas could be a result of competitive interactions with normal neighbours. Previous work has also demonstrated that the adult skin can eliminate aberrant cells through a mechanism that uses wild-type neighbours (Brown et al., 2017). Moreover, elimination has been observed in the murine intestine (Kon et al., 2017) and pancreatic ductal compartment (Sasaki et al., 2018). Therefore, these studies support a model of competitive epithelial interactions within the pancreas. However, these systems used mutational activation of *Hras* which although it shares a high sequence homology with *Kras* (Bar-Sagi, 2001), *Hras* is mutated in 0.1% of human pancreatic tumours (Forbes et al., 2017). Therefore, competitive interactions between normal and *Kras* mutated cells in the pancreas is a novel process that is more relevant to the initiation of pancreatic cancer. This could represent an inherent ability of the pancreas to remove aberrant cells. Rapidly dividing tissues such as the intestine can remove aberrant cells via neutral drift (Lopez-Garcia et al., 2010). Neutral drift is the theory that stem cell fate is determined stochastically and cells can be lost by differentiation and replacement by the stem cell pool. But this may not be suitable for slow dividing tissues such as the pancreas (Magami et al., 1990) that lack a well-defined stem cell niche (Minami, 2013). So cell competition provides a proliferation independent mechanism in the pancreas.

The tissue from low dose Cre positive; RFP positive pancreata was also generated and included as controls. This can provide insight into tissue homeostasis and dynamics (Alcolea et al., 2014). Using these controls, over time it was found that few changes occur to the labelled cell population. For example, no significant change in RFP percentage area occurred between 7 and 35 days post-induction and the analysis of cluster distribution showed that the two profiles were remarkably similar. However, overall proliferation decreased between 7 and 35 dpi in both control and experimental setting. This could be a remnant of postnatal development of the pancreas which can still stabilise up to 8 weeks after birth (Herbach et al., 2011; Magami et al., 2002). A previous study using *Nestin-Cre^{ERT2}* combined with rainbow labelling found evidence that within 28 days most acinar cells do not divide (Wollny et al., 2016). Even at 365 dpi the overall clone distribution was similar to shorter time points. This suggests that

tissue dynamics affecting cluster size and distribution are relatively slow in the pancreas and supports a mechanical mechanism of mutant cell elimination based on cell-cell interactions.

Elimination of less fit cells during normal development has been identified as highly important for embryogenesis (Bowling et al., 2018). In cell competition, cells with higher levels of p53 are recognised as less fit and lead to elimination of p53 high cells (Bowling et al., 2018; Zhang et al., 2017). Through the progression of PDAC, mutation of p53 has been shown to occur after the an initial $Kras^{G12D}$ mutation and is mutated in up to 85% of pancreatic cancers (Yachida et al., 2010). Thus, it could be hypothesised that mutation of p53 could promote the retention of $Kras^{G12D}$ mutant cells within the tissue as one mechanism by which p53 drives PDAC progression. Indeed, p53 mutant cells have recently been shown to undergo necroptosis when surrounded by normal neighbours but when under a Ras^{V12} mutant background these mutant cells survive (Watanabe et al., 2018). This highlights the importance of the order of oncogenic mutations in retention of mutant cells within a normal epithelium.

Precisely how risk factors can promote the initiation and progression of PDAC is also currently unclear. One study has demonstrated that a high-fat diet can suppress the extrusion of mutant cells from normal epithelia *in vivo* (Sasaki et al., 2018). Although the use of a *CK19*-driven Cre limited analysis to the ductal compartment, this study supports the hypothesis that Ras-transformed cells are extruded *in vivo* and indicates a potential mechanism how cell elimination may be overcome in patients. It is known that most late-stage PDAC contains $Kras^{G12D}$ mutations (Biankin et al., 2012) so this process must be overcome in the vast majority of cases. It is conceivable that alterations to cell-cell interactions caused by risk factors such as inflammation lead to retention of transformed cells, facilitating the initial steps of carcinogenesis. Indeed, it has been demonstrated that in pancreatitis cell contacts between acinar cells rapidly disassociate (Lerch et al., 1997; Schnekenburger et al., 2005). With pancreatitis known to accelerate PDAC in $Kras^{G12D}$ expressing mouse models (Guerra et al., 2007).

3.3.4 EphA2 is required for the loss of mutant cells surrounded by normal neighbours

EphA2 is a membrane-bound receptor tyrosine kinase that can regulate cell repulsion and adhesion to promote cell sorting (Pasquale et al., 2008). Differential EphA2 has previously been identified as the mechanism by which mutant cells are identified and extruded from MDCK monolayers *in vitro* (Porazinski et al., 2016). The study by Porazinski et al, describes a potential novel mechanism by which mutant cells could be detected and extruded by repulsive forces at the initial stages of cancer. Therefore, in this study the requirement of EphA2 in the elimination of Kras^{G12D} mutant cells from the pancreas was investigated. To this end a EphA2-deficient mouse model was crossed with KC animals to generate mutant cells surrounded by normal neighbours on a background of EphA2-deficiency. Previous characterisation of N-terminal and C-terminal EphA2 expression demonstrated that neither the full length nor a truncated form of EphA2 is present in these mice and thus can be considered an EphA2 deficient mouse (Amato et al., 2016). As whole-body LOF models can have wide-ranging effects throughout the body (Eisener-Dorman et al., 2009), it was necessary at each stage to control for any change induced by loss of EphA2. Importantly, it was observed that loss of functional EphA2 alone had no quantifiable impact on the labelling of cells or dynamics of RFP labelled cells over time in the pancreas; with all metrics similar to controls. Therefore, any change in KC-Eph animals can be considered a result of both mutant *Kras^{G12D}* expression and EphA2-deficiency. Using this model, it was found that the area of Kras^{G12D} cells significantly increased in EphA2-deficient animals and returned to levels comparable to controls. This suggests that EphA2-dependent elimination of Kras^{G12D} cells is occurring in the adult murine pancreas. Furthermore, it supports an emerging role for pathways previously implicated in axon guidance, but are now found to be implicated in cell competition (Vaughen and Igaki, 2016) and pancreatic cancer (Biankin et al., 2012).

Although a requirement for EphA2 in the elimination of mutant cells was identified, EphA2 can have a variety of different effects both autonomously and non-autonomously which may result in mutant cell retention. For example, EphA2 is a direct transcriptional target of the MAPK pathway and can negatively regulate Ras signalling (Macrae et al., 2005). Therefore, it could be hypothesised that loss of EphA2 could remove feedback inhibition of Kras further activating MAPK signalling, as observed in lung adenocarcinoma (Yeddula et al., 2015). However,

the increased proliferation associated with this mechanism was not observed suggesting another mechanism of EphA2-dependent clearance of mutant cells.

We have previously demonstrated that Ras-transformed cells are detected via elevated EphA2 in mutant cells compared to surrounding normal neighbours (Porazinski et al., 2016). With cell-cell interactions between normal and mutant cells triggering EphA2 dependent repulsion of Ras-transformed cells. In combination with increased contractility of mutant cells this drives the separation and extrusion of mutant cells from normal neighbours. In this study, several lines of evidence were found to support this hypothesis. A decrease in mutant cells was observed to occur in a process that requires non-transformed neighbours and EphA2. Moreover, the difference in cluster sizes observed at 7 dpi in KC and controls is consistent with a model of elimination based on repulsion at the boundary between normal and mutant cells; driving a decrease in clusters >800 μm^2 and resulting in an increase in clusters <800 μm^2. The loss of mutant clusters without an observed increase apoptosis could also indicate that cell competition is not leading to apoptosis but supports a mechanical extrusion of mutant cells via cell competition (Hogan et al., 2009).

This study identifies a fundamental role of EphA2 in the elimination of $Kras^{G12D}$ mutant cells by normal neighbours. It could then be expected that mutations to EphA2 are associated with human PDAC cases. However, mutations to EphA2 occur in less than 1% of PDAC cases in the COSMIC database (Forbes et al., 2017). This could be in part explained by the different roles EphA2 could play through PDAC tumourigenesis. It has been found that EphA2 is present in 95% of human pancreatic cancer patient samples and levels change with disease stage (Mudali et al., 2006). Levels of EphA2 were found to be higher in primary carcinomas than PanIN lesions and advanced, metastatic carcinomas showed relatively less strong staining than primary carcinomas that had not metastasised. EphA2 has also been implicated in driving PDAC dissemination with cell:cell repulsion generated by trafficking of EphA2 causing metastasis (Gundry et al., 2017). As the role of EphA2 in pancreatic cancer progression is still unclear, it is possible that wild-type EphA2 is important for pancreatic cancer progression. Therefore, inactivation of EphA2 would promote retention of transformed cells but could inhibit tumour growth or spread. It is also

possible that EphA2 is not regulated at the genetic level but at the protein level by endocytosis and degradation (Boissier et al., 2013). Another possible explanation is that cell-cell contacts are lost at the initial stages of tumourigenesis for example by pancreatitis (Lerch et al., 1997) which would overcome direct cell-cell interactions. Although further characterisation of EphA2 in pancreatic cancer is required to understand the role it plays in tumourigenesis. These results suggest that EphA2 has a functional role in the removal of mutant cells to maintain homeostasis, however if these cells are retained they can go on to initiate carcinogenesis (Hingorani et al., 2003).

3.3.5 Elimination of small clusters of $Kras^{G12D}$ mutant cells

Cell competition is considered to be a short-range phenomenon with the direct interaction of neighbouring cells allowing fitness comparison and elimination (Martín et al., 2009). Therefore, in this study clusters of $Kras^{G12D}$ cells were discretely investigated. It was found that the total number of mutant clusters decreased in a EphA2 dependent manner. Moreover, clusters up to 4400 μm^2 were significantly underrepresented with an increase to control levels of these clusters in EphA2-deficient mice.

It has been demonstrated in *Drosophila* that juxtaposition of aberrant cells with normal neighbours leads to an enrichment of actomyosin at the interface (Bielmeier et al., 2016). This increased contractility at the interface of normal and mutant cells is sufficient to alter the fate of aberrant cells in a cluster size-dependent manner. It was observed that single or small clusters of up to six cells were eliminated whereas clusters larger than this were retained. Contractility at the interface still occurs in larger clusters but this force drives mutant cluster invagination and cyst formation. It was not possible in this study to differentiate clusters based on cell number due to the technical difficulty in visualising nuclei and retaining RFP signal. However, a significant underrepresentation of clusters up to 4400 μm^2 in KC mice at 35 dpi was observed. As the average acinar cell is approximately 200 μm^2 (Houbracken and Bouwens, 2017), this implies that clusters up to 22 cells are being eliminated. But cells can also become contractile from Eph signalling and repulsion (Porazinski et al., 2016) which would alter the size of an acinar cell and so the threshold number of cells being eliminated could

be higher. However, this work does suggest a higher threshold number of cells than previous work (Bielmeier et al., 2016) but lower than another study (Ballesteros-Arias et al., 2014). This could reflect tissue-specific differences or result from differences between *Drosophila* and murine models. Previous *Drosophila* models use 2D epithelial sheets whereas the *in vivo* pancreas is a 3D environment which could also alter the threshold of cells required to overcome elimination.

Another question arising from this study is the fate of mutant clusters over 4400 μm^2. Previous work has demonstrated that once clusters of oncogenic cells reach around 400 cells they overcome tumour suppressive cell-competition effects and form tumours in *Drosophila* (Ballesteros-Arias et al., 2014). Mutant cells at the boundary were still eliminated by cell competition, however those cells inside the large cluster and further away from the normal:mutant interface survive. Furthermore, the apoptosis of mutant cells by normal neighbours was found to drive proliferation and promote tumourigenesis. In this study, the range of sizes of large clusters and the low frequency made inferring any changes to larger clusters difficult. Apoptosis and proliferation was not found to be elevated in this study suggesting apoptosis is not promoting proliferation in the pancreas at this time point. However, this work could suggest a size threshold for the elimination of clusters. Moreover, if Eph-dependent repulsion is driving elimination of smaller clusters it could also be acting on larger clusters but with a different outcome. Interface contractility can drive cyst formation in *Drosophila* (Bielmeier et al., 2016). Moreover, EphB interactions in the intestine compartmentalises tumour cells into a cyst in the villus where tumour growth is restricted (Batlle et al., 2005; Cortina et al., 2007). Therefore, larger clusters could be compartmentalised into a cyst structure similar to PanIN lesions. So EphA2 signalling from cell-cell interactions may eliminate small clusters and segregate larger clusters into cysts.

3.4 Summary and Future Directions

In summary, three major conclusions can be drawn from the data in this chapter. First, Kras^{G12D} cells are lost when present at low numbers *in vivo*. Second, clusters below a critical size may be preferentially eliminated. Finally,

EphA2 is required for both of these processes to occur. Together, this work in combination with previous studies suggests that a mechanical form of cell competition is occurring between normal and mutant pancreatic cells *in vivo* to eliminated Ras-transformed cells.

These conclusions raise a number of interesting questions with regard to removal of mutant cells, heterotypic cell interactions and the role of EphA2 in PDAC, and provide a number of avenues that warrant further investigation.

The results in this chapter suggest Kras^{G12D} mutant cells are eliminated from the pancreas by normal neighbours. However, as Kras mutations are present in >90% of PDAC tumours it raises the question of how it is overcome for tumourigenesis to occur. To understand how single Kras^{G12D} cells overcome elimination, the model described in this chapter could be combined with known risk factors of PDAC to determine if it leads to retention of transformed cells. For example, pancreatitis is an established risk factor for pancreatic cancer and can be modelled by caerulein administration in murine models (Niederau et al., 1985). Therefore, caerulein could be given at 10 dpi to test if this promotes retention of transformed cells *in vivo*. Tissue health during aging could also be studied using this system. Age is the biggest risk factor in PDAC (Bosetti et al., 2014) but the mechanism of how aging increases risk is unclear. The mechanical properties of tissues are known to alter in aging which may alter the efficiency of mutant cell elimination (Phillip et al., 2015). With temporal control over emergence of Kras^{G12D} cells provided by this system, mutations could be induced in aged animals to study if elimination still occurs. Multiple mutations in a single cell can also alter the effect of cell competition on aberrant cells. In *Drosophila* epithelium, polarity deficient cells induced by mutations to *Scribble* are eliminated by apoptosis, but Ras mutation in the same cell causes synergistic effect and neoplastic overgrowth (Brumby and Richardson, 2003). Moreover, p53 mutant cells are basally extruded and undergo necroptosis when surrounded by normal neighbours but p53 mutant cell elimination does not occur in Ras-transformed epithelia (Watanabe et al., 2018). Therefore, combining this model with an inducible p53 mutation could investigate if Kras^{G12D} and p53 mutations would inhibit elimination by normal neighbours. One way to combine *Kras^{G12D}* mutations with a variety other genetic changes would be orthotopic injection of pancreatic cells with defined mutations. Mutations to p53 are highly prevalent in pancreatic

cancer with up to 85% of tumours carrying a mutation (Yachida et al., 2010), and are associated with more advanced PanIN3 lesions and therefore could provide a mechanism of overcoming cell elimination. This could further elucidate how cell competition influences the order of genetic mutations in tumour evolution (Watanabe et al., 2018). Thus, this model could be used to study a range of factors that may alter mutant cell elimination to promote tumourigenesis.

Further investigation is also required into the fate of transformed cells. Mechanical cell competition can drive both extrusion or apoptosis of mutant cells (Hogan et al., 2009; Wagstaff et al., 2016). Answering if either of these processes are occurring is key to understanding whether this process is tumour suppressive or could promote disease. For example, if mutant cells are being extruded into the circulatory system it could drive metastasis from the earliest stages of disease. To this end probing for circulating tumour DNA could be used to detect if mutant cells are entering the blood. Whole tissue imaging would also further our understanding of whether cells are being extruded or segregated. Recent genetic analysis has established that precancerous, mutant cells can spread through the pancreas and seed precursor lesions in distal sites (Makohon-Moore et al., 2018). By further elucidating whether this process promotes or suppresses cancer it will inform the research moving forward. If it tumours suppressive then therapies to promote mutant cell elimination could be tested. Conversely, if it promotes metastasis then it could provide novel targets to detect and inhibit the spread of PDAC from the earliest stages

Chapter 4: Modelling heterotypic cell-cell interactions in a 3D acinar cell culture model

4.1 Introduction

An increasing body of evidence indicates cell competition is occurring at the initiation of cancer (Hogan et al., 2009; Kon et al., 2017; Leung and Brugge, 2012). However, direct evidence for a role in tumourigenesis can be difficult to obtain *in vivo*. In chapter 3, by modelling these interactions *in vivo* it was found that mutant cells were eliminated from the pancreas. This process of elimination was only observed when Kras^{G12D} cells were present at low numbers but the mechanism of elimination and fate of transformed cells was unclear. Use of *ex vivo* models can provide a tractable system to study cell-cell interactions over time at the level of the single cell. Moreover, 3D acinar cell culture systems can model disease initiation (Liou et al., 2013; Shi et al., 2013) and hence may further elucidate the fate of mutant cells.

The initial stages of pancreatic ductal adenocarcinoma (PDAC) are poorly understood. Due to the duct-like nature of precursor lesions the ductal compartment was thought to be the cell of origin of PDAC (Cubilla and Fitzgerald, 1976). However, early targeting of *Kras^{G12D}* to the pancreas found the ductal compartment resilient to transformation. It was later found that expression of *Kras^{G12D}* in the acinar compartment was sufficient to give rise to pancreatic intraepithelial neoplasia (PanIN) lesions and PDAC (Habbe et al., 2008; Hingorani et al., 2003; Kopp et al., 2012). It is now believed that the acinar compartment goes through a de-differentiation process, known as acinar-ductal metaplasia (ADM), to give rise to the PDAC cell of origin (Crawford et al., 2002).

ADM is a common and reversible process upon pancreatic damage and is thought to protect the pancreas and aid regeneration once the injury has passed (Mills and Sansom, 2015; Storz, 2017). However, *Kras^{G12D}* mutations can initiate ADM and lock cells in this duct-like state, leading to precancerous lesion development (Kopp et al., 2012). During ADM, acinar cells shut off specific transcription factors characteristic of mature acinar cell fate. This involves downregulation of transcription factors that control acinar cell maturation and architecture (MIST1, PTF1A, NR5A2) and expression of mature duct cell

transcription factors like *Sox9* and *Hnf6*. They also express transcription factors associated with pancreatic embryonic progenitors (*Sox17*)(Jensen et al., 2005; Mills and Sansom, 2015; Morris et al., 2010). To better understand the processes underlying the early events in pancreatic cancer an *ex vivo* acinar model has been developed (Liou et al., 2013; Means et al., 2005).

Signalling mechanisms regulating early *Kras*^{G12D} driven changes to acinar have been studied using this *ex vivo* explant three-dimensional (3D) cell culture model in which primary acinar cells are isolated and cultured (Ardito et al., 2012). This allows visualisation of the de-differentiation process in real-time as clusters of cells undergoing ADM change from a "berry" shape to a duct-like cyst structure in 3 days (Shi et al., 2013). Therefore, ADM represents an early disease state that can be studied at the level of the single cell using this *ex vivo* explant model.

Recently, the microenvironment has been identified as a key component in the earliest stages of PDAC. It has been demonstrated that macrophages infiltrating the pancreas can drive the dedifferentiation process and promote PDAC development (Liou et al., 2013). Moreover, evidence that normal neighbouring cells inhibit the de-differentiation associated with ADM has also been found in a murine model (Krah et al., 2015). This suggests that normal acini can inhibit cells lacking key acinar transcription factors from undergoing ADM. Together, these results suggest that the local microenvironment can promote or suppress the progression of Ras-transformed cells through ADM. Thus, loss of this repressive environment by extrusion may promote tumourigenesis (Leung and Brugge, 2012).

In addition to altering progression through to an early disease state normal neighbours can also competitively interact with Ras-transformed cells leading to extrusion of mutant cells (Hogan et al., 2009; Kajita et al., 2014). Recent work has demonstrated that sporadic induction of *Ras*^{V12} in the murine intestine and using organoid culture can lead to extrusion of mutant cells (Kon et al., 2017). Aberrant activation of MAPK signalling has also been implicated in extrusion of single cells from 3D mammary acini (Leung and Brugge, 2012). This suggests that Ras-transformed cells can be extruded from a variety of different tissues and could indicate that Kras^{G12D} acinar cells are being extruded in the pancreas.

As a loss of acinar cells was identified *in vivo* the aim of this chapter was to develop an *ex vivo* model of these interactions. This would allow the

investigation of two main hypotheses: 1) do heterotypic interactions between normal and mutant acinar cells drive elimination of the mutant cell and 2) Do normal acinar cells promote or inhibit Kras^{G12D} cells undergoing ADM.

4.1 Results

4.2.1 Generation of a 3D *ex vivo* model of pancreatic acinar cells

To investigate the fate of mutant cells surrounded by normal neighbours in the acinar compartment it was first necessary to develop a mouse pancreatic acinar cell primary culture system (Liou et al., 2013). This ex vivo model is based on a previously established cell culture model in which growth factors or genetic changes, such as $Kras^{G12D}$, have been shown to induce ADM within 3 days (Shi et al., 2013). To investigate if this is conserved using the $Pdx1\text{-}Cre^{ER}$; LSL-$Kras^{G12D/+}$; $ROSA26^{tdRFP}$ animal model these mice were treated with tamoxifen via intraperitoneal injection (I.P) to activate $Kras^{G12D}$ expression. Pancreata were then harvested 48 hours later, digested with collagenase and individual acini clusters plated in a 3D collagen matrix (Figure 4.1A).

To determine if acinar cells generated using this system retained features of acinar biology immunofluorescence was carried out directly after plating (day zero; D0) (Figure 4.1B). As described previously, acinar cells initially retain normal apical-basal polarity with zymogen granules present at the apical pole, positive for the acinar specific marker amylase (Figure 4.1B). This demonstrates that both polarity and presence of acinar specific amylase are retained *ex vivo* suggesting that features of acinar cells are retained.

Induction of recombination within acinar cells was also examined using RFP as a readout. After *in vivo* induction with 1 mg of tamoxifen and plating, RFP expression (red) was present in a mosaic fashion in clusters (Figure 4.1B). As the pancreas was stochastically digested and mechanically broken-down to produce clusters, clusters with varying numbers of RFP positive cells were generated. This allowed clusters with different numbers of RFP positive cells to be compared within the same well.

A

Dissociation to clusters

Plate in collagen

B

| RFP | Nuclei | Amylase | Merge |

D0 Kras^G12D
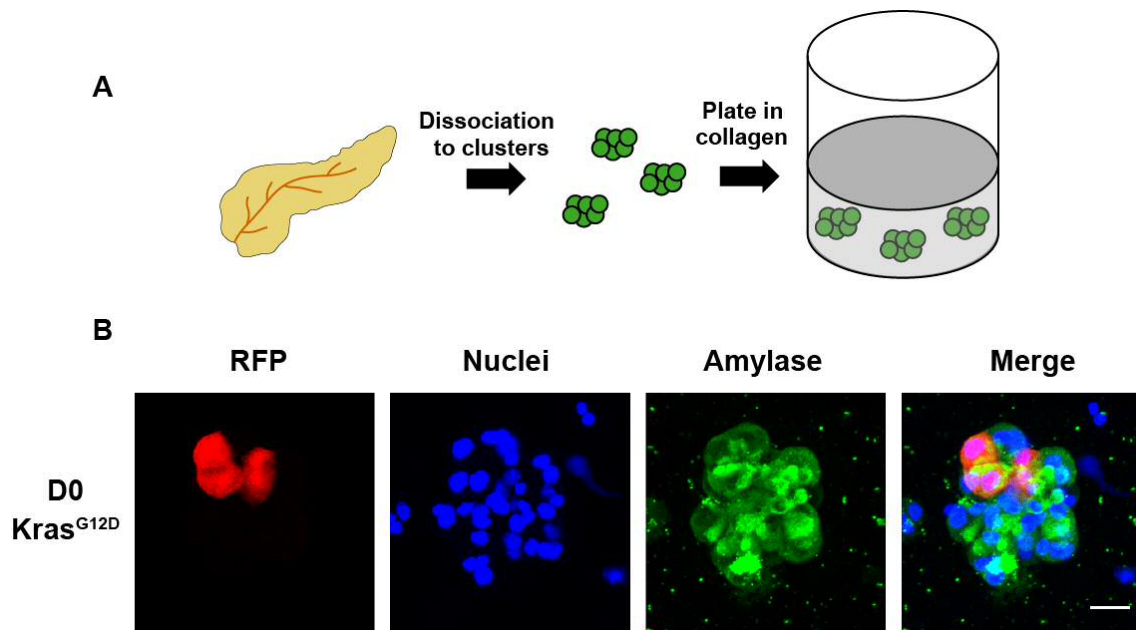
Figure 4.1: Generation of mosaic acinar clusters *ex vivo*. (A) Cartoon of protocol for acinar cell culture; the pancreas was broken down into clusters which were plated in collagen. (B) Following plating of mouse primary acinar cells *ex vivo* immunofluorescence was carried out on the same day as plating (day 0). Cells express the acinar specific marker amylase (green) at this time point. Administration of tamoxifen *in vivo* to *Pdx1-Cre; Rosa26^tdRFP; Kras^G12D* animals 48 hours before harvesting the pancreas for *ex vivo* culture, is sufficient to generate

4.2.2 Heterotypic cell-cell interactions associated with morphological changes in Kras^{G12D} cells

Once optimised, *ex vivo* cultures, were used to investigate the effects of heterotypic cell-cell interactions between *Kras^{G12D}* mutant acinar cells and normal neighbours. For this *Pdx1-Cre^{ER}; LSL-Kras$^{G12D/+}$; ROSA26^{tdRFP}* (KC) mice were induced and cultured. Acinar cultures derived from *Pdx1-Cre^{ER}; ROSA26^{tdRFP}* animals following the same induction procedure were included as controls.

Single cell induction of oncogenes has been demonstrated to lead to small, round and contractile cells that are extruded in 3D (Leung and Brugge, 2012). To investigate if single cell induction of *Kras^{G12D}* in clusters of acinar cells leads to a similar phenotype, acinar clusters were generated and fixed 24 hours after induction and stained for F-actin. After 24 hours in culture (day 1; D1) morphological changes were observed between normal and mutant cells. Single *Kras^{G12D}* (RFP positive) cells surrounded by RFP negative cells had an apparent decrease in volume, and F-actin accumulated at the interface between normal and transformed cells (Figure 4.2, top). Strikingly, elevated levels of F-actin appeared to occur within Ras-transformed cells; rather than from normal neighbouring cells (Rosenblatt et al., 2001; Slattum et al., 2014). These changes were not observed in clusters containing *Kras^{G12D}* cells only (Figure 4.2, middle) or RFP positive cells from *Pdx1-Cre^{ER}; ROSA26^{tdRFP}* control mice (Figure 4.2, bottom). This suggests that Kras^{G12D}cells are induced to undergo morphological changes indicative of repulsion when surrounded by normal neighbours. However, single RFP cells were uncommon at this time point, with the vast majority of clusters containing more mutant cells. Therefore, this this phenomenon was a rare event. Although mutant cells were found to adopt this morphology, evidence for extrusion of *Kras^{G12D}* was not observed in *ex vivo* cultures. Timelapse microscopy was also carried out, however the system was not sufficiently robust to allowing tracking of cells over time. Together, these observations indicate that *Kras^{G12D}* expressing acinar cells adopt a contractile morphology when surrounded by normal neighbours within 24 hours of *ex vivo* culture.
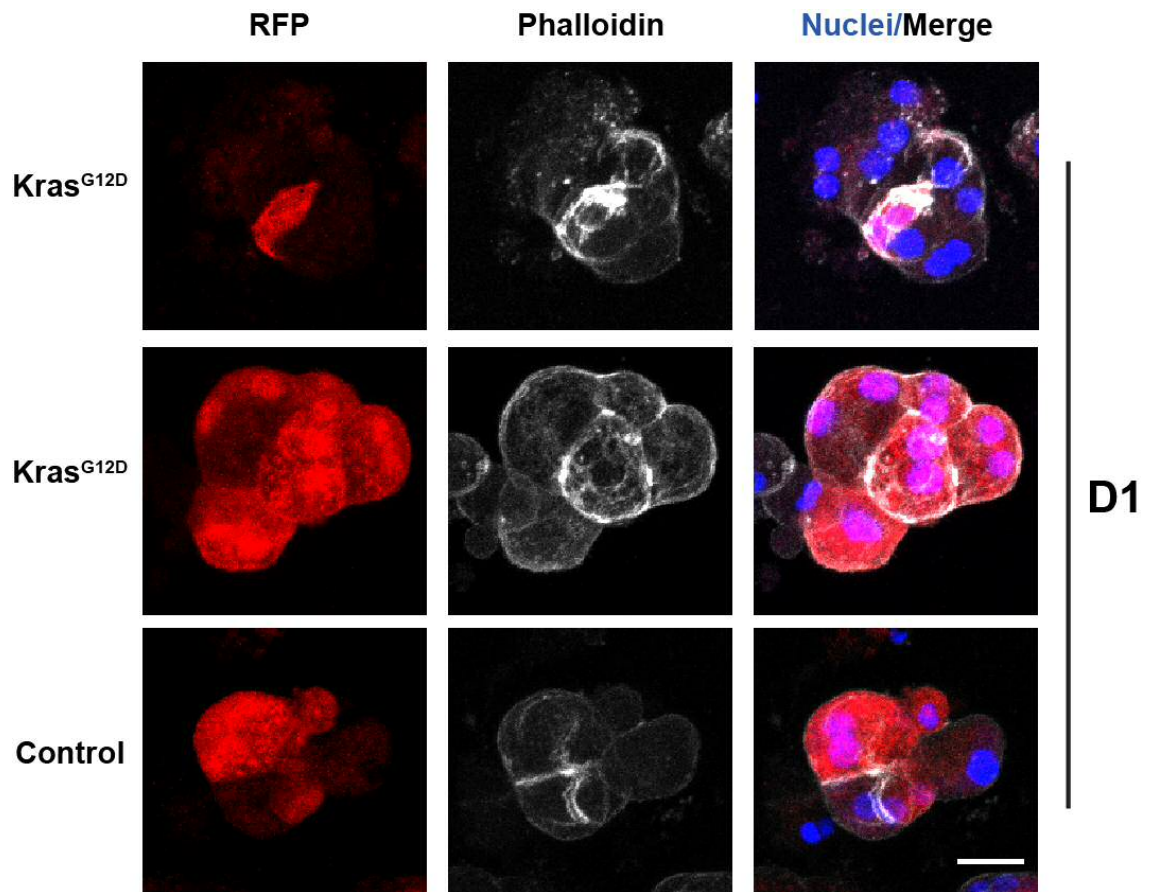
Figure 4.2: Kras^G12D acinar cells adopt a contractile morphology upon interaction with normal neighbours. After 24 hours in culture *Kras^G12D*(RFP; red) expressing cells adopt a small, contractile morphology when surrounded by normal neighbours and accumulate F-actin (top row). These changes do not occur when mutant cells are surrounded by mutant neighbours (middle row). Control acini from *Pdx1-Cre^ER;ROSA26^tdRFP* mice also did not undergo these morphological changes ex vivo (bottom row). Scale bar, 20 μm.

4.2.3 Characterisation of ADM in *Kras*^*G12D* expressing clusters *ex vivo*

The next aim was to investigate the role of normal neighbours in acinar-ductal metaplasia (ADM). Previous work has identified a role for the normal neighbourhood in inhibiting ADM *in vivo* upon mosaic loss of the acinar-specific transcription factor *Ptf1a* (Krah et al., 2015). Furthermore, during development the interaction with similar neighbours or a 'community effect', is required for the activation of certain genes and differentiation (Gurdon et al., 1993; Ho, 1992). It follows that non-transformed acinar cells may inhibit the ADM process. Therefore, the role of normal neighbours in inhibiting Kras-driven ADM was investigated using the established *ex vivo* model. ADM is associated with acinar cells dedifferentiating to a duct-like progenitor cell type which is associated with both transcriptional and morphological changes and so readouts of both of these changes were examined.

First it was necessary to validate that ADM was occurring in my model system using cells derived from *Pdx1-Cre*^*ER*^*; LSL-Kras*^*G12D/+*^*; ROSA26*^*tdRFP* animals following *in vivo* induction. It has previously been demonstrated that *Kras*^*G12D* expression drives the de-differentiation ADM process to a more duct-like cell (Habbe et al., 2008; Hingorani et al., 2003; Kopp et al., 2012). To test whether this process was conserved using the *Pdx1-Cre*^*ER*^*; LSL-Kras*^*G12D/+*^*; ROSA26*^*tdRFP* mouse model, acinar cells were plated 48 hours after *in vivo* induction and visualised over time. After plating (Day 0), both control and Kras^G12D cells were observed to have the many-lobed acinar morphology apparent from the F-actin stain (Figure 4.3, top). However, by day 3 it was observed that Kras^G12D expressing, RFP positive clusters adopted a ductal cyst morphology comprising of a single layer of epithelial cells in a circular ring with an expansion of the hollow, luminal space (Figure 4.3), similar to previously published reports (Ardito et al., 2012; Liou et al., 2013; Shi et al., 2013). Control acinar cultures from *Pdx1-Cre*^*ER*^*; ROSA26*^*tdRFP* animals did not undergo this morphological change by day 3 (Figure 4.3). Widespread cell death was observed at later time points in acinar cells not expressing *Kras*^*G12D* as observed previously (Shi et al., 2013). This indicates that clusters of *Kras*^*G12D* cells undergo the morphological changes associated with ADM over 3 days *ex vivo*.

The ADM de-differentiation process is also associated with changes in transcription. As ADM progresses, a number of ductal and pancreatic embryonic markers are expressed (Storz, 2017). One such transcription factor is Sox9, a ductal lineage specific marker that is upregulated ADM *in vivo* and *ex vivo* (Kopp et al., 2012; Prévot et al., 2012). As *Sox9* expression is required for ADM (Kopp et al., 2012), immunofluorescence for Sox9 was used as a second readout of ADM. After plating (day 0), Sox9 staining was not detectable in RFP positive cells in control or experimental cultures (Figure 4.4). After 3 days in culture, RFP positive, *Kras*^{G12D} mutant cells had adopted a ductal cyst shape that was strongly positive for nuclear Sox9 (Figure 4.4). Sox9 staining was not detected in clusters from *Pdx1-Cre*^{ER}*; ROSA26*^{tdRFP} after 3 days in culture. This suggests that the morphological changes associated with ADM are accompanied by a transcriptional switch to a more duct-like fate in *Kras*^{G12D} cells *ex vivo*.

Together, this work describes the generation of a 3D acinar model that recapitulates ADM in clusters of cells expressing oncogenic *Kras*^{G12D} as observed by both morphological and transcriptional changes consistent with previous reports (Ardito et al., 2012; Liou et al., 2015; Shi et al., 2013). It also highlights some of the limitations of the system with most non-transformed acini unable to survive beyond 3 days in culture.
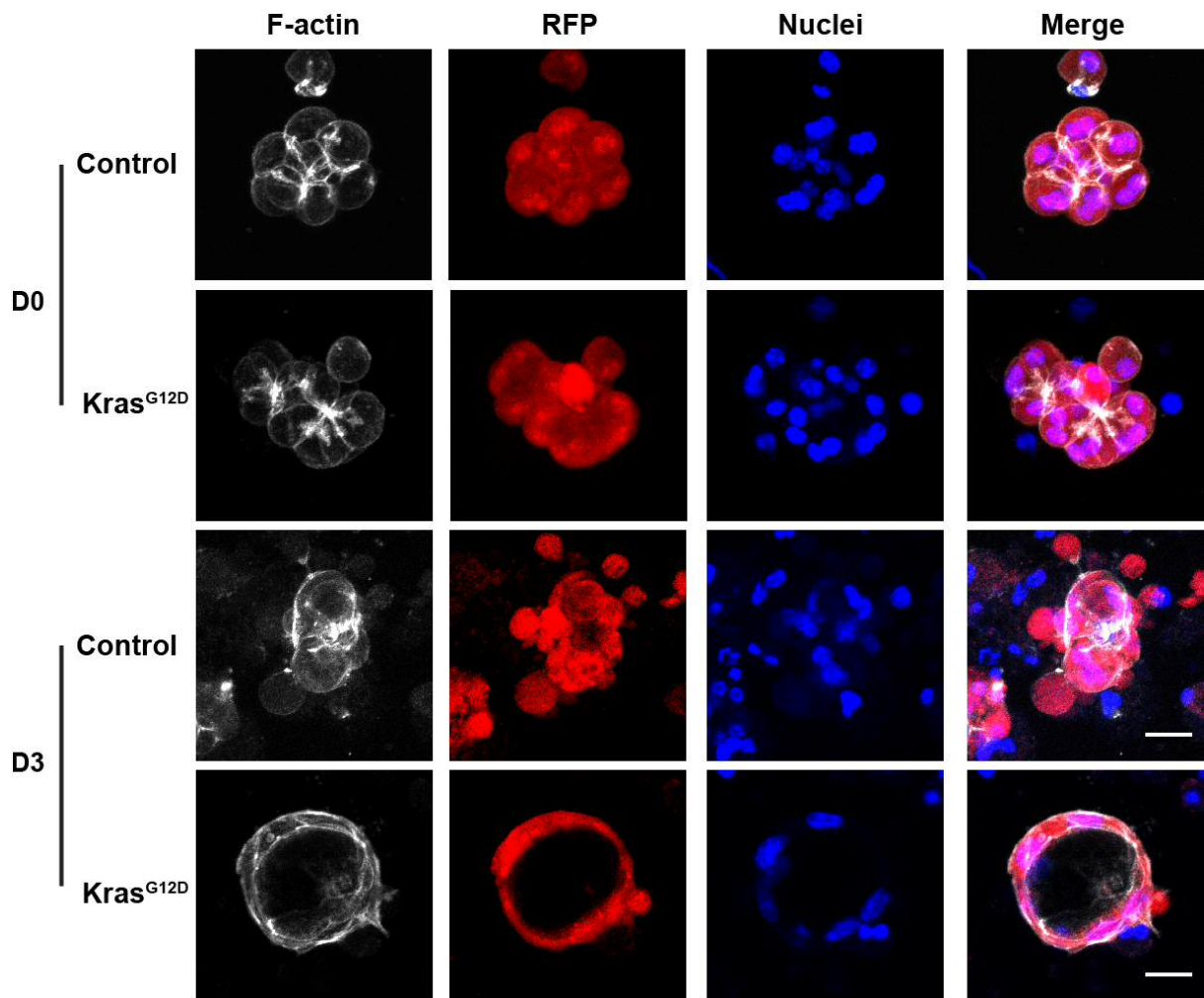
Figure 4.3: Kras^{G12D} drives morphological changes to a duct-like cyst *ex vivo*. Acinar cells isolated from *Pdx1-Cre^{ER};LSL-Kras$^{G12D/+}$;ROSA26^{tdRFP}* (Kras^{G12D}) animals 48 hours post-induction were cultured *ex vivo*. After 3 days in culture (D3) Kras^{G12D} cells identified by RFP (red) have lost the round shape and adopted a duct-like structure with lumen expansion as apparent from F-actin (grey). Control cultures from *Pdx1-Cre^{ER}; ROSA26^{tdRFP}* did not undergo this morphological transformation and retained an acinar morphology. Scale bar, 20 μm.
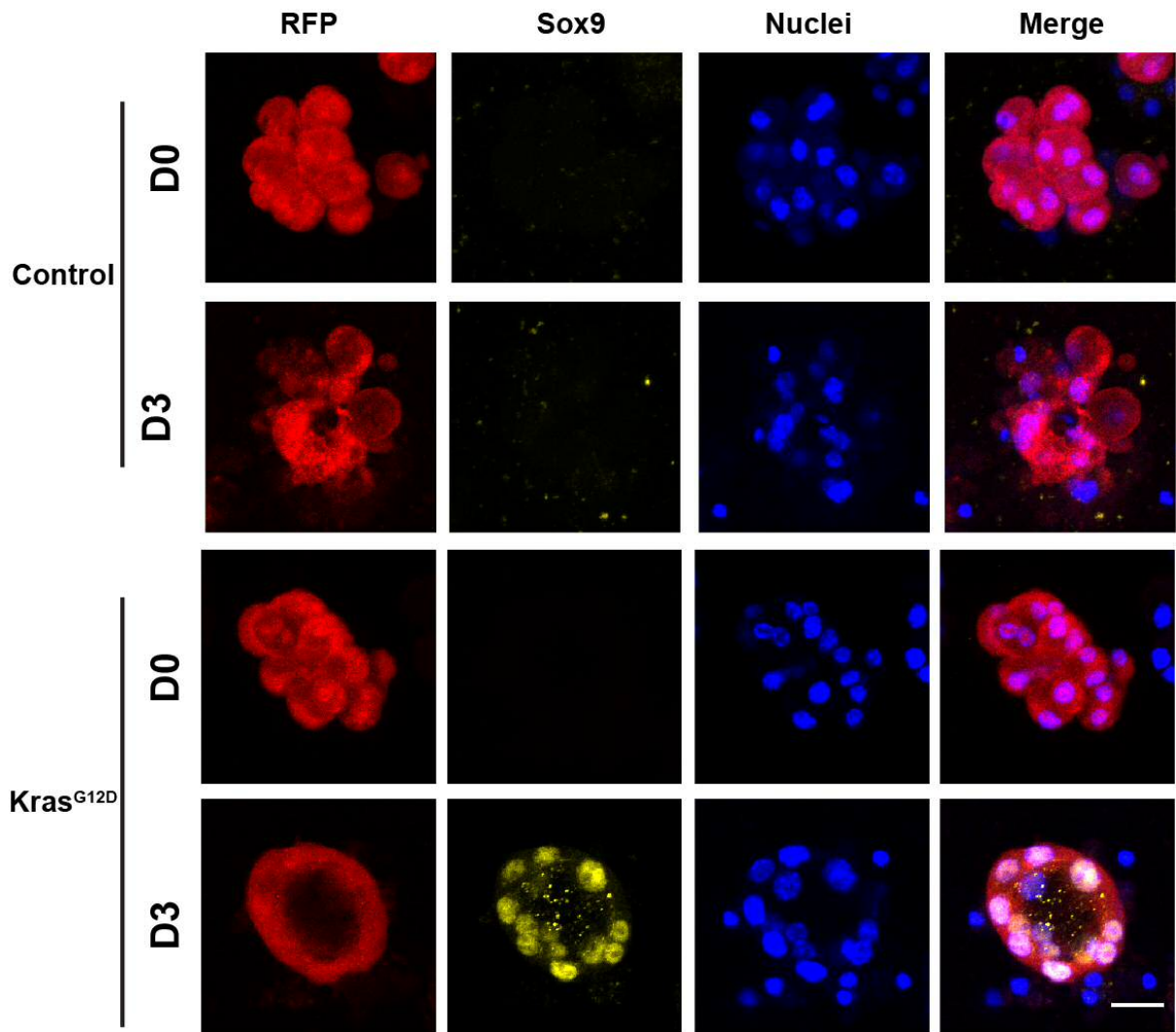
Figure 4.4. ADM *ex vivo* is associated with genetic reprogramming to express *Sox9*. *Ex vivo* cultures were isolated from *Pdx1-Cre^ER^;LSL-Kras^G12D/+^;ROSA26^tdRFP^* (Kras^G12D^) animals 48 hours after *in vivo* induction. On day 0 (D0) clusters have a 'berry' like shape and no Sox9 (yellow) was detectable. After 3 days in culture (D3) Kras^G12D^ clusters have adopted a ductal cyst morphology, positive for the ductal marker Sox9. In control *Pdx1-Cre^ER^; ROSA26^tdRFP^* acini, Sox9 was not observed at day 0 or day 3. Scale bar, 20 μm.

4.2.4 Normal neighbours decrease the efficiency of duct-like cyst formation of *Kras*^{G12D} transformed cells.

ADM is an initiating event for the development of PDAC in mice. It is associated with changes to a duct-like progenitor gene expression profile and morphological changes. After establishing that clusters of Kras^{G12D} cells can progress through ADM in this system the effect of mosaic *Kras*^{G12D} expression was explored.

To investigate this question the impact of normal neighbours was studied in two ways: i) with respect to morphological changes with the formation of a ductal cyst as a readout, and ii) at the level of cell fate with Sox9 as a readout.

This *ex vivo* model has been widely used to elucidate the underlying signalling mechanisms of ADM and role of the tumour microenvironment in both mice and humans (Ardito et al., 2012; Liou et al., 2017; Liu et al., 2016; Shi et al., 2013). So to examine the role of normal epithelial neighbours in ADM, *ex vivo* acinar clusters were generated from *Pdx1-Cre*^{ER}*;LSL-Kras*$^{G12D/+}$*;ROSA26*^{tdRFP} (KC) animals 48 hours after induction with 1 mg of tamoxifen. After 3 days in culture, the percentage of a clusters positive for RFP was calculated and each cluster was then scored as either converting to a duct-like cyst with an expanded lumen and associated cell shape changes, or retaining acinar features. After plating (day 0) no ductal cyst structures were observed (Figure 3.5A). However, by day 3 a stark difference was observed between clusters with low and high percentages of mutant cells. Clusters consisting of less than 60% RFP positive cells had an approximately 10% likelihood of forming a duct-like cyst (Figure 3.5B). This could indicate a basal level of transformation within the system as clusters from KC mice that contained no mutant cells (0%), or in control clusters, a similar level of duct-like cyst formation was observed. Conversely, clusters consisting of over 60% RFP positive cells (and hence Kras^{G12D} cells) would efficiently progress through ADM, with the vast majority forming a duct-like cyst. This suggests that to form a duct-like cyst *ex vivo* a threshold number of *Kras*^{G12D} cells per cluster is required.

It was noted that clusters with a high proportion of mutant cells (but less than 100%) are able to form a duct-like cyst. This suggests that normal cells when present at low numbers can also be induced to the duct-like cyst morphology (Figure 4.6). Strikingly, it was found that non-transformed cells surrounded by

Kras^{G12D} cells are able to undergo ADM and become part of the duct-like cyst structure. These normal cells were also found to genetically reprogram and express *Sox9* (Figure 3.6, asterisks), suggesting that mutant cells recruit non-transformed cells to form a duct-like cyst.

These data illustrate that in order to efficiently progress to a duct-like cyst a threshold of mutant cells is required *ex vivo*. This suggests that normal neighbours have an inhibitory effect on mutant cell disease progression as clusters with low numbers of Kras^{G12D} cells are unable to efficiently adopt a duct-like cyst morphology. It also indicates that once *Kras^{G12D}* cells overcome this effect they can recruit normal cells into a duct-like cyst in culture.
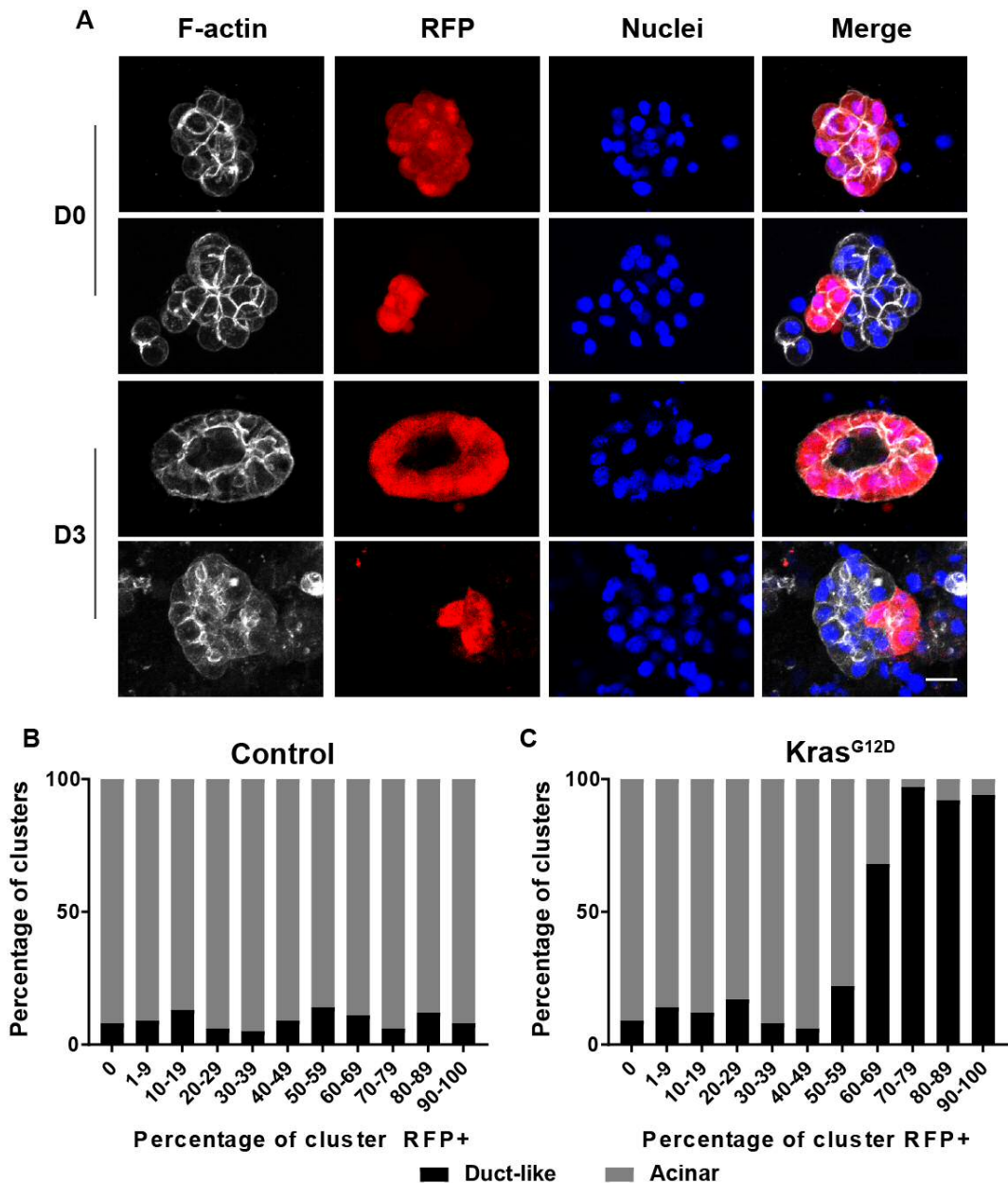
Figure 4.5: A threshold of *Kras^G12D* cells is required to efficiently progress through ADM *ex vivo*. (A) After plating *Pdx1-Cre^ER;LSL-Kras^G12D/+;ROSA26^tdRFP* acini cells have a round morphology (day 0). At day 3, clusters with a high percentage of RFP (red) and hence mutant cells adopted a duct-like structure with an expanded lumen. Whereas clusters with a low percentage of transformed cells retain acinar-like features. At day 3, the proportion of RFP positive (red) cells in a cluster was counted and then each cluster was scored as whether duct-like with a lumen or retaining acinar morphology (B,C). (B) In control clusters (*Pdx1-Cre^ER;ROSA26^tdRFP*) a low number of clusters were observed to have undergone ADM independent of the percentage of RFP positive cells within the cluster.(C) However, in clusters where RFP marks Kras^G12D cells the ratio of normal to mutant cells plays an important factor in determining whether a cluster progresses through ADM. A cluster with less than 60 % mutant cells has a similar efficiency of ADM as the basal control level whereas the vast majority of clusters with over 60 % transformed cells went through ADM efficiently within 3 days. Data represents >30 clusters/experiment, n = 3 biological replicates. Scale bar, 20 μm.
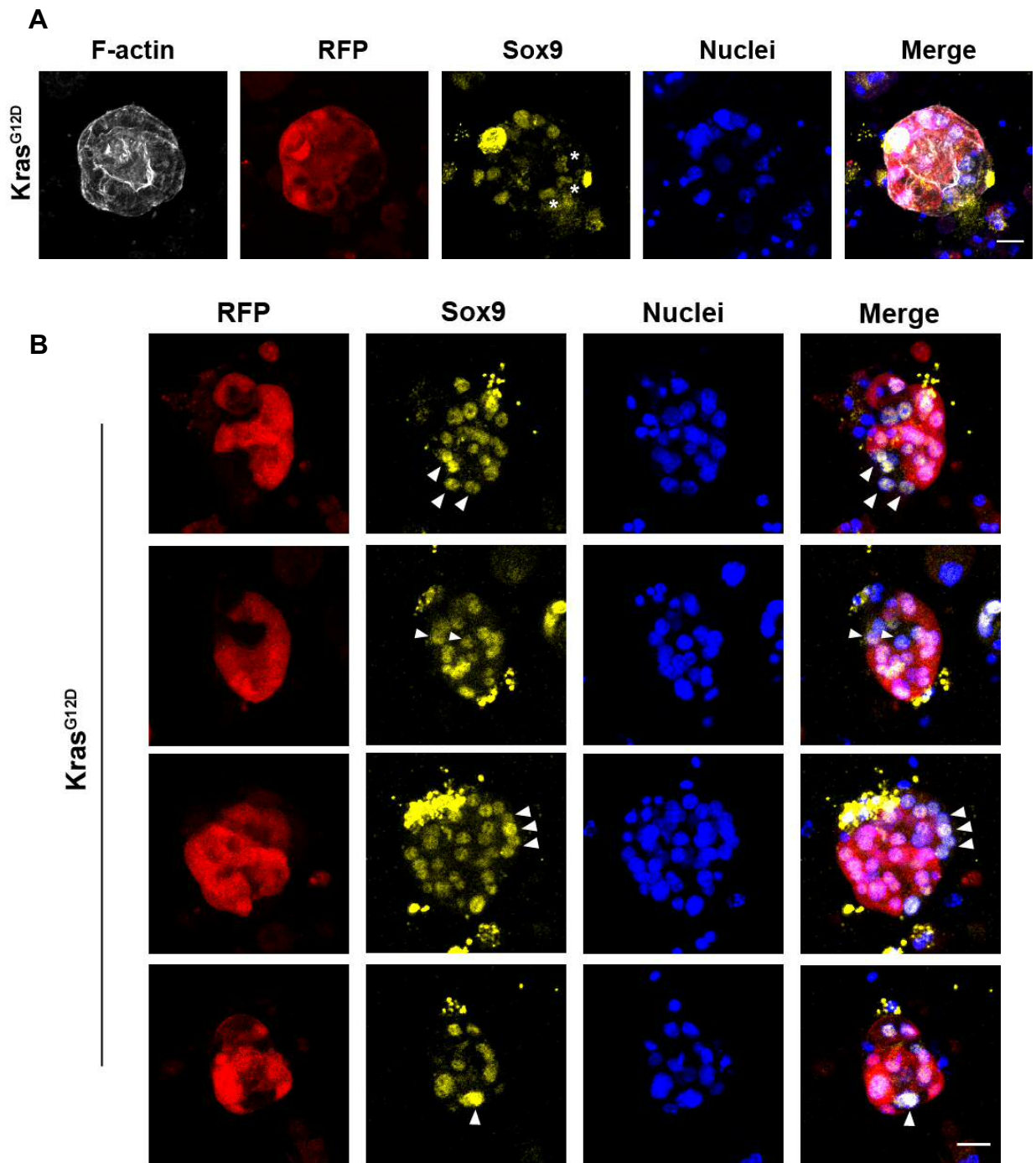
Figure 4.6: Recruitment and reprogramming of wild-type cells by Kras^G12D mutant neighbours. (A) Non-transformed, RFP negative cells are recruited to form a duct-like cyst the normal cells (asterisks) and reprogram to express Sox9 (yellow). Cells were fixed at day 3 and stained for F-actin (grey), RFP (red), Sox9 (yellow) and Nuclei (blue). (B) RFP negative cells (white arrows) from clusters with a large proportion of Kras^G12D cells reprogram to Sox9 positive cells. Images are representative of 4 biological replicates. Scale bar, 20 μm.

4.2.5 *Kras^G12D* transformed cells reprogram to express *Sox9* autonomously.

ADM requires both a genetic reprogramming process and a morphological change. Having found evidence suggesting that normal neighbours decrease the efficiency of forming duct-like cysts in 3 days the next aim was to investigate if normal neighbours were inhibiting the genetic changes associated with ADM in single Kras^G12D cells.

Acinar cell cultures were generated from KC and control mice 48 hours after *in vivo* induction of Cre recombinase by tamoxifen. After plating, Sox9 was not detectable in single *Kras^G12D* expressing acinar cells or RFP positive, Kras wild-type controls (Figure 4.7). However, after 3 days in culture de-differentiation to a Sox9 positive cell was observed. Single *Kras^G12D* expressing acinar cells surrounded by RFP negative, normal cells stained positively for nuclear Sox9 (Figure 3.7 bottom, white arrowhead). This suggests that single mutant cells surrounded by normal neighbours autonomously reprogram to *Sox9* expressing duct-like cells. Clusters containing single RFP positive cells from *Pdx1-Cre^ER*; *ROSA26^tdRFP* controls did not show any positive staining for Sox9 (Figure 3.7, white asterisks).

These data indicate that normal neighbours do not inhibit the transition of *Kras^G12D* to Sox9 positive cells on day 3 in an *ex vivo* model of ADM and it is autonomous.
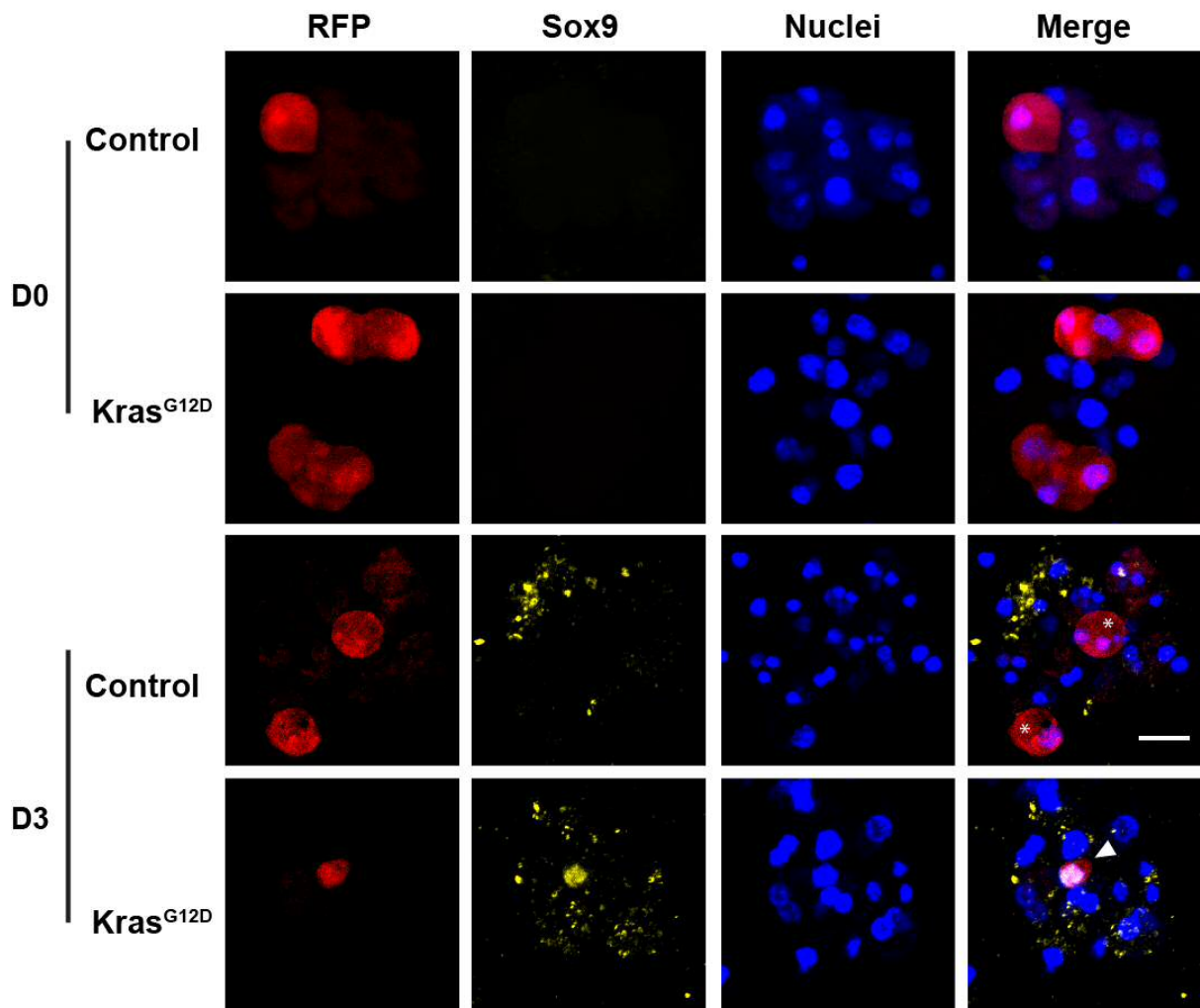
Figure 4.7: Single Kras^{G12D} acinar cells autonomously reprogram to Sox9 positive cells. Acinar cells from either *Pdx1-Cre^{ER};LSL-Kras$^{G12D/+}$;ROSA26^{tdRFP}* (Kras^{G12D}) or *Pdx1-Cre^{ER}; ROSA26^{tdRFP}* (Control) animals following Cre induction *in vivo* were cultured for 3 days *ex vivo*. On day 0, Sox9 (yellow) staining was not observed in RFP positive cells controls or *Kras^{G12D}* expressing cells. At day 3, single *Kras^{G12D}* cells stained positively for the ductal marker Sox9 (white arrow, bottom row), whilst single RFP positive cells in controls were Sox9 negative (asterisks). Scale bar, 20 μm.

Chapter 4.3 Discussion.

Previous work has found that targeting Kras[G12D] to the acinar compartment drives precancerous lesion development *in vivo* (Habbe et al., 2008; Kopp et al., 2012), suggesting that the acinar cell is the cell of origin for PDAC and activating mutations in *Kras* are sufficient to drive the early stages beginning with ADM (Collins et al., 2012, 2014; Zhu et al., 2007). The microenvironment plays an important role in ADM with macrophages shown to drive ADM (Liou et al., 2013). In chapter 3, acinar cells are eliminated *in vivo* when surrounded by normal neighbours the aim of this chapter was to develop an *ex vivo* model of heterotypic cell-cell interactions in the acinar compartment, to provide insight on this interaction at the level of the single cell. Extrusion of oncogenic cells has also been shown to promote disease progression after evasion of the suppressive epithelial microenvironment (Leung and Brugge, 2012). As this model also allows short-term modelling of ADM it allowed examination of whether normal neighbours repress the initiation of disease with extrusion promoting ADM.

4.3.1 Morphological changes in Kras[G12D] cells surrounded by normal neighbours

To examine the fate of a *Kras[G12D]* cell surrounded by normal neighbours an acinar cell culture system was employed as described previously (Shi et al., 2013). KC and control animals were first injected with tamoxifen to activate Cre, and 48 hours later the pancreas was harvested and acinar cells isolated and cultured in collagen. This resulted in a large number of clusters with different numbers of RFP positive cells. To investigate short term morphological changes in *Kras[G12D]* mutant cells surrounded by normal neighbours; cells were fixed 24 hours after plating and immunofluorescence carried out for the cytoskeletal component F-actin. It was found that subset of *Kras[G12D]* expressing cells undergo morphological changes to a compact, contractile shape when surrounded by normal acinar neighbours. Importantly, this was not observed when transformed cells were surrounded by other transformed cells suggesting it is a result of the heterotypic interaction of normal and *Kras[G12D]* expressing cells. The increase in contractility and time frame is consistent with morphological changes identified

using *in vitro* models (Hogan et al., 2009), supporting the idea that *Kras*[G12D] cells are becoming contractile when surrounded by normal neighbours. In addition, F-actin accumulated at the periphery between normal and Kras[G12D] cells. Previous work has demonstrated that contractile rings form around cells destined to extrude either induced by overcrowding (Eisenhoffer et al., 2012) or apoptosis (Rosenblatt et al., 2001). The recruitment of F-actin did not occur between Kras[G12D] cells suggesting that heterotypic interactions between normal and Kras[G12D] cells results in actin cytoskeleton rearrangements (Hogan et al., 2009). E-cadherin-based cell-cell contacts can couple with the actin cytoskeleton leading to junctional contractility, which has also been implicated in apical constriction and extrusion (Roh-Johnson et al., 2012; Wu et al., 2015). Further characterisation of the interface of normal and transformed acini by immunofluorescence for E-cadherin and other cytoskeletal markers such as phosphorylated myosin-II would further elucidate the mechanism underlying increased contractility of mutant cells surrounded by normal neighbours (Hogan et al., 2009; Porazinski et al., 2016). These results suggest that non-autonomous changes occur to Kras[G12D] acinar cells surrounded by normal neighbours with parallels to other competitive interactions.

Although increased contractility and modulation of cytoskeleton of Kras[G12D] cells were observed (Hogan et al., 2009; Leung and Brugge, 2012), cells were not extruded within the time frame. Extrusion is reported to occur over 8 days in other 3D mammary cultures (Leung and Brugge, 2012) and so extrusion may occur over longer periods in pancreatic acinar cultures. It has also been reported that loss of tight junctions and polarity can occur in acinar culture after 24 hours (Amsterdam and Jamieson, 1974; Marciniak et al., 2013; Park et al., 2004). Moreover, extrusion of Src-transformed cells in zebrafish requires mitosis and proliferation is not observed in this acinar *ex vivo* model (Anton et al., 2018; Shi et al., 2013). Therefore, further investigation is required to elucidate if Kras[G12D] acinar cells are extruded by normal neighbours.

In summary, the acinar *ex vivo* culture is not a robust system however Kras[G12D] cells adopt a contractile morphology when surrounded by normal neighbours. This could suggest that competitive interactions are initiated between normal and Kras[G12D] mutant acinar cells. This could be expanded on in

the future to further investigate the molecular signalling underlying these interactions.

4.3.2 Characterising the impact of normal neighbours on Kras^{G12D} cells progressing through ADM *ex vivo*

Next, to investigate the role of normal epithelial neighbours in ADM recombination was induced with tamoxifen in *Pdx1-Cre^{ER}; LSL-Kras$^{G12D/+}$; ROSA26^{tdRFP}* mice and *Pdx1-Cre^{ER+}; ROSA26^{tdRFP}* controls and 3D acinar cultures were produced. For the identification of cells undergoing ADM two readouts were used: the morphological change to a duct-like cyst and the genetic change to a *Sox9* expressing cell. Firstly, it was necessary to validate the model. It was observed that over time clusters of *Kras^{G12D}* cells adopted a duct-like cyst morphology and expressed *Sox9*. Whereas, control acinar retained acinar morphology and did not genetically reprogram, suggesting that this model faithfully recapitulates previously defined features of ADM *ex vivo* (Kopp et al., 2012; Shi et al., 2013).

Using the morphological change to a duct-like cyst as a read-out of ADM it was found that clusters consisting of over 60% *Kras^{G12D}* cells efficiently underwent ADM whereas activation of Kras in <60% of cells did not produce duct-like cyst formation above the background level. This suggests a non-cell autonomous protective mechanism working to offset ADM or retain the acinar-specific lineage (Krah et al., 2015), similar to the community effect in embryonic development (Gurdon et al., 1993). Although the mechanisms of a community effect are not well understood it has been demonstrated that cell-cell interactions drive homogeneous fate changes in small clusters of cells. Using micropatterning to produce small colonies of 1-8 human embryonic stem (hESC) cells, it has been shown that the community impacts differentiation (Nemashkalo et al., 2017). In response to very low concentrations of BMP, clusters of cells differentiated together whereas non-contacting neighbouring colonies often had alternate fates. It was found that cell-cell interactions maintain a high BMP signalling response and enforce differentiation in the whole cluster. Single cell colonies lacked this reinforcement and consequently differentiated less efficiently. Moreover, it has been demonstrated that single cells transplanted to developing

embryos change fate but clusters do not (Gurdon et al., 1993; Ho, 1992). Thus, single Kras^{G12D} cells may be inhibited to progress through ADM by the surrounding normal neighbours through a community effect and this suggests a signalling threshold underlies ADM.

Interestingly, normal cells surrounded by *Kras^{G12D}* neighbours were found to be recruited into the duct-like cyst structure when a cluster consists of >60% Kras^{G12D} cells. This could indicate that the presence of Kras^{G12D} cells drive a pro-ADM signal to the whole cluster which has been theorised to drive the community effect (Bolouri and Davidson, 2010; Saka et al., 2011). Examination of pancreatic cancer patient samples has shown an upregulation of epidermal growth factor receptor (EGFR) (Tobita et al., 2003) and ligands (Zhu et al., 2000). Moreover, treatment of *ex vivo* acinar cultures with EGFR ligands, such as transforming growth factor alpha (TGF-α) drives ADM (Means et al., 2005). Expression of *Kras^{G12D}* can upregulate EGFR expression and activation which can activate wild-type *Kras* alleles (Ardito et al., 2012; Ji et al., 2009). Therefore, EGFR is a good candidate for the underlying mechanism of how Kras^{G12D} cells promote ADM in normal neighbouring cells.

A recent study found adjacent healthy tissue can be induced by PDAC to form PanIN-like lesions (Ferreira et al., 2017), suggesting wild-type cells can progress through ADM and form a PanIN-like lesion. Although multicolour lineage tracing demonstrated that malignant PanIN lesions are clonal (Maddipati and Stanger, 2015), a meta-analysis of low-grade PanIN lesions from human PDAC samples found that over half of PanIN lesions do not harbour a *Kras* mutation (Löhr et al., 2005). A more recent study using sensitive sequencing techniques detected Kras mutations in most human PanIN lesions, but only in a subset of cells within the lesion (<10% of cells) which does not fit with a clonal origin (Kanda et al., 2012). This strongly supports these findings that *Kras* induces metaplastic features in normal adjacent epithelial cells lacking *Kras* mutations, recruiting them to form a precancerous lesion. Further work to investigate the molecular mechanism underlying this interaction is required and this could lead to the development of therapeutics that promote the protective effect of normal neighbours and decrease the likelihood of precancerous lesion development.

Together, these findings support the hypothesis of a community effect in two contrasting ways; firstly, that normal cells inhibit the morphological formation of a precancerous lesion and secondly that clusters of *Kras* mutant cells can recruit adjacent, normal neighbours into a metaplastic lesion.

After investigating ADM from a histological perspective, the underlying genetic alterations associated with ADM were explored. In normal conditions Sox9 is expressed in ductal cells and not acinar cells (Seymour et al., 2007). Furthermore, Sox9 promotes and is required for PanIN formation from the acinar compartment (Kopp et al., 2012). Immunofluorescence for Sox9 in this *ex vivo* model found that initially all acinar cells are negative for Sox9 and that *Sox9* is expressed in duct-cyst like structures that form from *Kras*^G12D mutant clusters.

After 3 days in culture, single Kras^G12D cells surrounded by normal neighbours were positive for Sox9. The expression of the ductal marker Sox9 in single *Kras*^G12D mutant cells within a cluster of transformed cells suggests that the genetic reprogramming to Sox9 positive cell is a cell-autonomous process and normal neighbours do not influence this change in this model. This is consistent with a recent study that found in human pancreatic ductal cells overexpression of oncogenic *Kras* induces *Sox9* expression (Zhou et al., 2018). However, this is only looking at one marker of ADM and further confirmation is required looking at the loss of acinar specific markers such as amylase or Cpa1. This is important because previous work has demonstrated that Sox9 expression is initiated before Kras-active acinar cells progress to a duct-like state (Kopp et al., 2012). This study used the acinar specific Cre *Ptf1a* to drive *Kras*^G12D expression *in utero* and found that at 2 months after birth a subset of cells with acinar morphology co-expressed the acinar marker Cpa1 and the ductal marker Sox9. Therefore, although Kras^G12D cells surrounded by normal neighbours can express *Sox9* by day 3 it is unclear whether mutant cells could go on to form a lesion at later time points.

4.4 Summary and Future Directions

In summary, several major conclusions can be made from the data presented in this chapter. Firstly, that interaction with normal acinar cells induces morphological changes in single Kras[G12D] cells after 24 hours *ex vivo*. Secondly, that normal acinar neighbours inhibit the progression of Kras[G12D] cells to a precancerous lesion. Finally, when Kras[G12D] cells are present at high numbers they can promote ADM in neighbouring normal cells. This provides further evidence that heterotypic interactions are occurring between normal and transformed cells in the pancreas and they may impact upon pancreatic cancer initiation. However, several interesting questions arise from this work regarding the heterotypic cell-cell interaction of normal and Kras[G12D] acinar cells.

Although this model has provided a number of insights into cell-cell interactions in the pancreas it has several limitations. Proliferation does not occur within the system and normal cells undergo either apoptosis or spontaneous ADM at low levels after several days. Therefore, it is important to investigate the role of normal neighbours using *in vivo* models. This study provides evidence that wild-type cells can be included in precancerous lesions similar to previous reports (Kanda et al., 2012). The implications of this for disease progression are unclear. It raises the question of whether these normal cells are "bystanders" (Ferreira et al., 2017), or play an active role in early lesion development to suppress tumourigenesis. Further characterising these normal-mutant cell interactions *in vivo* could provide insight into a potential role of the normal cells in precancerous lesions. Recent work has supported the stepwise progression of PanIN lesions to pancreatic ductal adenocarcinoma but also that multiple lesions can progress in parallel through the pancreas (Makohon-Moore et al., 2018). With PanIN lesions present in up to 77% of patients without clinically evident pancreatic neoplasia (Matsuda et al., 2017) it suggests precursor lesions have different capacities to progress to PDAC. It is conceivable that interaction of normal neighbouring cells with mutant cells in precursor lesions inhibits precursor lesion progression and could elucidate how low grade lesions differ from malignant lesions. Analysis of human samples of normal pancreas in combination with recent *in situ* mutational detection techniques (Baker et al.,

2017) could test for the presence of *Kras* wild-type cells in PanIN lesions and if there is an association with disease stage.

Using *ex vivo* acinar model this study has identified a threshold of *Kras*^{G12D} mutant cells required to efficiently drive ADM. How this threshold is reached independent of proliferation to allow PanIN formation in human tissue is not clear. Risk-factors such as pancreatitis may help mutant cells overcome the suppressive environment of normal cells. As pancreatitis is associated with immune infiltrate (Montecucco et al., 2014) combining the culture system and model with macrophages as used previously (Liou et al., 2013) could test whether immune cells could facilitate mutant cells to reach this threshold. Chronic pancreatitis can increase the risk of pancreatic cancer by more than tenfold (Bosetti et al., 2014) and pancreatitis promotes pancreatic cancer via EGFR signalling (Ardito et al., 2012). If Kras^{G12D} cells are promoting ADM in normal neighbours via EGFR signalling pancreatitis may also alter the threshold of mutant cells required to form a duct-like cyst and could promote normal neighbours to undergo ADM. Use of EGFR inhibitors could test if this signalling is driving normal neighbouring cells to undergo ADM when surrounded by Kras^{G12D} cells (Ardito et al., 2012) and hence increase the threshold of mutant cells required to drive a cluster to form a duct-like cyst.

Chapter 5: Characterisation of the interface between normal and Kras^{G12D} pancreatic ductal epithelia *in vitro*

5.1 Introduction

It is increasingly apparent that extrusion of aberrant cells provides a mechanism for normal epithelial tissues to maintain homeostasis (Brown et al., 2017; Hogan et al., 2009). However, precisely what happens at the interface between newly emerged transformed cells and the surrounding normal epithelial cells is unclear.

Previous studies have revealed that various molecules and signalling pathways are modulated in transformed cells during apical extrusion. Prior to apical extrusion, Ras^{V12} cells significantly increase in cell height, accumulate F-actin and demonstrate higher activity of myosin-II and Cdc42 (Hogan et al., 2009). This and other studies (Kajita et al., 2010, 2014) have identified that normal neighbouring cells influence the cytoskeletal organisation of mutant cells. Activation of myosin-II and F-actin accumulation leads to enhanced surface tension and cell-cell adhesion of mutant cells, respectively (Lecuit and Yap, 2015); With these two parameters reported to be involved in cell sorting (Canty et al., 2017; Cayuso et al., 2015).

More recently, elevated EphA2 has been identified as the mechanism by which normal cells detect Ras-transformed neighbours (Porazinski et al., 2016). Eph-ephrin signalling has a general role in cell repulsion and cell segregation required for tissue boundary formation in development and maintenance in homeostasis (Batlle and Wilkinson, 2012). Cell-autonomous upregulation of EphA2 in Ras-transformed cells (Macrae et al., 2005; Porazinski et al., 2016) leads to detection by normal neighbours. EphA2 forward signalling then occurs in a ligand dependent manner driving repulsion and segregation of mutant cells. This drives increased contractility of Ras^{V12} cells and extrusion from epithelial monolayers. Extrusion is dependent on E-cadherin-based cell-cell adhesions (Hogan et al., 2009) and signalling via Src family kinases (SFK) and myosin-II are required for RasV12 cell contractility downstream of EphA2 (Porazinski et al., 2016). Moreover, it has been demonstrated that even small clusters of normal cells can induce repulsion of Ras-transformed cells indicating a cell-cell signalling

event driving repulsion (Hill and Hogan, 2017) and not a mechanical compressive force induced by proliferation (Shraiman, 2005).

In this thesis, I present data to show that Kras^{G12D} cells are eliminated from the pancreas via a process that requires non-transformed neighbours and EphA2. To further delineate the heterotypic cell-cell interactions between Kras^{G12D} and normal cells at the single cell level, primary ductal epithelial (PDE) cell culture were used. These cells provided a robust model of epithelial cell interactions in the pancreas and hence allowed further characterisation of normal-mutant cell-cell interactions. This chapter set out to explore: i) whether Kras^{G12D} ductal epithelial cells were segregated by normal neighbours, ii) if signalling pathways previously identified in EphA2-dependent extrusion of mutant cells by normal neighbours are conserved in this system (Hogan et al., 2009; Porazinski et al., 2016), iii) and whether cell mediated changes identified *in vitro* are relevant *in vivo*.

5.2 Results

5.2.1 Segregation of Kras^{G12D} cells in an EphA2 dependent manner *in vitro*

Heterotypic interactions between normal and oncogenic Ras epithelial cells can drive extrusion of mutant cells (Hogan et al., 2009; Kajita et al., 2014; Kon et al., 2017; Ohoka et al., 2015; Wu et al., 2015). Previous work using MDCK cell lines has demonstrated that mutant cells are repulsed leading to extrusion when surrounded by normal neighbours (Porazinski et al., 2016). In this study Kras^{G12D} mutant cells were also found to be eliminated in a process that requires normal neighbours *in vivo*. Modelling and characterising these interactions using an acinar model was difficult as the system was not robust; normal acinar cells surviving only days in culture. Therefore, to better understand heterotypic cell-cell interactions in the pancreas a 2D pancreatic ductal epithelial (PDE) model was used, similar to previous work (Morton et al., 2010; Tape et al., 2016). This allowed mixing of normal and transformed cells at defined ratios and characterisation of Kras^{G12D} cells surrounded by normal neighbours at the level of the single cell over time.

First, Kras^{G12D} mutant cells surrounded by normal neighbours were modelled using PDE and the fate of transformed cells quantified. For this, the pancreas of wild-type animals was harvested and digested before plating on to collagen. Once confluent monolayers of epithelia had formed, normal PDE cells were split and mixed with primary PDE tumour-derived cell lines (with different mutational status) at 1:50 (normal:mutant) ratios. This generates a system of heterotypic cell-cell interactions with a small number of Kras^{G12D} mutant cells surrounded by normal epithelia. Mutant cells were labelled *in vitro* using a commercial cell tracker dye (Porazinski et al., 2016). Following mixing, cells were plated and upon reaching confluency (48 hours after plating) cells were fixed and stained for F-actin to visualise cell morphology (Figure 5.1A). When surrounded by normal neighbours, clusters of *Kras^{G12D}* expressing cells adopted a tightly packed morphology with a smooth border at the interface between normal and mutant cells (Figure 5.1A, top). Pre-labelled Kras^{G12D} cells mixed with non-labelled Kras^{G12D}cells at 1:50 ratios had a regular morphology consisting of random shapes and intermingled with an uneven border (Figure 5.1A, second

row). Furthermore, mixing pre-labelled wild-type PDE cells with non-labelled wild-type cells at 1:50 ratio also resulted in intermingling with jagged borders and a uniform morphology in both cell populations (Figure 5.2). This suggests Kras^{G12D} PDE cells are undergoing morphological changes when surrounded by normal neighbours.

To investigate the observed changes in Kras^{G12D} cell shape, cell area was used as a readout of contractility and area of labelled cells was quantified using ImageJ (Figure 5.1B). A significant decrease in Kras^{G12D} cell (KR) area was observed when surrounded by normal (N) neighbours (KR:N = 172.7 μm^2 ± 25.3 Vs. KR:KR = 355.2 ± 109.5, Welch's t-test p = 0.0412). This shows that Kras^{G12D} cells surrounded by normal neighbours have decreased cell area indicating increased compactness and contractility of mutant cells.

At the interface of Kras^{G12D} mutant and normal cells a smooth boundary was formed. Quantification of the linearity of the boundary between cells can provide a readout of the local intermingling of cells (Canty et al., 2017; Javaherian et al., 2015). Here the Index of Sphericity was used to quantify how much an irregular 2D shape deviates from the ideal shape of a circle (Figure 5.1C) (Ionescu-Tirgoviste et al., 2015). As the value tends more towards 1, the object becomes rounder. It was observed that clusters of Kras^{G12D} mutant cells were significantly more round when surrounded by normal (KR:N) neighbours than Kras^{G12D} cells (KR:KR) (KR:N = 1.092 ± 0.029 Vs KR:KR = 1.319 ± 0.073, Welch's unpaired t-test p=0.0048). This suggests that Kras^{G12D} cells segregate from normal neighbours and separate to form a smooth boundary. Together, these data suggest that Kras^{G12D} cells surrounded by normal neighbours become more tightly packed and segregated indicative of cell repulsion by normal neighbours.

Eph-ephrin signalling regulates cell segregation and cell repulsion (Xu et al., 1999), and EphA2 has previously been demonstrated to drive repulsion of Ras-transformed cells from normal cells (Porazinski et al., 2016). To test the functional role of EphA2 in this system, primary cells with Kras^{G12D} mutation and EphA2-deficiency (KRE) were used in cell mixing experiments. A replacement vector within the extracellular domain of *EphA2* results in a non-functional, truncated protein (Brantley-Sieders, 2004; Brantley-Sieders et al., 2008), the

same EphA2-deficient model as used *in vivo* in chapter 3. When KRE cells were mixed with non-transformed, normal cells it was observed that mutant clusters no longer adopted a tightly packed morphology, however a smooth boundary was still observed at the interface with normal neighbours (Figure 5.1A, third row). KRE mutant cells mixed with non-labelled KRE cells had a regular morphology similar to N:N co-cultures and intercalated with neighbours (Figure 5.1A, bottom). Quantification of cell area showed KRE cells had significantly larger cell area compared to Kras^{G12} cells when surrounded by normal cells (KR:N = 172.7 μm^2 ±25.3 Vs. KRE:N = 426.9 μm^2 ± 68.2, Welch's unpaired *t*-test p = 0.0026). This indicates KRE cells do not adopt a contractile and compact morphology when surrounded by normal neighbours. Moreover, KRE cells surrounded by normal cells had a similar area to KRE:KRE co-cultures (KRE:N = 426.9 μm^2 ± 68.2 Vs. KRE:KRE = 494.5 μm^2 ± 71.5). Analysis of mutant cell segregation by Index of Sphericity also demonstrated that KRE clusters are significantly less round and hence intermingle more with normal neighbours than KR cells (KR:N = 1.092 ± 0.029 Vs. KRE:N = 1.196 ± 0.061, Welch's unpaired *t*-test, p = 0.034). Mixing of KRE:KRE cells (Figure 5.1A, bottom row) demonstrated that KRE cells have a comparable Index of Sphericity (Figure 5.1B,C) (KRE:N = 1.196 ± 0.061 Vs. KRE:KRE = 1.285 ± 0.044, Welch's unpaired *t*-test, p= 0.08). Overall, this suggests that KRE cells surrounded by normal neighbours are not compacted or triggered to become round, suggesting a requirement for EphA2 in the repulsion of Kras^{G12D} cells by normal neighbours. However, the boundary between KRE cells and normal neighbours was found to be more blunt than controls, and Index of Sphericity is lower than KRE:KRE mixes indicating a level of segregation of KRE cells from normal neighbours. In summary, Kras^{G12D} PDE cells are triggered to become contractile and compact when surrounded by normal neighbours, which is dependent on functional EphA2 in mutant cells. Moreover, although mutant cells are triggered to become round in an EphA2-dependent manner other factors are involved in segregation of the two cell populations as KRE cells have a smooth boundary with wild-type cells.

Interestingly, it was observed that some clusters of Kras^{G12D} cells surrounded by normal neighbours had rounded up and were apically extruded from the monolayer (Figure 5.3A). In KR:N co-cultures, 49% of Kras^{G12D} clusters

(38/77 clusters, n = 2) were extruded out of the monolayer within 48 hours. Extrusion was observed at low levels in KR:KR co-cultures (Figure 5.3B) (3/71 cells n = 2). When Kras^{G12D} cells were EphA2-deficient (Figure 5.3C) the efficiency of extrusion decreased to 18% (14/76 cells n = 2). Although, the rate of extrusion in KRE:N mixing assays did not decrease to comparable levels to KRE:KRE mixes (Figure 5.3D)(4/68 cell n = 2).

Overall, this suggests that Kras^{G12D} transformed cells are actively repulsed by normal neighbouring cells which can result in apical extrusion of mutant cells. Moreover, it suggests this process is dependent on EphA2 in the mutant cell population.

A

	F-actin	CMRA	Nuclei/Merge
KR:N			
KR:KR			
KRE:N			
KRE:KRE			

B

C
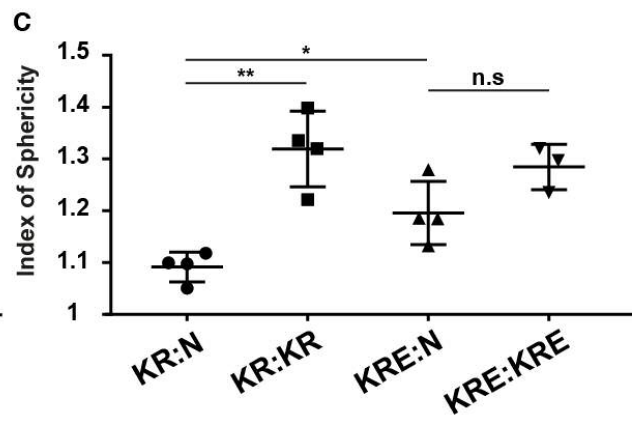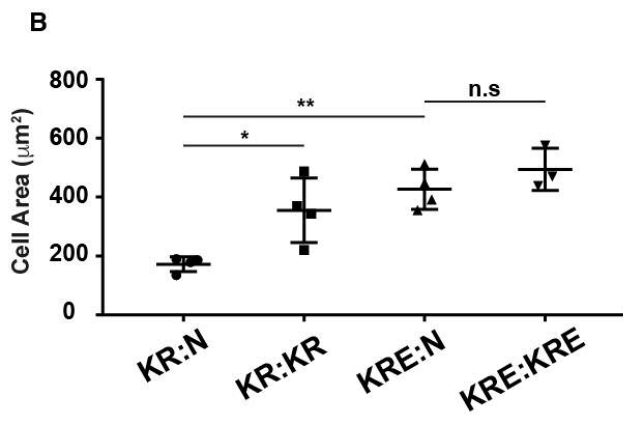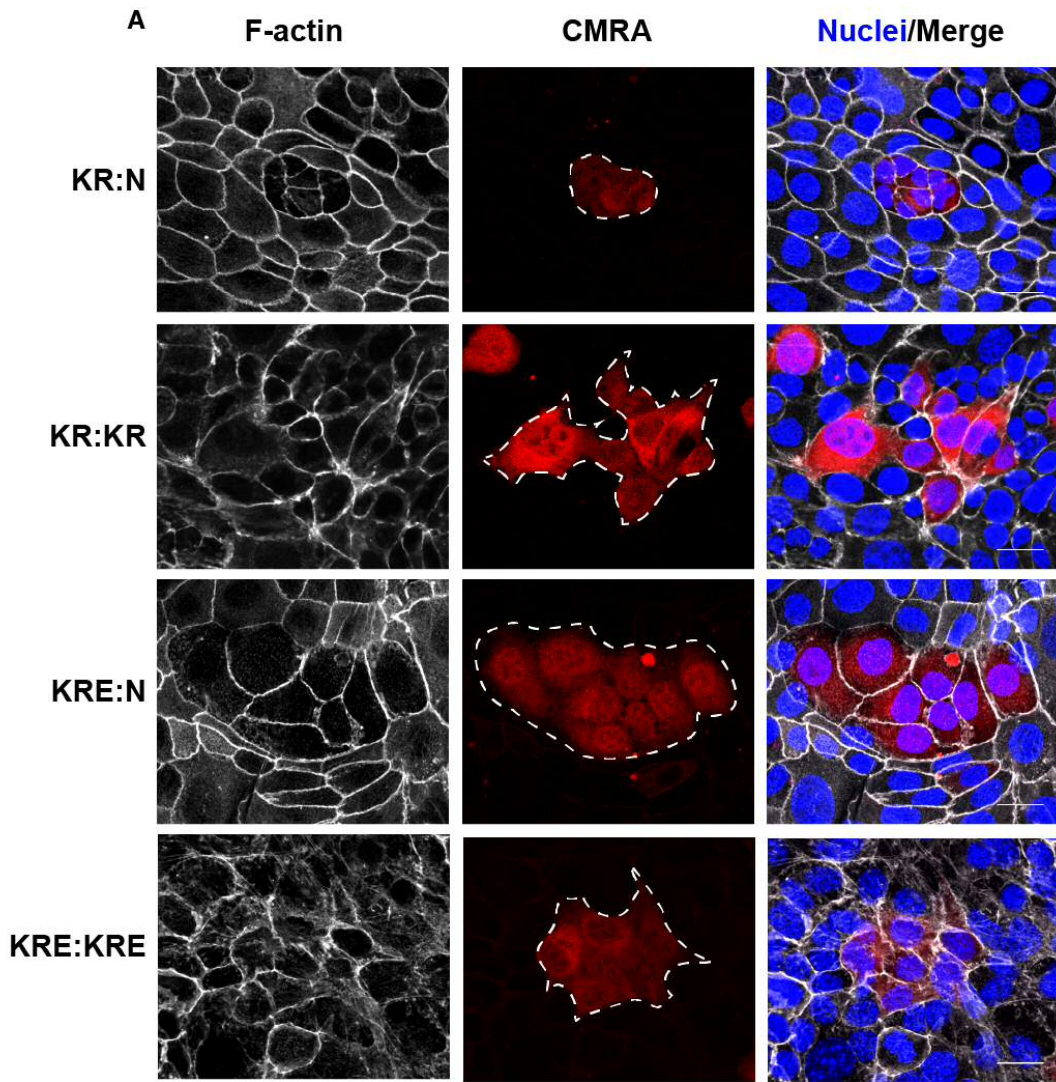
Figure 5.1: Increased contractility and segregation of Kras^{G12D} cells when surrounded by normal neighbour. (A) Representative images of mixing assays of normal (N) and labelled mutant cells populations (red) of either Kras^{G12D} (KR) mutated cells or Kras^{G12D}, EphA2 deficient (KRE) cells. F-actin grey; CMRA cell tracker red; Hoescht blue. Clusters of Kras^{G12D} mutant cells adopt a compact and round morphology when surrounded by normal neighbours in an EphA2 dependent manner. This suggests mutant cells are repulsed by normal neighbours via EphA2. (B) Quantification of cell area shows a significant decrease in Kras^{G12D} cells surrounded by normal cells (n= 552 cells) compared to Kras^{G12D}:Kras^{G12D} assays (n=241 cells). EphA2 deficiency in KRE cells surrounded by normal cells (n= 316 cells) significantly increased the area of transformed cells. KRE cells surrounded by normal neighbours have similar area as KRE:KRE cell assays (n= 119 cells). (C) Index of Sphericity quantifies how much an irregular shape deviates from a circle with rounder shapes tending towards 1. KR clusters surrounded by normal cells (n= 25 clusters) are significantly rounder than clusters from KR:KR assays (n= 36 clusters). Loss of functional EphA2 in Kras^{G12D} cells significantly increased Index of Sphericity (n=21 clusters) and were more similar to KRE cells from KRE:KRE assays (n= 22 clusters). Data represents mean ± s.d. with each point representing a biological replicate. Statistical analysis was carried out using Welch's unpaired *t*-test. $P < 0.05$ = *, $P<0.001$ = **. Scale bar, 20 μm.

N:N

F-actin   CMRA   Nuclei/Merge
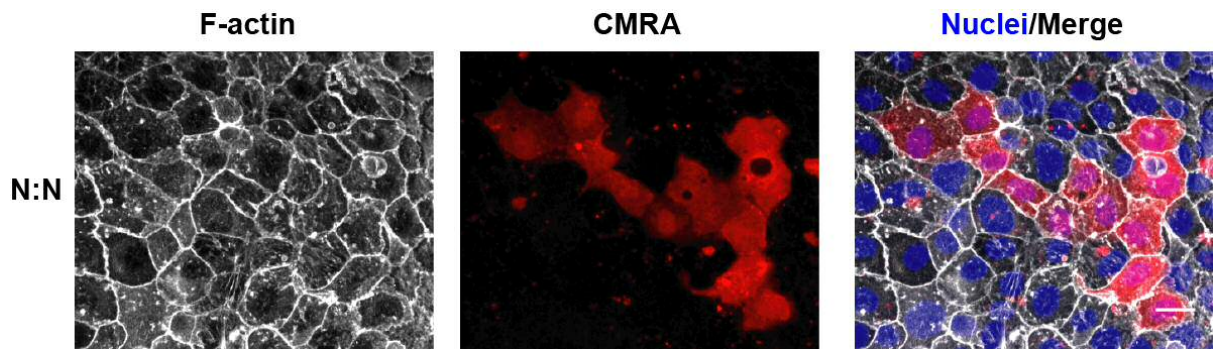
Figure 5.2 Normal cell interactions do not drive morphological changes in labelled normal cells. F-actin (grey) was used to analyse morphological changes to CMRA (red) labelled normal cells (N) mixed with non-labelled populations of normal cells (N). No apparent changes to morphology were observed in labelled normal cells. This suggests normal:normal (N:N) interactions do not lead to segregation of labelled cells. Scale bar, 20 μm.
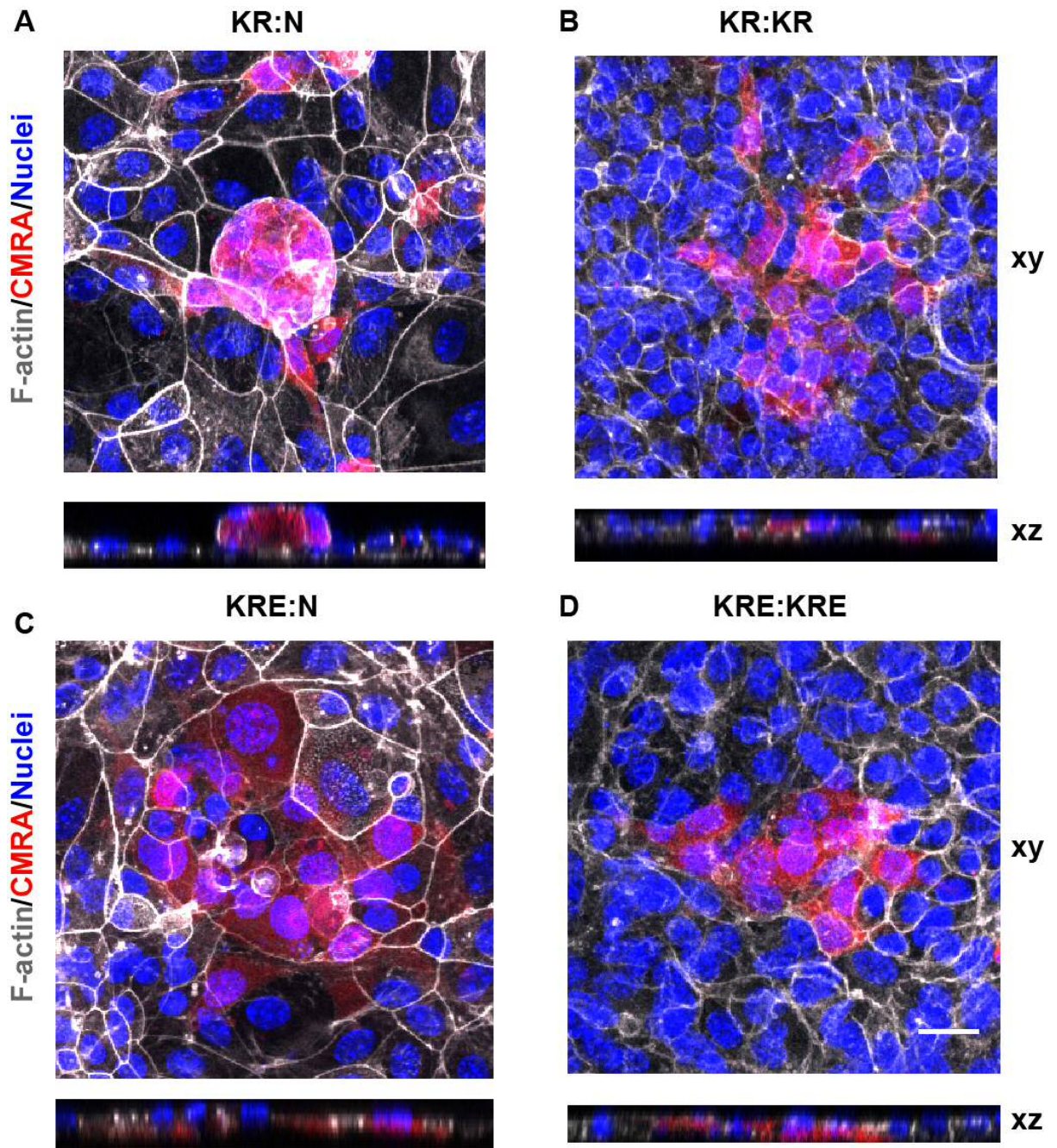
Figure 5.3: Extrusion of Kras^{G12D} cells surrounded by normal neighbours. (A) Clusters of Kras^{G12D} labelled (red) cells are extruded out of the monolayer by normal neighbours. Whereas Kras^{G12D} cells (KR) integrate and form a flat 2D monolayer with other Kras^{G12D} cells (KR:KR, B). Kras^{G12D}; EphA2-deficient cells integrate and are not extruded when surrounded by normal (C) or other KRE (D) cells. This suggests Kras^{G12D} are extruded by normal neighbours in an EphA2 dependent manner. xy images are max projections in z and are representative of 2 independent experiments. xz are orthogonal views. F-actin grey; CMRA cell tracker red; Hoescht blue. Scale bar, 20 μm.

5.2.2 Characterisation of EphA2 downstream signals *in vitro*

Signalling through Eph receptors and ephrin ligands is highly complex and acts through multiple pathways (Cayuso et al., 2015; Pasquale et al., 2008) to affect cell migration, proliferation and differentiation. EphA receptors bind to glycosylphosphatidylinositol (GPI) –anchored ephrinA ligands and with both components membrane-bound, signalling requires direct cell-cell contact (Davis et al., 1994). To investigate the downstream signals from heterotypic cell-cell interactions in PDE cells immunofluorescence was carried out on cell mixing assays as before.

Ras-transformed MDCK cells are detected by normal neighbours by autonomous upregulation of EphA2 in mutant cells (Macrae et al., 2005; Porazinski et al., 2016). To investigate levels of EphA2 in normal and transformed pancreatic cells mixing assays were stained for EphA2. When Kras[G12D] cells were surrounded by normal neighbours EphA2 levels appeared high at cell-cell contacts between transformed cells than in the surrounding wild-type cells (Figure 5.4, top), suggesting EphA2 levels are higher in mutant cells. Moreover, a large amount of EphA2 positive puncta were observed in mutant cells surrounded by normal neighbours but with a lack of membrane EphA2 staining observed at the heterotypic cell-cell boundary. When Kras[G12D] cells were mixed with labelled Kras[G12D] cells low levels of membrane localised EphA2 was observed, whereas a large number of EphA2 positive punctate were observed (Figure 5.4, second row). This suggests that EphA2 is autonomously higher, similar to previous reports (Macrae et al., 2005; Porazinski et al., 2016), but localisation appears to be primarily cytoplasmic. Importantly, EphA2 levels were depleted in KRE cells surrounded by normal neighbours and monolayers of KRE cells formed by KRE:KRE co-cultures (Figure 5.4 bottom). This indicates that EphA2 protein is depleted in KRE cells. Together, these results suggest that EphA2 protein is upregulated in Ras-transformed cells and that KRE cells are depleted of EphA2 protein.

Following investigation of EphA2 levels the activation of EphA2 signalling was studied. Initially, immunofluorescence for markers of EphA2 activation such as phosphorylated EphA2 (Y594) were used but this proved inconsistent so activity of EphA2 downstream signals was examined. Global phosphoproteome

analysis has demonstrated that activated Ephs function upstream of RAS/RHO GTPases, Src, phospholipase Cγ2 and mitogen-activated protein kinases (MAPKs) (Fang et al., 2008; Jørgensen et al., 2009). Signalling via the Src has previously been shown to be required for RasV12 cell extrusion (Hogan et al., 2009) and to be activated downstream of EphA2 (Porazinski et al., 2016). Therefore, immunofluorescence for phosphorylated (Y416) active Src was carried out. Elevated phosphorylated Src (pSrc), and hence active Src, was specifically detected in Kras^{G12D} cells surrounded by normal neighbours (Figure 5.5); inferring that EphA2 is activated specifically in Kras^{G12D} cells when surrounded by normal neighbours. However this requires further investigation to confirm the accurate staining of the pSrc antibody, including a control with no secondary antibody staining and a control with only secondary antibody staining to test for auto-fluorescence and non-specific staining respectively. Therefore this work only tentatively suggests pSrc is activated in KR cells surrounded by normal neighbours.

To test that Epha2 on mutant cells is functional a ligand-cell repulsion assay was used. Pre-clustered recombinant ephrin ligand can bind to Eph receptors on cells and induce Eph receptor clustering and activate signalling (Davis et al., 1994; Knöll et al., 2007; Porazinski et al., 2016). This can be observed as a repulsion phenotype upon interaction with pre-clustered ligand. Using this approach PDE cells were seeded into one of two compartments of a cell culture insert separated by a fixed gap. Pre-clustered recombinant ephrin-Fc proteins were used to coat the second compartment (Knöll et al., 2007; Porazinski et al., 2016). After removing the culture insert cells migrate and close the gap and interact with immobilised ligand. EphA2 interacts with ephrinA1 which results in forward EphA2 signalling and inhibition of cell migration (Deroanne et al., 2003; Fero et al., 2011; Miao et al., 2000), therefore ephrinA1 was used to coat the second compartment. As KR cells lacked motility and did not grow to confluence forming clusters rather than sheets, another PDE tumour-derived line was used which had Kras^{G12D} and p53^{R127H} mutations. These data were generated by Rebecca Bennion, a Cardiff University undergraduate, under my supervision.

First, it was necessary to confirm that Fc alone did not inhibit the migration of KP or KRE cells (Figure 5.6). Both cell populations migrated over Fc stripes. However, KP cells failed to efficiently migrate over ephrinA1 ligands, indicating cell repulsion by ephrinA1 (Figure 5.6). In contrast, KRE cells were not inhibited by ephrinA1 ligand and migrated over EphrinA1-Fc stripes similar to Fc control. This indicates that in tumourigenic PDE cells, EphA2 is functional. Moreover, this is consistent with the hypothesis that EphA2 expressed on mutant cells is activated by ephrin-presenting normal neighbours. Although further work is required to investigate this interaction in KR cells with EphrinA1 as it is not possible to extrapolate the results of KP cells due to the additional p53 mutation.

Another key aspect of EphA2 downstream signalling is modulation of cytoskeletal dynamics. Eph-ephrin signalling is associated with increased phosphorylated MLC (Rohani et al., 2011) and EphA2 is a known regulator of RhoA (Brantley-Sieders et al., 2008; Wakayama et al., 2011), which acts upstream of myosin-II (Gallo, 2006). This can regulate the contractile properties of a cell to generate force between cells and drive extrusion (Bielmeier et al., 2016; Hogan et al., 2009; Kajita et al., 2014; Wu et al., 2015). To study myosin-II activity, staining for phosphorylated MLC (pMLC) was carried out in cell mixing assays. In contrast to previous studies, elevated levels of phosphorylated MLC were not observed in Kras^{G12D} when surrounded by normal cells (Figure 5.7). A ring of membrane localised staining of pMLC was observed at the boundary between normal and mutant cells, however this appears to arise from the normal cell population and is at a similar intensity to other normal:normal interfaces (Figure 5.7). When Kras^{G12D} cells were mixed with labelled Kras^{G12D} cells, a low level of diffuse pMLC was observed. Thus, pMLC staining of Kras^{G12D} cells when surrounded by normal neighbours is not elevated in mutant cells and appears similar to Kras^{G12D} monolayers. This indicates that myosin-II activity is autonomously lower in Kras^{G12D} cells than non-transformed pancreatic cells and is not increased when mutant cells are surrounded by normal neighbours. However, a ring of p-myosin-II is observed at the boundary between normal and clusters of Kras^{G12D} cells. Changes to pMLC requires further investigation to confirm the accurate staining of the pMLC antibody to pMLC protein. This would include a negative control with no secondary antibody staining and a control with only secondary antibody staining to test for auto-fluorescence and non-specific

staining respectively. A positive control such as the previously characterised cell lines MDCK could also be used to confirm specific staining of the antibody to pMLC (Porazinski etal., 2016).
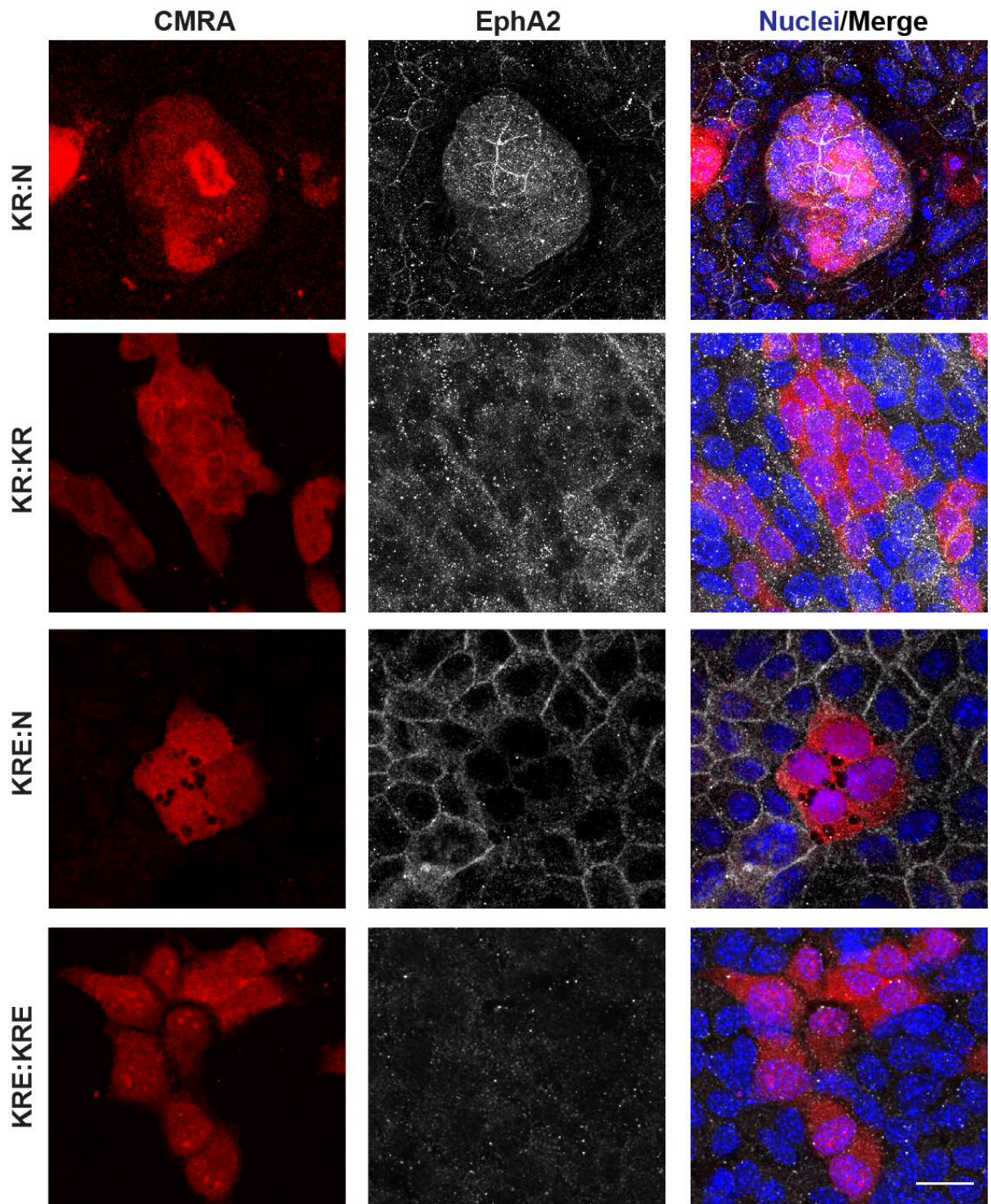
Figure: 5.4: Characterisation of EphA2 in cell mixing assays. Normal (N) cells were mixed with pre-labelled (CMRA, red) Kras^{G12D} (KR) cells or pre-labelled EphA2-deficient Kras^{G12D} cells (KRE) at a ratio of 1:50 and stained for EphA2 (grey). Levels of EphA2 appear higher in KR cells than surrounding normal neighbours and localises at the membrane between mutant cells and as punctate cytoplasmic staining. EphA2 in KR:KR mixes appears diffuse and cytoplasmic. KRE cells appear depleted of EphA2 when surrounded by normal neighbours (KRE:N) or non-labelled KRE cells (KRE:KRE). Images are representative of 2 biological replicates. CMRA cell tracker red; EphA2 grey; Nuclei blue. Scale bar, 20 μm.
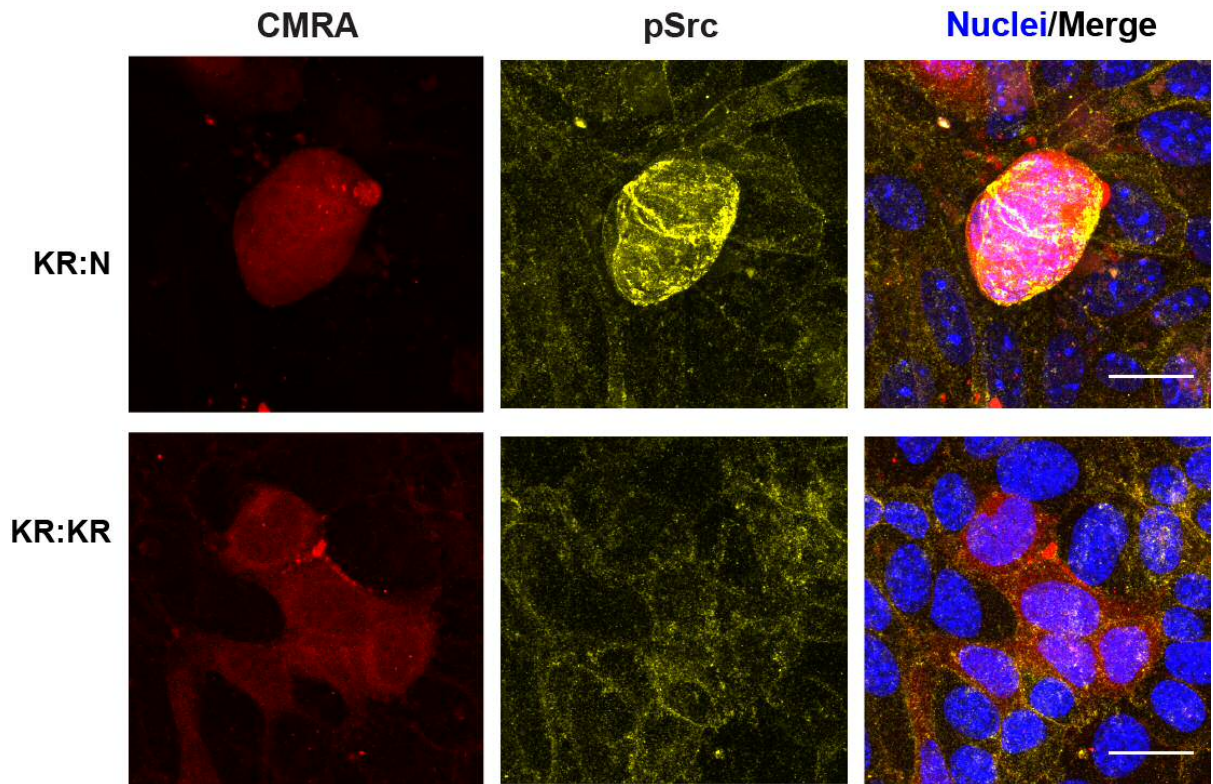
Figure 5.5 Characterisation of EphA2 downstream signalling in Kras^{G12D} cells. Mixing CMRA (red) labelled Kras^{G12D} (KR) mutant cells with normal (N) have elevated pSrc (yellow) compared to KR:KR mixing assays. Images are representative of 2 biological replicates. CMRA cell tracker red; pSrc yellow; Hoescht blue; F-actin grey. Scale bar, 20 μm
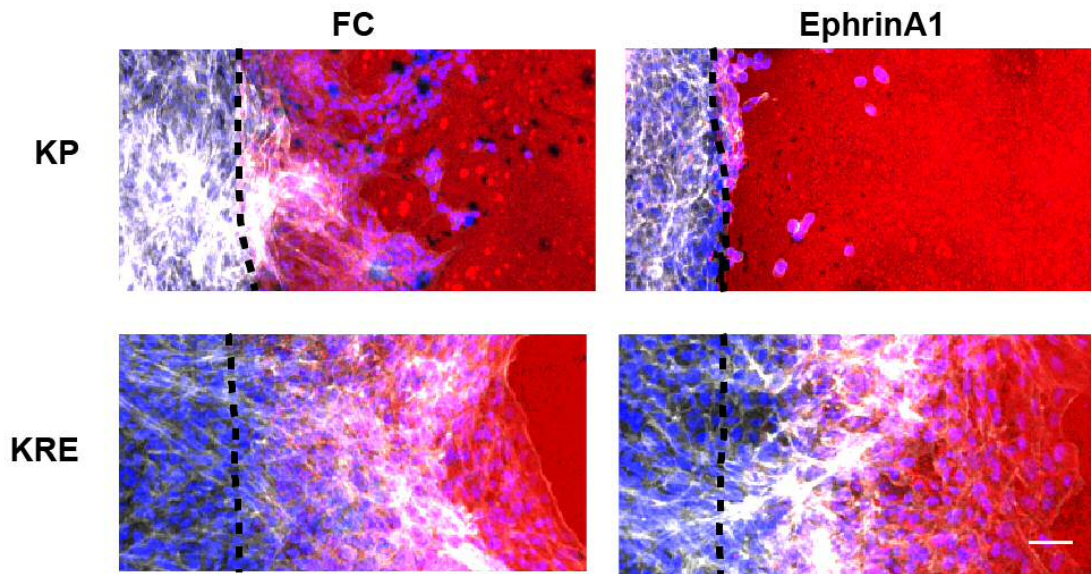
Figure 5.6 Cell-ligand repulsion assay. Kras^{G12D}; p53^{R172H} (KP) cells and Kras^{G12D}; EphA2^{tm1jrui} (KRE) cells were plated in one well of an insert and Fc or Fc-ephrinA1 ligand used to coat the second compartment. Once the insert is removed cells migrate and interact with Fc-stripe. Both KP and KRE cells migrate over Fc-stripes. However, KP cells are unable to migrate over ephrinA1 ligand whereas EphA2 depleted KRE cells efficiently migrate over ephrinA1-stripes. Images are representative of 3 biological replicates. Black dotted line indicates stripe boundary; F-actin grey; Nuclei blue; Fc stripe red. Scale bar, 20 μm.
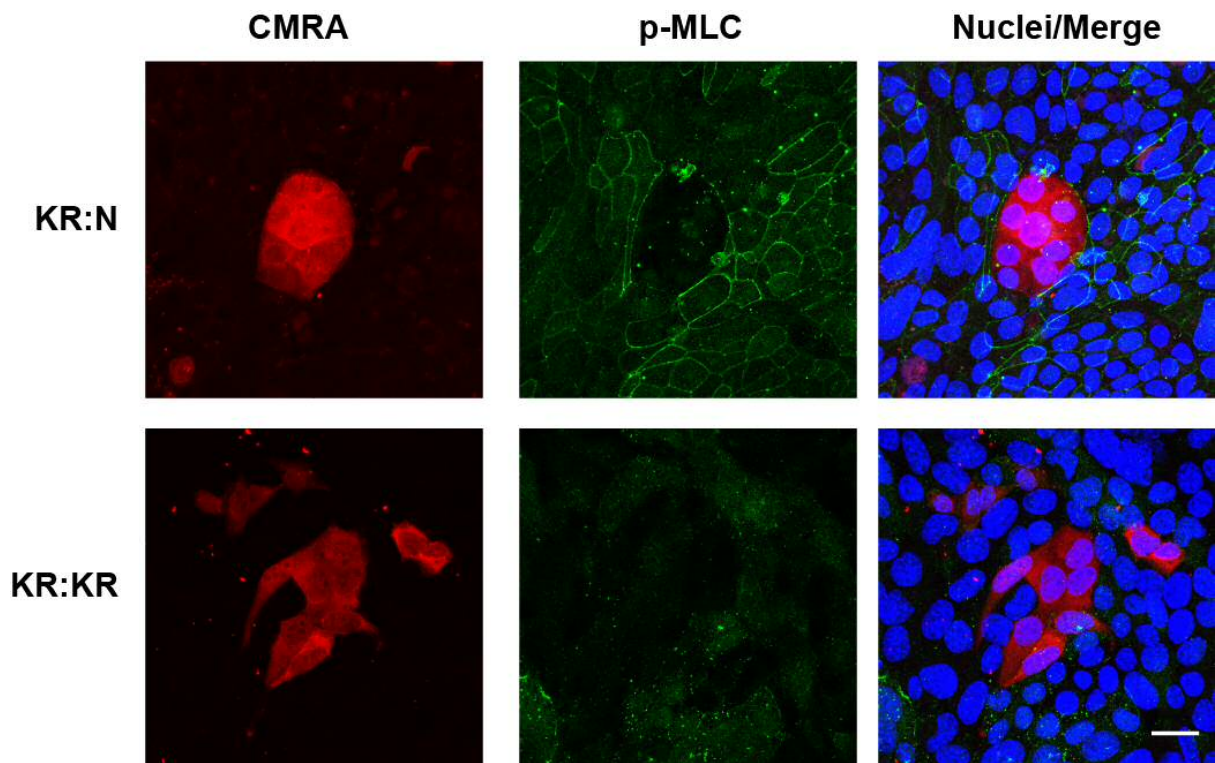
Figure 5.7 Characterisation of p-MLC in Kras^{G12D} cells surrounded by normal neighbours. Co-cultures of CMRA (red) labelled Kras^{G12D} (KR) mutant cells and normal (N) or KR:KR co-cultures were stained for phosphorylated-myosin-II (p-MLC; green). Levels of phosphorylated p-MLC appears autonomously lower in KR cells than non-labelled normal cells and pMLC is not elevated in KR cells surrounded by normal neighbours. CMRA cell tracker red; pSrc yellow; Hoescht blue; F-actin grey; phosphor-MLC cyan. Scale bar, 20 μm

5.2.3 Characterisation of E-cadherin in Kras^{G12D} cells surrounded by normal neighbours

Eph-ephrin signalling regulates the cytoskeleton as well as cadherin and integrin mediated adhesion to control segregation and boundary formation (Arvanitis and Davy, 2008). Previously, it has been demonstrated that E-cadherin is required in normal cells for the extrusion of mutant cells (Hogan et al., 2009). Super resolution microscopy also identified endocytosis of E-cadherin in Ras-transformed cells as a key driver of extrusion (Saitoh et al., 2017). Ligand-induced EphA2 forward signalling can also increase E-cadherin-based cell-cell contacts in Ras^{V12} cells and E-cadherin is required in normal cells for boundary formation and segregation (Porazinski et al., 2016). Thus, immunofluorescence for E-cadherin was carried out in Kras^{G12D} pancreatic cell mixing assays.

As expected, when KR:KR cells were mixed to generate monolayers of Kras^{G12D} cells, E-cadherin mainly localised at cell-cell contacts (Figure 5.8, second row). However, when Kras^{G12D} cells were surrounded by normal cells an accumulation of cytoplasmic puncta positive for E-cadherin was observed (Figure 5.8, top). This was accompanied by an apparent decrease in E-cadherin at cell-cell contacts of Kras^{G12D} cells. E-cadherin cytoplasmic puncta were also observed in Kras^{G12D} cells not in direct contact with normal cells. E-cadherin puncta were not diffuse throughout the cytoplasm as described previously in cell competition (Saitoh et al., 2017) but appeared polarised and adjacent to the nucleus, possibly indicative of endocytosis (Kimura et al., 2006; Lu et al., 2003). This suggests E-cadherin is internalised in Kras^{G12D} cells surrounded by normal neighbours and mutant cells are segregating from normal neighbours.

Kras^{G12D} cells segregate in an EphA2 dependent manner therefore E-cadherin was also examined in KRE pancreatic cells mixed with normal cells. In monolayers of KRE cells from KRE:KRE mixing E-cadherin was detected mostly at cell-cell contacts (Figure 5.8, bottom), similar to monolayers of Kras^{G12D} cells. Next KRE clusters surrounded by normal cells were investigated. E-cadherin was not observed to accumulate in KRE cells surrounded by normal neighbours, with membrane localisation of E-cadherin observed between normal and KRE cells (Figure 5.8, third row). This suggests EphA2-deficiency in Kras^{G12D} cells permits the formation of E-cadherin-based cell-cell contacts between normal and mutant

cells. Furthermore, it indicates that EphA2 acts upstream of E-cadherin internalisation to drive segregation of Kras^{G12D} cells by normal cells.

The association of p120 catenin with E-cadherin at epithelial cell membranes is critical for the formation and maintenance of adherens junctions (Ireton et al., 2002). The loss or mislocalisation of p120 catenin can destabilise E-cadherin and impact the adhesive properties of a cell. Furthermore, p120 catenin has shown to be required for apical and basal extrusion of Kras^{G12D} cells from pancreatic PanIN lesions *in vivo* (Hendley et al., 2016). To investigate context-dependent changes in p120 catenin, immunofluorescence was carried out using the mixing assay. When Kras^{G12D} cells (KR) were mixed with labelled Kras^{G12D} cells, p120 catenin was predominately localised to the membrane in both cell populations (Figure 5.9). However, when Kras^{G12D} cells were surrounded by normal cells diffuse cytoplasmic staining was observed in mutant cells (Figure 5.9). This was accompanied by an apparent decrease of p120 catenin at the interface between normal and transformed cells. However, membrane localised p120 catenin was observed between Kras^{G12D} mutant cells within a cluster. This supports the observed loss of E-cadherin-based cell-cell contacts between normal and Ras-transformed cells and could indicate decreased adhesion between the two cell populations.

In summary, the data presented here suggest that adherens junctions are absent between Kras^{G12D} cells and surrounding normal cells, indicative of segregation of mutant cells by normal neighbours. As EphA2-deficient Kras^{G12D} cells can form E-cadherin-based cell-cell contacts with normal neighbours this suggests EphA2-dependent repulsion of Kras^{G12D} cells by normal neighbours is leading to loss of cell-cell contacts.
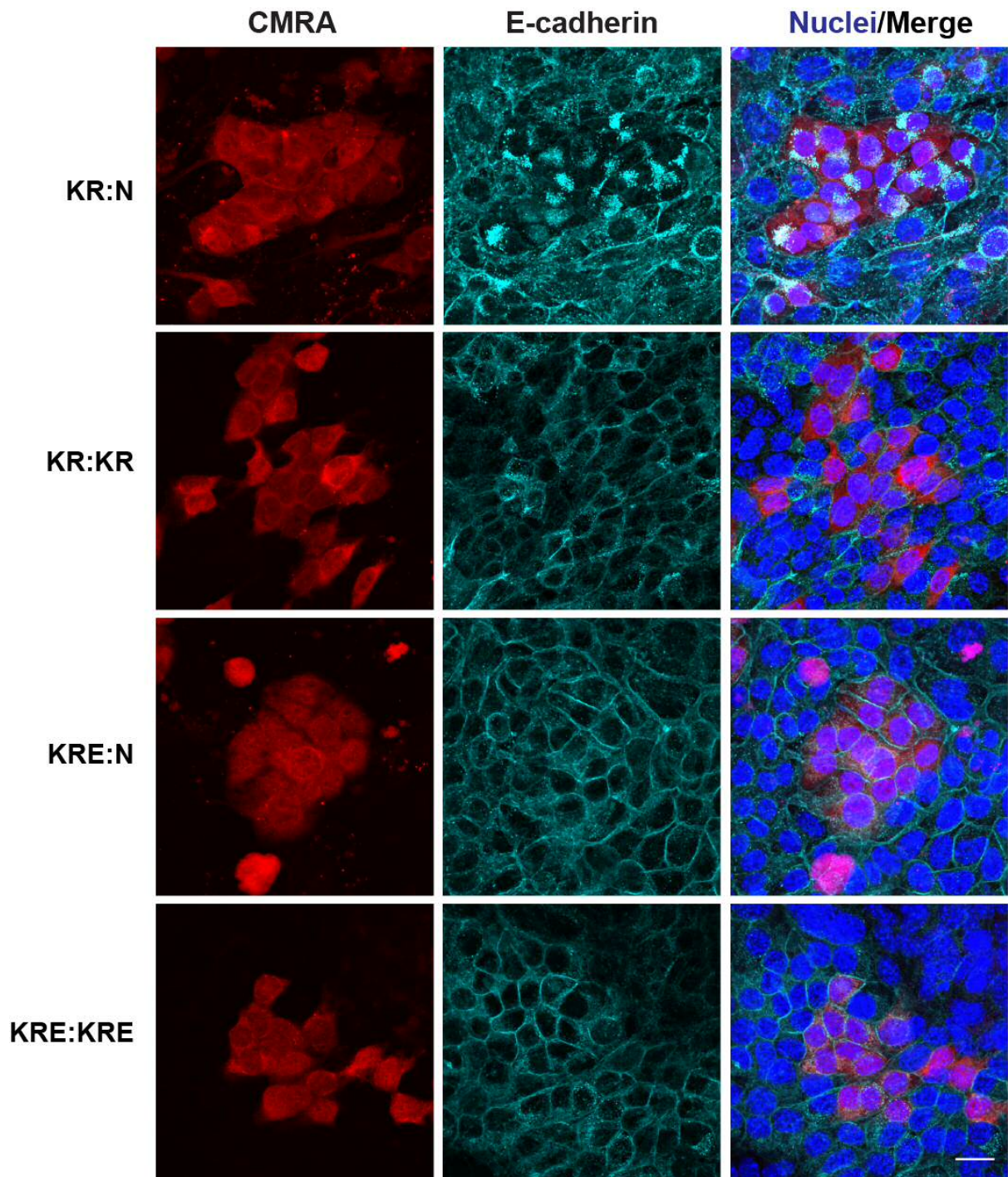
Figure: 5.8: Internalisation of E-cadherin in Kras^{G12D} cells surrounded by normal neighbours. Normal (N) cells were mixed with labelled (CMRA, red) Kras^{G12D} (KR) or Kras^{G12D};EphA2-deficient (KRE) cells at a ratio of 1:50. E-cadherin (cyan) decreased from the membrane of KR cells surrounded by normal cells and accumulates in the cytoplasm. This was not observed in KR:KR, KRE:N or KRE:KRE mixing assays suggesting it is a result of heterotypic cell-cell interactions dependent on EphA2. CMRA red; E-cadherin cyan; Hoescht blue. Images are representative of three independent experiments. Scale bar, 20 μm
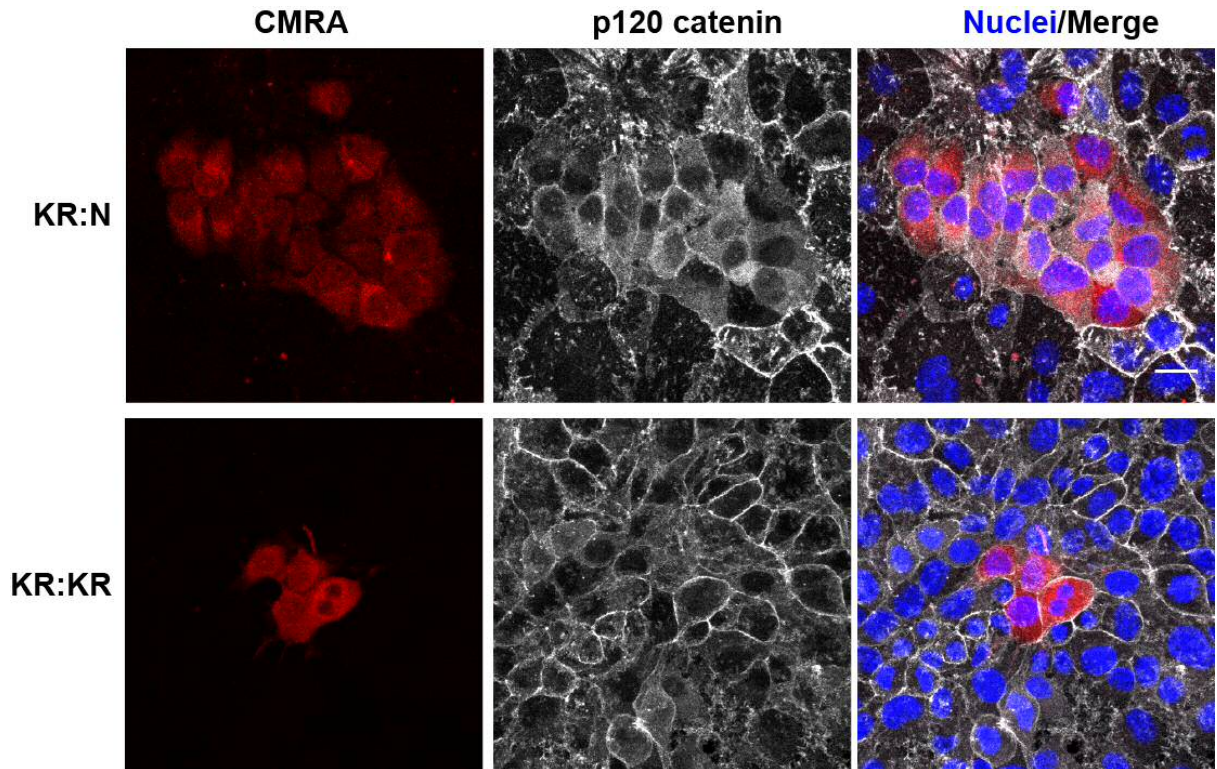
Figure: 5.9: Investigation of p120-catenin in Kras^{G12D} cells surrounded by normal neighbours. Normal (N) cells were mixed with labelled (CMRA, red) Kras^{G12D} (KR) cells at a ratio of 1:50. Immunofluorescence for p120 catenin (grey) was observed to decrease at the membrane of KR cells surrounded by normal cells and appeared diffuse in the cytoplasm. This was not observed in KR:KR mixing assays suggesting it is a result of heterotypic cell-cell interactions. CMRA red; p120-catenin grey; Hoescht blue. Scale bar, 20 μm

5.2.5 Segregation of Kras^{G12D} cells surrounded by normal neighbours *in vivo*

In chapter 3 it was found that Kras^{G12D} cells are eliminated when surrounded by normal neighbours in an EphA2 dependent manner. Mixing of primary pancreatic ductal cells in this chapter demonstrated that mutant cells undergo repulsion when surrounded by normal neighbours and adopt a compact, contractile morphology. To investigate whether these characterised changes in cell morphology are also occurring *in vivo*, a three-dimensional (3D) imaging approach was carried out.

Computer reconstruction of physical serial sections has been demonstrated to allow visualisation of large tissue volumes (mm^3) whilst maintaining high resolution (<1 μm) (Parfitt et al., 2012). This novel technique known as immunofluorescent computed tomography (ICT) was carried out on pancreata harvested 7 days post-induction (dpi) with low dose from both KC (*Pdx1-Cre^{ERT}; ROSA26^{RFP}; Kras$^{G12D/+}$*) and control (*Pdx1-Cre^{ERT}; ROSA26^{RFP}*) mice. Two-dimensional sections 2 μm thick were stained for E-cadherin and anti-RFP and imaged (Figure 5.8A), serial sections were then aligned and stacked to generate a 3D reconstruction of RFP positive clusters (Figure 5.10B). The volume of RFP positive cells could then be quantified using Imaris software (Bitplane). At 7 dpi, a decrease in the volume of Kras^{G12D} cells surrounded by normal neighbours compared to Kras wild-type controls was observed (Figure 5.8C). After 7 dpi Kras^{G12D} cells have a median volume of 2.08 x10^4 μm^3 compared to the volume of control RFP cells (2.83 x10^4 μm^3). This suggests an increase in contractility of Kras^{G12D} cells surrounded by normal neighbours *in vivo*. Moreover, changes to E-cadherin at the interface between Kras^{G12D} and normal cells may be occurring *in vivo*, with less apparent membrane staining between Kras^{G12D};RFP positive cluster and normal cells compared to control (Figure 5.8A). Although more biological replicates are required to allow statistical comparison, this is consistent with the hypothesis that mutant cells surrounded by normal neighbours *in vivo* are increasing in contractility.
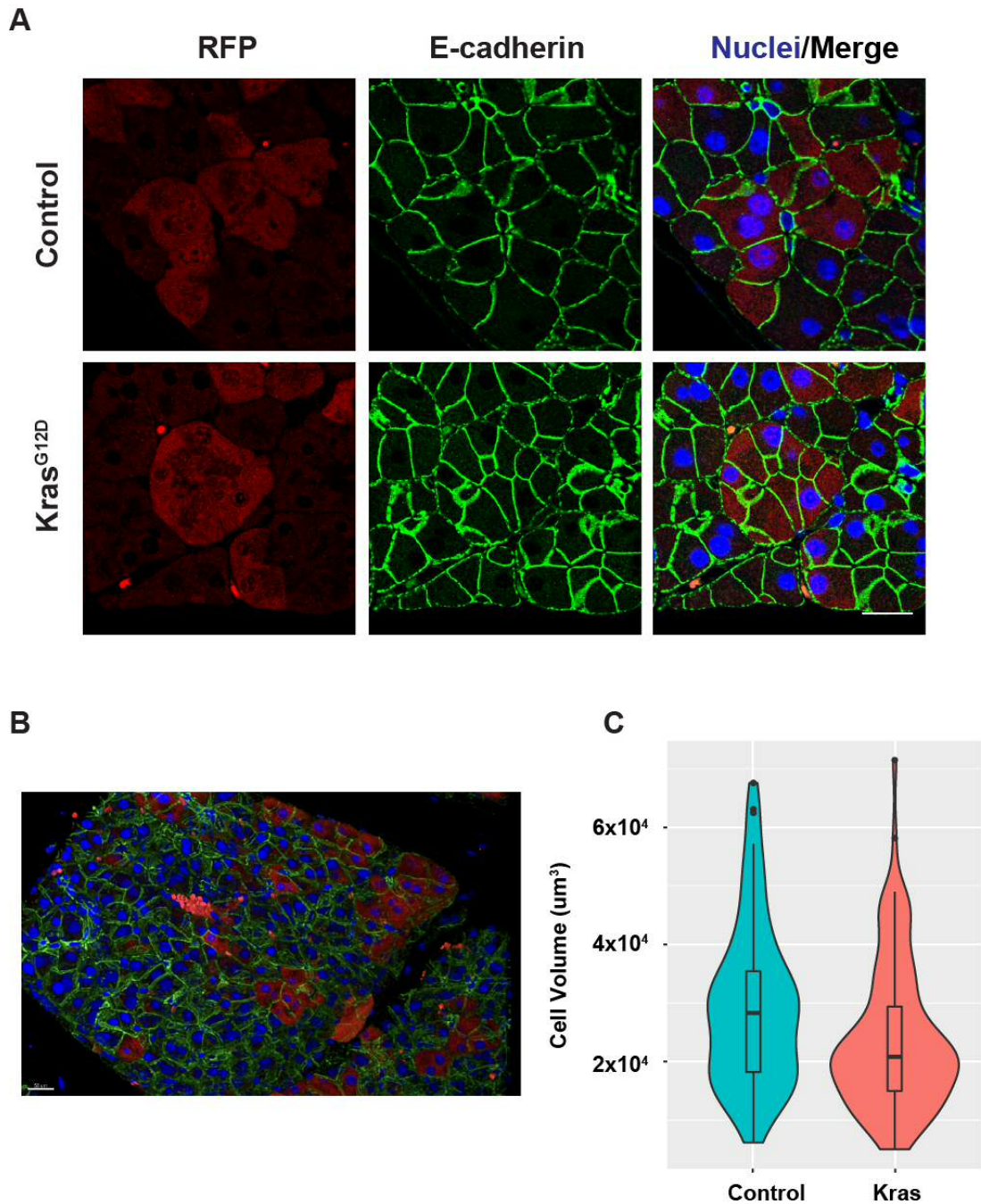
Figure 5.10: Quantification of Kras^{G12D} cell volume *in vivo*. Pancreata containing RFP (red) labelled cells from control (*Pdx1-Cre; Rosa26^{RFP}*) or Kras^{G12D} (*Pdx1-Cre;Rosa26^{RFP}; Kras^{G12D}*) 7 days post-induction were serial sectioned and imaged. (A) Representative 2D images of a single section from control and Kras^{G12D} showing segregation of transformed cells. (B) Representative 3D image of aligned serial sections. RFP red; E-cadherin green; Hoescht blue. (C) Violin plot showing cell volume of control (n=100 cells) or Kras^{G12D} (n=100 cells) at 7 days post-induction. The Tukey-style boxplot within violin plot has the median depicted as a horizontal line across the box, box edges are 25th and 75th percentile with whiskers 1st to 99th percentile. Data represents 2 independent experiments with 50 cells/experiment. Scale bar, 20 μm (A); 50 μm (B).

5.3 Discussion

Cell competition is a cell fitness-sensing mechanism that eliminates cells that, although viable, are less fit than the surrounding neighbours. Ras-transformed cells have been shown to undergo cell competition resulting in the extrusion and elimination of mutant cells (Hogan et al., 2009; Kajita et al., 2014; Kon et al., 2017; Wu et al., 2015). Extrusion depends on E-cadherin-based cell-cell adhesion, activation of myosin-II and accumulation of F-actin at the interface between normal and transformed cells (Hogan et al., 2009; Wu et al., 2015). More recently, we have demonstrated that elevated EphA2 on Ras-transformed cells leads to ephrinA-EphA2 forward signalling driving repulsion and increased contractility of mutant cells (Porazinski et al., 2016). Oncogenic cells emerge within normal epithelial sheets and so extrusion may be occurring at the earliest stages of disease. However, whether segregation of abnormal cells is promoting or suppressing tumourigenesis is unclear. Previously in chapter 3 evidence for the selective elimination of Kras^{G12D} cells by normal neighbours was found *in vivo*. To further elucidate the underlying mechanism of mutant cell elimination, primary pancreatic ductal cells were used in cell mixing assays.

Although acinar cells were primarily being labelled *in vivo*, modelling heterotypic acinar cell-cell interactions *ex vivo* was technically challenging (Chapter 4). This system is not robust as non-transformed cells rapidly undergo cell death in culture after several days (Liou et al., 2013; Shi et al., 2013). Therefore, this chapter set out to characterise a primary ductal epithelial (PDE) cell culture model to investigate heterotypic cell-cell interactions between normal and Kras^{G12D} cells. This provided a more robust system *in vitro*, as non-transformed cells grow as 2D monolayers on collagen and can be serially passaged and allowed elucidation of the underlying mechanism of heterotypic Kras^{G12D}:normal cell interactions (Chen et al., 2009; Morton et al., 2010; Reichert et al., 2013). There is evidence that both acinar and ductal compartments can give rise to PDAC (Bailey et al., 2016; Ferreira et al., 2017). Furthermore, acinar cells are known to transdifferentiate to duct-like cells, via acinar-ductal metaplasia (ADM), that give rise to pancreatic intraepithelial neoplasia (PanIN), precursor lesions (Guerra et al., 2007; Habbe et al., 2008; Kopp et al., 2012). Human PanIN lesions also contain both Kras^{G12D} cells and Kras wild-type cells

(Kanda et al., 2012), therefore heterotypic cell-cell interactions could occur in these lesions. Thus, ductal cultures can provide important information about pancreatic heterotypic cell-cell interactions between normal and Kras^{G12D} cells that is pertinent to the earliest stages of pancreatic cancer.

5.3.1 Segregation of Kras^{G12D} cells in an EphA2 dependent manner

Differential EphA2 signalling drives repulsion and segregation of Ras-transformed MDCK cells from surrounding normal cells (Porazinski et al., 2016). To investigate whether Kras^{G12D} pancreatic ductal epithelial cells are also segregated; mutant and normal cells were mixed at a ratio of 1:50. This generated monolayers of normal cells with clusters of transformed cells at low densities; recapitulating the *in vivo* scenario. Quantification of cell area and the Index of Sphericity of a cluster can give an indication of contractility of cells and segregation and compactness of clusters (Javaherian et al., 2015; Kippert et al., 2009). Quantification of mutant clusters demonstrated that Kras^{G12D} cells increase in contractility and segregate from normal pancreatic cells. This is consistent with previous findings where Ras-transformed cells are repulsed by normal neighbours and adopt a contractile morphology (Porazinski et al., 2016). Loss of EphA2 in the mutant cell population was sufficient to significantly decrease contractility and segregation from surrounding normal cells. Furthermore, quantification of Kras^{G12D} cells *in vivo* indicates that transformed acinar cells decrease in volume supporting the hypothesis that mutant cells *in vivo* are becoming contractile. It was also found that Kras^{G12D} PDE cells could be extruded from the monolayer in an EphA2-dependent manner consistent with previous reports *in vitro* (Porazinski et al., 2016). Moreover, it supports the hypothesis that cell competition is occurring in healthy epithelial tissues to remove aberrant cells (Brown et al., 2017; Kon et al., 2017).

It is conceivable that extrusion of mutant cells could have a tumour-suppressive or tumour-promoting role *in vivo*. Single transformed cells have been identified disseminating precursor lesions which can lead to metastasis (Hendley et al., 2016; Rhim et al., 2012). With Kras^{G12D} mutant and Kras-wild type cells identified in precursor lesions it is conceivable that EphA2 signalling may drive extrusion of mutant cells from PanIN lesions. Extrusion of single cells has also

been shown to promote mutant cell growth (Leung and Brugge, 2012). Thus, this could suggest a tumour-promoting role for competitive interactions with inhibition of extrusion potentially inhibiting tumour growth and metastasis.

However, heterotypic interactions between Kras[G12D] cells and normal neighbours may also protect against tumour formation. If apical extrusion is occurring *in vivo* it could lead to mutant cells in the pancreatic ductal network. Presumably this would expose mutant cells to harsh conditions such as altered pH and could be cleared into the intestine and out via the gastrointestinal tract (Kon et al., 2017; Saitoh et al., 2017). Although apical extrusion was observed in PDE *in vitro* monolayers the direction of extrusion and effects of potential repulsion by normal neighbours within a 3D space of the pancreas tissue is less clear and requires further investigation. In summary, this chapter provides evidence than competitive interactions with normal cells are driving increased compactness of Kras[G12D] cells both *in vitro* and *in vivo*.

5.3.2 Characterisation of EphA2/ephrin and downstream signalling in pancreatic cells *in vitro*

In order for aberrant cells to be eliminated they must first be detected by normal neighbouring cells. We have previously demonstrated that EphA2 is autonomously upregulated in Ras-transformed MDCK cell lines which promotes detection by normal neighbours (Porazinski et al., 2016). In this study levels of EphA2 appear to be higher in Kras[G12D] cells as observed by elevated levels observed between mutant cells surrounded by normal neighbours however, the localisation was primarily cytoplasmic when surrounded by normal neighbours or Kras[G12D] cells. Staining of EphA2 in MDCK cells is punctate when plated on collagen and membrane localised on glass. Therefore, the punctate EphA2 staining of pancreatic cells could be a result of plating on top of collagen. Importantly, EphA2 levels were depleted in KRE cells indicating a loss of EphA2. Moreover, these cells were previously derived from animals with the same genetic disruption of EphA2 as KC-Eph mice supporting the *in vivo* model from the chapter 3.

As a requirement for EphA2 in Kras[G12D] cells had been observed for segregation from normal cells it was investigated whether the downstream

signalling pathway was similar to previous reports (Porazinski et al., 2016). Increased levels of phosphorylated Src were observed specifically in Kras^{G12D} cells surrounded by normal neighbours supporting the hypothesis that EphA2 signalling is activated in Kras^{G12D} mutant cells. Although activation of pSrc requires further confirmation to confirm the accuracy of antibody staining. Moreover, use of stripe assay found that Kras^{G12D} p53^{R172H} mutant PDE cells were unable to efficiently migrate over pre-clustered ephrinA1 ligand. Further characterisation of ephrin-receptor interaction is required to as KP (Kras^{G12D} p53^{R172H}) cells may interact differently to Kras^{G12D}cells upon collision with EphrinA1 stripes. However, EphA2-deficient Kras^{G12D} cells could efficiently migrate over stripes of pre-clustered ephrinA1. This suggests EphA2 is functional on Kras^{G12D} PDE cells.

It was previously observed that levels of phosphorylated myosin light chain were elevated in Ras-transformed cell surrounded by normal neighbours (Hogan et al., 2009). Also, it was previously found that signalling via myosin-II was lost in Ras-transformed cells depleted of EphA2 when collided with normal cells (Porazinski et al., 2016), suggesting activation of actomyosin downstream of EphA2. In contrast to previous studies, this work found tentative evidence that elevated phosphorylated myosin-II was not observed in Kras^{G12D}:normal cell interactions. Levels of active myosin-II were lower in Kras^{G12D} cells than non-transformed neighbours and appeared similar to monolayers of Kras^{G12D} cells. This requires further characterisation in the form of a no secondary antibody control and staining only with a secondary antibody to check auto-fluorescence and non-specific staining respectively. However, this could suggest repulsion and cytoskeletal rearrangement in Kras^{G12D} cells by normal neighbours could be different in primary pancreatic cells to MDCK cell lines and occurs via another pathway. Several other pathways have been associated downstream of EphA2 to drive repulsion. For example, EphA2 can mediate actin cytoskeletal reorganisation via the Rac1/PAK pathway (Deroanne et al., 2003). Moreover, mDia1 and mDia3, members of the formin protein family, act downstream of EphA4-dependent axon repulsion (Toyoda et al., 2013) and so could also be acting downstream of EphA2 in repulsion of Kras^{G12D} cells in primary pancreatic cells. Although active myosin-II was not elevated in Kras^{G12D} cells surrounded by normal neighbours differential levels of phosphorylated myosin-II were observed

between mutant cells and the surrounding neighbours. Myosin-II can generate tension within a cell (Franke et al., 2005) and so this could indicate differential tension between normal and Kras^{G12D} cells, which is important for cell sorting (Brodland, 2002; Krieg et al., 2008). In developing *Drosophila* a myosin-II cable forms at the boundary between different tissues (Monier et al., 2010). Therefore, although myosin-II does not appear to act downstream of EphA2 to drive repulsion, the contractile ring of myosin-II observed at the boundary between normal and Kras^{G12D} cells is indicative of repulsion and segregation of mutant cells by normal neighbours. Therefore, further work is required to understand the role of myosin-II in Kras^{G12D} pancreatic cells surrounded by normal neighbours.

In Eph-ephrin-mediated cell sorting cell-cell adhesion have been shown to be important (Steinberg, 2007) and EphA2 can weaken E-cadherin-mediated cell-adhesions (Fang et al., 2008). Previous work has demonstrated than endocytosis of E-cadherin via Rab-5 GTPase is vital for extrusion (Saitoh et al., 2017). Moreover, E-cadherin is required within normal cells for extrusion of Ras-transformed neighbours (Hogan et al., 2009). In PDE cells it was found that E-cadherin was internalised in an EphA2 dependent manner. This could indicate that upon interaction with normal cells, E-cadherin in Kras^{G12D} cells undergoes endocytosis by Rab-5 as observed in previous work (Saitoh et al., 2017), which is supported by the specific localisation of E-cadherin observed in PDE cells. Moreover, Eph-ephrin interactions can lead to adhesive forces between cells which must be overcome in order for cellular repulsion to occur. This can either occur through metalloproteinase cleavage of ephrin ligand (Hattori et al., 2000) or endocytosis of phosphorylated-Eph receptor and ligand into the receptor expressing cell (Marston et al., 2003). With EphA2 known to interact with E-cadherin (Guo et al., 2014; Van Itallie et al., 2014; Zantek et al., 1999), it is possible that EphA2 and E-cadherin are endocytosed together which could explain the punctate EphA2 staining in mutant cells surrounded by normal neighbours. It is worth noting that active Eph signal transduction persists following endocytosis (Marston et al., 2003) and so repulsive signals would be maintained. In this chapter, EphA2 deficiency in Kras^{G12D} cells was sufficient to allow formation of E-cadherin-based cell-cell contacts between normal and mutant cells. This is supported by previous studies where EphA2 has been demonstrated to drive E-cadherin loss from adherens junctions (Fang et al.,

2008). Furthermore, staining for E-cadherin *in vivo* indicated loss of membrane E-cadherin between normal and Kras[G12D] cells suggesting a similar process may occur *in vivo*. Knockdown of E-cadherin in single cells in a normal epithelia has been demonstrated to be sufficient to drive extrusion (Vaughen and Igaki, 2016) inferring that loss of E-cadherin-based cell-cell contacts is an important step in the segregation of Kras[G12D] cells by normal neighbours.

The p120 catenin protein associates with E-cadherin at the cell membrane to stabilise E-cadherin, inhibit E-cadherin endocytosis and promote adherens junction formation (Ishiyama et al., 2010; Wildenberg et al., 2006). A decrease in p120 catenin at the membrane, specifically between Kras[G12D] and normal PDE cells was observed in cell mixing assay, which further supports the hypothesis that E-cadherin-based cell-cell contacts are lost at heterotypic cell-cell contacts. Loss of p120 catenin has also been shown to promote extrusion of Kras[G12D] cells from pancreatic PanIN lesions (Hendley et al., 2016), which suggests EphA2-dependent junctional remodelling may occur in PanIN lesions. Moreover, extruding cells from PanIN lesions were found to have decreased E-cadherin and epithelial-mesenchymal transition (EMT) characteristics. With loss of E-cadherin a hallmark of EMT and metastasis (Wheelock et al., 2008), it is conceivable that heterotypic Kras[G12D]:normal cell interactions may promote neoplastic cell invasion. Although p120 catenin was internalised in Kras[G12D] cells surrounded by normal neighbours, membrane-localised p120 catenin was observed between Kras[G12D] cells. p120 catenin can bind other cadherins such as P-catenin (Albergaria et al., 2011) so could remain at the membrane during E-cadherin internalisation. Together, these data suggest that EphA2 is driving extrusion of mutant cells which results in loss of E-cadherin-based cell-cell contacts in mutant cells surrounded by normal neighbours.

The segregation and sorting of different cell populations has been extensively studied in development and homeostasis. With several hypotheses proposed for the segregation of cells; differential adhesion (Nose et al., 1988; Steinberg, 1963), induction of actomyosin contractility (Krieg et al., 2008) and Eph-ephrin signalling (Xu et al., 1999) which can alter both cadherin mediated adhesion (Hattori et al., 2000) and modulate the actin cytoskeleton (Marston et al., 2003). In this study, differences in myosin-II activity and a loss of E-cadherin-based cell-cell contacts, which could imply differential tension and adhesion

between normal and mutant cells, respectively. Therefore, differential tension and adhesion could be leading to the observed segregation of mutant cells surrounded by normal neighbours. Loss of EphA2 in mutant cells resulted in a loss of contractile morphology when surrounded by normal neighbours and retention of transformed cells within normal monolayers. However, a smooth boundary was still observed at the interface of normal and mutant cells. This could suggest that repulsion of Kras^{G12D} cells occurs via EphA2 but that other mechanisms contribute to segregation of mutant by normal pancreatic cells. Further characterisation of active myosin-II and use of the myosin-II inhibitor blebbistatin would further elucidate the segregation of EphA2-deficient Kras^{g12D} cells by normal neighbours. In summary, the repulsion of Kras^{G12D} mutant cells by normal neighbours occurs via an EphA2-dependent mechanism, resulting in loss of E-cadherin-based cell-cell contacts.

5.4 Summary and Future Directions.

Using the pancreatic ductal epithelial model in this chapter has further elucidated the mechanism of heterotypic cell-cell interaction between Kras^{G12D} cells and normal neighbours at the level of the single cell. In summary, several conclusions can be made from the data presented in this chapter. Firstly, that Kras^{G12D} cells segregate and are repulsed by normal neighbours which can result in extrusion. Secondly, that EphA2 is elevated in mutant cells and required for repulsion and extrusion. Finally, EphA2-dependent repulsion results in loss of E-cadherin-based cell-cell contacts but does not appear to involve phosphorylated myosin-II in mutant cells.

Taken together, and in combination with previously published data, these results suggest that segregation of Kras^{G12D} cells via EphA2 signalling could lead to the elimination of mutant cells. This raises several interesting questions regarding the maintenance of homeostasis in the pancreas by removal of aberrant cells.

Segregation or compacting of cells can have a variety of effects on a cell. In this chapter and other studies the contractile force is sufficient to drive extrusion of mutant cells (Hogan et al., 2009; Kon et al., 2017). The effect of this *in vivo* is still unclear; apical extrusion exposes cells to typically harsh

environments such as urine or digestive fluids and is in the opposite direction from metastasis and so could be considered cancer-preventative. Although the pathological consequences of apical extrusion are controversial (Leung and Brugge, 2012; Makohon-Moore et al., 2018) and heterotypic cell-cell interaction can also drive basal extrusion (Hogan et al., 2009). To address this issue, the fate of eliminated cells needs to be studied *in vivo*. Analysis of 3D reconstructions at later time points may identify extrusion events *in vivo* and provide information on the fate of transformed cells. This could also be carried out in EphA2-deficient animals to confirm that increased contractility of Kras^{G12D} cells *in vivo* is occurring in an EphA2-dependent manner. This would support the hypothesis that EphA2-deficieny is leading to retention of mutant cells by removing EphA2 dependent repulsion between normal and mutant cells. Furthermore, if extrusion of Kras^{G12D} cells is promoting metastasis, analysis of the liver, the primary site of metastasis, or searching for circulating cancer cells using FACS for RFP cells could further elucidate this.

It is also important to further characterise the signalling cascade in vitro. The work in this chapter suggests that pSrc is activated and E-cadherin is internalised upon interaction of Kras^{G12D} and normal cells in an EphA2 dependent manner. It has previously been demonstrated that pSrc is downstream of EphA2 signalling (Porazinski et al., 2016), and that E-cadherin endocytosis plays an active role in apical extrusion of transformed cells (Saitoh et al., 2017). The requirement of these signals for extrusion in this system could be investigated with the use of pharmacological inhibitors of endocytosis such as chlorpromazine (Dutta and Donaldson, 2012; Saitoh et al., 2017). Analysis of pSrc in EphA2-deficient Kras^{G12D} cells could also confirm that SFK signalling is activated downstream of EphA2 as in previous work (Porazinski et al., 2016). With inhibition of pSrc shown to decrease Ras repulsion (Porazinski et al., 2016) and the extrusion of Src-transformed cells by non-transformed neighbours, inhibition of pSrc could further elucidate the molecular mechanism underlying EphA2-dependent extrusion.

The contractility of a cell is regulated by the actin-myosin cytoskeleton which in turn are dynamically controlled by Rho-family GTPases (Lawson et al., 2017). Further work could investigate whether Rho GTPases are important for the contractility observed in Kras^{G12D} cells surrounded by normal neighbours.

The role of Rho-family GTPases could be further elucidated using an active Rho pull-down. Furthermore, the addition of inhibitors would test the requirement of Rho-family GTPases in mutant cell contractility. This would further elucidate the molecular mechanism of repulsion of Kras^{G12D} pancreatic cells by normal neighbours.

Intriguingly this work infers that endocytosis of E-cadherin and potentially EphA2 is occurring in Ras-transformed cells. EphA2 endocytosis is necessary to overcome the adhesive properties of Eph-ephrin interactions required for cell repulsion (Marston et al., 2003; Zimmer et al., 2003). As EphA2 can interact and localise with E-cadherin (Guo et al., 2014; Van Itallie et al., 2014) and internalisation of E-cadherin was observed it could infer that both are endocytosed. This could be explored further by investigating early endosome markers such as EEA1 (Simonsen et al., 1998). Caveolin-1 has also been involved in the internalisation of EphA2 (Vihanto et al., 2006). As caveolin-1 has been demonstrated to be required for Ras-transformed cell competition and extrusion (Kadeer et al., 2017; Ohoka et al., 2015), this could link EphA2 and other cell competition mechanisms. Further elucidation of the implications of E-cadherin internalisation will improve our understanding of EphA2-dependent Kras^{G12D} cell extrusion and may link EphA2 to other regulators of cell competition (Kadeer et al., 2017; Kajita et al., 2014; Ohoka et al., 2015).

Eph-ephrin signalling has been well characterised in other tissues such as intestine (Batlle et al., 2002) where EphB/EphrinB signalling mediates cell positioning. Understanding Eph-ephrin signalling in pancreas homeostasis may provide further understanding of how this signal is altered in disease. To this end functional characterisation of Eph and ephrin family members could begin with generating an expression profile for the different cell types within the pancreas. Indeed, little is known about the role of EphA2 except in pancreas development (Park et al., 2013). Thus, understanding the role of EphA2 in pancreas homeostasis may help elucidate how signalling changes upon emergence of Kras^{G12D} transformed cell within a normal pancreatic epithelium.

In vitro cell culture systems are an invaluable tool for understanding cell biology and to characterise the underlying mechanisms of disease. However, 2D cell cultures can differ from the *in vivo* situation in a number of different ways, for example tissue culture conditions can select for clones that no longer model the

primary tumour (Boj et al., 2015; Lee et al., 2006). Moreover, 2D systems do not accurately recapitulate the complexity and organisation of a tissue with interactions limited between cells to only side-by-side contact which can alter cell morphology and adherens junctions (Soares et al., 2012). Recently, primary organoid models have been established for normal and neoplastic murine and human pancreatic tissue (Boj et al., 2015). Therefore, investigating heterotypic cell-cell interactions in normal human pancreatic tissue that is amenable to genetic manipulation could provide new insight into these processes and their relevance to human disease.

Chapter 6 General Discussion

At the initial stages of carcinogenesis, mutant cells emerge within an epithelial layer. Competitive interactions between normal and transformed cells can lead to the elimination of mutant cells from the epithelium to protect from carcinogenesis (Alcolea et al., 2014; Hogan et al., 2009; Kon et al., 2017; Norman et al., 2012; Wagstaff et al., 2016). Strikingly, oncogenic cells such as Ras-transformed cells can be eliminated by normal neighbours (Hogan et al., 2009; Kajita et al., 2014). In pancreatic ductal adenocarcinoma Kras^{G12D} mutations are considered the initial transformation and are sufficient to drive malignant disease (Collins et al., 2012; Habbe et al., 2008; Hingorani et al., 2003). Although Kras^{G12D} expressing cells (Kras^{G12D} cells) initiate and drive the earliest stages of pancreatic cancer it is unclear if normal pancreatic cells can eliminate oncogenic cells. In this study, I have used low level, stochastic induction of Kras^{G12D} mutation in vivo to model these interactions. I found that Ras-transformed cells adopt a contractile morphology and are eliminated from healthy tissue when present at low numbers. Using in vitro co-cultures, Kras^{G12D} cells surrounded by normal neighbours become segregated, increase in compactness and are often extruded. I find that E-cadherin-based cell-cell contacts are downregulated and internalised in mutant cells when surrounded by normal neighbours in an EphA2-dependent manner. Our evidence also suggests that normal cells suppress progression of Ras-transformed cells to an early disease state. Together, this study suggests that non-transformed pancreatic epithelial cells can eliminate Kras^{G12D} cells from the tissue via EphA2 signalling (Figure 6.1). These data identify a novel putative tumour-suppressive mechanism in the adult pancreas that mutant cells must first overcome to drive tumourigenesis. Understanding the fate of eliminated cells and how cells are retained will further elucidate the role of cell competition in pancreatic cancer. Moreover, this may provide insight into how risk factors promote disease and how pancreatic cancer spreads around the body.
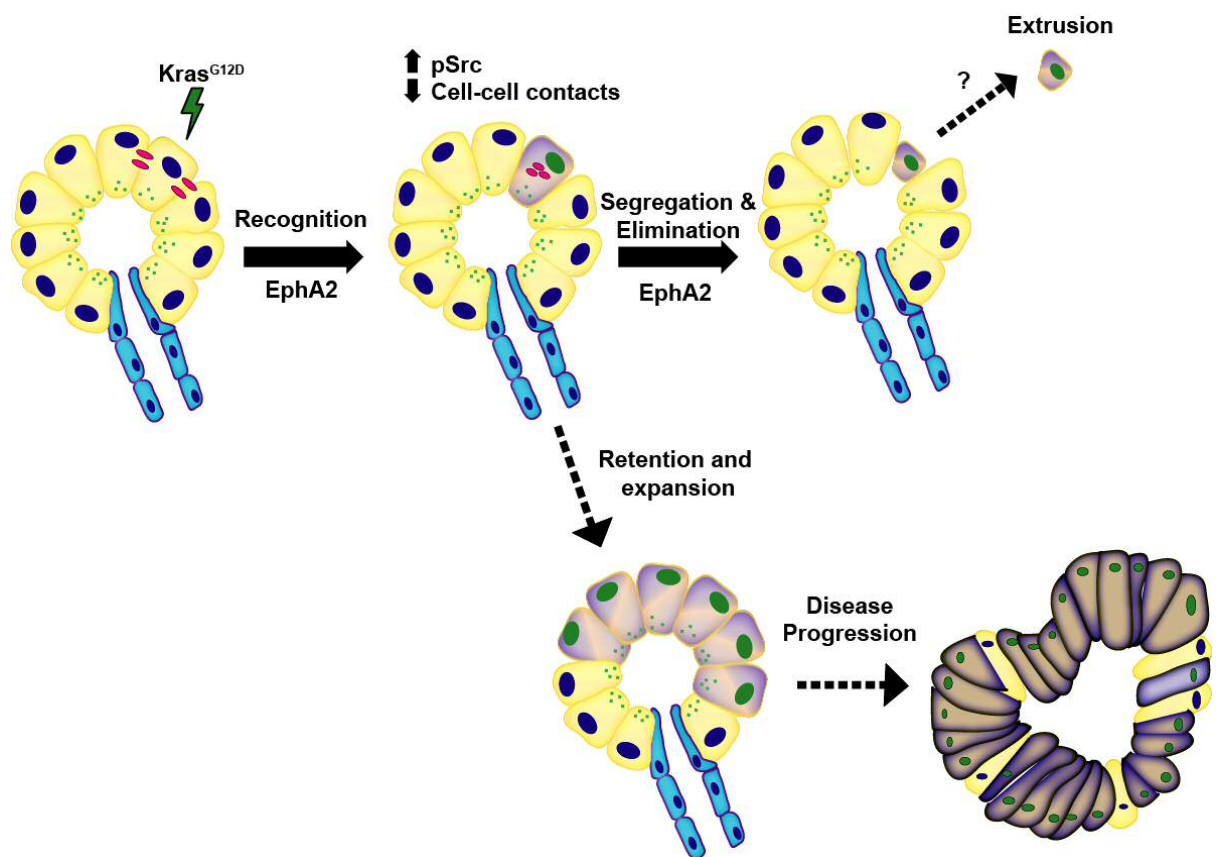
Figure 6.1 Proposed mechanism of Kras^{G12D} cell elimination from the pancreas.
Upon mutational activation of Kras the altered cell is recognised by normal
neighbours via EphA2 signalling. This leads to loss of cell-cell contacts (pink) and
elimination of mutant cells. Retention and proliferation of the transformed cell will
then lead to disease initiation.

6.1 Extrusion of KrasG12D cells via EphA2 signalling triggered by normal neighbours

How mutant cells are identified by normal neighbours and how they trigger competitive interactions is an area of ongoing research. A growing body of work suggests a positive role for cell repulsion signals that classically have a role in axon guidance, have been identified in cell competition. For example, Slit-Robo2 signalling drives extrusion of polarity deficient cells (Vaughen and Igaki, 2016), and we have identified EphA2 signalling as a mechanism of Ras-transformed cell repulsion and extrusion (Porazinski et al., 2016). Eph receptor tyrosine kinases regulate cell position by imposing repulsive signals and modulating adhesion between cells (Marston et al., 2003; Shamah et al., 2001). In pancreatic cancer, EphA2 is associated with early PanIN lesions and pre-mestastatic tumours (Mudali et al., 2006). In this thesis, I found that EphA2 is required for the detection and repulsion of KrasG12D cells from the pancreas. As KrasG12D cells were not triggered to become contractile by other Kras-transformed cells this suggests a requirement for normal neighbours to initiate repulsion via heterotypic interactions possibly via EphrinA1 ligand on non-transformed neighbours (Porazinski et al., 2016).

   Using primary co-culture experiments an EphA2 dependent increase in cell contractility occurred in KrasG12D pancreatic cells when surrounded by normal neighbours. This work also indicated the possible upregulation of active Src as observed previously in MDCK cell cultures (Porazinski et al., 2016). Activation of Src can promote tumour invasion and metastasis by destabilisation of epithelial cell-cell junctions. This occurs via direct phosphorylation of E-cadherin which promotes internalisation (Behrens et al., 1993; Lilien et al., 2005; Yap et al., 1998). Importantly, I found that E-cadherin was internalised in an EphA2 dependent manner specifically in Kras^{G12D} cells surrounded by normal neighbours. This suggests activation of EphA2 is the initial event which triggers internalisation of E-cadherin possibly via Src activation. Src activation can also lead to RhoA GTPase activation which can disrupt adherens junctions via ROCK (Fang et al., 2008; Wójciak-Stothard et al., 2001). Finally, Eph receptor activation can lead to Rac1-dependent endocytosis of E-cadherin (Akhtar and Hotchin,

2001; Marston et al., 2003). Therefore, several possible mechanisms downstream of EphA2 could promote the loss of E-cadherin-based junctions. Figure 6.2 provides a summary of the proposed mechanisms by which EphA2 could be regulating the internalisation of E-cadherin. The co-culture technique developed in this thesis in combination with specific inhibitors could be used in future studies to further elucidate the mechanism of KrasG12D cell extrusion and loss of E-cadherin via EphA2. It is important to understand the underlying mechanism as it could improve our understanding of how extrusion is overcome *in vivo* to promote pancreatic tumourigenesis.

In order for cells to be extruded they must lose contact with neighbouring cells. Using co-culture assays in vitro and mosaic expression of *Kras^G12D* in vivo models I found evidence for the loss of E-cadherin in Kras^G12D cells upon interaction with normal neighbours. Intriguingly, loss of E-cadherin can promote metastasis and is a key hallmark of epithelial-mesenchymal transition (Cano et al., 2000; Onder et al., 2008). Thus, it could be hypothesised that repulsion of Kras^G12D cells by normal neighbours is promoting a metastatic phenotype in transformed cells. Future studies could test if extruded Kras^G12D cells are more invasive than Kras^G12D cells cultured next to Kras^G12D cells. Although extrusion was not directly observed in vivo, analysis of further intermediate time points could capture pancreatic cells extruding. Another important implication in the loss of E-cadherin-based cell-cell junctions is the loss of cell polarity. Epithelial tissues display apical-basal polarity which is organised by polarity complexes physically associated with cell junction architecture. Consequently, loss of epithelial junctions confers a loss of polarity. This could be important for the direction of extrusion with loss of polarity potentially able to alter where oncogenic cells are extruded (Slattum & Rosenblatt, 2014). Apically extruded cells would be extruded in the lumen and could cleared through the ductal system (Kon et al., 2017), whereas basally extruded cells could invade and enter the circulation. Intriguingly, circulating tumour cells have been found in genetically engineered mouse models of pancreatic cancer circulating before primary tumours (Rhim et al., 2012). Moreover, pancreatic cancer is rarely diagnosed in humans without metastasis suggesting these tumours spread early (Das & Batra, 2015). Although I screened livers for RFP, robust RFP fluorescence was not detected in KrasG12D mice. This could be due to detection of RFP in the liver and future

experiments would need to stain for the pancreatic specific marker Pdx1. Another hypothesis is that cells require additional oncogenic transformations such as loss of p53 to promote survival after extrusion (Rhim et al., 2012). Recently, genetic analysis has demonstrated that spatially distal lesions share a common ancestral cell of origin suggesting precancerous cells spread and colonise the pancreas via the ductal network (Makohon-Moore et al., 2018). In 4/8 patients, a precursor cell had obtained one or two mutations to driver oncogenes such as Kras and spread through the pancreas to produce additional neoplastic lesions. Therefore, extrusion of Kras^{G12D} cells by normal neighbours could drive the invasion and metastasis of pancreatic cancer from the earliest stages of tumourigenesis.
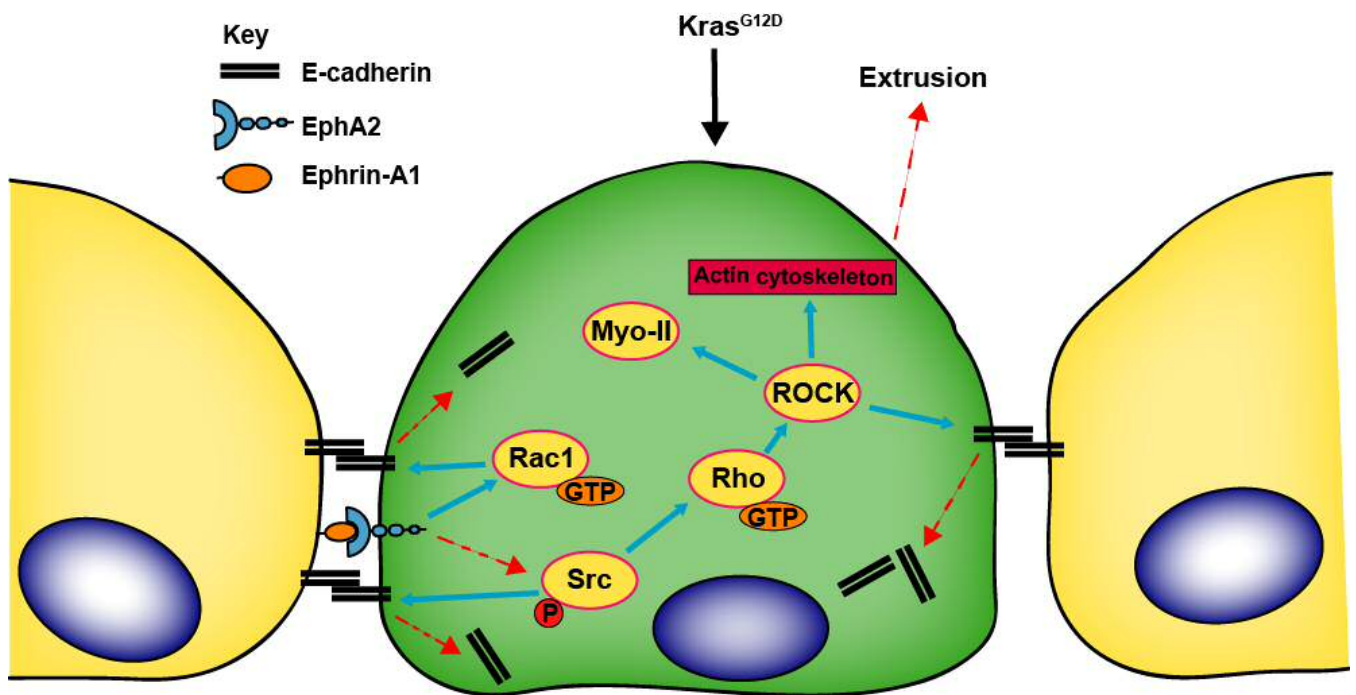
Figure 6.2: Proposed molecular mechanism of Kras^{G12D} cell elimination from the pancreas. In Kras^{G12D} mutant cells, EphA2 interacts with EphrinA1 on normal neighbouring cells which leads to activation of Src. Once active, Src can directly promote E-cadherin internalisation by phosphorylation and also activates RhoA GTPase. RhoA can activate ROCK which promotes E-cadherin internalisation. It has also been demonstrated that ROCK leads to Myosin-II activation and cytoskeletal rearrangements driving increased contractility. EphA2 can also activate another GTPase, Rac1, which can disrupt cell-cell contacts through endocytosis of E-cadherin. In summary, activation of EphA2 in Kras^{G12D} cells by normal neighbours could trigger repulsion and loss of cell-cell contacts via activation of Rho GTPases and Src. Together, this promotes extrusion of mutant cells from normal pancreatic monolayers. Blue arrows indicate published studies and red arrows the findings of this thesis.

6.2 Evidence of a Cell community effect in pancreatic acinar cells

In order to act efficiently cells are required to act in a coordinated manner to maintain homeostasis. Epithelial tissues are a tightly regulated system that must finely balance proliferation and cell turnover (Macara et al., 2014). It has long been established that cells acts as a coherent unit (Gurdon et al., 1993; Ho, 1992). In the pancreas, there is evidence that wild type cells promote a differentiated state of surrounding mis-specified cells and inhibit acinar ductal metaplasia (ADM) (Krah et al., 2015). Yet how a cellular community reacts when a KrasG12D cell emerges is unclear. It has been proposed that single oncogenic cells must escape via extrusion from this tightly regulated system in order to proliferate (Leung and Brugge, 2012; Sasaki et al., 2018). From this and other work I hypothesised that sporadic expression of KrasG12D would be phenotypically silent when surrounded by normal neighbours but upon extrusion mutant cells could proliferate and undergo ADM (Dolberg and Bissell, 1984; Jonason et al., 1996; Leung and Brugge, 2012; Martincorena et al., 2015). With the limitations of examining single cell evolution in vivo, an acinar 3D culture system was used that recapitulates the organisation of the pancreas but in a tractable system. This allowed investigation of the fate of eliminated cells in vivo and testing of whether elimination promotes or suppreses disease. However, although KrasG12D cells appeared to adopt a contractile morphology and undergo cytoskeletal rearrangement when surrounded by non-transformed neighbours, elimination of mutant cells via extrusion was not apparent. This could be for several reasons; acinar cell culture is not robust with alterations to cell-cell junctions and cellular signalling such as calcium signalling known to be altered after 6 hours in culture (Amsterdam and Jamieson, 1974; Marciniak et al., 2013; Orabi et al., 2013). Therefore, further optimisation of acinar cell culture may be required in order to allow extrusion of mutant cells. This ruled out the possibility to investigate the progression of extruded KrasG12D cells through acinar-ductal metaplasia (ADM) or proliferation. Nonetheless, the effects of normal neighbours on Ras-transformed cells progressing through ADM could be investigated. It was found that small numbers of KrasG12D cells were suppressed from forming a

duct-like cyst in clusters of non-transformed cells. This supports the theory that expression of oncogenic mutations are not sufficient to predict the fate of sporadic aberrant cells (Dolberg and Bissell, 1984; Jonason et al., 1996; Leung and Brugge, 2012; Martincorena et al., 2015). However, single KrasG12D cells autonomously reprogrammed and expressed Sox9 when surrounded by normal neighbours (Zhou et al., 2018). This could suggest that normal neighbours slow the progression of ADM as Sox9 can be expressed in morphologically normal acinar cells before progression to a duct-like cyst in vivo (Kopp et al., 2012). Analysis of clusters with a high proportion of mutant cells demonstrated that clusters of acinar cells containing > 60% KrasG12D cells were able to overcome this inhibitory effect and efficiently progressed through ADM. Strikingly, in clusters with a large number of Ras-transformed cells, wild type cells were induced to progress through ADM, suggesting community effect with clusters of cells acting as a coherent unit (Gurdon et al., 1993). As non-transformed cells are known to make up a proportion of cells in human pancreatic intraepithelial neoplasia (PanIN) lesions (Kanda et al., 2012), this could suggest that mutant cells are recruiting normal neighbours at the earliest stages of pancreatic cancer. Future work could examine lesions containing Kras wild-type cells in vivo to investigate whether the presence of wild-type cells alters the fate of precursor lesions.

6.3 Future Directions

Pancreatic ductal adenocarcinoma (PDAC) is a lethal disease with a 5-year survival rate of <5%. Over 80% of patients present with advanced, metastatic PDAC at diagnosis, ruling out surgical intervention. Current diagnostic techniques are expensive and invasive with no established screening technique demonstrated to be specific or sensitive enough to distinguish cancer from non-cancer related disease. An understanding of the biology of disease initiation and progression is imperative to developing effective screening and diagnostic techniques (Ying et al., 2016). Moreover, further elucidation of how disease

develops and spread could identify novel targets for therapeutics and improve our understanding of how risk factors promote PDAC.

This study found supporting evidence that the pancreas epithelium has an intrinsic ability to eliminate KrasG12D mutant cells, similar to other systems (Brown et al., 2017; Hogan et al., 2009; Kon et al., 2017). Yet, virtually all PDAC tumours have KrasG12D mutations (Biankin et al., 2012). If elimination of Ras-transformed cells is tumour suppressive it follows that there are mechanisms which overcome this process to permit disease initiation. The biggest risk factor for pancreatic cancer is age although the link between age and cancer risk not clear (Bosetti et al., 2014; Raimondi et al., 2009; Siegel et al., 2016). It has been demonstrated that the mechanical properties of tissue can change during aging (Phillip et al., 2015). With increasing stiffness strongly correlated with older epithelial cells in vitro and remodelling of the ECM observed in elderly individuals (Berdyyeva et al., 2005; Labat-Robert, 2004). Therefore, the intrinsic properties of normal epithelial cells or the surrounding microenvironment may reduce the efficiency of eliminating mutant neighbours. Altering the stiffness of the collagen matrix in vitro could further elucidate these changes; with matrix stiffness demonstrated to alter cell adhesive properties (Pelham & Wang, 1997) and could be studied by investigating cell competition in aged mice.

Obesity is a major risk factor for pancreatic cancer and has been increasing worldwide (Afshin 2012). Obesity can alter lipid metabolism, hormone secretion and induce chronic inflammation but it is unclear how obesity is involved in tumour initiation (Gonzalez-Muniesa 2017; Heymsfield and Wadden 2017; Kopelman 2000; Rosenbaum 1997). Recently, evidence has suggested that obesity can suppress Ras-transformed cell extrusion from epithelial tissues (Sasaki et al., 2018). To further elucidate how obesity affects cell competition and disease initiation a high-fat diet in combination with this model could be used.

Another important risk factor for pancreatic cancer is pancreatitis (Freelove and Walling, 2006). Pancreatitis promotes an inflammatory state and it has been suggested that chronic inflammation inhibits the extrusion of Ras-transformed cells in the intestine and pancreas (Sasaki et al., 2018). To better understand the relevance to disease initiation mosaic expression of KrasG12D could be combined with caerulein administration which recapitulates many aspects of pancreatitis (Niederau et al., 1985). It has also been reported that

pancreatitis results in a breakdown of adherens junctions so the segregation of mutant cells via internalisation E-cadherin may be altered (Lerch et al., 1997). Understanding how risk factors alter mutant cell elimination may help stratify patients and help inform diagnostic decisions and could be used to compliment developing diagnostic techniques. As if extrusion is a tumour suppressive mechanism this would suggest that identifying KrasG12D cells or oncogenic DNA in the circulatory system is a normal protective mechanism.

Extrusion of Ras-transformed cells was first observed using MDCK cell culture systems as a model of epithelial biology (Hogan et al., 2009). Evidence for extrusion was then identified in intestinal crypts (Kon et al., 2016), breast epithelia (Leung and Brugge, 2012) and more recently from CK19+ cells in the pancreas and lung (Sasuki et al., 2018). The work present here provides evidence for the elimination of KrasG12D cells from the pancreas building on previous cell competition studies using Hras (Kon et al., 2017; Saitoh et al., 2017). It therefore could be hypothesised that extrusion is a general epithelial biological process in response to constitutive activation of RAS/MAPK pathway. Understanding the impact of extrusion on Ras-transformed cells from epithelial tissues in the body could provide insight into the earliest stages of multiple different cancer types. This could potentially also expand to malignancies not typically associated with Ras mutations such as breast cancer. Ras is negatively regulated by Ras GTPase-activating proteins (RasGAPs) that catalyse the hydrolysis of Ras-GTP to the inactivate Ras-GDP form. As such, RasGAPs are poised to function as tumour suppressors. Indeed, The RasGAP Nf1 is lost or suppressed in sporadic cancers such as glioblastoma (McGillicuddy et al., 2009; Williams Parsons et al., 2008), non-small cell lung cancer (Ding et al., 2008) neuroblastoma (Hölzel, 2010) and melanoma (Maertens et al., 2013). Moreover, the RAS/MAPK pathway is hyperactivated in >50% of breast cancers (von Lintig et al., 2000; Mueller et al., 2000; Sivaraman et al., 1997). With the RasGAP RASAL2 demonstrated to have a causal role in breast cancer development (McLaughlin et al., 2013). Therefore, extrusion could be happening in a wide range of epithelial cancers.

List of References

Abercrombie, M., and Heaysman, J.E.M. (1954). Observations on the social behaviour of cells in tissue culture. II. "Monolayering" of fibroblasts. Exp. Cell Res. 6, 293–306.

Agrawal, N., Kango, M., Mishra, A., and Sinha, P. (1995). Neoplastic Transformation and Aberrant Cell–Cell Interactions in Genetic Mosaics of lethal(2)giant larvae (lgl),a Tumor Suppressor Gene of Drosophila. Dev. Biol. 172, 218–229.

Von Ahrens, D., Bhagat, T.D., Nagrath, D., Maitra, A., and Verma, A. (2017). The role of stromal cancer-associated fibroblasts in pancreatic cancer. J. Hematol. Oncol. 10.

Akhtar, N., and Hotchin, N.A. (2001). RAC1 Regulates Adherens Junctions through Endocytosis of E-Cadherin. Mol. Biol. Cell.

Albergaria, A., Ribeiro, A.S., Vieira, A.F., Sousa, B., Nobre, A.R., Seruca, R., Schmitt, F., and Paredes, J. (2011). P-cadherin role in normal breast development and cancer. Int. J. Dev. Biol.

Alberts, B., Johnson, A., Lewis, J., Raff, M., Roberts, K., and Walter, P. (2002). Molecular Biology of the Cell.

Alcolea, M.P., and Jones, P.H. (2015). Cell competition: Winning out by losing notch. Cell Cycle 14, 9–17.

Alcolea, M.P., Greulich, P., Wabik, A., Frede, J., Simons, B.D., and Jones, P.H. (2014). Differentiation imbalance in single oesophageal progenitor cells causes clonal immortalization and field change. Nat. Cell Biol. 16, 612–619.

Almoguera, C., Shibata, D., Forrester, K., Martin, J., Arnheim, N., and Perucho, M. (1988). Most human carcinomas of the exocrine pancreas contain mutant c-K-ras genes. Cell 53, 549–554.

Amato, K.R., Wang, S., Tan, L., Hastings, A.K., Song, W., Lovly, C.M., Meador, C.B., Ye, F., Lu, P., Balko, J.M., et al. (2016). EPHA2 blockade overcomes acquired resistance to EGFR kinase inhibitors in lung cancer. Cancer Res. 76, 305–318.

Amoyel, M., Bach, E.A., Abrams, J.M., Abrams, J.M., White, K., Fessler, L.I., Steller, H., Agrawal, N., Kango, M., Mishra, A., et al. (2014). Cell competition: how to eliminate your neighbours. Development 141, 988–1000.

Amsterdam, A., and Jamieson, J.D. (1974). Studies on dispersed pancreatic exocrine cells: I. dissociation technique and morphologic characteristics of separated cells. J. Cell Biol. 63, 1037–1056.

Andres, A.C., Reid, H.H., Zurcher, G., Blaschke, R.J., Albrecht, D., and Ziemiecki, A. (1994). Expression of two novel eph-related receptor protein tyrosine kinases in mammary gland development and carcinogenesis. Oncogene 9, 1461–1467.

Anton, K.A., Kajita, M., Narumi, R., Fujita, Y., and Tada, M. (2018). Src-transformed cells hijack mitosis to extrude from the epithelium. BioRxiv 246199.

Apodaca, G., Gallo, L.I., and Bryant, D.M. (2012). Role of membrane traffic in the generation of epithelial cell asymmetry. Nat. Cell Biol. 14, 1235–1243.

Ardito, C.M., Grüner, B.M., Takeuchi, K.K., Lubeseder-Martellato, C., Teichmann, N., Mazur, P.K., DelGiorno, K.E., Carpenter, E.S., Halbrook, C.J., Hall, J.C., et al. (2012). EGF Receptor Is Required for KRAS-Induced Pancreatic Tumorigenesis. Cancer Cell 22, 304–317.

Arvanitis, D., and Davy, A. (2008). Eph/ephrin signaling: Networks. Genes Dev. 22, 416–429.

Astin, J.W., Batson, J., Kadir, S., Charlet, J., Persad, R.A., Gillatt, D., Oxley, J.D., and Nobes, C.D. (2010). Competition amongst Eph receptors regulates contact inhibition of locomotion and invasiveness in prostate cancer cells. Nat. Cell Biol. 12, 1194–1204.

Avila, J.L., Troutman, S., Durham, A., and Kissil, J.L. (2012). Notch1 Is Not Required for Acinar-to-Ductal Metaplasia in a Model of Kras-Induced Pancreatic Ductal Adenocarcinoma. PLoS One 7, e52133.

Baer, R., Cintas, C., Dufresne, M., Cassant-Sourdy, S., Schönhuber, N., Planque, L., Lulka, H., Couderc, B., Bousquet, C., Garmy-Susini, B., et al. (2014). Pancreatic cell plasticity and cancer initiation induced by oncogenic Kras is completely dependent on wild-type PI 3-kinase p110α. Genes Dev. 28, 2621–2635.

Bailey, J.M., Hendley, A.M., Lafaro, K.J., Pruski, M.A., Jones, N.C., Alsina, J., Younes, M., Maitra, A., McAllister, F., Iacobuzio-Donahue, C.A., et al. (2016). P53 mutations cooperate with oncogenic Kras to promote adenocarcinoma from pancreatic ductal cells. Oncogene 35, 4282–4288.

Baker, A.M., Huang, W., Wang, X.M.M., Jansen, M., Ma, X.J., Kim, J., Anderson, C.M., Wu, X., Pan, L., Su, N., et al. (2017). Robust RNA-based in situ mutation detection delineates colorectal cancer subclonal evolution. Nat. Commun. 8.

Ballesteros-Arias, L., Saavedra, V., and Morata, G. (2014). Cell competition may function either as tumour-suppressing or as tumour-stimulating factor in Drosophila. Oncogene 33, 4377–4384.

Bar-Sagi, D. (2001). A Ras by any other name. Mol. Cell. Biol. 21, 1441–1443.

Bardeesy, N., and DePinho, R.A. (2002). Pancreatic cancer biology and genetics. Nat. Rev. Cancer 2, 897–909.

Barreto, S.G., Carati, C.J., Toouli, J., and Saccone, G.T.P. (2010). The islet-acinar axis of the pancreas: more than just insulin. Am. J. Physiol. Gastrointest. Liver Physiol. 299, 10–22.

Barrios, A., Poole, R.J., Durbin, L., Brennan, C., Holder, N., and Wilson, S.W. (2003). Eph/Ephrin signaling regulates the mesenchymal-to-epithelial transition of the paraxial mesoderm during somite morphogenesis. Curr. Biol. 13, 1571–1582.

Batlle, E., and Wilkinson, D.G. (2012). Molecular mechanisms of cell segregation and boundary formation in development and tumorigenesis. Cold Spring Harb. Perspect. Biol. 4, 1

Batlle, E., Henderson, J.T., Beghtel, H., Van den Born, M.M.W., Sancho, E., Huls, G., Meeldijk, J., Robertson, J., Van de Wetering, M., Pawson, T., et al. (2002). β-catenin and TCF mediate cell positioning in the intestinal epithelium by controlling the expression of EphB/EphrinB. Cell 111, 251–263.

Batlle, E., Bacani, J., Begthel, H., Jonkeer, S., Gregorieff, A., Van De Born, M., Malats, N., Sancho, E., Boon, E., Pawson, T., et al. (2005). EphB receptor activity suppresses colorectal cancer progression. Nature 435, 1126–1130.

Becker, A.E., Hernandez, Y.G., Frucht, H., and Lucas, A.L. (2014). Pancreatic ductal adenocarcinoma: Risk factors, screening, and early detection. World J. Gastroenterol. 20, 11182–11198.

Behrens, G., Jochem, C., Schmid, D., Keimling, M., Ricci, C., and Leitzmann, M.F. (2015). Physical activity and risk of pancreatic cancer: a systematic review and meta-analysis. Eur. J. Epidemiol. 30, 279–298.

Berdyyeva, T.K., Woodworth, C.D., and Sokolov, I. (2005). Human epithelial cells increase their rigidity with ageing in vitro: Direct measurements. Phys. Med. Biol. 50, 81.

Berndt, J.D., Clay, M.R., Langenberg, T., and Halloran, M.C. (2008). Rho-kinase and myosin II affect dynamic neural crest cell behaviors during epithelial to mesenchymal transition in vivo. Dev. Biol. 324, 236–244.

Biankin, A. V., Waddell, N., Kassahn, K.S., Gingras, M.C., Muthuswamy, L.B., Johns, A.L., Miller, D.K., Wilson, P.J., Patch, A.M., Wu, J., et al. (2012). Pancreatic cancer genomes reveal aberrations in axon guidance pathway genes. Nature 491, 399–405.

Bielmeier, C., Alt, S., Weichselberger, V., La Fortezza, M., Harz, H., Jülicher, F., Salbreux, G., and Classen, A.-K. (2016). Interface Contractility between Differently Fated Cells Drives Cell Elimination and Cyst Formation. Curr. Biol. 26, 563–574.

Böhni, R., Riesgo-Escovar, J., Oldham, S., Brogiolo, W., Stocker, H., Andruss, B.F., Beckingham, K., and Hafen, E. (1999). Autonomous control of cell and organ size by CHICO, a Drosophila homolog of vertebrate IRS1-4. Cell 97, 865–875.

Boissier, P., Chen, J., and Huynh-Do, U. (2013). Epha2 signaling following endocytosis: Role of tiam1. Traffic 14, 1255–1271.

Boj, S.F., Hwang, C. Il, Baker, L.A., Chio, I.I.C., Engle, D.D., Corbo, V., Jager, M., Ponz-Sarvise, M., Tiriac, H., Spector, M.S., et al. (2015). Organoid models of human and mouse ductal pancreatic cancer. Cell. 160, 324-338.

Bolouri, H., and Davidson, E.H. (2010). The gene regulatory network basis of the "community effect," and analysis of a sea urchin embryo example. Dev. Biol. 340, 170-178.

Bondar, T., and Medzhitov, R. (2010). p53-Mediated Hematopoietic Stem and Progenitor Cell Competition. Cell Stem Cell 6, 309–322.

Bonnans, C., Chou, J., and Werb, Z. (2014). Remodelling the extracellular matrix in development and disease. Nat. Rev. Mol. Cell Biol. 15, 786–801.

Bosetti, C., Bertuccio, P., Negri, E., La Vecchia, C., Zeegers, M.P., and Boffetta, P. (2012). Pancreatic cancer: Overview of descriptive epidemiology. Mol. Carcinog. 51, 3–13.

Bosetti, C., Rosato, V., Li, D., Silverman, D., Petersen, G.M., Bracci, P.M., Neale, R.E., Muscat, J., Anderson, K., Gallinger, S., et al. (2014). Diabetes, antidiabetic medications, and pancreatic cancer risk: an analysis from the International Pancreatic Cancer Case-Control Consortium. Ann. Oncol. 25, 2065–2072.

Bove, A., Gradeci, D., Fujita, Y., Banerjee, S., Charras, G., and Lowe, A.R. (2017). Local cellular neighbourhood controls proliferation in cell competition. Mol. Biol. Cell. 28, 3215-3228

Bowling, S., Gregorio, A., Sancho, M., Pozzi, S., Aarts, M., Signore, M., Schneider, M., Barbera, J.P.M., Gil, J., and Rodríguez, T.A. (2018). P53 and mTOR signalling determine fitness selection through cell competition during early mouse embryonic development. Nat. Commun. 9, 1763.

Braakhuis, B.J.M., Tabor, M.P., Kummer, J.A., Leemans, C.R., and Brakenhoff, R.H. (2003). A genetic explanation of slaughter's concept of field cancerization: Evidence and clinical implications. Cancer Res. 63, 1727–1730.

Brantley-Sieders, D.M. (2004). EphA2 receptor tyrosine kinase regulates endothelial cell migration and vascular assembly through phosphoinositide 3-kinase-mediated Rac1 GTPase activation. J. Cell Sci. 117, 2037–2049.

Brantley-Sieders, D.M., Zhuang, G., Hicks, D., Wei, B.F., Hwang, Y., Cates, J.M.M., Coffman, K., Jackson, D., Bruckheimer, E., Muraoka-Cook, R.S., et al. (2008). The receptor tyrosine kinase EphA2 promotes mammary adenocarcinoma tumorigenesis and metastatic progression in mice by amplifying ErbB2 signaling. J. Clin. Invest. 118, 64–78.

Brembeck, F.H., Schreiber, F.S., Deramaudt, T.B., Craig, L., Rhoades, B., Swain, G., Grippo, P., Stoffers, D.A., Silberg, D.G., and Rustgi, A.K. (2003). The mutant K-ras oncogene causes pancreatic periductal lymphocytic infiltration and gastric mucous neck cell hyperplasia in transgenic mice. Cancer Res. 63, 2005–2009.

Brodland, G.W. (2002). The Differential Interfacial Tension Hypothesis (DITH): A Comprehensive Theory for the Self-Rearrangement of Embryonic Cells and Tissues. J. Biomech. Eng. 124, 188.

Bronner-Fraser, M. (1999). 9 Rostrocaudal Differences within the Somites Confer Segmental Pattern to Trunk Neural Crest Migration. Curr. Top. Dev. Biol. 47, 279–296.

Brown, S., Pineda, C.M., Xin, T., Boucher, J., Suozzi, K.C., Park, S., Matte-Martone, C., Gonzalez, D.G., Rytlewski, J., Beronja, S., et al. (2017). Correction of aberrant growth preserves tissue homeostasis. Nature 548, 334–337.

Brumby, A.M., and Richardson, H.E. (2003). Scribble mutants cooperate with oncogenic Ras or Notch to cause neoplastic overgrowth in Drosophila. EMBO J. 22, 5769–5779.

Brunicardi, F.C., Shavelle, D.M., and Andersen, D.K. (1995). Neural regulation of the endocrine pancreas. Int. J. Pancreatol. 18, 177–195.

Cancer Research UK Pancreatic cancer statistics. 2017. https://www.cancerresearchuk.org/health-professional/cancer-statistics/statistics-by-cancer-type/pancreatic-cancer.

Cano, A., Pérez-Moreno, M.A., Rodrigo, I., Locascio, A., Blanco, M.J., Del Barrio, M.G., Portillo, F., and Nieto, M.A. (2000). The transcription factor Snail controls epithelial-mesenchymal transitions by repressing E-cadherin expression. Nat. Cell Biol.

Canty, L., Zarour, E., Kashkooli, L., François, P., and Fagotto, F. (2017). Sorting at embryonic boundaries requires high heterotypic interfacial tension. Nat. Commun. 8, 157.

Carriere, C., Seeley, E.S., Goetze, T., Longnecker, D.S., and Korc, M. (2007). The Nestin progenitor lineage is the compartment of origin for pancreatic intraepithelial neoplasia. Proc. Natl. Acad. Sci. 104, 4437–4442.

Cayuso, J., Xu, Q., and Wilkinson, D.G. (2015). Mechanisms of boundary formation by Eph receptor and ephrin signaling. Dev. Biol. 401, 122–131.

Chen, C.-L., Schroeder, M.C., Kango-Singh, M., Tao, C., and Halder, G. (2012). Tumor suppression by cell competition through regulation of the Hippo pathway. Proc. Natl. Acad. Sci. 109, 484–489.

Chen, K.L., Zheng, X.L., Li, Y., Yang, L., Zhou, Z.G., Zhou, X.Y., Zhou, B., Wang, R., Jiang, J.J., Chen, L.H., et al. (2009). An improved primary culture system of pancreatic duct epithelial cells from Wistar rats. Cytotechnology 60, 23–31.

Chiba, T., Ishihara, E., Miyamura, N., Narumi, R., Kajita, M., Fujita, Y., Suzuki, A., Ogawa, Y., and Nishina, H. (2016). MDCK cells expressing constitutively active Yes-associated protein (YAP) undergo apical extrusion depending on neighboring cell status. Sci. Rep. 6.

Clavería, C., Giovinazzo, G., Sierra, R., and Torres, M. (2013). Myc-driven endogenous cell competition in the early mammalian embryo. Nature. 500, 39–44.

Collins, M.A., Bednar, F., Zhang, Y., Brisset, J., Galbán, S., Galbán, C.J., Rakshit, S., Flannagan, K.S., Adsay, N.V., Pasca di Magliano, M., et al. (2012). Oncogenic Kras is required for both the initiation and maintenance of pancreatic cancer in mice. J. Clin. Invest. 122, 639-653.

Collins, M.A., Yan, W., Sebolt-Leopold, J.S., and Pasca Di Magliano, M. (2014). MAPK signaling is required for dedifferentiation of acinar cells and development of pancreatic intraepithelial neoplasia in mice. Gastroenterology 146.

Collisson, E.A., Trejo, C.L., Silva, J.M., Gu, S., Korkola, J.E., Heiser, L.M., Charles, R.P., Rabinovich, B.A., Hann, B., Dankort, D., et al. (2012). A Central role for RAF→MEK→ERK signaling in the genesis of pancreatic ductal adenocarcinoma. Cancer Discov. 2, 685–693.

Cortina, C., Palomo-Ponce, S., Iglesias, M., Fernández-Masip, J.L., Vivancos, A., Whissell, G., Humà, M., Peiró, N., Gallego, L., Jonkheer, S., et al. (2007). EphB-ephrin-B interactions suppress colorectal cancer progression by compartmentalizing tumor cells. Nat. Genet. 39, 1376–1383.

Cowan, C.A., and Henkemeyer, M. (2001). The SH2/SH3 adaptor Grb4 transduces B-ephrin reverse signals. Nature 413, 174–179.

Cox, A.D., and Der, C.J. (2010). Ras history: The saga continues. Small GTPases 1, 2–27.
Crawford, H.C., Scoggins, C.R., Kay Washington, M., Matrisian, L.M., and Leach, S.D. (2002). Matrix metalloproteinase-7 is expressed by pancreatic cancer precursors and regulates acinar-to-ductal metaplasia in exocrine pancreas. J. Clin. Invest. 109, 1437-1444.

Cubilla, A.L., and Fitzgerald, P.J. (1976). Morphological Lesions Associated with Human Primary Invasive Nonendocrine Pancreas Cancer. Cancer Res. 36, 2690–2698.

D'Amico, T.A., Aloia, T.A., Moore, M.B.H., Conlon, D.H., Herndon, J.E., Kinch, M.S., and Harpole, D.H. (2001). Predicting the sites of metastases from lung cancer using molecular biologic markers. Ann. Thorac. Surg. 72, 1144–1148.

Dail, M., Richter, M., Godement, P., and Pasquale, E.B. (2006). Eph receptors inactivate R-Ras through different mechanisms to achieve cell repulsion. J. Cell Sci. 119, 1244–1254.

Dang, C. V. (2012). MYC on the path to cancer. Cell 149, 22–35.

Davis, S., Gale, N.W., Aldrich, T.H., Maisonpierre, P.C., Lhotak, V., Pawson, T., Goldfarb, M., and Yancopoulos, G.D. (1994). Ligands for EPH-related receptor tyrosine kinases that require membrane attachment or clustering for activity. Science. 266, 816–819.

Deroanne, C., Vouret-Craviari, V., Wang, B., and Pouysségur, J. (2003). EphrinA1 inactivates integrin-mediated vascular smooth muscle cell spreading via the Rac/PAK pathway. J. Cell Sci. 116, 1367–1376.

Deutsch, M., Rosenstein, M.M., and Ramanathan, R.K. (1999). Pancreatic cancer in a young adult after treatment for Hodgkin's disease. Clin. Oncol. (R. Coll. Radiol). 11, 280–282.

DiGiuseppe, J.A., Hruban, R.H., Offerhaus, G.J., Clement, M.J., van den Berg, F.M., Cameron, J.L., and van Mansfeld, A.D. (1994). Detection of K-ras mutations in mucinous pancreatic duct hyperplasia from a patient with a family history of pancreatic carcinoma. Am. J. Pathol. 144, 889–895.

Ding, L., Getz, G., Wheeler, D.A., Mardis, E.R., McLellan, M.D., Cibulskis, K., Sougnez, C., Greulich, H., Muzny, D.M., Morgan, M.B., et al. (2008). Somatic mutations affect key pathways in lung adenocarcinoma. Nature 455, 1069–1075.

Dolberg, D.S., and Bissell, M.J. (1984). Inability of Rous sarcoma virus to cause sarcomas in the avian embryo. Nature. 309, 522

Dolenšek, J., Rupnik, M.S., and Stožer, A. (2015). Structural similarities and differences between the human and the mouse pancreas. Islets 7.

Le Douarin, N., and Kalcheim, C. (1999). The Neural Crest. Cambridge University Press.

Duffy, M.J., Sturgeon, C., Lamerz, R., Haglund, C., Holubec, V.L., Klapdor, R., Nicolini, A., Topolcan, O., and Heinemann, V. (2010). Tumor markers in pancreatic cancer: a European Group on Tumor Markers (EGTM) status report. Ann. Oncol. 21, 441–447.

Dutta, D., and Donaldson, J.G. (2012). Search for inhibitors of endocytosis. Cell. Logist. 2, 203–208.

Duxbury, M.S., Ito, H., Zinner, M.J., Ashley, S.W., and Whang, E.E. (2004). EphA2: A determinant of malignant cellular behavior and a potential therapeutic target in pancreatic adenocarcinoma. Oncogene 23, 1448–1456.

Eagle, H., and Levine, E.M. (1967). Growth regulatory effects of cellular interaction. Nature 213, 1102–1106.

Ehrlicher, A.J., Nakamura, F., Hartwig, J.H., Weitz, D.A., and Stossel, T.P. (2011). Mechanical strain in actin networks regulates FilGAP and integrin binding to filamin A. Nature 478, 260–263.

Eilers, M., and Eisenman, R.N. (2008). Myc's broad reach. Genes Dev. 22, 2755–2766.

Eisener-Dorman, A.F., Lawrence, D.A., and Bolivar, V.J. (2009). Cautionary insights on knockout mouse studies: The gene or not the gene? Brain. Behav. Immun. 23, 318–324.

Eisenhoffer, G.T., Loftus, P.D., Yoshigi, M., Otsuna, H., Chien, C. Bin, Morcos, P.A., and Rosenblatt, J. (2012). Crowding induces live cell extrusion to maintain homeostatic cell numbers in epithelia. Nature 484, 546–549.

Eser, S., Reiff, N., Messer, M., Seidler, B., Gottschalk, K., Dobler, M., Hieber, M., Arbeiter, A., Klein, S., Kong, B., et al. (2013). Selective requirement of PI3K/PDK1 signaling for kras oncogene-driven pancreatic cell plasticity and cancer. Cancer Cell 23, 406–420.

Fagotto, F., Rohani, N., Touret, A.S., and Li, R. (2013). A Molecular Base for Cell Sorting at Embryonic Boundaries: Contact Inhibition of Cadherin Adhesion by Ephrin/Eph-Dependent Contractility. Dev. Cell. 27, 72-87.

Fagotto, F., Winklbauer, R., and Rohani, N. (2014). Ephrin-Eph signaling in embryonic tissue separation. Cell Adhes. Migr. 8, 308-326

Fan, H.-Y., Shimada, M., Liu, Z., Cahill, N., Noma, N., Wu, Y., Gossen, J., and Richards, J.S. (2008). Selective expression of KrasG12D in granulosa cells of the mouse ovary causes defects in follicle development and ovulation. Development 135, 2127–2137.

Fang, W.B., Ireton, R.C., Zhuang, G., Takahashi, T., Reynolds, A., and Chen, J. (2008). Overexpression of EPHA2 receptor destabilizes adherens junctions via a RhoA-dependent mechanism. J. Cell Sci. 121, 358–368.

Feil, R., Brocard, J., Mascrez, B., LeMeur, M., Metzger, D., and Chambon, P. (1996). Ligand-activated site-specific recombination in mice. Proc. Natl. Acad. Sci. 93, 10887–10890.

Feldmann, G., Mishra, A., Hong, S.M., Bisht, S., Strock, C.J., Ball, D.W., Goggins, M., Maitra, A., and Nelkin, B.D. (2010). Inhibiting the cyclin-dependent kinase CDK5 blocks pancreatic cancer formation and progression through the suppression of Ras-Ral signaling. Cancer Res. 70, 4460–4469.

Feng, Y., Santoriello, C., Mione, M., Hurlstone, A., and Martin, P. (2010). Live imaging of innate immune cell sensing of transformed cells in zebrafish larvae: Parallels between tumor initiation and wound inflammation. PLoS Biol. 8.

Fero, D., Wang, K.C., Nguyen, P., Hur, S.S., Hu, Y., and Li, Y.S. (2011). Ephrin-a1 regulates cell remodeling and migration. Cell. Mol. Bioeng. 4, 648–655.

Ferreira, R.M.M., Sancho, R., Messal, H.A., Nye, E., Spencer-Dene, B., Stone, R.K., Stamp, G., Rosewell, I., Quaglia, A., and Behrens, A. (2017). Duct- and Acinar-Derived Pancreatic Ductal Adenocarcinomas Show Distinct Tumor Progression and Marker Expression. Cell Rep. 21, 968-978

Forbes, S.A., Beare, D., Boutselakis, H., Bamford, S., Bindal, N., Tate, J., Cole, C.G., Ward, S., Dawson, E., Ponting, L., et al. (2017). COSMIC: Somatic cancer genetics at high-resolution. Nucleic Acids Res. 45, 777-783

Franke, J.D., Montague, R.A., and Kiehart, D.P. (2005). Nonmuscle myosin II generates forces that transmit tension and drive contraction in multiple tissues during dorsal closure. Curr. Biol. 15, 2208–2221.

Freelove, R., and Walling, A.D. (2006). Pancreatic cancer: Diagnosis and management. Am. Fam. Physician 73, 485–492.

Frier, B.M., Saunders, J.H., Wormsley, K.G., and Bouchier, I.A. (1976). Exocrine pancreatic function in juvenile-onset diabetes mellitus. Gut 17, 685–691.

Frisch, S.M., and Francis, H. (1994). Disruption of epithelial cell-matrix interactions induces apoptosis. J. Cell Biol. 124, 619–626.

Froldi, F., Ziosi, M., Garoia, F., Pession, A., Grzeschik, N.A., Bellosta, P., Strand, D., Richardson, H.E., Pession, A., and Grifoni, D. (2010). The lethal giant larvae tumour suppressor mutation requires dMyc oncoprotein to promote clonal malignancy. BMC Biol. 8.

Fuchs, Y., and Steller, H. (2015). Live to die another way: Modes of programmed cell death and the signals emanating from dying cells. Nat. Rev. Mol. Cell Biol. 16, 329–344.

Gallo, G. (2006). RhoA-kinase coordinates F-actin organization and myosin II activity during semaphorin-3A-induced axon retraction. J. Cell Sci. 119, 3413–3423.

Gateff, E. (1978). Malignant neoplasms of genetic origin in Drosophila melanogaster. Science (80-.). 200, 1448–1459.

Gidekel Friedlander, S.Y., Chu, G.C., Snyder, E.L., Girnius, N., Dibelius, G., Crowley, D., Vasile, E., DePinho, R.A., and Jacks, T. (2009). Context-dependent transformation of adult pancreatic cells by oncogenic K-Ras. Cancer Cell 16, 379–389.

Gong, J., Körner, R., Gaitanos, L., and Klein, R. (2016). Exosomes mediate cell contact-independent ephrin-Eph signaling during axon guidance. J. Cell Biol. 214, 35–44.

Gopinathan, A., Morton, J.P., Jodrell, D.I., and Sansom, O.J. (2015). GEMMs as preclinical models for testing pancreatic cancer therapies. Dis. Model. Mech. 8, 1185–1200.

Grapin-Botton, A. (2005). Ductal cells of the pancreas. Int. J. Biochem. Cell Biol. 37, 504–510.

Grippo, P.J., Nowlin, P.S., Demeure, M.J., Longnecker, D.S., and Sandgren, E.P. (2003). Preinvasive pancreatic neoplasia of ductal phenotype induced by acinar cell targeting of mutant Kras in transgenic mice. Cancer Res. 63, 2016–2019.

Gu, G., Dubauskaite, J., and Melton, D.A. (2002). Direct evidence for the pancreatic lineage: NGN3+ cells are islet progenitors and are distinct from duct progenitors. Development. 129, 2447-2457.

Gu, Y., Forostyan, T., Sabbadini, R., and Rosenblatt, J. (2011). Epithelial cell extrusion requires the sphingosine-1-phosphate receptor 2 pathway. J. Cell Biol. 193, 667–676.

Gu, Y., Shea, J., Slattum, G., Firpo, M.A., Alexander, M., Golubovskaya, V.M., and Rosenblatt, J. (2015). Defective apical extrusion signaling contributes to aggressive tumor hallmarks. Elife 2015. e04069.

Guerra, C., Schuhmacher, A.J., Cañamero, M., Grippo, P.J., Verdaguer, L., Pérez-Gallego, L., Dubus, P., Sandgren, E.P., and Barbacid, M. (2007). Chronic Pancreatitis Is Essential for Induction of Pancreatic Ductal Adenocarcinoma by K-Ras Oncogenes in Adult Mice. Cancer Cell 11, 291–302.

Guerra, C., Collado, M., Navas, C., Schuhmacher, A.J., Hernández-Porras, I., Cañamero, M., Rodriguez-Justo, M., Serrano, M., and Barbacid, M. (2011). Pancreatitis-Induced Inflammation Contributes to Pancreatic Cancer by Inhibiting Oncogene-Induced Senescence. Cancer Cell 19, 728–739.

Gumbiner, B.M. (1996). Cell adhesion: The molecular basis of tissue architecture and morphogenesis. Cell 84, 345–357.

Gundry, C., Marco, S., Rainero, E., Miller, B., Dornier, E., Mitchell, L., Caswell, P.T., Campbell, A.D., Hogeweg, A., Sansom, O.J., et al. (2017). Phosphorylation of Rab-coupling protein by LMTK3 controls Rab14-dependent EphA2 trafficking to promote cell:cell repulsion. Nat. Commun. 8, 14646.

Guo, Z., Neilson, L.J., Zhong, H., Murray, P.S., Zanivan, S., and Zaidel-Bar, R. (2014). E-cadherin interactome complexity and robustness resolved by quantitative proteomics. Sci. Signal. 7.

Gurdon, J.B., Kato, K., and Lemaire, P. (1993). The community effect, dorsalization and mesoderm induction. Curr. Opin. Genet. Dev. 3, 662-667

Habbe, N., Shi, G., Meguid, R.A., Fendrich, V., Esni, F., Chen, H., Feldmann, G., Stoffers, D.A., Konieczny, S.F., Leach, S.D., et al. (2008). Spontaneous induction of murine pancreatic intraepithelial neoplasia (mPanIN) by acinar cell targeting of oncogenic Kras in adult mice. Proc. Natl. Acad. Sci. 105, 18913–18918.

Hall, P.A., and Lemoine, N.R. (1992). Rapid acinar to ductal transdifferentiation in cultured human exocrine pancreas. J. Pathol. 166, 97–103.

Hattori, M., Osterfield, M., and Flanagan, J.G. (2000). Regulated cleavage of a contact-mediated axon repellent. Science. 289, 1360–1365.

Hendley, A.M., Wang, Y.J., Polireddy, K., Alsina, J., Ahmed, I., Lafaro, K.J., Zhang, H., Roy, N., Savidge, S.G., Cao, Y., et al. (2016). p120 catenin suppresses basal epithelial cell extrusion in invasive pancreatic neoplasia. Cancer Res. 76, 3351–3363.

Herbach, N., Bergmayr, M., Göke, B., Wolf, E., and Wanke, R. (2011). Postnatal development of numbers and mean sizes of pancreatic islets and Beta-Cells in healthy mice and giprdntransgenic diabetic mice. PLoS One 6. e22814.

Hezel, A.F., Gurumurthy, S., Granot, Z., Swisa, A., Chu, G.C., Bailey, G., Dor, Y., Bardeesy, N., and DePinho, R.A. (2008). Pancreatic Lkb1 Deletion Leads to Acinar Polarity Defects and Cystic Neoplasms. Mol. Cell. Biol. 28, 2414–2425.

Hill, W., and Hogan, C. (2017). Normal epithelial cells trigger EphA2-dependent RasV12 cell repulsion at the single cell level. Small GTPases 1–6.

Hingorani, S.R., Petricoin, E.F., Maitra, A., Rajapakse, V., King, C., Jacobetz, M.A., Ross, S., Conrads, T.P., Veenstra, T.D., Hitt, B.A., et al. (2003a). Preinvasive and invasive ductal pancreatic cancer and its early detection in the mouse. Cancer Cell 4, 437–450.

Hingorani, S.R., Wang, L., Multani, A.S., Combs, C., Deramaudt, T.B., Hruban, R.H., Rustgi, A.K., Chang, S., and Tuveson, D.A. (2005). Trp53R172H and KrasG12D cooperate to promote chromosomal instability and widely metastatic pancreatic ductal adenocarcinoma in mice. Cancer Cell 7, 469–483.

Hirai, H., Maru, Y., Hagiwara, K., Nishida, J., and Takaku, F. (1987). A novel putative tyrosine kinase receptor encoded by the eph gene. Science. 238, 1717–1720.

Hiramoto-Yamaki, N., Takeuchi, S., Ueda, S., Harada, K., Fujimoto, S., Negishi, M., and Katoh, H. (2010). Ephexin4 and EphA2 mediate cell migration through a RhoG-dependent mechanism. J. Cell Biol. 190, 461–477.

Ho, R.K. (1992). Cell movements and cell fate during zebrafish gastrulation. Dev. Suppl. 73, 65–73.

Hobbs, G.A., Der, C.J., and Rossman, K.L. (2016). RAS isoforms and mutations in cancer at a glance. J. Cell Sci. 129, 1287–1292.

Hoess, R., Abremski, K., and Sternberg, N. (1984). The nature of the interaction of the P1 recombinase Cre with the recombining site loxP. Cold Spring Harb. Symp. Quant. Biol. 49, 761–768.

Hogan, C., Dupré-Crochet, S., Norman, M., Kajita, M., Zimmermann, C., Pelling, A.E., Piddini, E., Baena-López, L.A., Vincent, J.-P., Itoh, Y., et al. (2009). Characterization of the interface between normal and transformed epithelial cells. Nat. Cell Biol. 11, 460–467.

Hölzel, M. (2010). NF1 is a tumor suppressor in neuroblastoma that determines retinoic acid response and disease outcome. Nat. Rev. Cancer 10, 601.

Hornberger, M.R., Dütting, D., Ciossek, T., Yamada, T., Handwerker, C., Lang, S., Weth, F., Huf, J., Weßel, R., Logan, C., et al. (1999). Modulation of EphA receptor function by coexpressed EphrinA ligands on retinal ganglion cell axons. Neuron 22, 731–742.

Houbracken, I., and Bouwens, L. (2017). Acinar cells in the neonatal pancreas grow by self-duplication and not by neogenesis from duct cells. Sci. Rep. 7, 12643.

Houbracken, I., De Waele, E., Lardon, J., Ling, Z., Heimberg, H., Rooman, I., and Bouwens, L. (2011). Lineage tracing evidence for transdifferentiation of acinar to duct cells and plasticity of human pancreas. Gastroenterology. 141, 731-741.

Hruban, R.H., Takaori, K., Klimstra, D.S., Adsay, N.V., Albores-Saavedra, J., Biankin, A. V., Biankin, S.A., Compton, C., Fukushima, N., Furukawa, T., et al. (2004). An illustrated consensus on the classification of pancreatic intraepithelial neoplasia and intraductal papillary mucinous neoplasms. In American Journal of Surgical Pathology. 977–987.

Huch, M., Bonfanti, P., Boj, S.F., Sato, T., Loomans, C.J.M., Van De Wetering, M., Sojoodi, M., Li, V.S.W., Schuijers, J., Gracanin, A., et al. (2013). Unlimited

in vitro expansion of adult bi-potent pancreas progenitors through the Lgr5/R-spondin axis. EMBO J. 32, 2708–2721.

Hunter, S.G., Zhuang, G., Brantley-Sieders, D., Swat, W., Cowan, C.W., and Chen, J. (2006). Essential Role of Vav Family Guanine Nucleotide Exchange Factors in EphA Receptor-Mediated Angiogenesis. Mol. Cell. Biol. 26, 4830–4842.

Huynh-Do, U., Stein, E., Lane, A.A., Liu, H., Cerretti, D.P., and Daniel, T.O. (1999). Surface densities of ephrin-B1 determine EphB1-coupled activation of cell attachment through alphavbeta3 and alpha5beta1 integrins. EMBO J. 18, 2165–2173.

Igaki, T., Pagliarini, R.A., and Xu, T. (2006). Loss of Cell Polarity Drives Tumor Growth and Invasion through JNK Activation in Drosophila. Curr. Biol. 16, 1139–1146.

Ionescu-Tirgoviste, C., Gagniuc, P.A., Gubceac, E., Mardare, L., Popescu, I., Dima, S., and Militaru, M. (2015). A 3D map of the islet routes throughout the healthy human pancreas. Sci. Rep. 5, 14634.

Ireton, R.C., Davis, M.A., Van Hengel, J., Mariner, D.J., Barnes, K., Thoreson, M.A., Anastasiadis, P.Z., Matrisian, L., Bundy, L.M., Sealy, L., et al. (2002). A novel role for p120 catenin in E-cadherin function. J. Cell Biol. 159, 465-476.

Ishiyama, N., Lee, S.H., Liu, S., Li, G.Y., Smith, M.J., Reichardt, L.F., and Ikura, M. (2010). Dynamic and Static Interactions between p120 Catenin and E-Cadherin Regulate the Stability of Cell-Cell Adhesion. Cell 141, 117–128.

Van Itallie, C.M., Tietgens, A.J., Aponte, A., Fredriksson, K., Fanning, A.S., Gucek, M., and Anderson, J.M. (2014). Biotin ligase tagging identifies proteins proximal to E-cadherin, including lipoma preferred partner, a regulator of epithelial cell–cell and cell–substrate adhesion. J. Cell Sci. 127, 885–895.

Jackson, E.L., Willis, N., Mercer, K., Bronson, R.T., Crowley, D., Montoya, R., Jacks, T., and Tuveson, D.A. (2001). Analysis of lung tumor initiation and progression using conditional expression of oncogenic K-ras. Genes Dev. 15, 3243–3248.

Jain, R., and Lammert, E. (2009). Cell-cell interactions in the endocrine pancreas. Diabetes, Obes. Metab. 11, 159–167.

Javaherian, S., D'Arcangelo, E., Slater, B., Zulueta-Coarasa, T., Fernandez-Gonzalez, R., and McGuigan, A.P. (2015). An in vitro model of tissue boundary formation for dissecting the contribution of different boundary forming mechanisms. Integr. Biol. 7, 298-312.

Jensen, J.N., Cameron, E., Garay, M.V.R., Starkey, T.W., Gianani, R., and Jensen, J. (2005). Recapitulation of elements of embryonic development in adult mouse pancreatic regeneration. Gastroenterology. 128, 728-741.

Ji, B., Tsou, L., Wang, H., Gaiser, S., Chang, D.Z., Daniluk, J., Bi, Y., Grote, T., Longnecker, D.S., and Logsdon, C.D. (2009). Ras Activity Levels Control the Development of Pancreatic Diseases. Gastroenterology. 137, 1072-1082.

Johnson, P.W., Stankova, J., Dexter, D., and Roder, J.C. (1990). The in vivo clearance of Ha-ras transformants by natural killer cells. Clin. Exp. Metastasis 8, 13–25.

Jonason, A.S., Kunala, S., Price, G.J., Restifo, R.J., Spinelli, H.M., Persing, J.A., Leffell, D.J., Tarone, R.E., and Brash, D.E. (1996). Frequent clones of p53-mutated keratinocytes in normal human skin. Proc. Natl. Acad. Sci. 93, 14025-14029.

Jones, S., Zhang, X., Parsons, D.W., Lin, J.C.-H., Leary, R.J., Angenendt, P., Mankoo, P., Carter, H., Kamiyama, H., Jimeno, A., et al. (2008). Core signaling pathways in human pancreatic cancers revealed by global genomic analyses. Science 321, 1801–1806.

Jonsson, J., Carlsson, L., Edlund, T., and Edlund, H. (1994). Insulin-promoter-factor 1 is required for pancreas development in mice. Nature 371, 606–609.

Jørgensen, C., Sherman, A., Chen, G.I., Pasculescu, A., Poliakov, A., Hsiung, M., Larsen, B., Wilkinson, D.G., Linding, R., and Pawson, T. (2009). Cell-specific information processing in segregating populations of Eph receptor ephrin-expressing cells. Science. 326, 1502–1509.

Kadeer, A., Maruyama, T., Kajita, M., Morita, T., Sasaki, A., Ohoka, A., Ishikawa, S., Ikegawa, M., Shimada, T., and Fujita, Y. (2017). Plectin is a novel regulator for apical extrusion of RasV12-transformed cells. Sci. Rep. 7, 44328.

Kajita, M., and Fujita, Y. (2015). EDAC: Epithelial defence against cancer - Cell competition between normal and transformed epithelial cells in mammals. J. Biochem. 158, 15-23.

Kajita, M., Hogan, C., Harris, A.R., Dupre-Crochet, S., Itasaki, N., Kawakami, K., Charras, G., Tada, M., and Fujita, Y. (2010). Interaction with surrounding normal epithelial cells influences signalling pathways and behaviour of Src-transformed cells. J. Cell Sci. 123, 171–180.

Kajita, M., Sugimura, K., Ohoka, A., Burden, J., Suganuma, H., Ikegawa, M., Shimada, T., Kitamura, T., Shindoh, M., Ishikawa, S., et al. (2014). Filamin acts as a key regulator in epithelial defence against transformed cells. Nat. Commun. 5, 4428.

Kanda, M., Matthaei, H., Wu, J., Hong, S.M., Yu, J., Borges, M., Hruban, R.H., Maitra, A., Kinzler, K., Vogelstein, B., et al. (2012). Presence of somatic mutations in most early-stage pancreatic intraepithelial neoplasia. Gastroenterology. 142, 730-733.

Kania, A., and Klein, R. (2016). Mechanisms of ephrin–Eph signalling in development, physiology and disease. Nat. Rev. Mol. Cell Biol. 17, 240–256.

Karim, F.D., and Rubin, G.M. (1998). Ectopic expression of activated Ras1 induces hyperplastic growth and increased cell death in Drosophila imaginal tissues. Development 125, 1–9.

Kataoka, H., Igarashi, H., Kanamori, M., Ihara, M., Wang, J.D., Wang, Y.J., Li, Z.Y., Shimamura, T., Kobayashi, T., Maruyama, K., et al. (2004). Correlation of EPHA2 overexpression with high microvessel count in human primary colorectal cancer. Cancer Sci. 95, 136–141.

Kawaguchi, K., Kageyama, R., and Sano, M. (2017). Topological defects control collective dynamics in neural progenitor cell cultures. Nature 545, 327–331.

Kimura, T., Sakisaka, T., Baba, T., Yamada, T., and Takai, Y. (2006). Involvement of the Ras-Ras-activated Rab5 guanine nucleotide exchange factor RIN2-Rab5 pathway in the hepatocyte growth factor-induced endocytosis of E-cadherin. J. Biol. Chem. 281, 10598–10609.

Kippert, A., Fitzner, D., Helenius, J., and Simons, M. (2009). Actomyosin contractility controls cell surface area of oligodendrocytes. BMC Cell Biol. 10, 71.

Knöll, B., Weinl, C., Nordheim, A., and Bonhoeffer, F. (2007). Stripe assay to examine axonal guidance and cell migration. Nat. Protoc. 2, 1216–1224.

Kon, S., Ishibashi, K., Katoh, H., Kitamoto, S., Shirai, T., Tanaka, S., Kajita, M., Ishikawa, S., Yamauchi, H., Yako, Y., et al. (2017). Cell competition with normal epithelial cells promotes apical extrusion of transformed cells through metabolic changes. Nat. Cell Biol. 19, 530–541.

Kopp, J.L., von Figura, G., Mayes, E., Liu, F.-F., Dubois, C.L., Morris, J.P., Pan, F.C., Akiyama, H., Wright, C.V.E., Jensen, K., et al. (2012). Identification of Sox9-Dependent Acinar-to-Ductal Reprogramming as the Principal Mechanism for Initiation of Pancreatic Ductal Adenocarcinoma. Cancer Cell 22, 737–750.

Krah, N.M., De La O, J.-P., Swift, G.H., Hoang, C.Q., Willet, S.G., Chen Pan, F., Cash, G.M., Bronner, M.P., Wright, C.V., MacDonald, R.J., et al. (2015). The acinar differentiation determinant PTF1A inhibits initiation of pancreatic ductal adenocarcinoma. Elife 4, e07125.

Krieg, M., Arboleda-Estudillo, Y., Puech, P.H., Käfer, J., Graner, F., Müller, D.J., and Heisenberg, C.P. (2008). Tensile forces govern germ-layer organization in zebrafish. Nat. Cell Biol. 10, 429–436.

Kujoth, G.C., Hiona, A., Pugh, T.D., Someya, S., Panzer, K., Wohlgemuth, S.E., Hofer, T., Seo, A.Y., Sullivan, R., Jobling, W.A., et al. (2005). Mitochondrial

DNA mutations, oxidative stress, and apoptosis in mammalian aging. Science. 309, 481–484.

Kuo, C.S., and Krasnow, M.A. (2015). Formation of a Neurosensory Organ by Epithelial Cell Slithering. Cell 163, 394–405.

De La Cova, C., Abril, M., Bellosta, P., Gallant, P., and Johnston, L.A. (2004). Drosophila myc regulates organ size by inducing cell competition. Cell 117, 107–116.

De La Cova, C., Senoo-Matsuda, N., Ziosi, M., Wu, D.C., Bellosta, P., Quinzii, C.M., and Johnston, L.A. (2014). Supercompetitor status of drosophila Myc cells requires p53 as a Fitness sensor to reprogram metabolism and promote viability. Cell Metab. 19, 470–483.

Labat-Robert, J. (2004). Cell-matrix interactions in aging: Role of receptors and matricryptins. Ageing Res. Rev. 3, 233-247.

Landen, C.N., Lu, C., Han, L.Y., Coffman, K.T., Bruckheimer, E., Halder, J., Mangala, L.S., Merritt, W.M., Lin, Y.G., Gao, C., et al. (2006). Efficacy and antivascular effects of EphA2 reduction with an agonistic antibody in ovarian cancer. J. Natl. Cancer Inst. 98, 1558–1570.

Langenberg, T., and Brand, M. (2005). Lineage restriction maintains a stable organizer cell population at the zebrafish midbrain-hindbrain boundary. Development 132, 3209–3216.

Lankisch, P.G., Manthey, G., Otto, J., Koop, H., Talaulicar, M., Willms, B., and Creutzfeldt, W. (1982). Exocrine pancreatic function in insulin-dependent diabetes mellitus. Digestion 25, 211–216.

Lecuit, T., and Yap, A.S. (2015). E-cadherin junctions as active mechanical integrators in tissue dynamics. Nat. Cell Biol. 17, 533–539.

Lee, J., Kotliarova, S., Kotliarov, Y., Li, A., Su, Q., Donin, N.M., Pastorino, S., Purow, B.W., Christopher, N., Zhang, W., et al. (2006). Tumor stem cells derived from glioblastomas cultured in bFGF and EGF more closely mirror the phenotype and genotype of primary tumors than do serum-cultured cell lines. Cancer Cell 9, 391–403.

Lerch, M.M., Lutz, M.P., Weidenbach, H., Muller-Pillasch, F., Gress, T.M., Leser, J., and Adler, G. (1997). Dissociation and reassembly of adherens junctions during experimental acute pancreatitis. Gastroenterology 113, 1355–1366.

Leung, C.T., and Brugge, J.S. (2012). Outgrowth of single oncogene-expressing cells from suppressive epithelial environments. Nature 482, 410–413.

Levayer, R., Hauert, B., and Moreno, E. (2015). Cell mixing induced by myc is required for competitive tissue invasion and destruction. Nature 524, 476–480.

Li, J., Ma, Q., Liu, H., Guo, K., Li, F., Li, W., Han, L., Wang, F., and Wu, E. (2011). Relationship between neural alteration and perineural invasion in pancreatic cancer patients with hyperglycemia. PLoS One 6. e17385.

Liang, K., Liu, F., Fan, J., Sun, D., Liu, C., Lyon, C.J., Bernard, D.W., Li, Y., Yokoi, K., Katz, M.H., et al. (2017). Nanoplasmonic Quantification of Tumor-derived Extracellular Vesicles in Plasma Microsamples for Diagnosis and Treatment Monitoring. Nat. Biomed. Eng. 1, 21.

Lim, K.H., Baines, A.T., Fiordalisi, J.J., Shipitsin, M., Feig, L.A., Cox, A.D., Der, C.J., and Counter, C.M. (2005). Activation of RalA is critical for Ras-induced tumorigenesis of human cells. Cancer Cell 7, 533–545.

von Lintig, F.C., Dreilinger, A.D., Varki, N.M., Wallace, A.M., Casteel, D.E., and Boss, G.R. (2000). Ras activation in human breast cancer. Breast Cancer Res. Treat. 62, 51–62.

Liou, G.-Y., Döppler, H., Necela, B., Krishna, M., Crawford, H.C., Raimondo, M., and Storz, P. (2013a). Macrophage-secreted cytokines drive pancreatic acinar-to-ductal metaplasia through NF-κB and MMPs. J. Cell Biol. 202, 563–577.

Liou, G.-Y., Döppler, H., Braun, U.B., Panayiotou, R., Scotti Buzhardt, M., Radisky, D.C., Crawford, H.C., Fields, A.P., Murray, N.R., Wang, Q.J., et al. (2015). Protein kinase D1 drives pancreatic acinar cell reprogramming and progression to intraepithelial neoplasia. Nat. Commun. 6, 6200.

Liou, G.-Y., Bastea, L., Fleming, A., Döppler, H., Edenfield, B.H., Dawson, D.W., Zhang, L., Bardeesy, N., and Storz, P. (2017). The Presence of Interleukin-13 at Pancreatic ADM/PanIN Lesions Alters Macrophage Populations and Mediates Pancreatic Tumorigenesis. Cell Rep. 19, 1322–1333.

Liou, G.Y., Döppler, H., Necela, B., Krishna, M., Crawford, H.C., Raimondo, M., and Storz, P. (2013b). Macrophage-secreted cytokines drive pancreatic acinar-to-ductal metaplasia through NF-κB and MMPs. J. Cell Biol. 202, 563–577.

Liu, J., Willet, S.G., Bankaitis, E.D., Xu, Y., Wright, C.V.E., and Gu, G. (2013). Non-parallel recombination limits cre-loxP-based reporters as precise indicators of conditional genetic manipulation. Genesis 51, 436–442.

Liu, J., Akanuma, N., Liu, C., Naji, A., Halff, G.A., Washburn, W.K., Sun, L., and Wang, P. (2016). TGF-β1 promotes acinar to ductal metaplasia of human pancreatic acinar cells. 6, 30904.

Löhr, M., Klöppel, G., Maisonneuve, P., Lowenfels, A.B., and Lüttges, J. (2005). Frequency of K-ras Mutations in Pancreatic Intraductal Neoplasias Associated

with Pancreatic Ductal Adenocarcinoma and Chronic Pancreatitis: A Meta-Analysis. Neoplasia. 7, 17-23.

Lopez-Garcia, C., Klein, A.M., Simons, B.D., and Winton, D.J. (2010). Intestinal stem cell replacement follows a pattern of neutral drift. Science. 330, 822-825.

Lu, X., Xu, T., Qian, J., Wen, X., and Wu, D. (2002). Detecting K-ras and p53 gene mutation from stool and pancreatic juice for diagnosis of early pancreatic cancer. Chin. Med. J. (Engl). 115, 1632–1636.

Lu, Z., Ghosh, S., Wang, Z., and Hunter, T. (2003). Downregulation of caveolin-1 function by EGF leads to the loss of E-cadherin, increased transcriptional activity of β-catenin, and enhanced tumor cell invasion. Cancer Cell 4, 499–515.

Luche, H., Weber, O., Nageswara Rao, T., Blum, C., and Fehling, H.J. (2007). Faithful activation of an extra-bright red fluorescent protein in "knock-in" Cre-reporter mice ideally suited for lineage tracing studies. Eur. J. Immunol. 37, 43–53.

Macara, I.G., Guyer, R., Richardson, G., Huo, Y., and Ahmed, S.M. (2014). Epithelial homeostasis. Curr. Biol. 24, 815-825.

Macrae, M., Neve, R.M., Rodriguez-Viciana, P., Haqq, C., Yeh, J., Chen, C., Gray, J.W., and McCormick, F. (2005). A conditional feedback loop regulates Ras activity through EphA2. Cancer Cell 8, 111–118.

Maddipati, R., and Stanger, B.Z. (2015). Pancreatic cancer metastases harbor evidence of polyclonality. Cancer Discov. CD-15.

Maertens, O., Johnson, B., Hollstein, P., Frederick, D.T., Cooper, Z.A., Messiaen, L., Bronson, R.T., McMahon, M., Granter, S., Flaherty, K., et al. (2013). Elucidating distinct roles for NF1 in melanomagenesis. Cancer Discov. 3, 338–349.

Magami, Y., Azuma, T., Inokuchi, H., Kawai, K., and Hattori, T. (1990). Turnover of acinar cells in mouse pancreas. J. Gastroenterol. 25, 514.

Magami, Y., Azuma, T., Inokuchi, H., Moriyasu, F., Kawai, K., and Hattori, T. (2002). Heterogeneous cell renewal of pancreas in mice: [3H]-thymidine autoradiographic investigation. Pancreas 24, 153–160.

Magnuson, M.A., and Osipovich, A.B. (2013). Pancreas-specific Cre driver lines and considerations for their prudent use. Cell Metab. 18, 9–20.

Makohon-Moore, A., and Iacobuzio-Donahue, C.A. (2016). Pancreatic cancer biology and genetics from an evolutionary perspective. Nat. Rev. Cancer. 16, 553.

Makohon-Moore, A.P., Matsukuma, K., Zhang, M., Reiter, J.G., Gerold, J.M., Jiao, Y., Sikkema, L., Attiyeh, M.A., Yachida, S., Sandone, C., et al. (2018). Precancerous neoplastic cells can move through the pancreatic ductal system. Nature. 1.

Mamada, H., Sato, T., Ota, M., and Sasaki, H. (2015). Cell competition in mouse NIH3T3 embryonic fibroblasts is controlled by the activity of Tead family proteins and Myc. J. Cell Sci. 128, 790–803.

Marciniak, A., Selck, C., Friedrich, B., and Speier, S. (2013). Mouse pancreas tissue slice culture facilitates long-term studies of exocrine and endocrine cell physiology in situ. PLoS One 8. e78706.

Marinari, E., Mehonic, A., Curran, S., Gale, J., Duke, T., and Baum, B. (2012). Live-cell delamination counterbalances epithelial growth to limit tissue overcrowding. Nature 484, 542–545.

Marston, D.J., Dickinson, S., and Nobes, C.D. (2003). Rac-dependent trans-endocytosis of ephrinBs regulates Eph-ephrin contact repulsion. Nat. Cell Biol. 5, 879–888.

Martín, F.A., Herrera, S.C., and Morata, G. (2009). Cell competition, growth and size control in the Drosophila wing imaginal disc. Development 136, 3747–3756.

Martincorena, I., Roshan, A., Gerstung, M., Ellis, P., Van Loo, P., McLaren, S., Wedge, D.C., Fullam, A., Alexandrov, L.B., Tubio, J.M., et al. (2015). High burden and pervasive positive selection of somatic mutations in normal human skin. Science. 348, 880–886.

Martins, V.C., Busch, K., Juraeva, D., Blum, C., Ludwig, C., Rasche, V., Lasitschka, F., Mastitsky, S.E., Brors, B., Hielscher, T., et al. (2014). Cell competition is a tumour suppressor mechanism in the thymus. Nature 509, 465–470.

Matsuda, Y., Furukawa, T., Yachida, S., Nishimura, M., Seki, A., Nonaka, K., Aida, J., Takubo, K., Ishiwata, T., Kimura, W., et al. (2017). The prevalence and clinicopathological characteristics of high-grade pancreatic intraepithelial neoplasia autopsy study evaluating the entire pancreatic parenchyma. Pancreas. 46, 658-664.

Mayo, S.C., Nathan, H., Cameron, J.L., Olino, K., Edil, B.H., Herman, J.M., Hirose, K., Schulick, R.D., Choti, M.A., Wolfgang, C.L., et al. (2012). Conditional survival in patients with pancreatic ductal adenocarcinoma resected with curative intent. Cancer 118, 2674–2681.

McGillicuddy, L.T., Fromm, J.A., Hollstein, P.E., Kubek, S., Beroukhim, R., De Raedt, T., Johnson, B.W., Williams, S.M.G., Nghiemphu, P., Liau, L.M., et al. (2009). Proteasomal and Genetic Inactivation of the NF1 Tumor Suppressor in Gliomagenesis. Cancer Cell 16, 44–54.

McLaughlin, S.K., Olsen, S.N., Dake, B., De Raedt, T., Lim, E., Bronson, R.T., Beroukhim, R., Polyak, K., Brown, M., and Kuperwasser, C. (2013). The RasGAP gene, RASAL2, is a tumor and metastasis suppressor. Cancer Cell 24, 365–378.

Means, A.L., Meszoely, I.M., Suzuki, K., Miyamoto, Y., Rustgi, A.K., Coffey, R.J., Wright, C.V., Stoffers, D.A., and Leach, S.D. (2005). Pancreatic epithelial plasticity mediated by acinar cell transdifferentiation and generation of nestin-positive intermediates. Development. 132, 3767-3776.

Menendez, J., Perez-Garijo, A., Calleja, M., and Morata, G. (2010). A tumor-suppressing mechanism in Drosophila involving cell competition and the Hippo pathway. Proc. Natl. Acad. Sci. 107, 14651–14656.

Merino, M.M., Rhiner, C., Portela, M., and Moreno, E. (2013). "Fitness fingerprints" mediate physiological culling of unwanted neurons in drosophila. Curr. Biol. 23, 1300-1309.

Meyer, N., and Penn, L.Z. (2008). Reflecting on 25 years with MYC. Nat. Rev. Cancer 8, 976–990.

Meyer, S.N., Amoyel, M., Bergantiños, C., De La Cova, C., Schertel, C., Basler, K., and Johnston, L.A. (2014). An ancient defense system eliminates unfit cells from developing tissues during cell competition. Science. 346, 1258236.

Miao, H., Burnett, E., Kinch, M., Simon, E., and Wang, B. (2000). Activation of EphA2 kinase suppresses integrin function and causes focal-adhesion-kinase dephosphorylation. Nat. Cell Biol. 2, 62–69.

Miao, H., Wei, B.R., Peehl, D.M., Li, Q., Alexandrou, T., Schelling, J.R., Rhim, J.S., Sedor, J.R., Burnett, E., and Wang, B. (2001). Activation of EphA receptor tyrosine kinase inhibits the Ras/MAPK pathway. Nat. Cell Biol. 3, 527–530.

Miao, H., Li, D.Q., Mukherjee, A., Guo, H., Petty, A., Cutter, J., Basilion, J.P., Sedor, J., Wu, J., Danielpour, D., et al. (2009). EphA2 Mediates Ligand-Dependent Inhibition and Ligand-Independent Promotion of Cell Migration and Invasion via a Reciprocal Regulatory Loop with Akt. Cancer Cell 16, 9–20.

Mills, J.C., and Sansom, O.J. (2015). Reserve stem cells: Differentiated cells reprogram to fuel repair, metaplasia, and neoplasia in the adult gastrointestinal tract. Sci. Signal. 8, re8.
Minami, K. (2013). Searching for stem cells in the adult pancreas: A futile effort? J. Diabetes Investig. 4, 331–333.

Monier, B., Pélissier-Monier, A., Brand, A.H., and Sanson, B. (2010). An actomyosin-based barrier inhibits cell mixing at compartmental boundaries in Drosophila embryos. Nat. Cell Biol. 12, 60–65.

Montecucco, F., Mach, F., Lenglet, S., Vonlaufen, A., Gomes Quinderé, A.L., Pelli, G., Burger, F., Galan, K., Dallegri, F., Carbone, F., et al. (2014). Treatment with Evasin-3 abrogates neutrophil-mediated inflammation in mouse acute pancreatitis. Eur. J. Clin. Invest. 44, 940-950

Morata, G., and Ripoll, P. (1975). Minutes: Mutants of Drosophila autonomously affecting cell division rate. Dev. Biol. 42, 211–221.

Moreno, E. (2008). Is cell competition relevant to cancer? Nat. Rev. Cancer 8, 141–147.

Moreno, E., and Basler, K. (2004). dMyc transforms cells into super-competitors. Cell 117, 117–129.

Moreno, E., Basler, K., and Morata, G. (2002). Cells compete for decapentaplegic survival factor to prevent apoptosis in Drosophila wing development. Nature 416, 755–759.

Morris, J.P., Wang, S.C., and Hebrok, M. (2010a). KRAS, Hedgehog, Wnt and the twisted developmental biology of pancreatic ductal adenocarcinoma. Nat. Rev. Cancer 10, 683–695.

Morris, J.P., Cano, D.A., Sekine, S., Wang, S.C., and Hebrok, M. (2010b). β-catenin blocks Kras-dependent reprogramming of acini into pancreatic cancer precursor lesions in mice. J. Clin. Invest. 120, 508–520.

Morton, J.P., Timpson, P., Karim, S.A., Ridgway, R.A., Athineos, D., Doyle, B., Jamieson, N.B., Oien, K.A., Lowy, A.M., Brunton, V.G., et al. (2010). Mutant p53 drives metastasis and overcomes growth arrest/senescence in pancreatic cancer. Proc. Natl. Acad. Sci. 107, 246–251.

Mudali, S. V, Fu, B., Lakkur, S.S., Luo, M., Embuscado, E.E., and Iacobuzio-Donahue, C.A. (2006). Patterns of EphA2 protein expression in primary and metastatic pancreatic carcinoma and correlation with genetic status. Clin. Exp. Metastasis 23, 357–365.

Mueller, H., Flury, N., Eppenberger-Castori, S., Kueng, W., David, F., and Eppenberger, U. (2000). Potential prognostic value of mitogen-activated protein kinase activity for disease-free survival of primary breast cancer patients. Int. J. Cancer 89, 384–388.

Nakayama, D., Magami, Y., Azuma, T., Inokuchi, H., Furukawa, M., Ohyashiki, J., Yoshimoto, T., Mizuguchi, J., Moriyasu, F., Kawai, K., et al. (2003). Turnover of acinar and islet cells in the pancreas of monosodium glutamate-treated obese mice. Obes. Res. 11, 87–94.

Neesse, A., Algül, H., Tuveson, D.A., and Gress, T.M. (2015). Stromal biology and therapy in pancreatic cancer: A changing paradigm. Gut 64, 1476–1484.

Nemashkalo, A., Ruzo, A., Heemskerk, I., and Warmflash, A. (2017). Morphogen and community effects determine cell fates in response to BMP4 signaling in human embryonic stem cells. Development. 153239.

Neto-Silva, R.M., de Beco, S., and Johnston, L.A. (2010). Evidence for a growth-stabilizing regulatory feedback mechanism between Myc and Yorkie, the drosophila homolog of Yap. Dev. Cell 19, 507–520.

Niederau, C., Ferrell, L.D., and Grendell, J.H. (1985). Caerulein-Induced Acute Necrotizing Pancreatitis in Mice; Protective Effects of Proglumide Benzotript, and Secretin. Gastroenterology. 88, 1192-1204.

Noberini, R., Rubio de la Torre, E., and Pasquale, E.B. (2012). Profiling Eph receptor expression in cells and tissues. Cell Adh. Migr. 6, 102–156.

Noren, N.K., and Pasquale, E.B. (2004). Eph receptor-ephrin bidirectional signals that target Ras and Rho proteins. Cell. Signal. 16, 655–666.

Norman, M., Wisniewska, K.A., Lawrenson, K., Garcia-Miranda, P., Tada, M., Kajita, M., Mano, H., Ishikawa, S., Ikegawa, M., Shimada, T., et al. (2012). Loss of Scribble causes cell competition in mammalian cells. J. Cell Sci. 125, 59–66.

Nose, A., Nagafuchi, A., and Takeichi, M. (1988). Expressed recombinant cadherins mediate cell sorting in model systems. Cell 54, 993–1001.

Oertel, M., Menthena, A., Chen, Y.-Q., and Shafritz, D.A. (2006). Properties of Cryopreserved Fetal Liver Stem/Progenitor Cells That Exhibit Long-Term Repopulation of the Normal Rat Liver. Stem Cells 24, 2244–2251.

Offield, M.F., Jetton, T.L., Labosky, P.A., Ray, M., Stein, R.W., Magnuson, M.A., Hogan, B.L., and Wright, C. V (1996). PDX-1 is required for pancreatic outgrowth and differentiation of the rostral duodenum. Development 122, 983–995.

Ohoka, A., Kajita, M., Ikenouchi, J., Yako, Y., Kitamoto, S., Kon, S., Ikegawa, M., Shimada, T., Ishikawa, S., and Fujita, Y. (2015). EPLIN is a crucial regulator for extrusion of RasV12-transformed cells. J. Cell Sci. 128, 781–789.

Oliver, E.R., Saunders, T.L., Tarle, S.A., and Glaser, T. (2004). Ribosomal protein L24 defect in Belly spot and tail (Bst), a mouse Minute. Development 131, 3907–3920.

Onder, T.T., Gupta, P.B., Mani, S.A., Yang, J., Lander, E.S., and Weinberg, R.A. (2008). Loss of E-cadherin promotes metastasis via multiple downstream transcriptional pathways. Cancer Res.

Orabi, A.I., Muili, K.A., Wang, D., Jin, S., Perides, G., and Husain, S.Z. (2013). Preparation of Pancreatic Acinar Cells for the Purpose of Calcium Imaging, Cell Injury Measurements, and Adenoviral Infection. J. Vis. Exp. 77.

Palmer, A., Zimmer, M., Erdmann, K.S., Eulenburg, V., Porthin, A., Heumann, R., Deutsch, U., and Klein, R. (2002). EphrinB phosphorylation and reverse

signaling: Regulation by Src kinases and PTP-BL phosphatase. Mol. Cell 9, 725–737.

Parfitt, G.J., Xie, Y., Reid, K.M., Dervillez, X., Brown, D.J., and Jester, J. V. (2012). A Novel Immunofluorescent Computed Tomography (ICT) Method to Localise and Quantify Multiple Antigens in Large Tissue Volumes at High Resolution. PLoS One. 7, e53245.

Park, J.E., Son, A.I., and Zhou, R. (2013). Roles of EphA2 in development and disease. Genes. 4, 334-357.

Park, M.K., Lee, M., and Petersen, O.H. (2004). Morphological and functional changes of dissociated single pancreatic acinar cells: Testing the suitability of the single cells as a model for exocytosis and calcium signaling. Cell Calcium. 35, 367-379.

Parsons, B.L., and Meng, F. (2009). K-RAS mutation in the screening, prognosis and treatment of cancer. Biomark. Med. 3, 757–769.

Pasquale, E.B. (2010). Eph receptors and ephrins in cancer: Bidirectional signalling and beyond. Nat. Rev. Cancer 10, 165–180.

Pasquale, E.B., Aasheim, H.C., Munthe, E., Funderud, S., Smeland, E.B., Beiske, K., Logtenberg, T., Alfaro, D., Garcia-Ceca, J.J., Cejalvo, T., et al. (2008). Eph-ephrin bidirectional signaling in physiology and disease. Cell 133, 38–52.

Penzo-Méndez, A.I., Chen, Y.J., Li, J., Witze, E.S., and Stanger, B.Z. (2015). Spontaneous cell competition in immortalized mammalian cell lines. PLoS One 10. e0132437.

Phillip, J.M., Aifuwa, I., Walston, J., and Wirtz, D. (2015). The Mechanobiology of Aging. Annu. Rev. Biomed. Eng. 17, 113–141.

Pierreux, C.E., Cordi, S., Hick, A.C., Achouri, Y., Ruiz de Almodovar, C., Prévot, P.P., Courtoy, P.J., Carmeliet, P., and Lemaigre, F.P. (2010). Epithelial: Endothelial cross-talk regulates exocrine differentiation in developing pancreas. Dev. Biol. 347, 216-227.

Pommier, A., Anaparthy, N., Memos, N., Kelley, Z.L., Gouronnec, A., Yan, R., Auffray, C., Albrengues, J., Egeblad, M., Iacobuzio-Donahue, C.A., et al. (2018). Unresolved endoplasmic reticulum stress engenders immune-resistant, latent pancreatic cancer metastases. Science. 1–15.

Porazinski, S., de Navascués, J., Yako, Y., Hill, W., Jones, M.R., Maddison, R., Fujita, Y., and Hogan, C. (2016). EphA2 Drives the Segregation of Ras-Transformed Epithelial Cells from Normal Neighbors. Curr. Biol. 26, 3220–3229.

Poruk, K.E., Gay, D.Z., Brown, K., Mulvihill, J.D., Boucher, K.M., Scaife, C.L., Firpo, M.A., and Mulvihill, S.J. (2013). The clinical utility of CA 19-9 in pancreatic adenocarcinoma: diagnostic and prognostic updates. Curr. Mol. Med. 13, 340–351.

Prévot, P.-P., Simion, A., Grimont, A., Colletti, M., Khalaileh, A., Van den Steen, G., Sempoux, C., Xu, X., Roelants, V., Hald, J., et al. (2012). Role of the ductal transcription factors HNF6 and Sox9 in pancreatic acinar-to-ductal metaplasia. Gut 61, 1723–1732.

Prior, I.A., Lewis, P.D., and Mattos, C. (2012). A comprehensive survey of ras mutations in cancer. Cancer Res. 72, 2457–2467.

Prober, D.A., and Edgar, B.A. (2000). Ras1 promotes cellular growth in the Drosophila wing. Cell 100, 435–446.

Raff, M.C. (1992). Social controls on cell survival and cell death. Nature 356, 397–400.

Rahib, L., Smith, B.D., Aizenberg, R., Rosenzweig, A.B., Fleshman, J.M., and Matrisian, L.M. (2014). Projecting Cancer Incidence and Deaths to 2030: The Unexpected Burden of Thyroid, Liver, and Pancreas Cancers in the United States. Cancer Res. 74, 2913 LP-2921.

Raimondi, S., Maisonneuve, P., and Lowenfels, A.B. (2009). Epidemiology of pancreatic cancer: an overview. Nat. Rev. Gastroenterol. Hepatol. 6, 699.

Reichert, M., Takano, S., Heeg, S., Bakir, B., Botta, G.P., and Rustgi, A.K. (2013). Isolation, culture and genetic manipulation of mouse pancreatic ductal cells. Nat. Protoc. 8, 1354–1365.

Rhim, A.D., Mirek, E.T., Aiello, N.M., Maitra, A., Bailey, J.M., McAllister, F., Reichert, M., Beatty, G.L., Rustgi, A.K., Vonderheide, R.H., et al. (2012). EMT and dissemination precede pancreatic tumor formation. Cell 148, 349–361.

Rhim, A.D., Thege, F.I., Santana, S.M., Lannin, T.B., Saha, T.N., Tsai, S., Maggs, L.R., Kochman, M.L., Ginsberg, G.G., Lieb, J.G., et al. (2014). Detection of circulating pancreas epithelial cells in patients with pancreatic cystic lesions. Gastroenterology 146, 647–651.

Rhiner, C., López-Gay, J.M., Soldini, D., Casas-Tinto, S., Martín, F.A., Lombardía, L., and Moreno, E. (2010). Flower forms an extracellular code that reveals the fitness of a cell to its neighbors in Drosophila. Dev. Cell 18, 985–998.

Rodrigues, A.B., Zoranovic, T., Ayala-Camargo, A., Grewal, S., Reyes-Robles, T., Krasny, M., Wu, D.C., Johnston, L.A., and Bach, E.A. (2012). Activated STAT regulates growth and induces competitive interactions independently of Myc, Yorkie, Wingless and ribosome biogenesis. Development 139, 4051–4061.

Rodriguez-Boulan, E., and Macara, I.G. (2014). Organization and execution of the epithelial polarity programme. Nat. Rev. Mol. Cell Biol. 15, 225–242.

Roh-Johnson, M., Shemer, G., Higgins, C.D., McClellan, J.H., Werts, A.D., Tulu, U.S., Gao, L., Betzig, E., Kiehart, D.P., and Goldstein, B. (2012). Triggering a cell shape change by exploiting preexisting actomyosin contractions. Science. 335, 1232–1235.

Rohani, N., Canty, L., Luu, O., Fagotto, F., and Winklbauer, R. (2011). EphrinB/EphB signaling controls embryonic germ layer separation by contact-induced cell detachment. PLoS Biol. e1000597.

Rosenblatt, J., Raff, M.C., and Cramer, L.P. (2001). An epithelial cell destined for apoptosis signals its neighbors to extrude it by an actin- and myosin-dependent mechanism. Curr. Biol. 11, 1847–1857.

Saito, T., Masuda, N., Miyazaki, T., Kanoh, K., Suzuki, H., Shimura, T., Asao, T., and Kuwano, H. (2004). Expression of EphA2 and E-cadherin in colorectal cancer: Correlation with cancer metastasis. Oncol. Rep. 11, 605–611.

Saitoh, S., Maruyama, T., Yako, Y., Kajita, M., Fujioka, Y., Ohba, Y., Kasai, N., Sugama, N., Kon, S., Ishikawa, S., et al. (2017). Rab5-regulated endocytosis plays a crucial role in apical extrusion of transformed cells. Proc. Natl. Acad. Sci. 114, E2327–E2336.

Saka, Y., Lhoussaine, C., Kuttler, C., Ullner, E., and Thiel, M. (2011). Theoretical basis of the community effect in development. BMC Syst. Biol. 5, 54.

Sancho, M., Di-Gregorio, A., George, N., Pozzi, S., Sánchez, J.M., Pernaute, B., and Rodríguez, T.A. (2013). Competitive interactions eliminate unfit embryonic stem cells at the onset of differentiation. Dev. Cell 26, 19–30.

Sasaki, A., Nagatake, T., Egami, R., Gu, G., Takigawa, I., Ikeda, W., Nakatani, T., Kunisawa, J., and Fujita, Y. (2018). Obesity Suppresses Cell-Competition-Mediated Apical Elimination of RasV12-Transformed Cells from Epithelial Tissues. Cell Rep. 23, 974-982.

Sausen, M., Phallen, J., Adleff, V., Jones, S., Leary, R.J., Barrett, M.T., Anagnostou, V., Parpart-Li, S., Murphy, D., Li, Q.K., et al. (2015). Clinical implications of genomic alterations in the tumour and circulation of pancreatic cancer patients. Nat. Commun. 6, 7686.

Saw, T.B., Doostmohammadi, A., Nier, V., Kocgozlu, L., Thampi, S., Toyama, Y., Marcq, P., Lim, C.T., Yeomans, J.M., and Ladoux, B. (2017). Topological defects in epithelia govern cell death and extrusion. Nature 544, 212–216.

Schnekenburger, J., Mayerle, J., Krüger, B., Buchwalow, I., Weiss, F.U., Albrecht, E., Samoilova, V.E., Domschke, W., and Lerch, M.M. (2005). Protein

tyrosine phosphatase κ and SHP-1 are involved in the regulation of cell-cell contacts at adherens junctions in the exocrine pancreas. Gut 54, 1445–1455.

Scholzen, T., and Gerdes, J. (2000). The Ki-67 protein: From the known and the unknown. J. Cell. Physiol. 182, 311–322.

Senoo-Matsuda, N., and Johnston, L. a (2007). Soluble factors mediate competitive and cooperative interactions between cells expressing different levels of Drosophila Myc. Proc. Natl. Acad. Sci. 104, 18543-18548.

Seymour, P.A., Freude, K.K., Tran, M.N., Mayes, E.E., Jensen, J., Kist, R., Scherer, G., and Sander, M. (2007). SOX9 is required for maintenance of the pancreatic progenitor cell pool. Proc. Natl. Acad. Sci. 104, 1865-1870.

Shamah, S.M., Lin, M.Z., Goldberg, J.L., Estrach, S., Sahin, M., Hu, L., Bazalakova, M., Neve, R.L., Corfas, G., Debant, A., et al. (2001). EphA receptors regulate growth cone dynamics through the novel guanine nucleotide exchange factor ephexin. Cell. 105, 233-244.

Shi, G., DiRenzo, D., Qu, C., Barney, D., Miley, D., and Konieczny, S.F. (2013). Maintenance of acinar cell organization is critical to preventing Kras-induced acinar-ductal metaplasia. Oncogene 32, 1950–1958.

Shiozawa, Y., Pedersen, E.A., Havens, A.M., Jung, Y., Mishra, A., Joseph, J., Kim, J.K., Patel, L.R., Ying, C., Ziegler, A.M., et al. (2011). Human prostate cancer metastases target the hematopoietic stem cell niche to establish footholds in mouse bone marrow. J. Clin. Invest. 121, 1298–1312.

Shraiman, B.I. (2005). Mechanical feedback as a possible regulator of tissue growth. Proc. Natl. Acad. Sci. 102, 3318–3323.

Siegel, R.L., Miller, K.D., and Jemal, A. (2016a). Cancer statistics, 2016. CA. Cancer J. Clin. 66, 7–30.

Simonsen, A., Lippé, R., Christoforidis, S., Gaullier, J.M., Brech, A., Callaghan, J., Toh, B.H., Murphy, C., Zerial, M., and Stenmark, H. (1998). EEA1 links PI(3)K function to Rab5 regulation of endosome fusion. Nature. 394, 494.

Simpson, P. (1979). Parameters of cell competition in the compartments of the wing disc of Drosophila. Dev. Biol. 69, 182–193.

Simpson, P., and Morata, G. (1981). Differential mitotic rates and patterns of growth in compartments in the Drosophila wing. Dev. Biol. 85, 299–308.

Sivaraman, V.S., Wang, H., Nuovo, G.J., and Malbon, C.C. (1997). Hyperexpression of mitogen-activated protein kinase in human breast cancer. J. Clin. Invest. 99, 1478–1483.

Slaghter, D.P., Southwick, H.W., and Smejkal, W. (1953). Field canerisation in oral stratified squamous epithelium. Cancer 6, 963–968.

Slattum, G., Gu, Y., Sabbadini, R., and Rosenblatt, J. (2014). Autophagy in oncogenic K-Ras promotes basal extrusion of epithelial cells by degrading S1P. Curr. Biol. 24, 19–28.

Smith, F.M., Vearing, C., Lackmann, M., Treutlein, H., Himanen, J., Chen, K., Saul, A., Nikolov, D., and Boyd, A.W. (2004). Dissecting the EphA3/Ephrin-A5 interactions using a novel functional mutagenesis screen. J. Biol. Chem. 279, 9522–9531.

Snippert, H.J., van der Flier, L.G., Sato, T., van Es, J.H., van den Born, M., Kroon-Veenboer, C., Barker, N., Klein, A.M., van Rheenen, J., Simons, B.D., et al. (2010). Intestinal crypt homeostasis results from neutral competition between symmetrically dividing Lgr5 stem cells. Cell. 143, 134-144.

Soares, C.P., Midlej, V., de Oliveira, M.E.W., Benchimol, M., Costa, M.L., and Mermelstein, C. (2012). 2D and 3D-organized cardiac cells shows differences in cellular morphology, adhesion junctions, presence of myofibrils and protein expression. PLoS One 7. e38147.

Solanas, G., Cortina, C., Sevillano, M., and Batlle, E. (2011). Cleavage of E-cadherin by ADAM10 mediates epithelial cell sorting downstream of EphB signalling. Nat. Cell Biol. 13, 1100–1109.

Sousa, C.M., and Kimmelman, A.C. (2014). The complex landscape of pancreatic cancer metabolism. Carcinogenesis. 35, 1441-1450.

St Johnston, D., and Ahringer, J. (2010). Cell polarity in eggs and epithelia: Parallels and diversity. Cell 141, 757–774.

Steinberg, M.S. (1963). Reconstruction of tissues by dissociated cells. Some morphogenetic tissue movements and the sorting out of embryonic cells may have a common explanation. Science. 141, 401–408.

Steinberg, M.S. (2007). Differential adhesion in morphogenesis: a modern view. Curr. Opin. Genet. Dev. 17, 281–286.

Stoker, M., and Rubin, H. (1967). Density dependent inhibition of cell growth in culture. Nature 215, 171–172.

Stopczynski, R.E., Normolle, D.P., Hartman, D.J., Ying, H., DeBerry, J.J., Bielefeldt, K., Rhim, A.D., DePinho, R.A., Albers, K.M., and Davis, B.M. (2014). Neuroplastic changes occur early in the development of pancreatic ductal adenocarcinoma. Cancer Res. 2050.

Storz, P. (2017). Acinar cell plasticity and development of pancreatic ductal adenocarcinoma. Nat. Rev. Gastroenterol. Hepatol. 14, 296–304.

Stromnes, I.M., DelGiorno, K.E., Greenberg, P.D., and Hingorani, S.R. (2014). Stromal re-engineering to treat pancreas cancer. Carcinogenesis 35.

Suijkerbuijk, S.J.E., Kolahgar, G., Kucinski, I., and Piddini, E. (2016). Cell competition drives the growth of intestinal adenomas in Drosophila. Curr. Biol. 26, 428–438.

Tamori, Y., and Deng, W.M. (2013). Tissue Repair through Cell Competition and Compensatory Cellular Hypertrophy in Postmitotic Epithelia. Dev. Cell 25, 350–363.

Tamori, Y., Bialucha, C.U., Tian, A.G., Kajita, M., Huang, Y.C., Norman, M., Harrison, N., Poulton, J., Ivanovitch, K., Disch, L., et al. (2010). Involvement of Lgl and mahjong/VprBP in cell competition. PLoS Biol. 8. e1000422.

Tape, C.J., Ling, S., Dimitriadi, M., McMahon, K.M., Worboys, J.D., Leong, H.S., Norrie, I.C., Miller, C.J., Poulogiannis, G., Lauffenburger, D.A., et al. (2016). Oncogenic KRAS Regulates Tumor Cell Signaling via Stromal Reciprocation. Cell. 165, 910-920.

Thiery, J.P., Acloque, H., Huang, R.Y.J., and Nieto, M.A. (2009). Epithelial-Mesenchymal Transitions in Development and Disease. Cell 139, 871–890.

Tobita, K., Kijima, H., Dowaki, S., Kashiwagi, H., Ohtani, Y., Oida, Y., Yamazaki, H., Nakamura, M., Ueyama, Y., Tanaka, M., et al. (2003). Epidermal growth factor receptor expression in human pancreatic cancer: Significance for liver metastasis. Int. J. Mol. Med. 11, 305-309.

Toyoda, Y., Shinohara, R., Thumkeo, D., Kamijo, H., Nishimaru, H., Hioki, H., Kaneko, T., Ishizaki, T., Furuyashiki, T., and Narumiya, S. (2013). EphA4-dependent axon retraction and midline localization of Ephrin-B3 are disrupted in the spinal cord of mice lacking mDia1 and mDia3 in combination. Genes to Cells. 18, 873-885.

Trajkovic-Arsic, M., Kalideris, E., and Siveke, J.T. (2013). The role of insulin and IGF system in pancreatic cancer. J. Mol. Endocrinol. 50, 67-74.

Trepat, X., and Sahai, E. (2018). Mesoscale physical principles of collective cell organization. Nat. Phys. 1.

Tuveson, D.A., Shaw, A.T., Willis, N.A., Silver, D.P., Jackson, E.L., Chang, S., Mercer, K.L., Grochow, R., Hock, H., Crowley, D., et al. (2004). Endogenous oncogenic K-rasG12Dstimulates proliferation and widespread neoplastic and developmental defects. Cancer Cell 5, 375–387.

Twigg, S.R.F., Kan, R., Babbs, C., Bochukova, E.G., Robertson, S.P., Wall, S.A., Morriss-Kay, G.M., and Wilkie, A.O.M. (2004). Mutations of ephrin-B1 (EFNB1), a marker of tissue boundary formation, cause craniofrontonasal syndrome. Proc. Natl. Acad. Sci. U. S. A. 101, 8652–8657.

Tyler, D.M., Li, W., Zhuo, N., Pellock, B., and Baker, N.E. (2007). Genes affecting cell competition in drosophila. Genetics 175, 643–657.

Vaughen, J., and Igaki, T. (2016). Slit-Robo Repulsive Signaling Extrudes Tumorigenic Cells from Epithelia. Dev. Cell 39, 683–695.

Verdu, J., Buratovicht, M.A., Wilder, E.L., and Birnbaum, M.J. (1999). Cell-autonomous regulation of cell and organ growth in Drosophila by Akt/PKB. Nat. Cell Biol. 1, 500–506.

Vihanto, M.M., Vindis, C., Djonov, V., Cerretti, D.P., and Huynh-Do, U. (2006). Caveolin-1 is required for signaling and membrane targeting of EphB1 receptor tyrosine kinase. J. Cell Sci. 119, 2299-2309.

Villa del Campo, C., Clavería, C., Sierra, R., and Torres, M. (2014). Cell competition promotes phenotypically silent cardiomyocyte replacement in the mammalian heart. Cell Rep. 8, 1741–1751.

Villasenor, A., Chong, D.C., Henkemeyer, M., and Cleaver, O. (2010). Epithelial dynamics of pancreatic branching morphogenesis. Development. 137, 4295-4305.

Vincent, J.P., Kolahgar, G., Gagliardi, M., and Piddini, E. (2011). Steep Differences in Wingless Signaling Trigger Myc-Independent Competitive Cell Interactions. Dev. Cell 21, 366–374.

Vooijs, M., Jonkers, J., and Berns, A. (2001). A highly efficient ligand-regulated Cre recombinase mouse line shows that LoxP recombination is position dependent. EMBO Rep. 2, 292-297.

Waddell, N., Pajic, M., Patch, A.M., Chang, D.K., Kassahn, K.S., Bailey, P., Johns, A.L., Miller, D., Nones, K., Quek, K., et al. (2015). Whole genomes redefine the mutational landscape of pancreatic cancer. Nature 518, 495–501.

Wagstaff, L., Goschorska, M., Kozyrska, K., Duclos, G., Kucinski, I., Chessel, A., Hampton-O'Neil, L., Bradshaw, C.R., Allen, G.E., Rawlins, E.L., et al. (2016a). Mechanical cell competition kills cells via induction of lethal p53 levels. Nat. Commun. 7, 11373.

Wahl, S., Barth, H., Ciossek, T., Aktories, K., and Mueller, B.K. (2000). Ephrin-A5 induces collapse of growth cones by activating Rho and Rho kinase. J. Cell Biol. 149, 263–270.

Wakayama, Y., Miura, K., Sabe, H., and Mochizuki, N. (2011). EphrinA1-EphA2 signal induces compaction and polarization of Madin-Darby canine kidney cells by inactivating Ezrin through negative regulation of RhoA. J. Biol. Chem. 286, 44243–44253.

Walker-Daniels, J., Coffman, K., Azimi, M., Rhim, J.S., Bostwick, D.G., Snyder, P., Kerns, B.J., Waters, D.J., and Kinch, M.S. (1999). Overexpression of the EphA2 tyrosine kinase in prostate cancer. Prostate 41, 275–280.

Wang, H.U., and Anderson, D.J. (1997). Eph family transmembrane ligands can mediate repulsive guidance of trunk neural crest migration and motor axon outgrowth. Neuron 18, 383–396.

Watanabe, H., Ishibashi, K., Mano, H., Kitamoto, S., Sato, N., Hoshiba, K., Kato, M., Matsuzawa, F., Takeuchi, Y., Shirai, T., et al. (2018). Mutant p53-Expressing Cells Undergo Necroptosis via Cell Competition with the Neighboring Normal Epithelial Cells. Cell Rep. 23, 3721–3729.

Watanabe, T., Sato, Y., Saito, D., Tadokoro, R., and Takahashi, Y. (2009). EphrinB2 coordinates the formation of a morphological boundary and cell epithelialization during somite segmentation. Proc. Natl. Acad. Sci. 106, 7467–7472.

Wheelock, M.J., Shintani, Y., Maeda, M., Fukumoto, Y., and Johnson, K.R. (2008). Cadherin switching. J. Cell Sci. 121, 727–735.

Wildenberg, G.A., Dohn, M.R., Carnahan, R.H., Davis, M.A., Lobdell, N.A., Settleman, J., and Reynolds, A.B. (2006). p120-Catenin and p190RhoGAP Regulate Cell-Cell Adhesion by Coordinating Antagonism between Rac and Rho. Cell 127, 1027–1039.

Wilentz, R.E., Geradts, J., Maynard, R., Offerhaus, G.J.A., Kang, M., Goggins, M., Yeo, C.J., Kern, S.E., and Hruban, R.H. (1998). Inactivation of the p16 (INK4A) tumor-suppressor gene in pancreatic duct lesions: Loss of intranuclear expression. Cancer Res. 58, 4740–4744.

Wilentz, R.E., Iacobuzio-Donahue, C.A., Argani, P., McCarthy, D.M., Parsons, J.L., Yeo, C.J., Kern, S.E., and Hruban, R.H. (2000). Loss of expression of Dpc4 in pancreatic intraepithelial neoplasia: Evidence that DPC4 inactivation occurs late in neoplastic progression. Cancer Res. 60, 2002–2006.

Williams Parsons, D., Jones, S., Zhang, X., Cheng-Ho Lin, J., Leary, R.J., Angenendt, P., Mankoo, P., Carter, H., Siu, I.-M., Gallia, G.L., et al. (2008). An Integrated Genomic Analysis of Human Glioblastoma Multiforme I An Integrated Genomic Analysis of Human Glioblastoma Multiforme. Source Sci. New Ser. 321, 1807–1812.

Witkiewicz, A.K., McMillan, E.A., Balaji, U., Baek, G.H., Lin, W.C., Mansour, J., Mollaee, M., Wagner, K.U., Koduru, P., Yopp, A., et al. (2015). Whole-exome sequencing of pancreatic cancer defines genetic diversity and therapeutic targets. Nat. Commun. 6.

Wójciak-Stothard, B., Potempa, S., Eichholtz, T., and Ridley, A.J. (2001). Rho and Rac but not Cdc42 regulate endothelial cell permeability. J. Cell Sci.

Wollny, D., Zhao, S., Everlien, I., Lun, X., Brunken, J., Brüne, D., Ziebell, F., Tabansky, I., Weichert, W., Marciniak-Czochra, A., et al. (2016). Single-Cell Analysis Uncovers Clonal Acinar Cell Heterogeneity in the Adult Pancreas. Dev. Cell 39, 289–301.

Woods, D.F., and Bryant, P.J. (1991). The discs-large tumor suppressor gene of Drosophila encodes a guanylate kinase homolog localized at septate junctions. Cell 66, 451–464.

Wu, S.K., Gomez, G.A., Michael, M., Verma, S., Cox, H.L., Lefevre, J.G., Parton, R.G., Hamilton, N.A., Neufeld, Z., and Yap, A.S. (2014). Cortical F-actin stabilization generates apical-lateral patterns of junctional contractility that integrate cells into epithelia. Nat. Cell Biol. 16, 167–178.

Wu, S.K., Lagendijk, A.K., Hogan, B.M., Gomez, G.A., and Yap, A.S. (2015). Active contractility at E-cadherin junctions and its implications for cell extrusion in cancer. Cell Cycle 14, 315–322.

Xu, N.J., and Henkemeyer, M. (2009). Ephrin-B3 reverse signaling through Grb4 and cytoskeletal regulators mediates axon pruning. Nat. Neurosci. 12, 268–276.

Xu, M., Jung, X., Hines, O.J., Eibl, G., and Chen, Y. (2018). Obesity and Pancreatic Cancer: Overview of Epidemiology and Potential Prevention by Weight Loss. Pancreas 47, 158–162.

Xu, Q., Mellitzer, G., Robinson, V., and Wilkinson, D.G. (1999). In vivo cell sorting in complementary segmental domains mediated by Eph receptors and ephrins. Nature 399, 267–271.

Yachida, S., Jones, S., Bozic, I., Antal, T., Leary, R., Fu, B., Kamiyama, M., Hruban, R.H., Eshleman, J.R., Nowak, M.A., et al. (2010). Distant metastasis occurs late during the genetic evolution of pancreatic cancer. Nature 467, 1114–1117.

Yakubovskaya, M.S., Spiegelman, V., Luo, F.C., Malaev, S., Salnev, A., Zborovskaya, I., Gasparyan, A., Polotsky, B., Machaladze, Z., Trachtenberg, A.C., et al. (1995). High frequency of K- ras mutations in normal appearing lung tissues and sputum of patients with lung cancer. Int. J. Cancer 63, 810–814.

Yamaguchi, J., Yokoyama, Y., Kokuryo, T., Ebata, T., and Nagino, M. (2017). Cells of origin of pancreatic neoplasms. Surg. Today 0, 1–9.

Yan, L., McFaul, C., Howes, N., Leslie, J., Lancaster, G., Wong, T., Threadgold, J., Evans, J., Gilmore, I., Smart, H., et al. (2005). Molecular analysis to detect pancreatic ductal adenocarcinoma in high-risk groups. Gastroenterology 128, 2124–2130.

Yeddula, N., Xia, Y., Ke, E., Beumer, J., and Verma, I.M. (2015). Screening for tumor suppressors: Loss of ephrin receptor A2 cooperates with oncogenic KRas in promoting lung adenocarcinoma. Proc. Natl. Acad. Sci. 112, E6476–E6485.

Yin, Y., Yamashita, Y., Noda, H., Okafuji, T., Go, M.J., and Tanaka, H. (2004). EphA receptor tyrosine kinases interact with co-expressed ephrin-A ligands in cis. Neurosci. Res. 48, 285–296.

Ying, H., Dey, P., Yao, W., Kimmelman, A.C., Draetta, G.F., Maitra, A., and Depinho, R.A. (2016). Genetics and biology of pancreatic ductal adenocarcinoma. Genes Dev. 30, 355-385.

Zantek, N.D., Azimi, M., Fedor-Chaiken, M., Wang, B., Brackenbury, R., and Kinch, M.S. (1999). E-cadherin regulates the function of the EphA2 receptor tyrosine kinase. Cell Growth Differ. 10, 629–638.

Zelinski, D.P., Zantek, N.D., Stewart, J.C., Irizarry, A.R., and Kinch, M.S. (2001). EphA2 overexpression causes tumorigenesis of mammary epithelial cells. Cancer Res. 61, 2301–2306.

Zhang, K., Myllymäki, S.M., Gao, P., Devarajan, R., Kytölä, V., Nykter, M., Wei, G.H., and Manninen, A. (2017). Oncogenic K-Ras upregulates ITGA6 expression via FOSL1 to induce anoikis resistance and synergizes with αV-Class integrins to promote EMT. Oncogene 36, 5681–5694.

Zhou, H., Qin, Y., Ji, S., Ling, J., Fu, J., Zhuang, Z., Fan, X., Song, L., Yu, X., and Chiao, P.J. (2018). SOX9 activity is induced by oncogenic Kras to affect MDC1 and MCMs expression in pancreatic cancer. Oncogene. 37, 912.

Zhu, L., Shi, G., Schmidt, C.M., Hruban, R.H., and Konieczny, S.F. (2007). Acinar Cells Contribute to the Molecular Heterogeneity of Pancreatic Intraepithelial Neoplasia. Am. J. Pathol. 171, 263–273.

Zhu, Z., Kleeff, J., Friess, H., Wang, L., Zimmermann, A., Yarden, Y., Büchler, M.W., and Korc, M. (2000). Epiregulin is up-regulated in pancreatic cancer and stimulates pancreatic cancer cell growth. Biochem. Biophys. Res. Commun. 273, 1019-1024.

Zhuang, G., Brantley-Sieders, D.M., Vaught, D., Yu, J., Xie, L., Wells, S., Jackson, D., Muraoka-Cook, R., Arteaga, C., and Chen, J. (2010). Elevation of receptor tyrosine kinase EphA2 mediates resistance to trastuzumab therapy. Cancer Res. 70, 299–308.

Zimmer, M., Palmer, A., Köhler, J., and Klein, R. (2003). EphB-ephrinB bi-directional endocytosis terminates adhesion allowing contact mediated repulsion. Nat. Cell Biol. 5, 869–878.

Ziosi, M., Baena-López, L.A., Grifoni, D., Froldi, F., Pession, A., Garoia, F., Trotta, V., Bellosta, P., Cavicchi, S., and Pession, A. (2010). dMyc functions downstream of yorkie to promote the supercompetitive behavior of hippo pathway mutant Cells. PLoS Genet. 6.